Medical Applications of In-line Laser Absorption Spectroscopy



Jennifer Louise Redmond

Worcester College

University of Oxford

A thesis submitted for the degree of

Doctor of Philosophy

Trinity 2023

For my parents, Sue and Steve,
and my grandparents,
Pat, Harold, Margaret and Albert

Medical Applications of In-line Laser Absorption Spectroscopy

Jennifer Louise Redmond

Worcester College
University of Oxford

A thesis submitted for the degree of Doctor of Philosophy

Trinity 2023

The recent development of the molecular flow sensor (MFS), a device which employs laser absorption spectroscopy to make in-line real-time measurements of gas exchange rates in humans, offers multiple exciting clinical applications. The concentration of O_2 is measured every 10 ms using cavity enhanced absorption spectroscopy alongside CO_2 and H_2O concentration measurements via direct laser absorption spectroscopy. This allows dynamic recalibration of the flow sensing system which provides simultaneous measurements of flow from which highly accurate gas exchange rates can be determined. This thesis aims to demonstrate the clinical utility of the device across multiple previously untested patient groups.

The work presented involves building and calibrating two custom-made MFS instruments, as well as instigating several modifications to optimise device performance. Both devices demonstrate excellent performance in terms of nitrogen balance over tens of minutes and are shown to work reliably across multiple clinical settings. One of the potentially most impactful applications of the device lies in monitoring O_2 consumption rates in critical care, where many patients display impaired oxygen utilisation. As a first example, the device is shown to perform well in the first study of its use in this setting, with intriguing observations about patient responses to interventions such as the adjustment of ventilator settings and the administration of vasoactive drugs.

A second major application of this technology involves using it in combination with another recent development, the lognormal lung model, a mathematical model of the lung which can be used to obtain parameters assessing lung inhomogeneity. This thesis describes the use of this technique in three groups, namely young smokers and patients with chronic obstructive pulmonary disease and cystic fibrosis (CF). The thesis provides early evidence that this novel method of determining lung inhomogeneity may provide a more sensitive assessment of lung abnormalities than conventional techniques. In particular the inhomogeneity parameter σ_{CL} can differentiate between controls and CF patients with preserved FEV_1. In the case of CF, patients undergo

lifelong monitoring of their lung function. To that end, a miniaturised device suitable for use in the paediatric population was designed and early data of its use in a clinical setting is also presented.

Acknowledgements

First and foremost, I would like to thank Grant for being such an inspirational tutor and then supervisor during my time in the Ritchie group. His unwavering enthusiasm, guidance and support has been invaluable throughout my time as an Oxford student. Sincere thanks must also go to both Peter and Gus for incredibly helpful discussions and sharing their physiology and spectroscopy wisdom as well as many entertaining stories.

I am very grateful to John for his incredible design work and knowledge of optical fibres (and houseplant rescue operations). Thank you also to Rob, for sharing his expertise of lasers and optical cavities. Luca, David, and Nick were all incredibly generous in sharing their knowledge of the project when I first joined, for which I am very grateful, and Nick also deserves recognition for his skilled navigation of the seven-lane highways of San Diego. Huge thanks must also go to Graham, who has been a continually patient source of knowledge and support, especially with his LabVIEW expertise. Thank you also to Chris and Dom for all their hard work furthering the development of the lung model.

There have been so many other fantastic colleagues in the Ritchie group over the years that have made being in the group so much fun: Katherine and her baking masterpieces, Lorenzo for introducing me to Italian hot chocolate, James for his skilful operation of the FTIR experiment and canal boats, Michele and Tomàs with our early evening chats, Dáire and Sam and everyone else for all the enjoyable PTCL teas and Uni Parks lunches. There have been so many great Part IIs over the years who have provided both entertainment and baking, but special thanks must go to Fiona for all her help in searching for the smokers of Oxford. I appreciate all the support of the whole team in the PTCL electronics workshop - a trip downstairs was always fun and thank you for trusting me with the soldering iron.

Thank you to the team at the JR for their efforts to recruit patients for the ICU work, particularly Killian and Akshay for their perseverance. I am also extremely grateful to both Nick and Nayia, who made recruiting patients for both the CF and smoking studies possible and offered such valuable insights into the clinical applications of the technique. Both Keith and Snapper always brightened my trips to DPAG, thank you for all our chats, physiology related and otherwise.

I am grateful to all our collaborators at the RBH for their work in recruiting CF patients and for sharing their lung clearance index expertise.

I feel privileged to have also had the opportunity to work with the team at the UCSD Radiology Imaging Laboratory, who enabled our collaborative study and made us feel so welcome, with hiking, barbecues and attempts to teach us surfing.

To all the wonderful friends who've been there through thick and thin, including the Shoal, the Worcester MCR and my many lovely housemates over the years, I'm so happy to call you my friends.

Finally, none of this would have been possible without the continual love and support of my parents. You have always been there to provide love and encouragement and I wouldn't be where I am today without you.

Abbreviations

ABG	Arterial blood gas (test)
AD	Autogenic drainage
ADC	Analog to digital converter
AICU	Adult intensive care unit
ALI	Acute lung injury
APC	Angled physical contact
ARC	Advanced research computing
ARDS	Acute respiratory distress syndrome
ASE	Amplified spontaneous emission (filter)
BMI	Body mass index
BTPS	Body temperature and ambient pressure saturated with water vapour
CAD	Computer aided design
CBGS	Circulation and body gas stores
CEAS	Cavity enhanced absorption spectroscopy
CED	Cumulative effective dose
CF	Cystic fibrosis
CFTR	Cystic fibrosis transmembrane conductance regulator
CMOS	Complementary metal oxide semiconductor
COPD	Chronic obstructive pulmonary disease
CoV	Coefficient of variation
COVID-19	Coronavirus disease 2019
CT	Computerised tomography
DBR	Distributed Bragg reflectors
DFB	Distributed-feedback
EE	Energy expenditure
EELV	End-expiratory lung volume
EGDT	Early Goal Directed Therapy
ERS	European Respiratory Society

ERV	Expiratory reserve volume
FC	Fibre connector
FEF_{75}	Maximal expiratory flow when 75% of FVC expired
FEV_1	Forced expiratory volume in 1 second
FOT	Forced oscillation technique
FRC	Functional residual capacity
FSR	Free spectral range
FVC	Forced vital capacity
FWHM	Full-width at half maximum
GOLD	Global Initiative for Obstructive Lung Disease
HALI	Hyperoxic acute lung injury
HFCWO	High frequency chest wall oscillation
HITRAN	High-resolution transmission molecular absorption database
HME	Heat and moisture exchange
HRCT	High resolution computerised tomography
HS	Hypertonic saline
IC	Inspiratory capacity
ICU	Intensive care unit
IR	Infra-red
IRV	Inspiratory reserve volume
IV	Intravenous
IVC	Inspiratory vital capacity
JR	John Radcliffe (Hospital)
LCI	Lung clearance index
LD	Laser diode
LNL	Lognormal lung
MAP	Mean arterial pressure
MBW	Multiple breath washout
MFS	Molecular flow sensor
MFS-P	Paediatric molecular flow sensor
MIGET	Multiple inert gas elimination technique
MRI	Magnetic resonance imaging
NBS	Newborn screening
NHS	National Health Service
NTM	Non-tuberculous mycobacterium
PAC	Pulmonary artery catheter

PC	Physical contact
PD	Photodetector
PD	Postural drainage with percussion
PEEP	Positive end-expiratory pressure
PEP	Positive expiratory pressure
PIS	Participant information sheet
PRT	Platinum resistance thermometer
PS	Pressure support
RASS	Richmond agitation and sedation score
RBH	Royal Brompton Hospital
REC	Research Ethics Committee
RF	Radio frequency
RQ	Respiratory quotient
RSS	Residual sum of squares
RV	Residual volume
SBW	Single breath washout
SM	Single-mode
SNR	Signal-to-noise ratio
TEC	Thermoelectric cooler
TLC	Total lung capacity
TV	Tidal volume
UCSD	University of California, San Diego
VAS	Visual analogue scale
VCSEL	Vertical-cavity surface-emitting laser
VILI	Ventilator-induced lung injury

Contents

Abstract v

Acknowledgements vii

Abbreviations ix

List of Figures xvii

List of Tables xxi

1 Introduction 1

1.1 Respiratory Physiology . . . 3
1.2 Existing Techniques for Monitoring Oxygen Consumption . . . 7
1.3 Existing Techniques for Assessing Pulmonary Function . . . 10
1.3.1 Spirometry . . . 10
1.3.2 Forced Oscillation Technique . . . 12
1.3.3 Body Plethysmography . . . 12
1.3.4 Multiple Inert Gas Elimination Technique . . . 13
1.3.5 Hyperpolarized Gas MRI . . . 14
1.3.6 Multiple Breath Washout and the Lung Clearance Index . . . 15
1.4 Thesis Outline . . . 17

2 Molecular Flow Sensing for Clinical Use in Adults 21

2.1 Design of the Molecular Flow Sensor . . . 21
2.2 Temperature and Pressure Sensing . . . 24
2.3 Spectroscopic Measurements . . . 27
2.3.1 Spectroscopic Transitions . . . 27
2.3.2 Data Acquisition . . . 29
2.3.3 Determining Concentration . . . 37
2.3.4 Application of RF . . . 45

2.4 Flow Sensing 46
2.5 Validation of MFS Performance 51

3 Monitoring Oxygen Consumption Rates in Critical Care 53
3.1 Motivation for Study 54
3.2 Methods 57
3.3 Results 59
3.3.1 Patient A 59
3.3.2 Patient B 66
3.4 Discussion 73
3.5 Conclusions and Future Work 75

4 Application of Molecular Flow Sensor to Assess Lung Inhomogeneity in Adults 77
4.1 Assessing Lung Inhomogeneity with the Lognormal Lung Model . . . 78
4.1.1 Multi-breath Nitrogen Washout Protocol 79
4.1.2 Lognormal Lung Model 80
4.2 Validation of Lognormal Lung Model by Comparison with MIGET . . 88
4.2.1 Methods 90
4.2.1.1 MIGET 91
4.2.1.2 MFS Washout and LNL Model 92
4.2.2 Results 93
4.2.2.1 Spirometry 93
4.2.2.2 MIGET 94
4.2.2.3 Lognormal Lung 99
4.2.3 Discussion 104
4.2.4 Conclusion 110
4.3 Cross-sectional Study of Lung Inhomogeneity in Young Smokers . . . 111
4.3.1 Methods 112
4.3.1.1 Experimental Methods 112
4.3.1.2 Statistical Analysis 113
4.3.2 Results 115
4.3.3 Discussion 119
4.3.4 Conclusions and Future Work 121

5 Investigation of Lung Inhomogeneity in Adults with Cystic Fibrosis 123
5.1 Preliminary Study of the Utility of the Lognormal Lung Model in the CF Population . . . 125
5.1.1 Methods . . . 126
5.1.1.1 Patient Recruitment . . . 126
5.1.1.2 Experimental Protocol . . . 126
5.1.1.3 Statistical Analysis . . . 127
5.1.2 Results . . . 128
5.1.2.1 Comparison between CF Patients and Healthy Controls 128
5.1.2.2 Comparison with Severity of Bronchiectasis . . . 135
5.1.2.3 CF Patients with Preserved FEV_1 . . . 137
5.1.2.4 Assessing the Effect of Physiotherapy . . . 139
5.1.3 Discussion . . . 141
5.2 Comparison of Lognormal Lung Model and Lung Clearance Index . . 146
5.2.1 Methods . . . 147
5.2.1.1 Conventional Multiple Breath Washout Parameters . 148
5.2.1.2 Lognormal Lung Model Parameters . . . 149
5.2.1.3 Statistical Analysis . . . 149
5.2.2 Results . . . 150
5.2.2.1 MBW Volume Measurements . . . 152
5.2.2.2 Lung Inhomogeneity Parameters . . . 157
5.2.2.3 Severity of Bronchiectasis . . . 162
5.2.3 Discussion . . . 163
5.2.4 Conclusions and Future Work . . . 167

6 Development of a Paediatric Molecular Flow Sensor 169
6.1 Motivation . . . 170
6.2 Miniaturisation of the Molecular Flow Sensor . . . 172
6.3 Methane and Acetylene Trace Gas Detection . . . 178
6.4 Modelling Optical Paths of the Multipass Cell . . . 182
6.5 Sample Patient Data . . . 186
6.6 Conclusions and Future Work . . . 191

7 Conclusions and Future Work 195

Bibliography 200

List of Figures

1.1 Diagram of the lung . . . 3
1.2 Lung volumes . . . 5
1.3 Phases of expiration . . . 16

2.1 Components of a molecular flow sensor . . . 22
2.2 Molecular flow sensor measurement head schematics . . . 23
2.3 Thermocouple calibration data . . . 25
2.4 Barometric pressure sensor calibration . . . 26
2.5 Barometric pressure and temperature data during breathing . . . 26
2.6 Laser ramps schematic . . . 30
2.7 Characterisation of the lasers . . . 31
2.8 Control unit diagram . . . 32
2.9 Fibre etalon residuals . . . 33
2.10 V-path schematic . . . 34
2.11 V-path calibration . . . 35
2.12 Cavity schematic . . . 36
2.13 Gaussian, Lorentzian and Voigt profiles . . . 42
2.14 Experimental absorption spectra, with Voigt fits and residuals . . . 43
2.15 Measured gas composition over the breathing cycle . . . 44
2.16 Effect of applying RF . . . 45
2.17 Flow sensing schematic . . . 47
2.18 Flow calibration data . . . 48
2.19 Flow sensor zeroing period data . . . 50
2.20 Nitrogen washout dry gas fractions and integrated volume plot . . . 52

3.1 Relationship between $\dot{D}_{O_2}$ and $\dot{V}_{O_2}$ . . . 55
3.2 MFS set-up in ICU . . . 58
3.3 Patient A gas fractions . . . 60
3.4 Ten sample breaths . . . 62

3.5 Patient A cumulative volume plot 63
3.6 Patient A washout 64
3.7 Patient A respiratory quotient 66
3.8 Patient B gas fractions and gas exchange rates 68
3.9 Patient B gas exchange rates during drug administration 70
3.10 Patient B respiratory quotient 72

4.1 MFS set-up for MBW 79
4.2 Lognormal lung model 82
4.3 Sample LNL model fitted expirograms 86
4.4 Sample LNL model fitted cumulative volume plot 87
4.5 UCSD-Oxford research team 89
4.6 Unimodal MIGET distribution 96
4.7 Bimodal MIGET distributions 96
4.8 Intra-subject LogSD$\dot{V}$ and LogSD$\dot{Q}$ comparison 98
4.9 End-tidal peak expiratory N_2 fraction 99
4.10 Measured and modelled arterial O_2 content 102
4.11 Measured and modelled arterial CO_2 content 103
4.12 Fractional deadspace ventilation and percentage shunt comparison . . 106
4.13 Calculated Shunt Comparison 107
4.14 LogSD$\dot{V}$ and LogSD$\dot{Q}$ comparison 108
4.15 MIGET LogSD$\dot{V}$ and LogSD$\dot{Q}$ vs. lognormal fit 109
4.16 Correlations between LNL and MIGET parameters 110
4.17 Smoking and never-smoking LNL model parameters 116
4.18 Relationship between σ_{CL} and pack years 117
4.19 Variation between primary LNL parameters with pack years 118
4.20 Variation between secondary LNL parameters with pack years 119

5.1 Spirometry results for healthy controls and CF patients 129
5.2 LNL model parameters for healthy controls and CF patients 131
5.3 Relationship between age and LNL parameters σ_{CL} and V_D/FRC . . 133
5.4 Comparison between spirometry values and degree of bronchiectasis . 135
5.5 Comparison between LNL parameters and bronchiectasis severity . . 136
5.6 Spirometry and LNL parameters in CF patients with preserved FEV_1 and controls 139
5.7 Sputum expectorated, dicomfort level and spirometry values pre- and post-physiotherapy 140

5.8 Change in LNL model parameters in response to physiotherapy . . . 141
5.9 Sample CF patient CT scans . . . 144
5.10 LNL model parameters for CF patients and controls . . . 152
5.11 FRC comparison between healthy controls and CF patients . . . 153
5.12 FRC comparison between the Exhalyzer D and MFS . . . 155
5.13 Predicted blood N_2 contribution to FRC over washout time . . . 155
5.14 Predicted contribution from blood N_2 *vs.* difference in FRC . . . 156
5.15 LNL lung distribution parameters . . . 158
5.16 Exhalyzer D MBW parameters . . . 159
5.17 Comparison of σ_{CL} and V_D/FRC with the $LCI_{2.5}$ in CF patients . . . 161
5.18 LNL model parameters in patients with varying degrees of bronchiectasis 162
5.19 Exhalyzer D FRC measurements after cross-talk correction . . . 164

6.1 Adult and paediatric measurement cells . . . 172
6.2 Redesign of light traps . . . 174
6.3 Sample MFS-P O_2, CO_2 and H_2O spectra . . . 177
6.4 Optical paths in MFS-P . . . 180
6.5 Sample MFS-P CH_4 and C_2H_2 spectra . . . 181
6.6 Calculated spots sizes in multipass cell and comparison between modelled positions . . . 185
6.7 Herriott cell calculated spot positions and sizes . . . 186
6.8 Sample MFS-P washout dry gas fractions . . . 187
6.9 Sample MFS-P washout cumulative volume plots . . . 188

List of Tables

2.1 Spectroscopic transitions for O_2, CO_2 and H_2O 29
2.2 Broadening coefficients for O_2, CO_2 and H_2O 41
2.3 Flow parameters 48
2.4 Density and viscosity data 49

4.1 Lognormal lung model parameters 81
4.2 MIGET subjects 90
4.3 MIGET spirometry 94
4.4 MIGET deadspace and shunt 95
4.5 MIGET ventilation and perfusion parameters 97
4.6 MIGET study LNL parameters 100
4.7 Physical characteristics of smokers vs. healthy controls 114

5.1 Physical characteristics for CF JR study 129
5.2 Correlation coefficients between LNL paramters and physical characteristics 132
5.3 Correlation coefficients between LNL parameters and spirometry . . . 134
5.4 Physical characteristics of CF patients with preserved FEV_1 and controls 138
5.5 Physical characteristics for CF patients and controls at the RBH . . . 151
5.6 CF patients vs. healthy controls spirometry 151
5.7 Coefficients of variation for the lung volumes measured at the RBH . 154
5.8 Coefficients of variation the lung inhomogeneity parameters measured at the RBH 160
5.9 Pearson's r values comparing LNL and conventional MBW parameters 161

6.1 Spectroscopic transitions and broadening coefficients for CH_4 and C_2H_2 179
6.2 Density and viscosity data for CH_4 and C_2H_2 182
6.3 Sample MFS-P washout LNL model parameters 190

Chapter 1

Introduction

In the UK government's 2021 Life Sciences Vision policy paper, the need to reduce the levels of morbidity and mortality from respiratory diseases was stated as one of the seven Healthcare Missions identified as some of the biggest healthcare challenges and key priorities for the NHS.[1] Even prior to the COVID-19 pandemic, the increased contribution to pressure on the NHS was recognised as a growing issue - from 2010-2017 the number of hospital admissions as a result of respiratory disease increased by 27%, a rate 3 times that of all admissions generally.[2] The COVID-19 pandemic has further increased the morbidity and mortality due to respiratory disease, and resulted in a significantly higher healthcare burden.[3] Between the financial years 2016/17 and 2021/22, the total prescribing costs in hospitals and the community to treat respiratory disease increased by 41%.[4] In addition, as new and more expensive drugs are developed to target specific respiratory diseases, the development of new and more effective techniques for monitoring patients becomes more important to target treatments in a cost effective way.[3] New methods for non-invasive assessment of lung function, enabling earlier and potentially more effective intervention are highly desirable or even necessary.

Advances in the application of laser absorption spectroscopy to monitor human breath offer the potential to determine gas exchange at the mouth with unparalleled accuracy. The device described in this thesis, the molecular flow sensor (MFS), employs near-IR absorption spectroscopy to afford simultaneous, in-line measurements of concentration and flow of gas in a patient's airway, from which the rate of gas consumption or production can be directly calculated. This technology has the potential to address the need for early assessment of impaired lung function.

The potential clinical applications of this device fall into two broad categories: monitoring oxygen consumption, particularly in ventilated patients, and providing a more sensitive assessment of lung function using a multi-breath washout (MBW)

test. The first of these applications has the potential for significant improvements to patient management in intensive care. At present there is no adequate method to monitor oxygen consumption ($\dot{V}_{O_2}$) in real time at the elevated and variable inspired O_2 levels used to treat patients in this setting.[5] One potential future application of $\dot{V}_{O_2}$ monitoring is in the management of patients with sepsis, a condition which affects between 100,000 and 200,000 people in the UK annually and results in approximately 40,000 deaths each year.[6] Sepsis is the body's response to infection, and in its most severe form leads to septic shock, characterised by the body's inability to deliver sufficient oxygen to its tissues and hence results in decreased oxygen consumption. If it were possible to directly measure $\dot{V}_{O_2}$, critical care physicians could potentially better weigh up the potential benefits and risks of administering a given treatment. This could result in more tailored treatment, less unnecessary treatments and therefore a lower cost of care, fewer unnecessary side effects and improved patient outcomes. This is the basis of precision medicine. The first part of this thesis focuses on the design and calibration of a molecular flow sensor and its first application in measuring respiratory gas exchange in intensive care and physiological studies.

The second application of this technology lies in its potential to provide a more sensitive assessment of early lung disease in patients with respiratory diseases. Recent decades have seen great strides in the development of new drugs and treatments for respiratory diseases, yet further improvement hinges on both earlier identification of pulmonary abnormalities and a more sensitive tool for assessing the effects of a treatment on a patient's lung function. The work in this thesis will touch on two diseases: chronic obstructive pulmonary disease (COPD) and cystic fibrosis (CF). The treatment of COPD has benefited from the development of bronchoscopic procedures, inhaled corticosteroids and bronchodilators.[7] Meanwhile the estimated median survival age of people with CF in the UK has increased to > 50 years for those born post-2000,[8] with the development of new treatments, such as airway clearance techniques, inhaled antibiotics, lung transplants and DNAse.[9] With the recent paradigm shift in CF treatment due to the arrival of cystic fibrosis transmembrane conductance regulator (CFTR) modulators, which treat the cause of CF at the cellular level for the first time, patients can be expected to live far longer with far better lung function,[10] so it is crucial that suitable techniques exist to assess lung function and guide treatment in these patients. At present, the most ubiquitous technique is still spirometry, a cheap and easily performed assessment of gross lung function. However, it is a somewhat 'blunt tool', which only informs on the presence of disease once it is well established and fails to identify early stage degeneration of the small airways.[11]

Other techniques such as the lung clearance index and hyperpolarized MRI are more sensitive to disease in the small airways, but these techniques all suffer from disadvantages which have prevented their widespread adoption in clinical practice. The latter part and majority of this thesis focuses on the potential application of the molecular flow sensor in conjunction with a computational model of the lungs to obtain more sensitive parameters to describe a person's lung function.

This introductory chapter begins with an overview of the physiology of the respiratory system, before introducing the current clinical techniques for assessing oxygen consumption, including their limitations. This is followed by a critical appraisal of current methods to assess pulmonary function in patients with respiratory diseases. The chapter concludes with an overview of the work presented in this thesis.

1.1 Respiratory Physiology

The primary purpose of the respiratory system is gas exchange to provide the body with oxygen for cellular aerobic respiration and remove the waste product carbon dioxide. Secondary functions include olfaction, phonation, immunological protection, pH regulation and body temperature regulation. Figure 1.1 shows a diagram of the lungs, including a detailed schematic of gas exchange via a single alveolus.

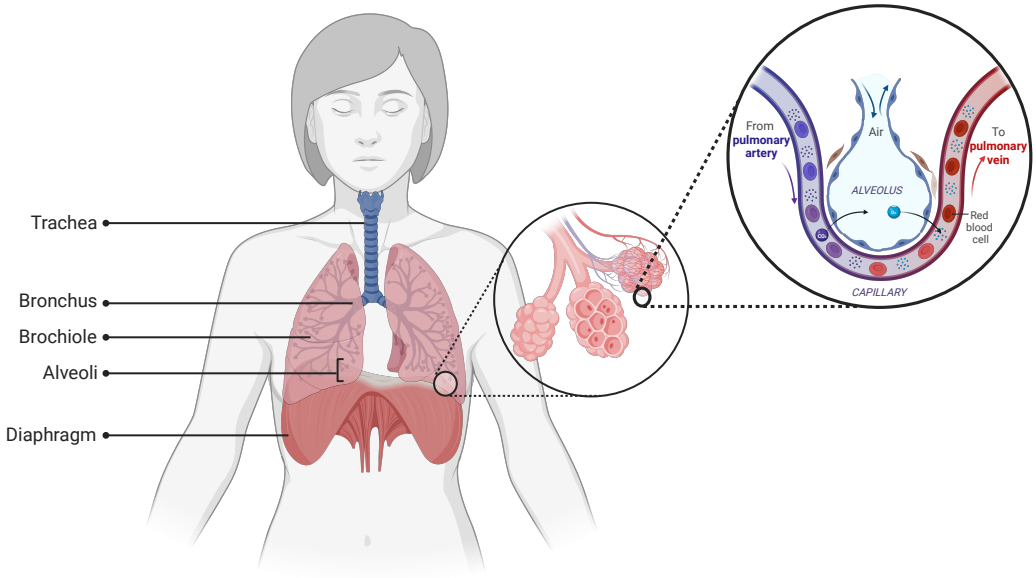


Figure 1.1: Diagram of the lung with a closer look at gas exchange by a single alveolus.[12]

Upon inspiration, the diaphragm contracts and flattens, while the external intercostal muscles contract to elevate the ribs and sternum. Between the inner surface of the thoracic cavity and the outer surface of the lungs lies the pleural space. Due to surface tension, the pleural fluid inside this space forms a seal between the surfaces, ensuring expansion of the lungs as the chest cavity volume increases. By Boyle's law, as the volume of the lungs increases, the pressure inside decreases. External atmospheric pressure then exceeds the internal pressure inside the lungs and gas moves into the lungs down the pressure gradient. Air enters through the oral or nasal cavity, then travels down the trachea, which splits into two bronchi at the fifth thoracic vertebra. The bronchi then branch into the smaller bronchioles, which terminate in tiny air sacs called alveoli.

The trachea, bronchi and bronchioles are all lined with a mucous membrane, which transitions from ciliated pseudostratified columnar epithelium to simple cuboidal and then to simple squamous epithelium on descending the pulmonary airways.[13] In healthy people, goblet cells in the ciliated pseudostratified columnar epithelium of the trachea produce mucus that traps airborne particles and microorganisms. Cilia then move the mucus upwards where it can be swallowed or expelled, defending the lungs from irritation and infection. In people with cystic fibrosis (CF), normal mucus production is compromised, leading to frequent infections and lung damage.

The alveoli are the final destination of the inspired air. The alveolar ducts and alveoli are lined with simple squamous epithelium, which facilitates the diffusion of O_2 into the capillaries that supply the lungs with blood and the diffusion of CO_2 out of the bloodstream. Oxygen diffuses across the alveolar membrane and binds reversibly to the haemoglobin in red blood cells. This is delivered to the body cells to be used in respiration. The waste product of respiration, CO_2, then dissolves into the blood directly and is transported back to the alveolar capillaries, where it diffuses across the alveolar membrane to then be expelled from the body upon exhalation.

During passive exhalation, the diaphragm relaxes to return to its resting position and the external intercostal muscles relax, depressing the ribs and sternum. This decreases the volume of the thoracic cavity and hence the lungs, thereby increasing the pressure relative to external atmospheric pressure so air is expelled. If the exhalation is forced, as it is during spirometry measurements, the internal and innermost intercostal muscles will contract to further depress the ribs and increase the volume of air that is removed from the lungs.

The volume of gas contained within the lungs over the course of the respiratory cycle is described according to Figure 1.2. Measuring some of these values forms the

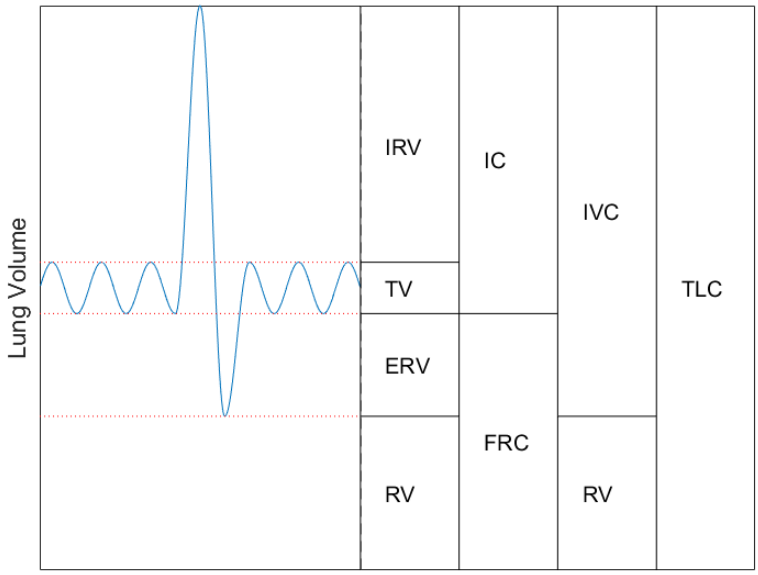


Figure 1.2: The definitions of the volumes and capacities used to describe the lung. On the left is a volume-time spirogram showing normal tidal breathing, followed by a larger inhalation to fill the lungs with the maximum volume of gas. The maximum possible amount of gas is then exhaled before returning to normal tidal breathing. The four standard volumes indicated on the right of the spirogram comprise the total volume of air resident in the lungs over the course of the respiratory cycle: tidal volume (TV), the inspiratory reserve volume (IRV), the expiratory reserve volume (ERV) and the residual volume (RV). The standard lung capacities are indicated to the right of the volumes: the inspiratory capacity (IC), the functional residual capacity (FRC), the inspiratory vital capacity (IVC) and the total lung capacity (TLC).

basis of many of the pulmonary function tests described in Section 1.3. Tidal volume (TV) is the volume of gas that is inspired and expired during a normal breath, which varies according to a person's breathing pattern and increases on exercise. The inspiratory reserve volume (IRV) is the additional volume of gas which can be inspired after a normal inhalation during tidal breathing and depends on factors such as muscle strength and lung compliance (the ability of the lung to expand). Similarly, the expiratory reserve volume (ERV) is the additional volume of gas that it is possible to expire beyond that of normal tidal breathing and relies on muscle strength and airway resistance. The residual volume (RV) is the volume of gas that remains in the lungs following maximal exhalation. This volume is increased in patients with obstructive lung disease, such as emphysema, due to bronchial spasm, airway inflammation and

loss of elastic recoil in the lungs. The total lung capacity (TLC) is the total volume of gas in the lungs following maximum inspiration. A person's TLC is considered to be within a normal range if it is between 80 % and 120 % of the predicted value based on an individual's height, age and sex.[14] A TLC greater than 120 % indicates hyperinflation due to obstructive lung disease,[15] while a TLC below 80 % indicates restrictive lung disease, with increasing disease severity at lower TLC values.[16] The RV/TLC ratio is also of clinical interest to track changes in the lung due to restrictive or obstructive lung disease and has been shown to have significant prognostic value in monitoring patients with chronic obstructive pulmonary disease (COPD).[17] Inspiratory capacity (IC) is defined as the amount of gas that can be inhaled following normal exhalation. The functional residual capacity (FRC) is the volume of gas that remains in the lungs following normal exhalation. The maximal volume of gas that can be inspired is the inspiratory vital capacity (IVC).

The volume of the lung that is ventilated, but does not participate in gas exchange, is referred to as deadspace and is classified as either anatomical or alveolar deadspace. The former refers to the volume of the lung which comprises the conducting zone, the nose, trachea and bronchi, and is estimated at 2 ml kg^{-1} of body weight in adults (approximately 1/3 of the TV).[18] If a patient is ventilated, the ventilator equipment will effectively increase the anatomical deadspace.[18] Alveolar deadspace refers to the volume of the respiratory zone of the lung which does not participate in gas exchange. In healthy adults this volume is negligible, but may be elevated in patients with respiratory diseases.[19] For example, alveolar tissue is destroyed in patients suffering from emphysema, so the surface area available for diffusion is reduced and deadspace volume increases.[20]

The pulmonary system works in tandem with the cardiovascular system; therefore efficient gas exchange at the alveoli is dependent on sufficient blood supply as well as good ventilation. The volume of gas inhaled and exhaled from the lungs over a given time period is known as the ventilation rate, $\dot{V}$, calculated by multiplying the TV by the respiratory rate (normally given in breaths per minute). The perfusion rate, $\dot{Q}$, refers to the total volume of blood reaching the lungs per unit time. Both $\dot{V}$ and $\dot{Q}$ are usually given in L/min. The ratio between these quantities, the $\dot{V}/\dot{Q}$ ratio, is used to assess the efficiency of the pulmonary system. In a perfectly efficient lung, the rates of ventilation and perfusion would be equal, resulting in a $\dot{V}/\dot{Q}$ ratio of 1. In regions of deadspace within the lung which are ventilated but not perfused, the $\dot{V}/\dot{Q}$ ratio equals infinity, while a $\dot{V}/\dot{Q}$ of zero would indicate an unventilated region of the lung, a condition known as a pulmonary shunt.[21]

1.2 Existing Techniques for Monitoring Oxygen Consumption

The ability to accurately measure the rate of oxygen consumption is of great interest in several clinical settings: patient monitoring in critical care, lung function testing in respiratory clinics and cardiopulmonary exercise testing. Its use in single and multi-breath washout tests in lung function testing will be discussed in the next section of this chapter, while this section will focus primarily on measuring oxygen consumption in critical care.

Impaired oxygen delivery and utilisation is common in patients with a critical illness, and successful resuscitation, reversal of shock, and prevention of organ failure are all goals of an intensive care physician.[22] Real-time monitoring of a patient's ability to use oxygen and eliminate carbon dioxide is informative, and early intervention to increase the delivery of oxygen ($\dot{D}_{O_2}$) to optimise oxygen consumption ($\dot{V}_{O_2}$) may result in improved clinical outcomes.[23–25] $\dot{V}_{O_2}$ and $\dot{D}_{O_2}$ are also considered superior to conventional parameters as resuscitation endpoints, and failure to increase $\dot{V}_{O_2}$ upon resuscitation may predict a poor outcome.[26]

Accurate assessment of metabolic rate is also of great interest for tailoring a patient's feeding to their individual requirements in intensive care.[27] At present, predictive equations are employed to determine a patient's caloric requirements,[28] but these have been shown to deviate from direct measurements of metabolic activity.[29,30] The ICU population is largely heterogeneous and additional confounding factors such as their comorbidities, degree of consciousness and individual treatments, make basic demographic information such as age, height, weight and gender insufficient to obtain a satisfactory estimate.[30] As both under-feeding and over-feeding are associated with adverse effects,[31–34] an improved estimation of metabolic energy requirements to allow optimal nutrition is desirable.[35,36]

One way of measuring oxygen consumption uses the 'reverse Fick' method. The Fick equation uses the fractional arterial oxygen content, C_{a,O_2}, the fractional venous oxygen content, C_{v,O_2}, and the cardiac output, $\dot{Q}$, to calculate the rate of oxygen uptake, $\dot{V}_{O_2}$:

$$\dot{V}_{O_2} = \dot{Q}(C_{a,O_2} - C_{v,O_2}) \tag{1.1}$$

However, this method requires the use of a pulmonary artery catheter (PAC) to measure pulmonary blood flow via thermodilution and hence determine cardiac output. While the use of PACs as a diagnostic tool in intensive care is common,[37] the

invasive nature of the procedure means the effectiveness of routine use is disputed,[38,39] based on multinational trials investigating patient management across a range of conditions treated in intensive care.[40–47] The PAC is also unlikely to remain in place for the duration of recovery from illness due to risk of infection and complications, so is not a suitable tool for long term monitoring.[36] When using the PAC readings to compare $\dot{D}_{O_2}$ with $\dot{V}_{O_2}$, the use of the arterial oxygen content and cardiac output to measure both $\dot{D}_{O_2}$ with $\dot{V}_{O_2}$ also introduces mathematical coupling errors, which may introduce an erroneous positive correlation between $\dot{D}_{O_2}$ and $\dot{V}_{O_2}$ in response to interventions.[22] The use of PACs is also not appropriate outside of the critical care setting, so would not be suitable for monitoring oxygen consumption in respiratory clinics.

Monitoring respiratory gas exchange directly at the mouth removes the requirement for invasive procedures. The rate of oxygen consumption is determined from the difference between the volume of oxygen inspired and the volume of oxygen expired per unit time, which is calculated from the inspiratory and expiratory flow rates, $\dot{V}_I$ and $\dot{V}_E$, and oxygen fractions, F_{I,O_2} and F_{E,O_2}:

$$\dot{V}_{O_2} = \dot{V}_I \; F_{I,O_2} - \dot{V}_E \; F_{E,O_2} \tag{1.2}$$

Collection of exhaled air for subsequent analysis has been performed since the 19th century.[48] In the early 20th century, the innovation of impermeable bags to collect expiratory samples via a mask or mouthpiece was used to improve these measurements in exercising or bed-ridden subjects.[49] This intermittent sampling has continued to be used as a reference to validate modern technology. A natural progression of this method involves taking automated intermittent samples from expired gas using either a mixing chamber or breath by breath sampling procedure.[50] Analysis of the samples of mixed expired air then relies on the Haldane transformation to obtain the oxygen consumption. This equation assumes that there is zero nitrogen exchange by the body (i.e. $\dot{V}_I F_{I,N_2} = \dot{V}_E F_{E,N_2}$). Therefore the oxygen consumption can be calculated without measuring the inspiratory flow rate, according to:

$$\dot{V}_{O_2} = \frac{\dot{V}_E F_{E,N_2}}{F_{I,N_2}} \; F_{I,O_2} - \dot{V}_E \; F_{E,O_2} \tag{1.3}$$

By considering the gas to consist solely of O_2, CO_2 and N_2, and assuming that the inspired fractions, F_{I,O_2} and F_{I,CO_2} are known, $\dot{V}_{O_2}$ may be calculated from just the expired fractions of O_2 and CO_2 and the expiratory flow, $\dot{V}_E$:

$$\dot{V}_{O_2} = \frac{\dot{V}_E(1-(F_{E,O_2}+F_{E,CO_2}))}{(1-(F_{I,O_2}+F_{I,CO_2}))}\ F_{I,O_2} - \dot{V}_I\ F_{I,O_2} \tag{1.4}$$

However, this result is only valid for a constant, known inspired fraction of O_2. This assumption does not hold for intubated patients in critical care, who may receive elevated partial pressures of oxygen for prolonged periods to improve oxygen delivery or a higher F_{I,O_2} may be required in short bursts to prevent desaturation during airway management procedures. There is also a preference for moving away from the reliance on the Haldane transformation in cardiopulmonary exercise testing.[51]

Alternatively, monitoring both inspiratory and expiratory flow removes the requirement for the Haldane transformation. However, due to the sidestream design of most analysers, additional sources of error are introduced, including the increased instrument deadspace and the requirement to time-align the sampled oxygen and carbon dioxide concentrations with the measured flow.[52] There are numerous techniques for measuring the concentrations of gases necessary to determine oxygen consumption for both blood gas measurements and inspiratory/expiratory gas. Blood gas analysis is largely performed using electrochemical sensors,[53] while for airway monitoring a variety of techniques are employed for measurements in the gas phase, including paramagnetic sensing, mass spectrometry and IR spectroscopy. The most common technique for measuring oxygen concentration in inhaled and exhaled gas in an operating theatre relies on a paramagnetic cell.[54] This is based on the large paramagnetic susceptibility of oxygen gas compared to other gases present in breath and used in anaesthesia. The notable exception to this is nitric oxide, which is also strongly paramagnetic, but far less abundant.[55]

Mass spectrometry is capable of determining gas concentrations with a high degree of accuracy. If mass spectrometry is used, oxygen concentration in samples can be measured alongside an exogenous tracer gas such as argon, which can be added to inspired air, allowing calculation of $\dot{V}_{O_2}$ from the difference between O_2 and Ar concentrations in inspired vs expired gas.[56–58] However, mass spectrometers rely on powerful vacuum pumps, are expensive to purchase and maintain, and are unsuitable for in-line measurements.[59]

The most widely used method to determine CO_2 concentration in breath is infrared absorption spectroscopy, which uses a broadband source to excite multiple transitions,[54] as opposed to the molecular flow sensor which employs a laser to selectively probe a single transition. Nondispersive infrared spectroscopy is a suitable

technique for both sidestream and in-line measurements due to its compact components, and also benefits from its cheap cost to buy and maintain. However, it does require that all water vapour be removed before the gas reaches the measurement plane.[54]

Despite progress in monitoring technology, current techniques still do not show an acceptable level of agreement between methods for measuring $\dot{V}_{O_2}$ in critical care,[36] and there is a recognised need for improved equipment for measuring gas exchange in single and multiple breath washout experiments in lung function testing.[60] The molecular flow sensor (MFS) described in this thesis overcomes some of the limitations of previous techniques. Inspiratory and expiratory flow are measured so the Haldane equation is not required. Measurements are taken in-line in the main airway, so there is no sampling procedure, and concentration and flow rate is measured at the same point, so there is no error introduced from aligning the signals.

1.3 Existing Techniques for Assessing Pulmonary Function

Methods for assessing respiratory health are of vital importance to clinicians. They are used to identify damaged lungs, monitor patients as they receive treatment and assess the effectiveness of new interventions in clinical trials. A more sensitive technique can improve disease management and hence quality of life. In clinical trials, greater sensitivity reduces the number of participants required to produce statistically significant results, thereby reducing the substantial cost of testing new drug regimens.

Spirometry and body plethysmography are well established techniques which provide a global assessment of the lungs. A brief overview of these techniques is provided in this section. However, in the early stages of respiratory disease, the function of sections of the lungs may decline more rapidly than the lungs as a whole, leading to increased lung inhomogeneity.[61] There is therefore great interest in techniques able to assess this. The multiple inert gas elimination technique (MIGET), the lung clearance index (LCI) and hyperpolarised gas MRI are all existing techniques used to evaluate lung inhomogeneity and are described along with their relative strengths and limitations in this section.

1.3.1 Spirometry

Spirometry is the most commonly used technique in the diagnosis and monitoring of respiratory disease. A patient is asked to inhale as deeply as possible then exhale into

a spirometer as hard as possible while wearing a nose clip. Successful interpretation of spirometry readings relies on a subject being able to perform the manoeuvre within acceptable limits. This requires an instantaneous start to the exhalation with a rapid increase in flow rate to reach peak flow, followed by a smooth and continuous decrease in flow until the lung volume equals RV.[62]

The most important parameters obtained from spirometry are the Forced Vital Capacity (FVC) and the Forced Expiratory Volume in the first second of exhalation (FEV_1). FVC is defined as the maximal volume of air exhaled with maximum forced effort from a maximal inspiration, while the FEV_1 is the volume of air exhaled during the first second of this manoeuvre, both expressed in litres at body temperature and ambient pressure saturated with water vapour (BTPS). Patients are required to carry out at least three spirometry manoeuvres, the best two of which must fulfil the criteria for reproducibility: within 150 ml or 5% of each other, whichever is greater.[63] These values are highly dependent on factors such as age, sex, height and race, and so FEV_1 and FVC values are reported as a percentage of the predicted value for a patient based on established normal values.[64–68] A value of 80-120% of the predicted FEV_1 is within the normal healthy range, while below 80% indicates disease.[69] For patients with Chronic Obstructive Pulmonary Disease, FEV_1 (% predicted) is used to classify the stage of the disease according to the GOLD (Global Initiative for Obstructive Lung Disease) staging system: Stage 1 at 80% or above is mild COPD, Stage 2 is moderate at 50-80%, Stage 3 is severe between 30-50% and below 30% indicates very severe COPD at Stage 4.[70] FEV_1 may be reduced in both obstructive and restrictive lung disease, but FVC is reduced to a greater degree in restrictive lung disease, due to poor lung expansion.[71] Consequently the FEV_1/FVC ratio is used clinically to distinguish obstructive lung disease specifically where the FEV_1/FVC ratio falls below 0.7.[72]

The advantages of spirometry as a diagnostic tool are principally its low cost, simplicity to perform and well-established range of normal values. However, the technique does have several limitations. Spirometry only assesses function across the lungs as a whole, so is relatively insensitive to the early stages of airways disease when damage is generally more localised. The test can be challenging to perform for those with severe disease, due to the forced nature of the breathing pattern required. Due to the strict protocol for carrying out the tests, patient comprehension and compliance is necessary, restricting its use in young children and other patients who lack capacity.

1.3.2 Forced Oscillation Technique

The Forced Oscillation Technique (FOT) provides a measurement of the impedance of the respiratory system. An oscillating frequency is applied to the airway opening by an external pressure generator during tidal breathing. The amplitude of the oscillation is small enough that it causes a reaction by the respiratory system without perturbing its behaviour. The measured changes in pressure and flow in response to the applied pressure oscillations undergo analysis to calculate the respiratory system impedance, Z_{rs}. This term encapsulates the impedance of the airways, lungs and chest wall and can be split further into respiratory system resistance (R_{rs}) and reactance (X_{rs}).[73] R_{rs} reflects both airway and tissue resistance, while X_{rs} accounts for the elastance of the pulmonary and chest wall tissues, as well as the inertance of the large airways. The test is repeated three to five times and the mean values are calculated.[74]

As only passive cooperation is required and the test itself can be completed in as little as 20 seconds, it is of particular interest in the management of paediatric lung disease.[75] Parameters obtained from oscillometry have been shown to correlate with other markers of inflammation in pre-school children with CF.[76] However, there is still a lack of standardisation in the application of this technique and a range of different reference values have been reported depending on the equipment and protocol used. For example, reported values are higher when a facemask is used instead of a mouthpiece.[77] With significant variability between healthy children, it has been proposed that the FOT may be better suited to detecting changes in one individual following intervention than assessing the presence and severity of disease.[78]

1.3.3 Body Plethysmography

Body plethysmography offers several important measurements which spirometry is unable to provide, allowing assessment of functional residual capacity (FRC) and specific airway resistance (sR_{aw}) as the primary parameters of interest. Total lung capacity (TLC) and residual volume (RV) can also be calculated.[79]

This technique uses the principle of Boyle's law which equates the pressure and volume of a gas under two sets of isothermal conditions according to $P_1V_1 = P_2V_2$. The patient is connected to a pneumotachograph while sitting inside a sealed cubicle fitted with a pressure transducer, enabling simultaneous measurements of pressure inside the cubicle and at the mouth. As the patient inhales, a pressure gradient between the airways and outside the body is induced, so the volume of the lungs increases. The thoracic cavity volume increase is equivalent to that of the lungs due

to the incompressibility of the other internal organs. There is a slight delay in air flow due to the resistance of the airways, delaying the equilibration of pressure. While air is flowing into the lungs, the increase in lung volume exceeds the volume of air delivered to the lungs, known as the shift volume. An equal but opposite shift volume is induced in the free volume of the box (estimated from a patient's weight), so the pressure change measured inside the box can be used to determine the shift volume of the lungs.[80] Volume and pressure measurements recorded during a breathing pattern similar to that shown in Figure 1.2 enables the determination of the lung capacities and volumes indicated on the diagram, such as TLC, RV and FRC. Tracking these values, as well as the RV/TLC ratio can inform clinicians about disease progression, as noted in the previous section. Specific airway resistance (sR_{aw}) is the ratio of shift volume to flow rate and can provide clinicians with information on the type of airway obstruction.[80]

While spirometry involves forced manoeuvres, body plethysmography measurements are made during breathing at rest, although the two techniques can be combined for a more complete evaluation of lung mechanics.[81] The absence of forced manoeuvres makes this technique less demanding for patients, but it is more time consuming than spirometry, as well as relying on larger equipment which is less portable.

1.3.4 Multiple Inert Gas Elimination Technique

The Multiple Inert Gas Elimination Technique (MIGET) is considered the gold standard to assess ventilation and perfusion distributions in the lungs and hence evaluate the degree of inhomogeneity of the ventilation-perfusion matching across the lung.[82] In normal lungs, the distribution follows a relatively narrow unimodal distribution, which broadens with ageing. In patients with severe obstructive lung disease such as COPD and asthma, a multimodal distribution is common, reflecting the increase in lung inhomogeneity in diseased lungs.[83]

To conduct the test, a saline solution containing six inert gases with differing solubility profiles is first delivered to the patient intravenously over a 20 minute period to reach a steady state. Arterial and venous blood samples and expired gas samples are then taken. Inert gas concentrations in the samples are measured using gas chromatography (electron capture detector in the case of SF_6 and flame ionisation detector for the other five gases).[84] Expired gas is analysed directly, whereas the inert gases in blood samples require prior extraction by equilibration with N_2 gas. The ratio of expired to venous concentrations of the six gases reflects the ventilation, while the ratio of arterial to venous partial pressures informs on the perfusion of different regions

of the lung. The principle of conservation of mass during gas exchange between alveoli and blood is then used to relate the alveolar and capillary pressures of these gases to the ventilation perfusion ratio. Each of the six gases used has a different solubility and hence sensitivity to a specific range of ventilation perfusion ratios. The data are fitted to a 50 compartment lung model, which considers each compartment to have a different ventilation perfusion ratio, to estimate the distribution of the ventilation perfusion ratio across the lungs.[85] The distributions derived from MIGET have been shown to identify lung abnormalities earlier than spirometry in COPD patients.[86]

The primary limitation of MIGET is its operational complexity. As both a venous and an arterial line are required, it is a demanding and invasive test for a patient. It requires a high degree of specialist operator training and considerable time to perform the test and analyse the samples, leading to a delay in obtaining results. Despite its significant use as a research tool, these practical considerations mean it has never evolved into a tool for clinical management.

1.3.5 Hyperpolarized Gas MRI

Hyperpolarized MRI offers an alternative method for assessing ventilation inhomogeneity. Using conventional ^{1}H MRI to image the lungs is challenging, due to its low abundance in the lungs compared to surrounding structures, a long relaxation time and the inhomogeneous magnetic environment in the lungs.[87] Therefore exogenous trace gases (^{3}He or ^{129}Xe) are used to image the airways and airspaces as opposed to imaging the lung tissue. To overcome the problem of low trace gas concentration leading to low signal intensity, hyperpolarization is utilised to increase the magnetisation by approximately 5 orders of magnitude.[87]

To perform the test, a patient must inhale a single breath of the hyperpolarized gas mixture while an MRI scan is taken. In well-ventilated parts of the lung, a high signal intensity is seen, while regions of low signal indicate ventilation defects. This technique has been shown to be sensitive to changes in the lung in COPD, CF and asthma.[87]

^{3}He has traditionally been the preferred gas for hyperpolarized MRI, due to its greater gyromagnetic ratio and hence superior image quality, as well as its lack of physiological side effects, such as the anaesthetising behaviour of ^{129}Xe at high concentrations.[88]. However, ^{3}He is produced as a by-product of manufacturing nuclear warheads, so supplies are limited and much of the current supply is reserved for border security scanners.[89] The subsequent increase in cost of ^{3}He has therefore led to renewed interest in using ^{129}Xe;[87] with improved polarisation techniques a higher

image quality is possible at lower ^{129}Xe concentrations.[90] The safety of ^{129}Xe is well established[91] and has a long history of use as a contrast agent in CT imaging.[92]

Hyperpolarized MRI benefits from its non-invasive nature and lack of ionising radiation. However, the production of hyperpolarized gas is still an expensive process and the half-life of hyperpolarized ^{129}Xe is only 1 hour,[87] so production and administration to the patient must be carefully controlled. The expense of the equipment and gases used has prevented this technique from achieving widespread clinical use.

1.3.6 Multiple Breath Washout and the Lung Clearance Index

Nitrogen elimination rate was identified as a quantitative measure for the effectiveness of ventilation more than 70 years ago, with mass spectrometry used for gas analysis.[93] This principle has been applied in both single breath and multiple breath inert gas washout tests (SBW and MBW respectively). As the names indicate, SBW assesses the gas mixing in the lungs in a single breath, while MBW quantifies the efficiency of inert gas clearance from the lungs. Inert gases used can be endogenous, such as N_2 and Ar, or exogenous, such as He, SF_6, and CH_4. These gases are selected for their low solubility in blood, which means they do not participate significantly in gas exchange and they are safe to inhale at the concentrations used in these tests.[60].

Single breath washout (SBW) tests are most commonly performed using N_2. The subject is asked to perform a vital capacity manoeuvre, where they exhale to the residual volume (RV) point, then inhale 100% O_2 to total lung capacity (TLC) then exhale to RV again. The expirogram from this final exhalation is analysed to determine the phase III slope (S_{III}), as shown in Figure 1.3. If an exogenous gas is used instead of N_2, the inert gas is washed in during the inhalation period from RV to TLC before being washed out during exhalation from TLC to RV. A modification of this protocol involves beginning the washout from FRC instead of RV, as this provides a better assessment of inhomogeneity during tidal breathing and inhomogeneity of the peripheral airways.[94]

The SBW test benefits from its shorter duration, but the MBW is preferred due to its superior sensitivity.[95] To perform a nitrogen washout, the subject is switched from breathing air to pure oxygen and the expired nitrogen is measured. Alternatively, an exogenous tracer gas such as SF_6 can be used but the subject must first undergo a washin procedure.[96] The MBW test has seen renewed interest as a technique in recent years due to advances in gas sensing technology, in particular as a technique for monitoring paediatric CF patients.[97]

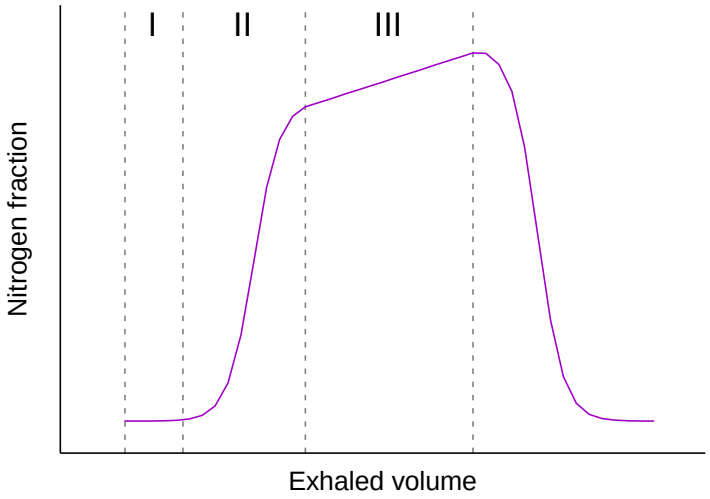


Figure 1.3: Diagram of the three phases of expiration: phase I where the exhaled gas is solely from the conducting airways, phase II where the gas is mixed from the conducting airways and alveoli and phase III when the gas is solely from clearing the alveoli.

The most commonly reported index from the MBW test is the lung clearance index (LCI), which provides a global assessment of inhomogeneity across the whole lung. For a nitrogen MBW, the LCI is defined as the number of lung turnovers (total litres of ventilation/FRC) required to reduce the alveolar nitrogen concentration to 1/40th of its initial concentration. When the concentration is at 1/40th of the initial concentration, FRC is calculated as follows:

$$\text{FRC} = \frac{V_{N_2}}{F_{N_2,initial} - F_{N_2,final}} \tag{1.5}$$

where V_{N_2} is the cumulative exhaled N_2 volume and $F_{N_2,initial}$ and $F_{N_2,final}$ are the initial and final nitrogen fractions respectively. The LCI can then be calculated according to:

$$\text{LCI} = \frac{V_{N_2}}{\text{FRC}} \tag{1.6}$$

The LCI is of particular interest in monitoring cystic fibrosis disease progression and post-lung transplant recipients.[98–100] Vermeulen *et al.* showed that the LCI can be used to predict pulmonary exacerbations in patients with CF aged 5-19, even when there was no change in FEV_1.[101] The technique only requires tidal breathing instead of forced manoeuvres, making it an attractive technique to use in children.

LCI values have also been shown to be semi-independent of lung growth,[102] and the effect of ageing on the index is small.[103]

Two other indices can be derived from an MBW test: S_{cond} and S_{acin}, which quantify ventilation inhomogeneity in the conductive and acinar zones of the lung respectively.[104–106] Each breath of the washout is analysed in a similar way to the SBW test and it is found that the gradient of the phase III slope increases over the course of an MBW. Plotting the phase III slopes for the MBW against lung turnover can differentiate between normal lungs and obstructive lung disease, as the gradient of this plot, S_{cond} increases with increased airway obstruction. S_{acin} is effectively equal to the intercept of the phase III slope plotted against lung turnover. These indices have been shown to be sensitive to inflammation,[107] airways hyper-responsiveness[108] and exacerbations[109] in asthma patients, as well as changing in response to various treatments.[110–113]

The absence of forced manoeuvres makes the MBW test suitable in children and patients where spirometry is contraindicated, however the need to maintain a consistent tidal volume can be challenging. Widespread application of the technique is also limited by the lack of standardisation of the equipment, experimental protocol and subsequent analysis. For example, values calculated from an N_2 washout differ from those obtained from an SF_6 washin.[114] Due to variation in end-expiratory volume and tidal volume, tests must be performed 3 times for each patient and LCI values within 10% of each other are accepted.[96]

1.4 Thesis Outline

The work detailed in this thesis is centred around the molecular flow sensor (MFS), a device which affords non-invasive, real time, in-line measurement of gas exchange rates through simultaneous measurement of gas concentrations and flow rate. Accurate real-time assessment of oxygen consumption offers great potential in improving the monitoring of intubated patients in intensive care. Data from the device can also be analysed using a computational model of the lung, the Lognormal Lung model (LNL), which shows promise as a sensitive technique for assessing lung inhomogeneity and identifying dysfunction in its early stages.

The next chapter of the thesis introduces the molecular flow sensor (MFS). The MFS employs laser absorption spectroscopy to measure the concentration of O_2, CO_2 and H_2O in human breath every 10 ms. In conjunction with simultaneous flow measurements from a custom Lilly-type pneumotachograph embedded within the mea-

surement head, this provides highly accurate measurements of gas exchange rates. The design of the MFS is explained in Chapter 2, along with details of further development of the device, including the use of a different absorption line to measure the water concentration and the application of radio frequency (RF) modulation to improve the signal to noise ratio. Details of the calibration procedures are outlined and sample data of a subject breathing through the device are shown.

In Chapter 3 the application of the MFS in ICU is addressed. The first study of intubated patients in the adult intensive care unit using the MFS is described, investigating their baseline oxygen consumption rate and response to standard interventions. The patients recruited for this study were ventilated with passive humidification to protect the airways, i.e. a heat and moisture exchanger was used between the patient and the MFS, which reduces the humidity inside the MFS. The scope of this study was drastically reduced due to the occurrence of the COVID-19 pandemic and subsequent implementation of COVID-19 restrictions after the recruitment of the first two patients, but does present the successful use of the device in this setting for the first time.

Chapter 4 begins with a brief introduction to the Lognormal Lung (LNL) model, a novel tool to analyse a nitrogen washout to return parameters which assess the degree of inhomogeneity in the lungs. As reported by Mountain *et al.*, the ability of the model to return parameters is only possible due to the accuracy and precision of the in-line measurements from the MFS.[115] The chapter details two small studies, the first of which is a validation study of the LNL model, comparing measurements obtained from MIGET with the standard deviation of the ventilation and perfusion distributions obtained from the LNL model in patients with chronic obstructive pulmonary disease (COPD). The second study investigates the potential of the LNL model parameters to detect early stage lung damage, by comparing parameters obtained for young smokers and non-smokers. In particular it demonstrates superior sensitivity compared to FEV_1 and is able to discriminate between never smokers and current smokers at a lower cumulative smoking history than existing techniques.

Investigating the potential of the technique in the assessment of lung inhomogeneity in adults with cystic fibrosis (CF) is the focus of Chapter 5. The chapter begins with a small pilot study at the John Radcliffe Hospital in Oxford, which includes a comparison of the LNL parameters from a series of CF patients with preserved FEV_1 ($FEV_1 > 70\%$) with a control group. In patients where a CT scan was available, the severity of bronchiectasis in CF patients is compared with their LNL parameters.

Several patients were also studied before and after a physiotherapy session to investigate any change in the LNL parameters in response to treatment. The latter part of the chapter presents a study at the Royal Brompton Hospital in London, where a second, larger cohort of CF patients with preserved FEV_1 was recruited alongside a healthy control group. Both groups performed spirometry, standard LCI tests, and an MBW using the MFS with subsequent analysis by the LNL model to allow comparison of these techniques. In both studies, lung inhomogeneity determined by the LNL model was able to discriminate between CF patients and healthy controls with greater sensitivity than FEV_1, and the comparison between the LNL model parameters and the LCI implies that an elevated LCI is only partially, but not primarily, driven by increased inhomogeneity in patients with preserved FEV_1.

Chapter 6 extends the potential application of the molecular flow sensing technology in the management of CF, with the development of a novel paediatric molecular flow sensor (MFS-P). This work aims to improve the assessment of early stage lung abnormalities in children with CF, so that routine monitoring can better direct treatment plans. In order to be suitable for paediatric use, a smaller instrument deadspace was required, as well as a shorter test to allow for the shorter attention span of young children. The miniaturisation process is detailed and a sample dataset is presented to illustrate the successful design and potential utility in the paediatric population. An additional optical path was included in the design of MFS-P to allow methane trace gas measurements. This has the potential for a shortened washin procedure as an alternative to longer LCI washouts used in current clinical practice.

To conclude the thesis, the findings of the different clinical studies are summarised and potential areas for future work are identified and discussed in Chapter 7.

Chapter 2

Molecular Flow Sensing for Clinical Use in Adults

Prior to the body of work detailed in this thesis, a molecular flow sensor (MFS) had been designed and used to monitor the oxygen consumption rate of adult patients under anaesthesia by Ciaffoni *et al.*.[5] This device records spectroscopic and flow data every 10 ms, allowing accurate, in-line, real-time measurement of O_2, CO_2 and H_2O concentrations and flow rate in a patient's main airway and hence accurate determination of a patient's O_2, CO_2 and H_2O consumption or production rates. For the work contained in this thesis, two more molecular flow sensors were built and calibrated. Multiple devices were required so that different devices could be used in studies in separate clinical locations. The first application of the MFS in monitoring patients in critical care is outlined in Chapter 3, while its use in assessing lung inhomogeneity is detailed in Chapters 4 and 5. This chapter outlines the design and calibration of an MFS device, as well as further technical developments to the design.

2.1 Design of the Molecular Flow Sensor

Designing an instrument for clinical use presents a variety of challenges. The device must be a portable self-contained unit and robust enough to be transported between rooms in a clinical setting. It is important that the device can easily be connected to a patient using standard connector interfaces used in hospital equipment. Any calibration required directly prior to use must be straightforward to perform by a clinician *in situ*. In addition, the device must be easy to clean between patients to enable infection control, which is of particular importance for patients with severe lung disease, such as CF patients.

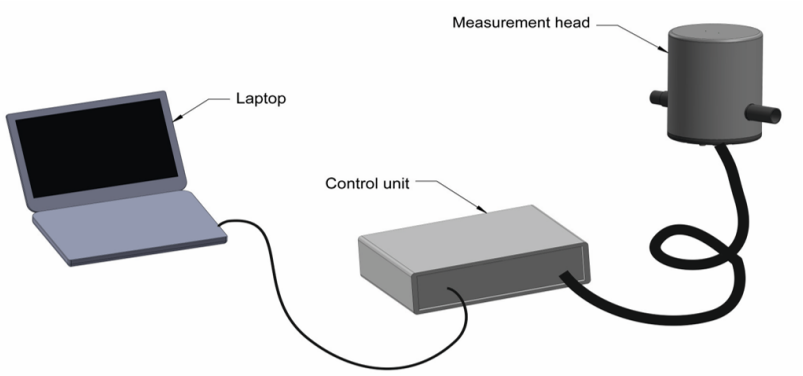


Figure 2.1: Three components of the molecular flow sensor

The MFS consists of the three elements shown in Figure 2.1: a laptop, a control unit and a measurement head. The controller, housed within the control unit, is responsible for the acquisition of optical, flow, temperature and pressure data. Real-time data processing is achieved via a custom-made LabVIEW program run on the laptop. The laptop is connected to the controller via a standard USB connection. Laser drivers for all three spectroscopic channels are also located in the control unit, along with the single-mode (SM) diode lasers for the H_2O and CO_2 measurements. The output radiation from the two lasers is spatially overlapped in the control unit and the multiplexed optical signals are carried to the measurement head via a LEMO optical cable. The use of time-division multiplexing simplifies the design by removing the need for a second set of fibres, collimators, optical paths and detectors. The diode laser used for the detection of O_2 is housed in the measurement head, along with the optical paths for the detection of all three gases. The spectroscopic measurements are described in greater detail in Section 2.3. Sensors for the measurement of barometric pressure, temperature and flow are also contained in the measurement head. These measurements are described in further detail in Section 2.2 and 2.4 respectively. The measurement head also contains a heating system, which ensures equilibrated and consistent temperature for the electrical and optical components. This ensures continued reliability of the measurements as room temperature varies and enables use of the device at higher humidity without condensation on optical surfaces interfering with the measurement. The design of the interior of the measurement head is illustrated in Figure 2.2.

The control unit, measurement head and laptop are all housed on a custom-made trolley, allowing easy transportation between rooms. The measurement head is secured to the trolley by a Manfrotto MHXPRO-BHQ2 ball mount on a Bytec HA Grey Pole Mount. This allows safe and easy movement of the measurement head so

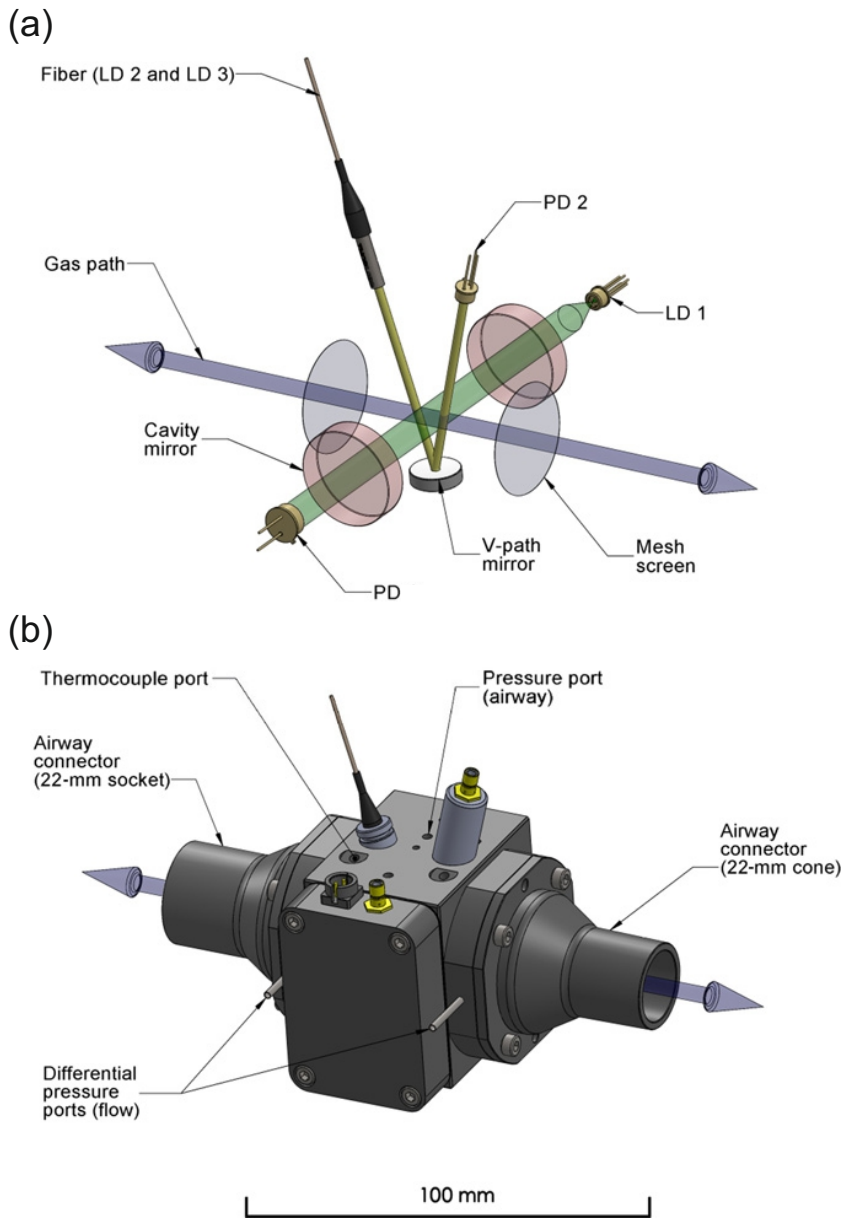


Figure 2.2: (a) Schematic of the gas path and the optical paths within the device (multiplexed CO_2 and H_2O path shown in brown and off-axis cavity enhanced O_2 path shown in green). The position of the cavity mirrors is shown in pink and the locations of the laser diodes (LD) and photodetectors (PD) are indicated. The wire meshes are used to create a pressure differential across the cell to enable flow measurement. (b) CAD diagram indicating the position of the thermocouple port, pressure port and differential pressure ports beside the mesh screens as well as the 22 mm airways connectors which connect to standard 22 mm medical tubing.

it can be adjusted to the desired position and connected to a patient's airway. A Liebert uninterruptible power supply (UPS) is also housed on the trolley. Powering the device through the UPS ensures that there is no effect on the data measurements when the mains supply is disconnected. Two 5 L cylinders are also located on the lower shelf of the trolley for ease of use for the clinicians carrying out the *in situ* calibration of the device which is detailed in Section 2.3.

All outer surfaces of the MFS are made of materials which can be wiped thoroughly with antibacterial wipes. The interior of the measurement head cannot be cleaned directly, but is always protected from the patient connected to it by either a bacterial filter or an HME filter, depending on the type of humidification used. A new filter is used for each subject and mouthpieces are sterilised between subjects.

2.2 Temperature and Pressure Sensing

Temperature and pressure measurements are recorded every 10 ms. This allows the total number density of all molecular species present in the gas in the measurement head to be calculated using the ideal gas law:

$$\frac{N}{V} = \frac{P}{kT} \tag{2.1}$$

where N/V denotes the number density, P is pressure, k is the Boltzmann constant and T is the temperature. Four welded-tip K-type thermocouples were custom-made for use in each device to measure the temperature of the gas in the gas path. A fast response time of the order of tens of ms is required to ensure good temporal alignment of the temperature and concentration measurements. Thin, 25 µm diameter sensors are used to improve the time resolution of temperature changes in the cell. The tips of the thermocouples protrude into the gas path by a few mm, ensuring good thermal contact with the gas in the measurement cell. The four thermocouples are spaced out around the gas path and their measurements averaged to account for spatial variation in temperature within the cell.

The custom-made thermocouples are calibrated against a precision calibrated Platinum Resistance Thermometer (PRT) which has an associated error of 0.04 °C. This is achieved by inserting the PRT into the measurement head through the light traps and sealing the measurement cell at either end. A series of measurements are taken with the cell heated to a range of temperatures from 30 °C to 42 °C and the current outputs scaled to match the temperature of the reference PRT. Figure 2.3 shows

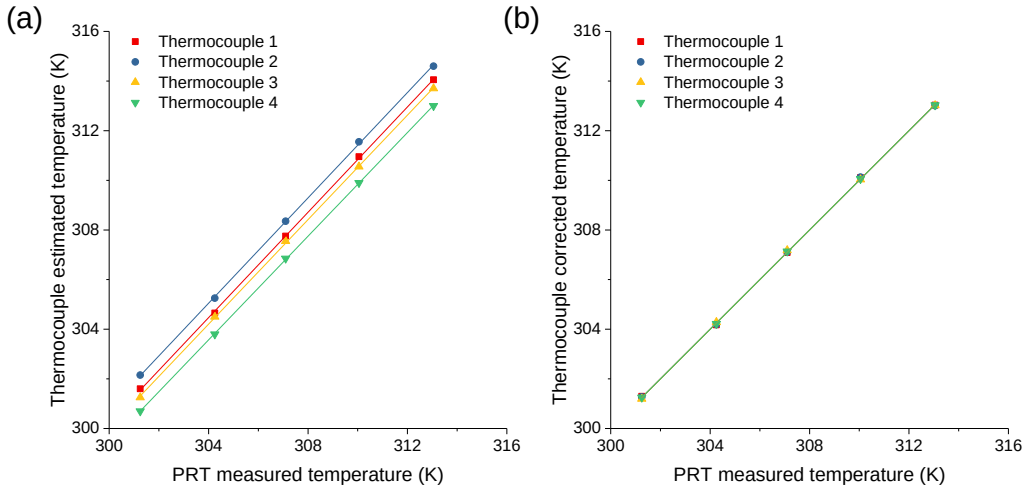


Figure 2.3: Sample calibration data from the four thermocouples in a MFS head against the precision calibrated PRT, with (a) the initial data collected using a scaling factor of 0.1 and an offset of 273 K for all sensors then (b) the corrected values determined from the linear fit to the data. R^2 values range from 0.99986 to 0.99996 for the linear fits shown in (b).

a sample set of measurements for the four thermocouples of one MFS unit. The corrected temperature measurements shown in Figure 2.3 (b) show excellent agreement with the PRT values, illustrated by R^2 values close to 1 for all four linear fits.

The barometric pressure is measured using a single HCA0811ARH8 sensor, manufactured by First Sensor AG, which is connected to the measurement cell by a flexible silicone tube. This sensor measures absolute pressure between 800 and 1100 mBar with 12-bit resolution and communicates with the system controller via an I2C bus.

The pressure sensor was calibrated by connecting it to the manifold shown in Figure 2.4 (a). A syringe is connected to a T-piece: the first output connects to the pressure sensor undergoing calibration and the second to a bank of 8 calibrated pressure sensors. As the syringe is depressed, the pressure change is recorded on the calibrated bank and the reading of the single sensor is scaled to match that of the bank. Sample calibration data is shown in Figure 2.4 (b).

Figure 2.5 shows measurements from a fully calibrated set of thermocouples and barometric pressure sensor when a volunteer breathes through an HME (Heat and Moisture Exchanger) filter connected to the MFS. The profile of the temperature variation over a breath cycle is highly dependent on the type of filter used. The variation in total number density over the breathing cycle calculated from the pressure and temperature measurements is also displayed.

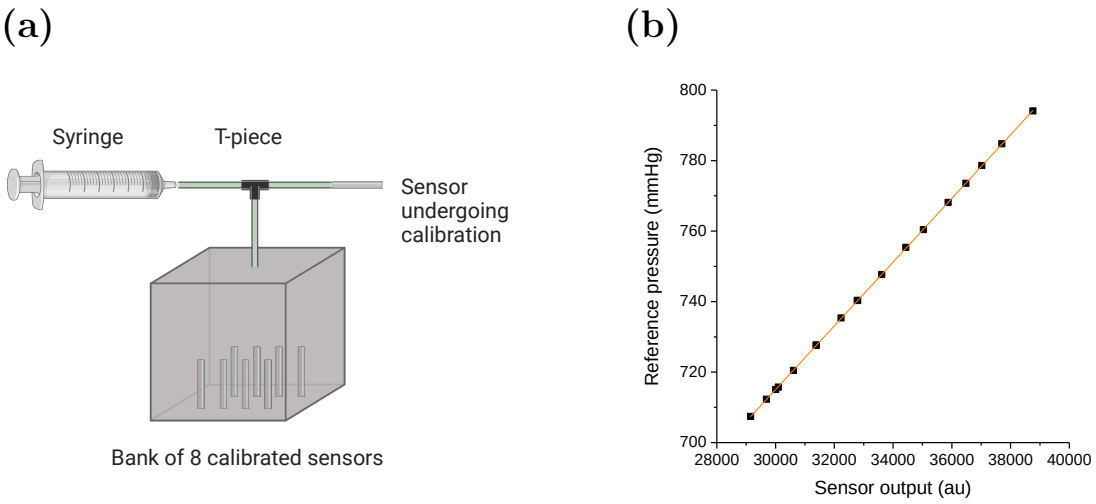


Figure 2.4: (a) Experimental set-up to calibrate a barometric pressure sensor.[12] (b) A sample set of calibration data for a pressure barometric sensor, from which the coefficients for scaling the sensor output to the measured reference pressure can be determined using an ordinary least squares fit (for displayed data intercept = 443.91 ± 0.29, gradient = $9.0380 \times 10^{-3} \pm 8.8 \times 10^{-6}$).

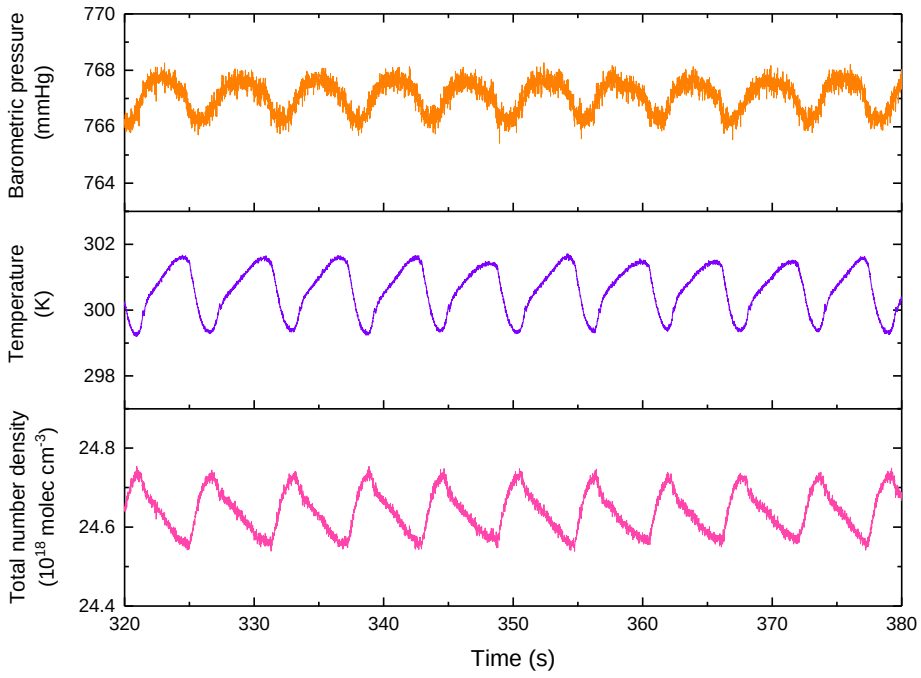


Figure 2.5: The barometric pressure, temperature and calculated total number density over 10 breath cycles of a volunteer breathing through the MFS.

2.3 Spectroscopic Measurements

The spectroscopic measurements described in this section provide the number density of O_2, CO_2 and H_2O and so the fraction of each of these three gases can be calculated, using the total number density obtained from the pressure and temperature measurements. The remaining gas fraction is the balance gas. The balance gas is primarily nitrogen, although other inert gases will also be present in smaller concentrations. Henceforth the balance gas will be referred to as nitrogen, although all calculations calculating the properties of the balance gas account for the presence of argon, which comprises 0.93 % of air in the atmosphere.

2.3.1 Spectroscopic Transitions

The attenuation of specific wavelengths of light due to the presence of different molecules was first observed by Wollaston over 200 years ago.[116] With the development of quantum mechanics and discovery of quantized energy levels in the 20th century, this phenomenon could be explained for the first time. A molecule can possess translational, electronic, vibrational and rotational energy. The first of these is essentially unquantized (at room temperature), while the latter three display discrete energy levels. When a photon, whose energy (hv) corresponds to a difference in molecular energy states, interacts with a molecule, there are 3 possible outcomes: stimulated absorption, stimulated emission and spontaneous emission. This body of work is concerned with the first of these processes, where a species, X, absorbs a photon and is excited to a higher energy state, X^*:

$$X + hv \longrightarrow X^* \tag{2.2}$$

The rate of absorption by the molecule from its initial state, with population density n_1, to its excited state, with population density n_2, is given by:

$$\frac{\mathrm{d}n_2}{\mathrm{d}t} = n_1 B_{12} \rho(v) \tag{2.3}$$

where B_{12} is the Einstein Coefficient for stimulated absorption and $\rho(v)$ is the radiation energy density. The radiation energy density is directly proportional to the square of the incident radiation field amplitude, which is determined by the intensity of the incident light. B_{12} is directly proportional to the square of the transition dipole moment, R_{12}, which is defined as the following matrix element formed by the

wavefunctions of the initial and final states of the molecule undergoing excitation and the electric dipole operator, $\hat{\mu}$:

$$R_{12} = \int \psi_2^* \, \hat{\mu} \, \psi_1 \, d\tau \tag{2.4}$$

Therefore the intensity of a transition depends on the value of R_{12}: for all allowed transitions, $R_{12} \neq 0$, while for forbidden transitions, $R_{12} = 0$. In most cases (and for transitions within a single electronic state), whether a transition between rovibrational states is allowed is governed by selection rules: $\Delta v_i = \pm 1$ and $\Delta J = \pm 1$, where v_i and J are the vibrational and rotational quantum numbers respectively.

The Einstein coefficient, B_{12} can be related to a more useful quantity, the integrated absorption cross section, σ_{12}, (a measure of the effective area over which a photon can be absorbed) according to:

$$\int_0^\infty \sigma_{12}(v)dv = \frac{hv}{c} B_{12} \tag{2.5}$$

which provides the integrated value of $\sigma(v)$ over an absorption profile in the frequency domain.

For the clinical work detailed in this thesis, two molecular flow sensors were built. The first MFS unit employs the same transitions as used by Ciaffoni *et al.* to monitor O_2, CO_2 and H_2O concentrations at 764 nm, 2004 nm and 1369 nm respectively. However, the 1369 nm H_2O laser is multiplexed with the 2004 nm laser and travels through a single mode fibre optimised for wavelengths between 1700 nm and 2300 nm. It is therefore desirable to explore potential H_2O transitions which fall within this range which could be used in future iterations of the MFS. Hence a second laser accessing a H_2O transition at 1854 nm was trialled in Unit 2. The cross section of this line is also larger, which could be beneficial if a measurement cell with a shorter optical path were required in the future. However, the cost of the 1854 nm laser is approximately double that of the 1369 nm laser, which may be a barrier if the MFS were to be produced as a commercial device. All wavelengths used in Units 1 and 2 are listed along with their spectroscopic assignment and absorption cross sections in Table 2.1.

The overtone/combination transitions probed to determine the CO_2 and H_2O concentrations are sufficiently strong to employ direct laser absorption spectroscopy. The CO_2 concentration is measured using the R(16) transition within the $2v_1 + v_3$ combination band, while R-branches within the $v_1 + v_2$ and $v_2 + v_3$ combination bands are employed to monitor the H_2O concentration in Units 1 and 2 respectively. In the case of the O_2 spectroscopy, the electronic b $^1\Sigma_g^+ \leftarrow$ X $^3\Sigma_g^-$ A-band transition is formally

Molecule	O_2	CO_2	H_2O	H_2O
Wavelength (nm)	764.28	2004.02	1368.60	1854.03
Wavenumber (cm^{-1})	13084.20	4989.97	7306.75	5393.65
Electronic transition	b $^1\Sigma_g^+ \leftarrow$ X $^3\Sigma_g^-$	-	-	-
Vibrational band	$0 \leftarrow 0$	$201 \leftarrow 000$	$101 \leftarrow 000$	$011 \leftarrow 000$
Rotational assignment	$^{P(11)}P(11)$	R(16)	$3_{13} \leftarrow 2_{12}$	$3_{13} \leftarrow 2_{12}$
Cross section ($cm^2\,cm^{-1}$)	6.13×10^{-24}	1.32×10^{-21}	1.80×10^{-20}	2.59×10^{-20}

Table 2.1: Parameters for the spectroscopic transitions employed in the molecular flow sensor. The wavelength is defined as the transition wavelength in a vacuum. Cross section is defined as the integrated absorption cross section at 296 K. For O_2 the electronic transition from the lower to the upper state is denoted by term symbols, which have the general form: $^{2S+1}\Lambda_{g/u}^{+/-}$. The vibrational band originates in the ground vibrational state, with the quanta of energy in the excited state in each vibrational mode given in the form $v_1v_2v_3$ for the CO_2 and H_2O transitions. The rotational assignment is reported as $^{\Delta N(N")}\Delta J(J")$, for O_2, $\Delta J(J")$ for CO_2 and $J_{K_aK_c}$ for H_2O.

spin forbidden,[117] and consequently has a much smaller cross-section than the CO_2 and H_2O transitions. However, the use of off-axis cavity enhanced absorption spectroscopy (CEAS) increases the effective path length and hence provides the required level of sensitivity for use in this device, *vide infra*.

2.3.2 Data Acquisition

The lasers used in the MFS are all single-mode (SM) diode lasers, with either a vertical-cavity surface-emitting laser (VCSEL) or a distributed-feedback (DFB) structure. A VCSEL consists of two distributed Bragg reflectors (DBR) with alternating layers of n- and p-doped semiconductor encasing a thin active region with quantum wells.[118] Unlike conventional edge emitting lasers, VCSELs emit radiation from their top surface, which allows many more lasers to be manufactured and tested at once, reducing production costs and hence laser price. DFB lasers improve on the basic Fabry-Perot laser design by including a grating above the active layer which only reflects the desired output wavelength into the laser cavity, resulting in a narrower

range of emitted wavelengths.

The lasers used in the MFS were selected for their low power consumption, small spectral bandwidth (∼100 MHz for VCSELs and ∼1 MHz for DFBs) and good tunability (> 10 MHz). They are all purchased in standard packages with a thermoelectric cooler (TEC). Each individual laser has its own custom-made laser driver in the control unit to provide a low noise current source and temperature control. Each laser driver has an analog to digital converter (ADC) with a sampling rate of 80000 samples per second, so 400 data points are recorded per 5 ms sampling period. For the O_2 measurements, two of these 5 ms spectra are averaged to provide a concentration measurement every 10 ms. As the CO_2 and H_2O radiation shares the same optical path, each laser is ramped successively for 2.5 ms over the wavelength range of their respective transitions. Two of these 2.5 ms spectra are averaged to give a measurement every 10 ms. The sequential laser ramps are illustrated in Figure 2.6.

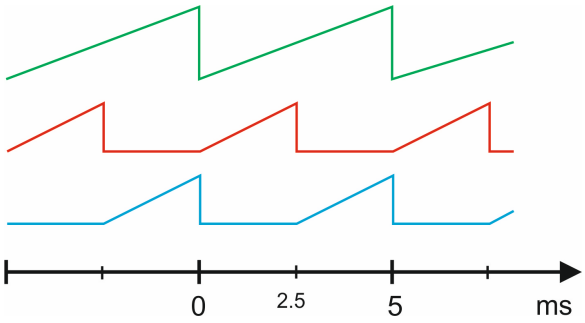


Figure 2.6: Plot showing data acquisition for the three channels: O_2 (green), CO_2 (red) and H_2O (blue). A single 5 ms measurement period is shown. Two of these measurements are averaged per 10 ms for each channel to provide a concentration measurement every 10 ms.

Each laser must be calibrated to determine its spectral tuning range around the current and temperature set point required to locate the centre of the absorption line at the centre of the ramp. This is achieved by directing the laser radiation into an optical spectrum analyser. For the O_2 laser, a spectrum analyser with a free spectral range (FSR) of 7.54 GHz (CVI, 3SAE036) is used and for the CO_2 and H_2O lasers a spectrum analyser with an FSR of 2.015 GHz (Melles Griot) is used. The output from the spectrum analysers is amplified and the output directed into the analog signal input in the controller within the MFS control unit for data acquisition. Data are averaged over 5 minutes as the laser is scanned in frequency and the resulting profile displays transmission maxima, as seen in sample data taken for the CO_2 and H_2O channels in Figures 2.7 (a) and (b). These maxima correspond to the resonant

frequencies of the spectrum analyser and are equally spaced in the frequency domain by the FSR of each spectrum analyser. The positions of these maxima are identified and a third order polynomial is fit to this data to obtain a set of regression coefficients relating time to wavenumber:

$$\tilde{\nu}(t) = c_0 + c_1 t + c_2 t^2 + c_3 t^3 \tag{2.6}$$

This produces the calibration curves such as those displayed in Fig. 2.7 (c) and (d).

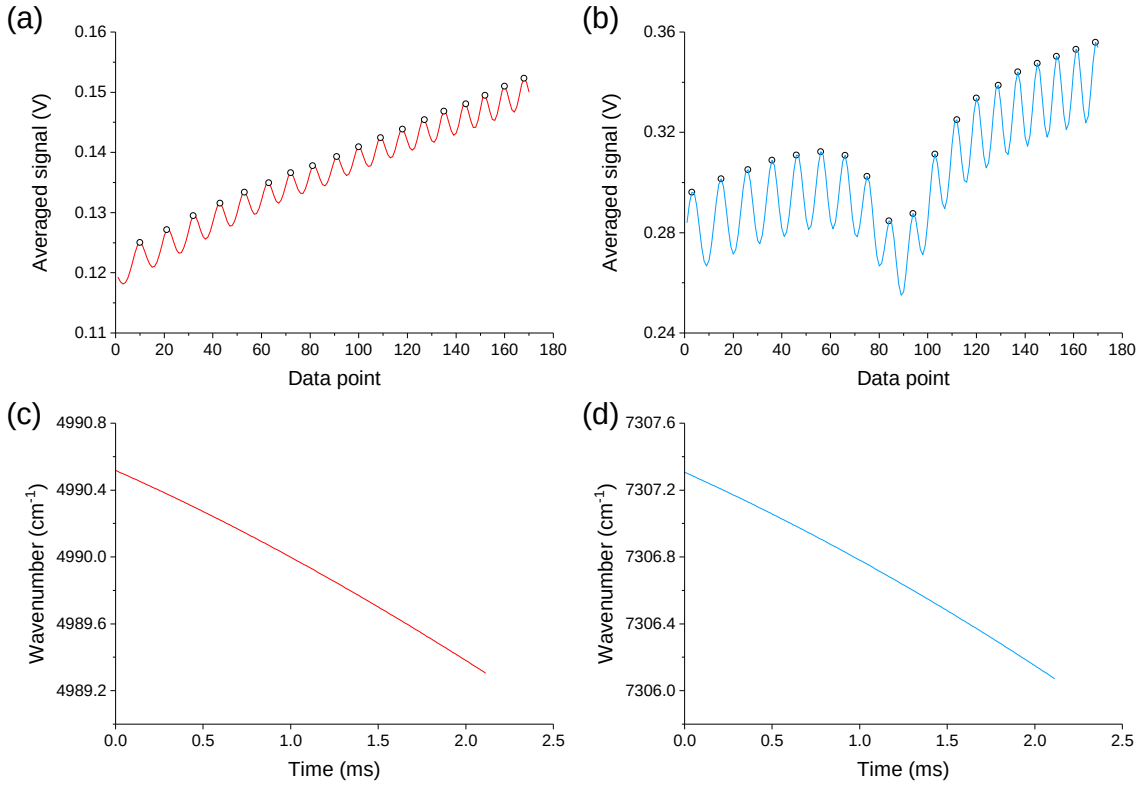


Figure 2.7: Example data recorded from an optical spectrum analyser for (a) the CO_2 channel and (b) the H_2O channel and their fitted time to wavenumber axes (c) and (d). N.B. Absorption from atmospheric H_2O is apparent on (b) between data points *ca.* 70-110.

The CO_2 and 1854 nm H_2O lasers are both Nanoplus DFB lasers, while the 1369 nm H_2O laser is an NEL DFB laser. All three lasers are supplied in standard 14-pin butterfly mounts and placed into custom-made laser mounts, designed to conserve space inside the control unit.

As noted earlier, the radiation from the CO_2 and H_2O lasers is spatially overlapped by a Thorlabs 2×2 SM fibre optic coupler so the measurement of both can be achieved using the same optical path. Couplers where the ferrule of the fibre was

cut at an angle, leaving an angled physical contact (APC) connector instead of a flat cut, physical contact (PC) connector, were used to minimise return losses and hence reduce the likelihood of optical feedback which may disrupt the free-running operation of each laser. For the two Nanoplus lasers, the fibre connectors (FCs) from the lasers are terminated with an FC-APC connection, which can be connected directly to the fibre optic coupler, while the NEL laser is terminated in an FC-PC connection, so requires an additional fibre to convert from a PC output to an APC output in order to connect to the APC input of the coupler. The layout of the control units is illustrated in Figure 2.8. The fibre optic coupler selected for each unit was carefully chosen to maximise throughput of light of the two wavelengths involved – this means the central wavelength, spectral bandwidth and split ratio were all considered.

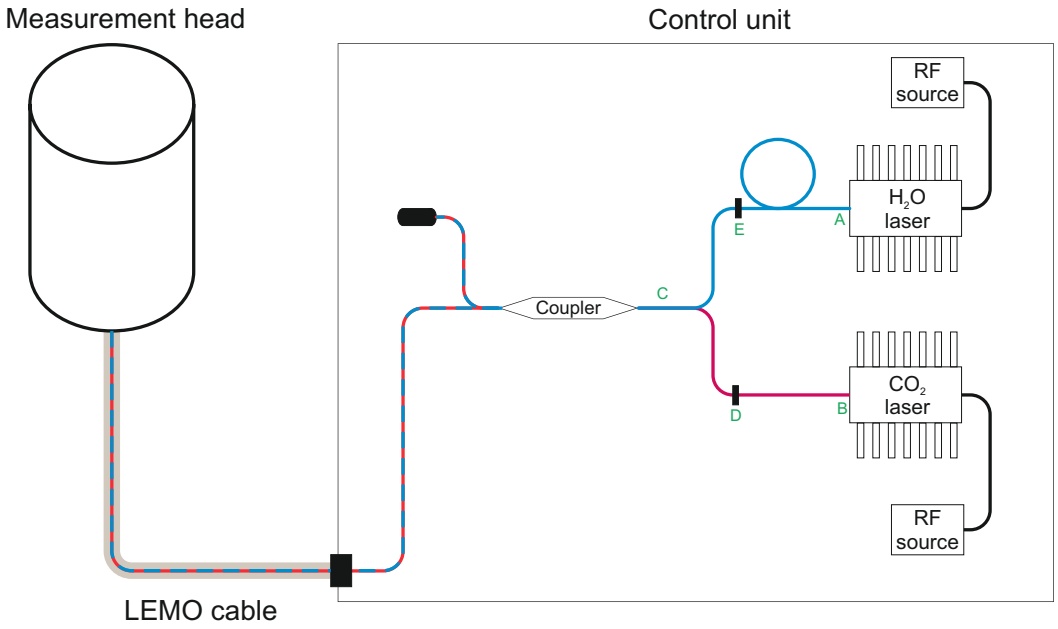


Figure 2.8: Generalised fibre diagram showing arrangement of components inside the MFS control unit.

For combining the 2004 nm and 1369 nm wavelengths, a dual window coupler optimised for transmission of light at central wavelengths of 1310 nm and 1550 nm with a bandwidth of ±100 nm was selected. The split ratio is 90:10 to account for the higher relative intensity of the NEL laser and additional attenuation of the 2004 nm light due to its greater spectral distance from the central wavelength of the coupler. A 3 dB Thorlabs attenuator was also added to the CO_2 laser to slightly attenuate the

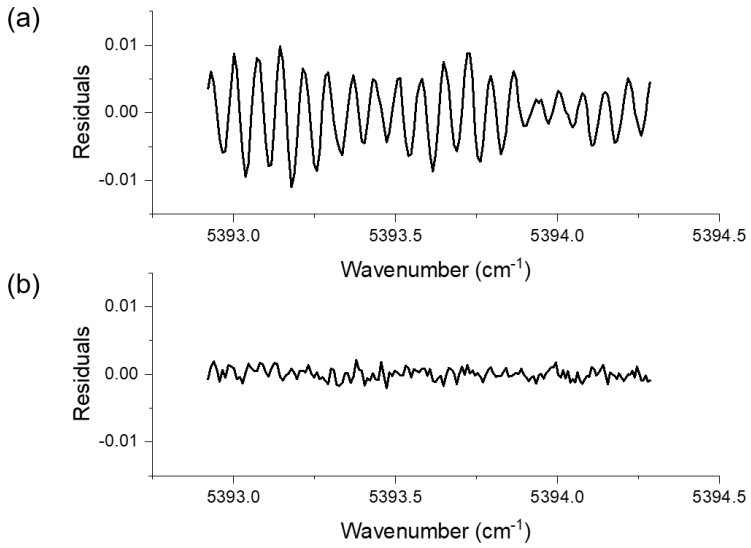


Figure 2.9: Residuals obtained by fitting the H_2O absorption spectrum, (a) without added fibre and (b) with the addition of an 8m fibre to the H_2O optical path.

power to better equalise the power outputs of the two channels. A generalised fibre diagram is shown in Figure 2.8.

The output powers of the 2004 nm and 1854 nm lasers used in Unit 2 are much more closely matched, and so a 75:25 coupler was used with a central wavelength of 2000 nm and a bandwidth of ±15 nm. Notably, the residuals from a fitting to the H_2O absorption profile obtained from Unit 2 showed a significant etalon, shown in Figure 2.9 (a), corresponding to an optical path difference of 4.73 cm in the fibre. The source of this etalon was investigated by adding an additional 3 dB attenuator with a fibre length of 2.1 cm, first at point D, then at point E, indicated on Figure 2.8. This resulted in a corresponding increase and decrease in path lengths, allowing the interfering paths to be identified as A-C-A and A-B-A. This etalon could then be removed by adding an 8 m long fibre at point E (shown by the blue circle) to significantly increase the path difference. This made the resulting residuals from the fitting of the 1854 nm data (Figure 2.9 (b)) comparable to those observed with the 1368 nm laser from Unit 1.

The output radiation from one arm of the coupler (see Figure 2.8) is carried to the measurement head by a LEMO 2 m optical cable (UKF.3K.B20.000200) when the MFS is used in lung function studies. However, a 5 m long cable (UKF.3K.B20.000500) is used in certain clinical settings, such as intensive care units, to allow a greater distance between the control unit and measurement head and hence maintain unrestricted access to the patient. The other unused output from the coupler is directed

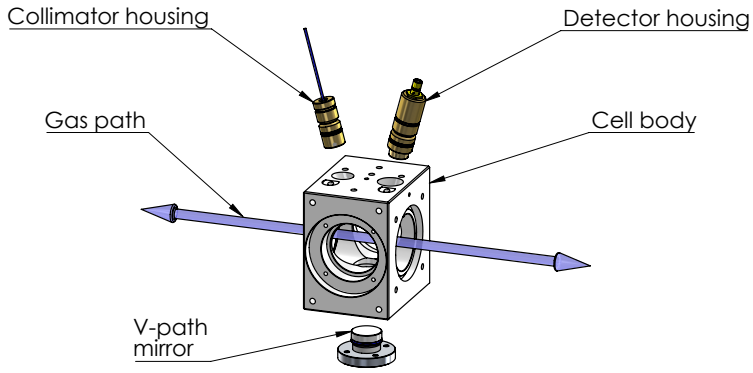


Figure 2.10: Schematic of the components of the optical V-path used for CO_2 and H_2O measurements. Radiation enters the measurement cell body via the collimator, is reflected by the aluminium coated mirror and is then detected by the photodiode in the detection module.

into a Thorlabs FTPC1 fibre optic light trap, which reduces back reflections into the input fibre by up to 50 dB.

Inside the measurement head the radiation is carried through 2 m of fibre before being injected into the optical V-path. This prevents interference effects between the PC/PC connection where the LEMO cable connects to the head and the surface of the collimating lens.

A diagram of the optical V-path within the measurement head is shown in Figure 2.10 and consists of three components connected to the cell body: a fibre collimator, a mirror at the base of the V-path and a photodetector. The mirror selected for use in the V-path is a half inch diameter, aluminium coated, concave mirror (Thorlabs, CM127-025-G01). It has a focal length of 25.0 mm, ensuring that the beam is focussed at the photodetector surface. The photodetector is an InGaAs photodiode (Hamamatsu G12182-020K) with a photosensitive area of 2.0 mm^2. Its spectral response range of 0.9 µm to 2.1 µm and peak sensitivity wavelength of 1.95 µm make it well suited for the wavelengths used to measure CO_2 and H_2O concentrations.

The V-path length is machined to a distance of (54.0 ± 1.0) mm and a device-specific V-path length is then determined by comparing the measured CO_2 concentration against a range of reference gases, certified to a gravimetric standard (Figure 2.11). As CO_2 and H_2O share the same optical path, this distance can also be used to calculate the H_2O concentration.

The O_2 concentration is measured along the axis perpendicular to both the V-path and gas flow axes within the measurement cell. The electrical signal from the

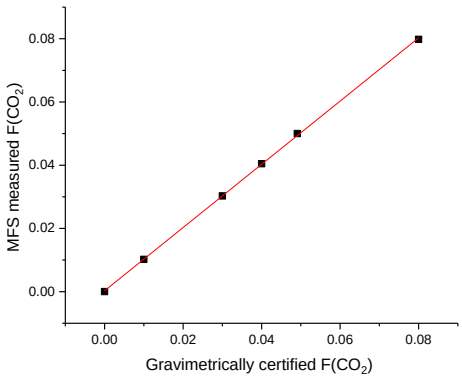


Figure 2.11: Measured CO_2 concentrations compared with a range of gravimetrically certified CO_2 gas mixtures following calibration of the V-path distance. Also shown is an ordinary least squares (OLS) fit to the data (gradient $= 1.00001 \pm 0.00650$, intercept $= 2.79 \times 10^{-4} \pm 2.84 \times 10^{-4}$, $R^2 = 0.99983$).

O_2 laser driver (which controls the temperature and current of the laser) is carried from the control unit to the measurement head through the custom-made electrical cable. An SM VCSEL laser (ULM763-01-TN-S46FTT, ULM Photonics), housed in the measurement head, is used to probe the transition at 764 nm, and has an output power of 0.3 mW. It is mounted in a custom-made assembly, consisting of a commercial 5-pin socket (BFI-Optilas, 612-1052314-001), which is hardwired to the cable connected to the laser driver and a collimation package (Thorlabs, LT220P-B) that focuses the output from the laser diode. The laser output is injected into the optical cavity, which comprises a pair of 25.0 mm diameter, 6 mm thick, spherical fused silica mirrors (Layertec, 134341), spaced 27 mm apart. These mirrors are coated with a partially reflective coating with a specified reflectivity of 99.80 % at 763 nm, increasing the effective path length by a factor of $\sim$ 500. The alignment of the cavity is off-axis, to minimise optical feedback and continuous excitation of higher order cavity modes, which ensures a smooth transmission function for the cavity.[119] Alignment is achieved by adjusting the input to the steering mirror, whose surface normal is at a 45° angle to the cavity transmission axis. A silicon photodetector with a photosensitive area of 18 mm $\times$ 18 mm and a spectral response range of $190 - 1100$ nm (Hamamatsu S1337-21) located behind the second mirror is used to detect light as it exits the cavity. An amplified spontaneous emission (ASE) filter is placed between the second cavity mirror and this detector to limit the wavelengths of light reaching the detector to the spectral region of interest and increase the signal-to-noise ratio (SNR). The components of the CEAS spectrometer are displayed in Figure 2.12.

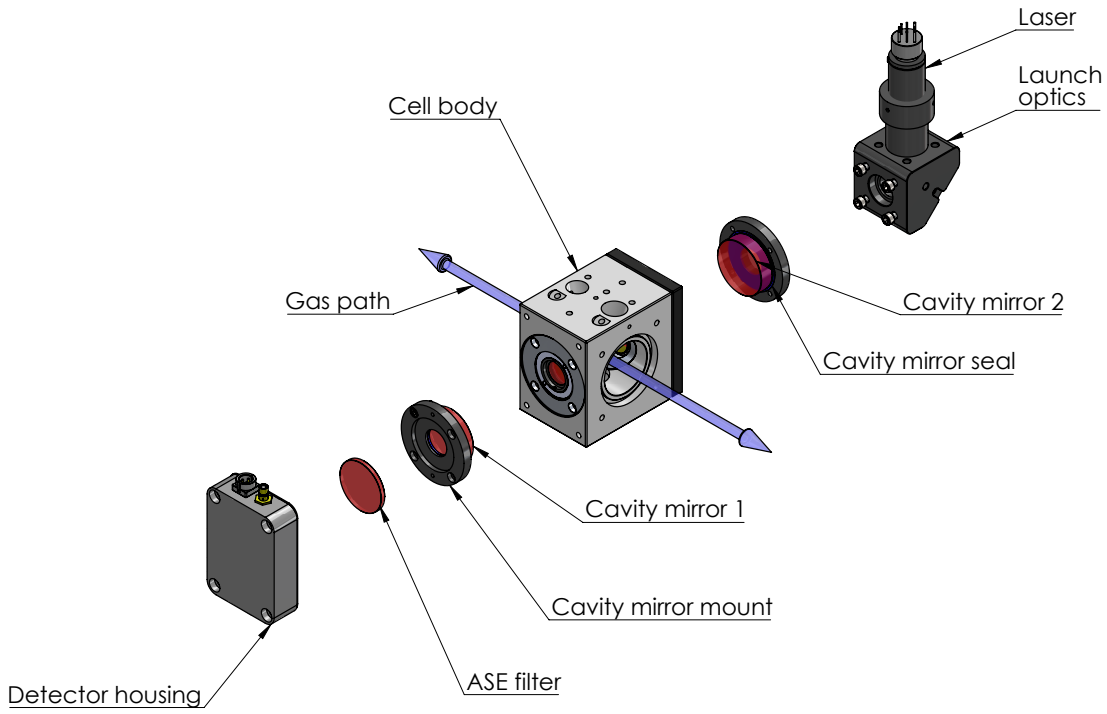


Figure 2.12: Schematic of the CEAS system for measuring O_2 concentration. The launch unit consists of the VSCEL laser, collimator and steering mirror. The optical cavity between the two high-reflectivity mirrors increases the effective path length for the O_2 optical path, which lies perpendicular to the gas flow path. Radiation leaves the cavity through the second mirror, travelling through an ASE filter before reaching the detection module.

Optimal alignment is achieved through imaging the mode field on the second mirror using a complementary metal oxide semiconductor (CMOS) sensor camera (Teledyne Dalsa Genie HM640) connected to a telecentric lens (Edmund Optics 56-675). While imaging and altering the mode field, the spectral output of the cavity is viewed contemporaneously to ensure sufficient signal is maintained and assess the etalons present in the baseline. A broader mode field results in a desirable improvement to baseline stability and etalon amplitudes through suppressing mode degeneracy. However, conversely, a more spatially extended mode field results in decreased mechanical stability and lower light intensities being detected. In addition, this effect is a function of gas flow. Therefore the final alignment reflects a compromise between optimal mechanical stability and measurement sensitivity.

2.3.3 Determining Concentration

The attenuation of the laser output in the MFS by the molecular species of interest involves light passing through a homogeneous, weak-absorbing medium, so can be described by the Beer-Lambert law:

$$I(v) = I_0(v)e^{-\sigma(v)c_i l} \tag{2.7}$$

where $I_0(v)$ is the intensity of the incident light, $I(v)$ is the intensity of the light transmitted through the absorbing medium, $\sigma(v)$ is the absorption cross-section for a specific frequency of incident radiation, l is the path length through the absorbing medium and c_i is the concentration of the absorbing species i. For a given transition, the absorption cross-section is generally reported as the integrated value across the transition, $\sigma_{int} = \int \sigma(v)\mathrm{d}v$. Such is the case for the values obtained from the HITRAN database and reported earlier in this chapter in Table 2.1.

When applying the Beer-Lambert law, a baseline I_0 would ideally be recorded immediately prior to or during acquisition of an absorption spectrum. However, this is not straightforward in the MFS, as the calibration must be performed prior to data collection from a human subject and then adjustments must be made according to instantaneous fluctuations in the performance of the optical and electrical systems. As highlighted earlier, it is vital that the calibration procedure is straightforward for a clinician to perform with minimal training and this is now described. Two calibration gases are used: Oxygen-free Nitrogen and 99.999 % pure (N5) Oxygen, both of which are stored on the lower shelf of the MFS trolley. Such a high purity of O_2 is needed to provide an accurate reference concentration for the calibration of the effective cavity mirror reflectivity. The LabVIEW software guides the user through the calibration, instructing them to first flow N_2 through the measurement head at 3 ml min^{-1}, while the lasers are automatically switched on and off according to the following six-step protocol:

1. All three lasers are switched off to record a baseline measurement, I_{off} for the O_2 channel with the laser switched off.

2. The CO_2 laser is switched on while the others are off to obtain I_{off} for the H_2O laser and I_{0,N_2} for the CO_2 laser.

3. The H_2O laser is switched on while the others are off to determine I_{off} for the CO_2 laser and I_{0,N_2} for the H_2O laser.

4. All three lasers are switched on for the I_{0,N_2} measurement for the O_2 laser.

The user is then instructed to change the flow of gas to 3 ml min^{-1} of N5 O_2 for the final two steps:

5. All three lasers are on to measure the H_2O concentration in the O_2 gas used to calibrate the O_2 cavity.

6. All three lasers are on to measure the effective reflectivity of the O_2 cavity mirrors.

Wherever possible, this calibration is carried out between subjects being studied with the MFS. Each step only lasts for 30 s and is easy to perform so the procedure is feasible to perform regularly in a clinical setting.

For the *nth* measurement of CO_2 and H_2O concentrations, c_n, the Beer-Lambert law can be applied directly, with baseline measurements calculated using the calibration procedure detailed above:

$$c_n \sigma l = \ln\left(\frac{I_0 - I_{off}}{I_n - I_{off}}\right) \tag{2.8}$$

where I_0 is the baseline signal in the absence of absorbing species, I_n is the recorded spectrum and I_{off} is the offset signal when the laser is switched off (but the other multiplexed laser is still emitting at its stationary frequency). This calibration procedure is simplified for the user by having the LabVIEW program automatically switch the lasers on and off. Because it is not possible to record simultaneous transmission spectra and baseline measurements, a correction factor is needed to account for random fluctuations in the baseline, due to causes such as drift by the laser or control electronics or changes to the performance of the optical components. It is assumed that the correction factor, q_1 translates the measurement linearly, according to:

$$\ln\left(\frac{I_0 - I_{off}}{I_n - I_{off}}\right) = \ln\left(\frac{I_{0,N_2} - I_{off}}{I_n - I_{off}}\right) + q_1 \tag{2.9}$$

where I_{0,N_2} is the baseline recorded during calibration with N_2. A second parameter, q_2 is defined to relate the determined concentration from a spectrum, c_n to an arbitrary reference concentration, c_{ref}, by:

$$c_n = q_2 c_{ref} \tag{2.10}$$

By combining these two corrections, a final equation to evaluate concentration is obtained:

$$q_2 c_{ref} \sigma l = \ln\left(\frac{I_{0,N_2} - I_{off}}{I_n - I_{off}}\right) + q_1 \tag{2.11}$$

LabVIEW's multiple linear regression model is then used to evaluate each data point on a spectrum to determine the best fit regression parameters q_1 and q_2.

To evaluate the quality of the fit, a simulated spectrum, $I_{n,fit}$ is constructed, according to:

$$I_{n,fit} = e^{-(q_2 c_n \sigma l - q_1)}(I_{0,N_2} - I_{off}) + I_{off} \tag{2.12}$$

For the O_2 measurement, a modified version of the Beer-Lambert Law must be used to account for the increased path length afforded by the use of an optical cavity with mirrors with reflectivity R located at a distance of l from each other:[120]

$$\frac{I_0(v) - I(v)}{I(v)} = \frac{\sigma c_n l}{1 - R} \tag{2.13}$$

Similarly, the equations used to calculate concentration from the CEAS measurements must be slightly altered from those described previously for the direct laser absorption spectroscopy measurements for CO_2 and H_2O. The nth value of $I_0(v)$ and $I(v)$ can be related to the measured spectrum and baseline according to:

$$\frac{(I_{0,n} - I_{off}) - (I_n - I_{off})}{I_n - I_{off}} = \frac{\sigma c_n l}{1 - R} \tag{2.14}$$

As described previously, it is not possible to directly measure a baseline, $I_{0,n}$ for each measurement, I_n. Therefore a correction factor, q_1 is introduced to account for deviations from the recorded baseline during calibration with N_2, I_{0,N_2}, according to:

$$I_{0,n} - I_{off} = q_1(I_{0,N_2} - I_{off}) \tag{2.15}$$

As with the CO_2 and H_2O fitting, the concentration of O_2 is related to a reference concentration c_n by: $c_n = q_2 c_{ref}$. Combining these equations yields:

$$I_n - I_{off} = q_1(I_{0,N_2} - I_{off}) - q_2\frac{\sigma c_{ref} l}{1 - R}(I_n - I_{off}) \tag{2.16}$$

Rearranging this equation and applying the multiple linear regression module in LabVIEW with q_1 and q_2 as the regression parameters produces an expression for the best-fit spectrum:

$$I_{n,fit} = \frac{I_{off}(1 + q_2\frac{\sigma c_{ref} l}{1-R}) + q_1(I_{0,N_2} - I_{off})}{1 + q_2\frac{\sigma c_{ref} l}{1-R}} \tag{2.17}$$

Concentration is determined by fitting an experimental absorption spectrum with a simulated lineshape. The width of the lineshape is affected by two types of factors: homogeneous broadening mechanisms, i.e. those that affect all molecules equally, and inhomogeneous mechanisms, in which the broadening depends upon particular properties of the absorbing species, in this case their velocities.

One source of homogeneous broadening arises from the Heisenberg uncertainty principle. Due to the process of spontaneous emission, an excited energy state never has an infinite lifetime and hence there will always be associated uncertainty in the energy levels. For this application, using radiation in the near-IR region and gas samples at room temperature and pressure, the contribution from this broadening mechanism to the spectral width is several orders of magnitude smaller than other sources and so is neglected in calculations in this work.

The lifetime of the upper state is however also reduced by collisional deactivation, leading to what is known as collisional broadening or pressure broadening. This decreases the lifetime of the excited state and hence introduces further associated uncertainty in the energy of the transition. A higher pressure and hence a greater collision rate increases the significance of this effect. As all molecules in the gas sample are affected to the same degree, this is a homogeneous effect and can be modelled by a Lorentzian lineshape:

$$L(v) = \frac{2}{\pi} \frac{\Delta v_l}{\Delta v_l^2 + 4(v - v_0)^2} \tag{2.18}$$

where Δv_l is the Lorentzian component of the full width at half maximum (FWHM), calculated by summing the contributions to broadening by all collision partners i:

$$\Delta v_l = 2 \sum_i \gamma_i \; p_i \tag{2.19}$$

where γ_i is the broadening coefficient for the probed molecule colliding with molecules of species i and p_i is the partial pressure of i. Broadening parameters are quoted in the HITRAN database for broadening by air, γ_{air}, and self-broadening, γ_{self}. These parameters were used to calculate lineshape as a first approximation. However, the constituent molecules in air do not broaden the line to the same degree,[121] and the relative concentrations of gases in inhaled and exhaled breath do not exactly match that of air. Therefore, broadening coefficients to quantify the contribution to the Lorentzian linewidth of each transition by collisions with O_2, CO_2, H_2O and N_2 had to be determined and are displayed in Table 2.2. Notably, the high polarity of H_2O results in a significantly greater contribution from self-broadening to the H_2O linewidth.

Molecule	O_2	CO_2	H_2O	H_2O
Wavelength (nm)	764.28	2004.02	1368.60	1854.03
γ_{N_2} (cm^{-1} atm^{-1})	0.048	0.077	0.104	0.108
γ_{O_2} (cm^{-1} atm^{-1})	0.047	0.066	0.055	0.057
γ_{CO_2} (cm^{-1} atm^{-1})	0.057	0.080	0.152	0.140
γ_{H_2O} (cm^{-1} atm^{-1})	0.070	0.135	0.541	0.525

Table 2.2: Broadening coefficients for the spectroscopic transitions employed in the molecular flow sensor. All broadening coefficients are defined at 296 K and reported in cm^{-1} atm^{-1}.

The broadening coefficients shown in Table 2.2 are defined for a reference temperature, T_{ref}, of 296 K. The temperature-dependent contribution to broadening from each molecular species is calculated according to:

$$\gamma(T) = \gamma(T_{ref})\left(\frac{T_{ref}}{T}\right)^n \tag{2.20}$$

where n is the broadening exponent, which is reported in HITRAN as ~ 0.7 for all molecules of interest in this work.[122]

Collisions between molecules also have the effect of shifting the transition energy relative to that in a vacuum, v_0 reported in Table 2.1 by:

$$v' = v_0 + \sum_i \delta_i \, p_i \tag{2.21}$$

with v' denoting the pressure-shifted transition energy and δ_i and p_i are the shift coefficient and partial pressure of species i respectively. These shift coefficients are also reported in HITRAN and are of the order of 0.005 cm^{-1} atm^{-1} and the effect was determined to have negligible effect on the measurements obtained from the MFS.

The dominant contribution to inhomogeneous broadening arises from the Doppler effect. This describes the frequency shift that results from the the relative motion of the absorbing molecule with respect to the radiation source. The Maxwellian distribution of molecular gas velocities gives rise to the Gaussian lineshape, which is described by:

$$G(v) = \frac{2}{\Delta v_g}\sqrt{\frac{\ln 2}{\pi}}\,\exp\left[-\frac{4\ln 2(v-v_0)^2}{\Delta v_g^2}\right] \tag{2.22}$$

where Δv_g is the full-width at half maximum (FWHM) Gaussian component, given by:

$$\Delta v_g = 2v_0\sqrt{\frac{2\ln 2\ k_B T}{Mc^2}} \tag{2.23}$$

for an absorber with molecular mass M and central transition frequency v_0. This effect does contribute substantially to the broadening in the IR region at gas temperatures found in human inspiration and expiration, so must be accounted for in calculating lineshape.

With significant Lorentzian and Gaussian contributions to the lineshape, a Voigt profile is required to best fit the measured spectrum. This is a convolution of the Lorentzian and Gaussian components, given by:

$$V(v) = \frac{2}{\Delta v_g}\sqrt{\frac{\ln 2}{\pi}}\ \frac{y}{\pi}\ \int_{-\infty}^{+\infty} \frac{e^{-t^2}}{y^2 + (x-t)^2}\ dt \tag{2.24}$$

where x and y are the detuning and Lorentzian widths respectively, both normalised to the Gaussian FWHM:

$$x = \sqrt{\ln 2}\ \frac{2(v - v_0)}{\Delta v_g} \tag{2.25}$$

$$y = \sqrt{\ln 2}\ \frac{\Delta v_l}{\Delta v_g} \tag{2.26}$$

For comparison of their respective lineshapes, Lorentzian, Gaussian and Voigt profiles are displayed in Figure 2.13. All three lineshapes have an equal FWHM of 1 au and the same integrated area of 1 au^2, where au is an arbitrary unit.

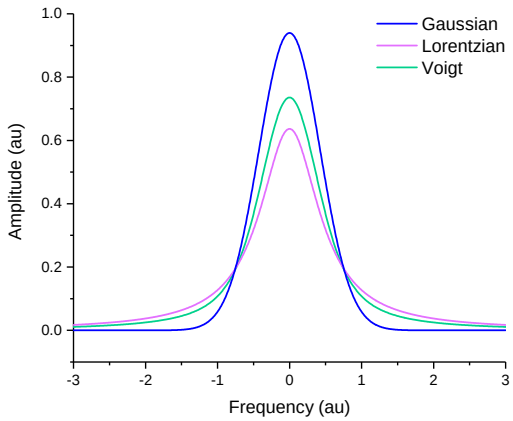


Figure 2.13: Comparison of Gaussian, Lorentzian and Voigt lineshapes. All three profiles have equal FWHM (1 au) and integrated areas (1 au^2). The Gaussian and Lorentzian contributions to the Voigt profile are equal in the above plot.

Sample absorption spectra, converted from the measured transmission spectra using the Beer-Lambert Law, are displayed in Figure 2.14. Their fitted Voigt profiles are also shown, as well as the residuals from subtracting the measured absorption spectrum from the fitted spectrum, which illustrate the excellent fits to the data.

The accuracy of concentration measurements for O_2 and CO_2 can be easily verified using gravimetrically certified reference gases, such as those used to determine V-path length in Figure 2.11. However, obtaining a reference measurement for the concentration of H_2O poses a greater challenge. To achieve this, an Optidew Series

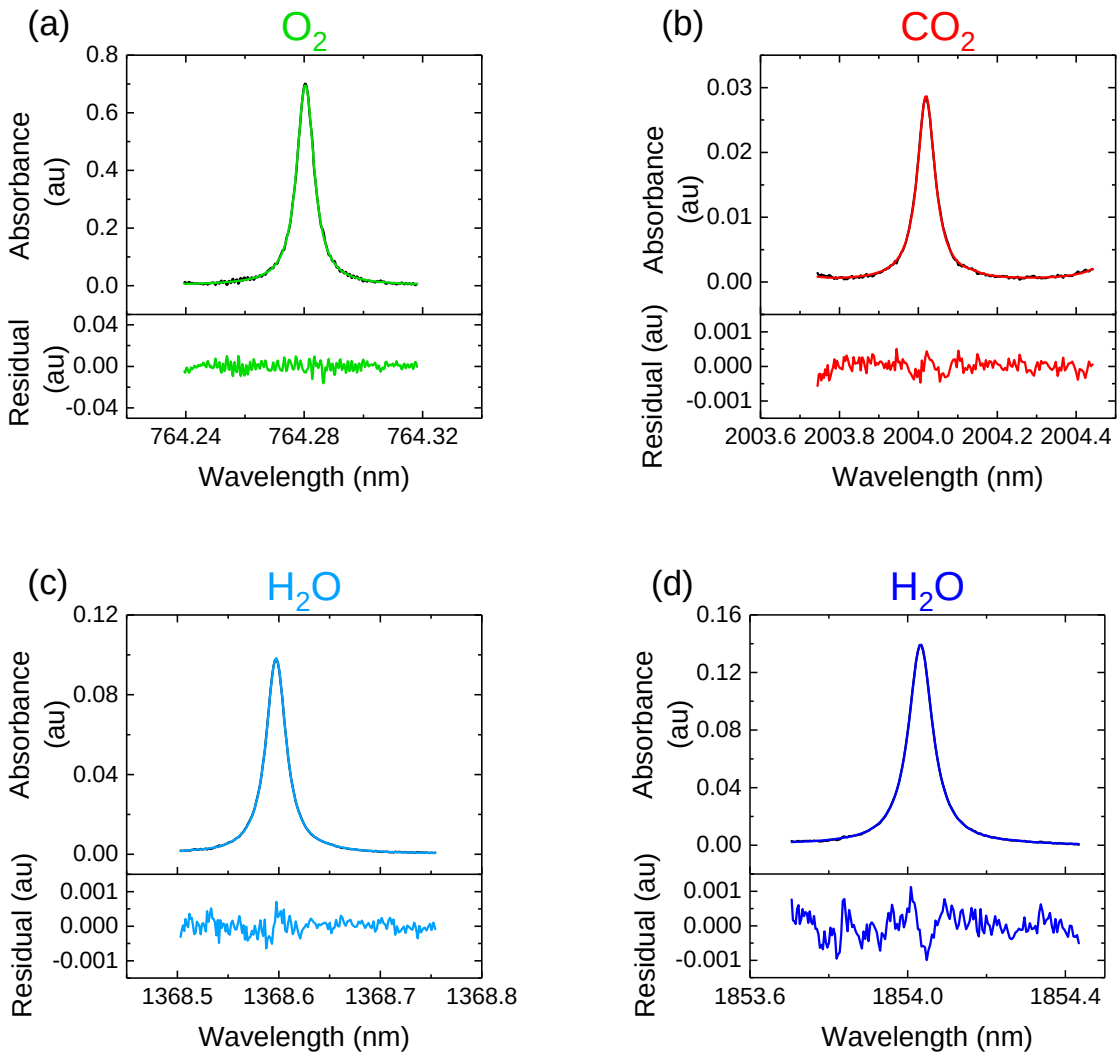


Figure 2.14: The four spectra for measuring (a) O_2 at 764nm, (b) CO_2 at 2004 nm, (c) H_2O at 1369 nm and (d) H_2O at 1854 nm are displayed and overlaid with fitted Voigt profiles. Residuals providing a measurement of the quality of the fit are also shown.

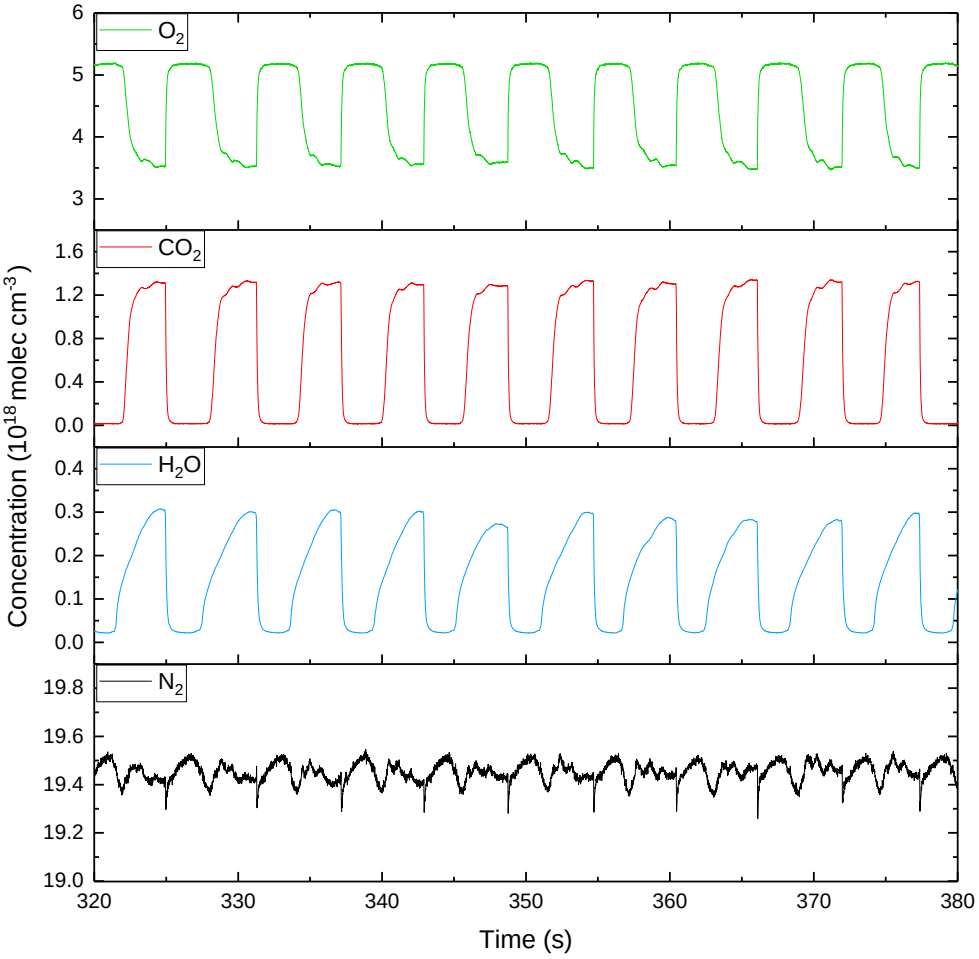


Figure 2.15: Calculated number densities of O_2, CO_2, H_2O and N_2 as a subject breathes air.

precision hygrometer (Michell Instruments), which measures the concentration of water using optical dew-point measurements, was connected in series with the MFS. Mass flow meters were then used to vary the balance of input dry N_2 directly from a cylinder and wet N_2 flowed through a humidifier. Simultaneous measurement of a range of water concentrations allowed further refinement of the H_2O channel, as the broadening coefficients (γ) and absorption cross sections (σ) are not well documented for these absorption lines.[122] As expected, the MFS showed a linear response to increasing H_2O concentration.

Using the concentration measurement calculations for O_2, CO_2 and H_2O detailed in this section alongside the total number density determined in the previous section

means that number densities and hence gas fractions can be calculated for O_2, CO_2, H_2O and N_2. Figure 2.15 shows the variation in number density of the four gas species over the same measurement period as the pressure, temperature and number density data shown in Figure 2.5.

2.3.4 Application of RF

The signal to noise ratio of a CEAS system using a 764 nm laser to detect O_2 was shown to be improved by the application of radio frequency (RF) noise to the laser injection current by Ciaffoni *et al.*.[123] This perturbation results in small, random fluctuations of the output wavelength. Hence residual mode structure is minimised, improving the SNR and minimum detectable concentration.

Despite refinement of the broadening coefficients used to fit the measured spec-

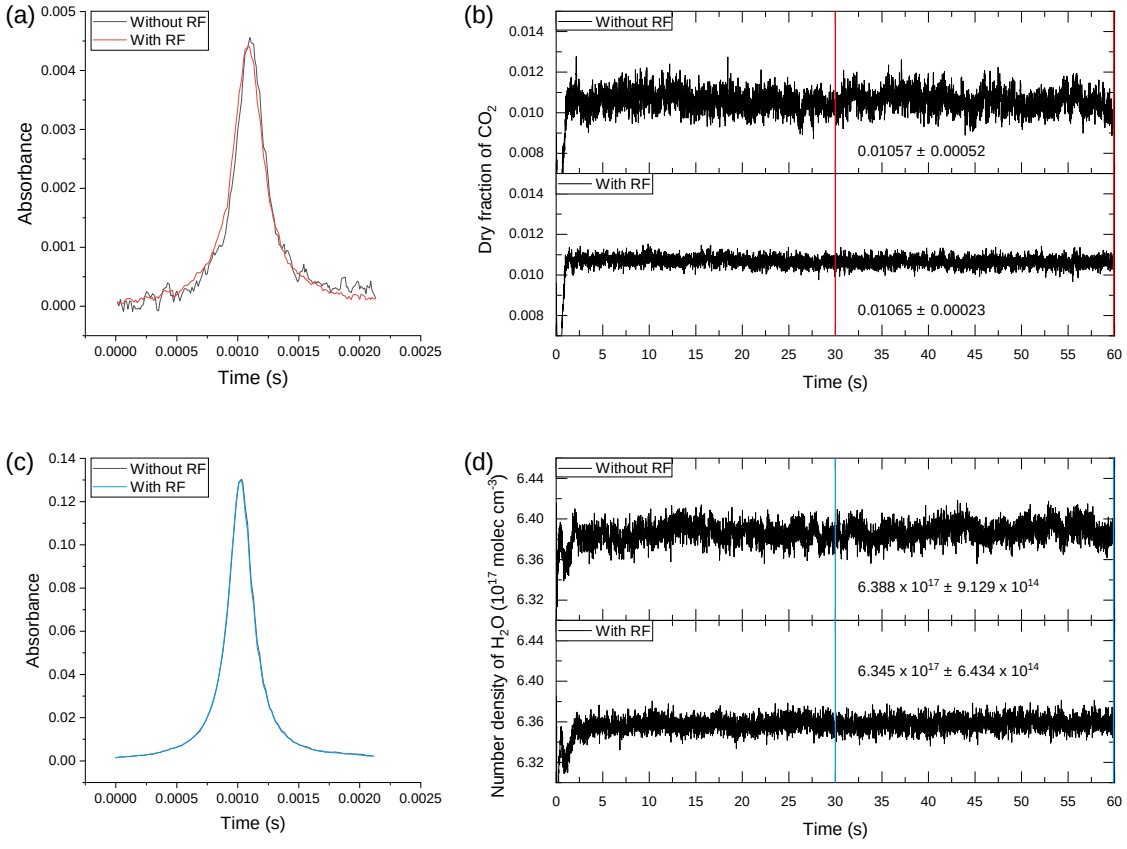


Figure 2.16: Sample spectra and measured dry gas fraction or number density for (a)-(b) CO_2 and (c)-(d) H_2O, in the absence and presence of RF modulation applied to each laser. Mean ± S.D., averaged between 30 s and 60 s (indicated by red or blue lines) is shown for both.

tra, the residuals still showed significant deviation from zero (particularly at high H_2O concentrations). The size of this effect varied between devices and spectroscopic channels and appeared to arise from unwanted back reflections within the lasers themselves, as changing other optical components had no effect on the magnitude of the residuals to the fits. The application of radio-frequency (RF) noise as a technique for improving signal to noise ratio (SNR) of the CO_2 and H_2O channels was investigated and found to significantly improve measurement sensitivity without having a significant effect on the spectral broadening. Figure 2.16 shows sample data comparing exemplar spectra and 1 minute of CO_2 and H_2O concentration data from a steady flow of 1% CO_2 and humidified N_2. The reduction in the standard deviation of the concentration measurements is evident for both spectroscopic channels when RF is applied.

2.4 Flow Sensing

Accurate flow sensing throughout the breath cycle is challenging due to the constant changes in temperature, pressure and gas composition. Continuous monitoring of these parameters within the MFS allows dynamic recalibration of the flow meter, providing a precision improvement of an order of magnitude when compared to other respiratory flow meters.[5] The MFS uses a modified Lilly-type pneumotachograph that uses a pair of wire mesh screens to produce a small pressure drop that is measured with two separate banks of pressure sensors. Each bank contains four ± 2.5 mbar piezoelectric membrane differential pressure sensors (HCLA, Sensortechnics) with 12-bit resolution that communicate with the controller via an I2C bus. Averaging the outputs of these four sensors improves the SNR of the differential pressure measurements.

The banks can be separately disconnected from the measurement cell using miniature changeover valves (X112SFB, Parker Hannifin) to enable alternating recalibration of the two banks while still recording flow data. It is necessary to recalibrate the zero point of the sensors at regular intervals due to the poor long-term drift rejections of piezoelectric membranes. Flow measurement ports provide the differential pressure sensors with gas at the ambient pressure of the measurement cell via thin, flexible, silicon tubes. Each port contains 16 holes spaced evenly around the ring to sample the gas in the measurement cell. A schematic of the flow sensor is displayed in Figure 2.17.

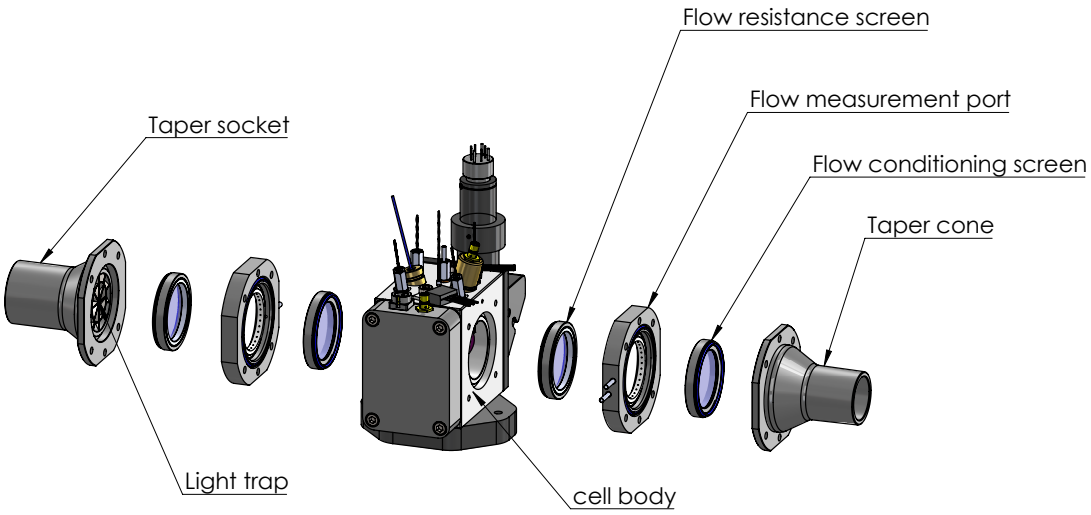


Figure 2.17: Components of the flow sensor which occupies the same axis as the gas flow path.

The nature of flow through a pipe depends on the dimensionless Reynolds number, calculated from the density, ρ, viscosity, μ, pipe diameter, d and gas velocity v:[124]

$$Re = \frac{\rho v d}{\mu} \tag{2.27}$$

If the Reynolds number is below 2320, the flow will be laminar; above 4000 it will be turbulent and between these values the flow will have laminar and turbulent contributions. As the Reynolds number exceeds 2320 during respiratory exchange, both laminar and turbulent flow must be considered when modelling flow through the MFS. The laminar component of the flow is dependent on the viscosity according to Poiseuille's law, while changes in geometry causing turbulent flow depends on the density.

To account for both factors, the pressure drop, ΔP across the wire meshes in the MFS, is related to the volumetric flow rate, $\dot{V}$, by:[125]

$$\Delta P = \alpha \mu \dot{V} + \beta \rho \dot{V}^2 \tag{2.28}$$

The parameters α and β are constants unique to each MFS unit and are determined through a flow calibration procedure.

The calibration procedure uses a mechanical pump programmed with two separate calibration schemes which consist of 22 pump strokes producing a range of known peak flow rates and stroke volumes. Flow data is recorded for 6 runs of each calibration

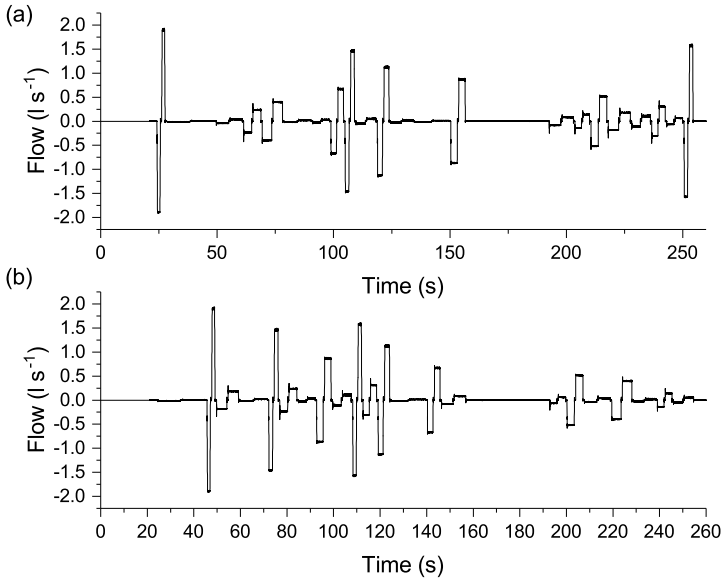


Figure 2.18: Example flow calibration data from the two calibration programs.

program. Data recorded for a single run of each program is displayed in Figure 2.18. The results from 12 calibration runs carried out on a single device are summarised in Table 2.3. The flow rate is integrated to provide measurements of the stroke volumes. These can then be compared to the known stroke volumes of the mechanical pump to obtain best fit values of α and β for the range of stroke volumes and peak flow rates in the calibration program. The final values of α and β are the mean of the values calculated from across the twelve runs. The sample results show that the means from the two calibration programs lie within the estimated error bars and hence the determined parameters are independent of the order of flow rates used in the calibration.

Importantly, the instantaneous viscosity and density used in Equation 2.28 are calculated from the spectroscopically determined gas composition. The instantaneous

Program	α ($\times 10^9$ mbar kg^{-1} m^{-2} s^2)	β ($\times 10^6$ mbar kg^{-1} m^{-3} s^2)
1	0.882 ± 0.008	0.252 ± 0.007
2	0.875 ± 0.005	0.249 ± 0.006
Mean	0.878 ± 0.007	0.250 ± 0.006

Table 2.3: Sample mean flow parameters determined from 6 runs on each calibration program. Errors shown represent $\pm 1\sigma$.

Molecule	Density (kg m^{-3})	Viscosity (µPa s)	Sutherland constant (K)
O_2	1.429	18.90	127
CO_2	1.977	13.90	240
H_2O	0.804	8.82	-
N_2	1.251	16.63	111
Ar	1.784	20.96	144

Table 2.4: Literature values for density and viscosity and Sutherland constants, all at 273.15 K and 1 atm.[126]

density of the gas in the MFS measurement cell is calculated according to:

$$\rho = \frac{P}{P_0}\frac{T_0}{T}\sum_{i=1}^{n}\rho_i F_i \tag{2.29}$$

where F_i is the fractional concentration of species i, T_0 is the reference temperature at which the density of the species, ρ_i is defined and P and T are the measured pressure and temperature values in the sample respectively. Literature values for the density, measured at a reference temperature of 273.15 K, are displayed in Table 2.4.

The temperature dependent viscosity, μ_i, of a pure gaseous species i can be calculated using the Sutherland equation:

$$\mu_i = \mu_0 \frac{T_0 + S}{T + S}\left(\frac{T}{T_0}\right)^{\frac{3}{2}} \tag{2.30}$$

where μ_0 is the viscosity at a reference temperature, T_0 of 273.15 K, T is the temperature of the gas flow and S is the Sutherland constant.[127] The literature values for the viscosities and the Sutherland constants are reported in Table 2.4. The Sutherland law used to calculate these viscosities assumes weak intermolecular interactions, which is sufficient for all molecules of interest in the MFS apart from H_2O, due to its highly polar nature. Therefore the viscosity of H_2O is instead calculated from coefficients determined experimentally by Teske *et al.*.[128] The determination of the dynamic viscosity of the gaseous mixtures measured by the MFS is based on Sutherland's approximation,[129] calculating the viscosity of a gas mixture, μ_{mix}, according to:

$$\mu_{mix} = \sum_{i=1}^{n}\frac{x_i\mu_i}{x_i + \sum\limits_{j=1,j\neq i}^{n}\Phi_{ij}x_j} \tag{2.31}$$

where x_i is the mole fraction of i and Φ_{ij} is determined using the method developed by Brokaw.[130] The calculation of Φ_{ij} uses the pure viscosities, molecular weights, boiling points, boiling point densities and dipole moments and is highly accurate under the conditions present within the MFS, with a reported error of $< 4\%$ for estimating the viscosity of mixtures of polar and non-polar gases.[130]

In the first 20 s of operation, the HCLA pressure sensors undergo a zeroing calibration period, which is repeated at intervals of 160 s throughout the operation of the device. A change in the measured gas concentrations was observed during these zeroing periods and was particularly evident on the O_2 channel, as seen in Figure 2.19 (a). This step-change was attributed to the sensitivity of the control electronics. Specifically, the electrical cable between the base unit and the head increases the impedance of the earth return. Therefore, when the valves are switched on and they draw current from the base unit, there is an increase in the voltage drop on the earth return. This resulted in a corresponding change in the photodiode readings measured in the base unit. Hence the measured gas concentrations showed a step-change at the beginning and end of the flow sensing zeroing periods. To correct this problem, an additional circuit board was added. This addition ensures that the head unit draws the same current whether the valves are operating or not. When the valves are switched off, as is the case during the zeroing period, the circuit draws an equivalent current through a resistor of the same impedance as the valves. This eliminates the increase in voltage drop on the earth return and hence eliminates the step change in oxygen concentration measurement, as demonstrated in Figure 2.19. This solution was implemented in both units.

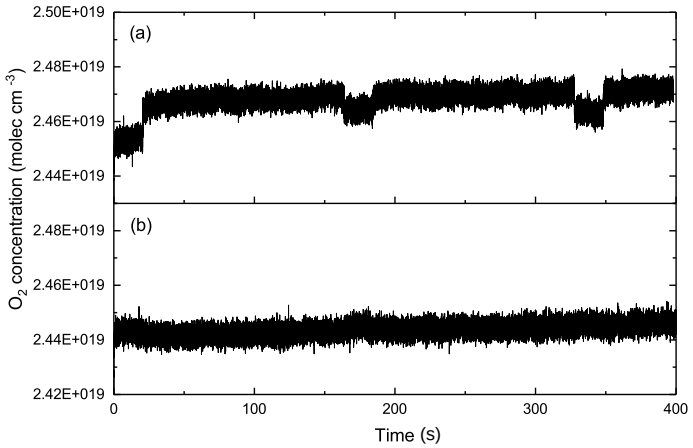


Figure 2.19: The measured O_2 concentration (a) prior to and (b) after adding the additional circuit board.

2.5 Validation of MFS Performance

The gas fractions of each molecular species can be calculated using the total number density (sample data shown in Figure 2.5) and the individual number densities (sample data shown in Figure 2.15). The contemporaneous measurements of fractional molecular concentrations, $F_i(t)$, and total flow, $\dot{V}(t)$, can then be used to calculate the cumulative volume uptake, V_i, and hence rate of consumption of each molecular species, $\dot{V}_i$, according to:

$$V_i = \int_t^{t+\Delta t} \dot{V}(t) \cdot F_i(t)\, dt \tag{2.32}$$

$$\dot{V}_i = \frac{1}{\Delta t} \int_t^{t+\Delta t} \dot{V}(t) \cdot F_i(t)\, dt \tag{2.33}$$

where i can be O_2, CO_2, H_2O or N_2.

A human participant can then breathe through the device via a mouthpiece from a supply of air/medical grade O_2. Figure 2.20 shows the measured O_2, CO_2, H_2O and N_2 cumulative volume uptake as a participant breathes air for 10 minutes followed by a period of 5 minutes of breathing medical grade O_2, which mimics the scenario in critical care of increasing a ventilated patient's fraction of inspired O_2 (discussed further in Chapter 3) or performing a N_2 MBW test (such as those detailed in Chapters 4-6). The device's precision is illustrated by integrating the N_2 flux and showing that this exchange is near zero, as a person's FRC lung volume should remain constant if they retain the same posture for the duration of the test and hence should neither produce nor consume N_2. The value of the air-breathing N_2 exchange rate for this washout shows a low N_2 consumption of 1.9 mL min^{-1}, demonstrating successful calibration. During the final minute of the O_2 breathing time period, the subject had successfully washed the N_2 from the their lungs, indicated by the low peak inspired fraction of N_2 and the asymptote observed on the N_2 cumulative volume uptake plot. The applications of this MBW procedure for assessing pulmonary function is detailed in subsequent chapters.

This chapter has outlined the operation, development and optimisation of two MFS devices, that differ only in the wavelengths at which they probe H_2O. Both show excellent performance in terms of nitrogen balance and are able to be deployed in small scale clinical trials in adults, which are described in the following chapters.

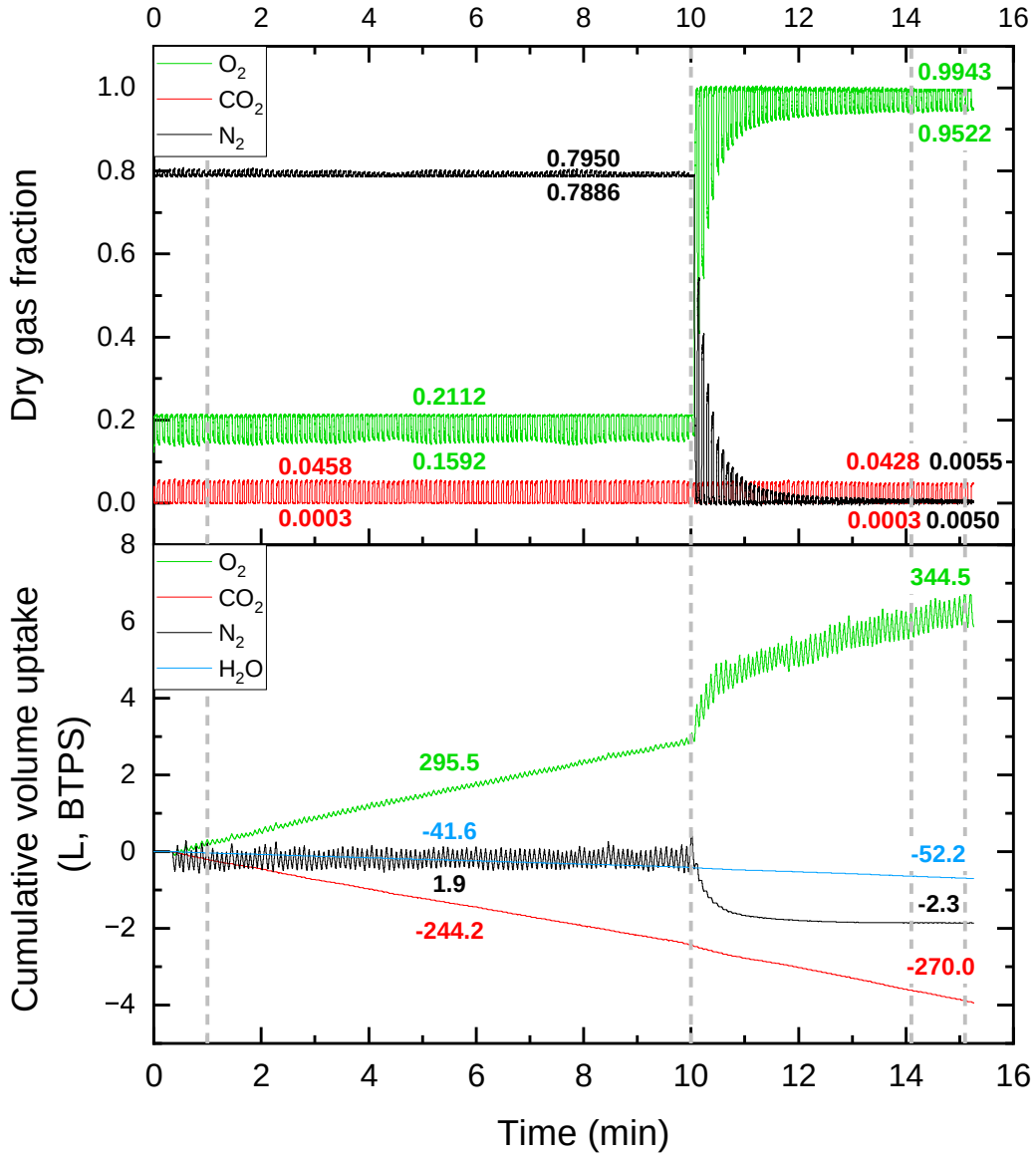


Figure 2.20: Sample dataset of a volunteer breathing through an MFS: 10 minutes of air followed by 5 minutes of medical grade O_2. The grey dashed lines indicate two time periods used in the calculations: the 9 minutes of complete breaths prior to the switch to breathing O_2 and the final 1 minute of complete breaths at the end of the washout. Displayed are the measured dry gas fractions, labelled with peak inspiratory and peak expiratory fractions and cumulative uptake volumes with the rate of exchange in L/min at BTPS for each gas indicated for the two time periods.

Chapter 3

Monitoring Oxygen Consumption Rates in Critical Care

The molecular flow sensor provides an accurate measure of gas exchange rates and as such has great potential for patient monitoring in critical care. Insufficient supply of oxygen to the body's tissues is a common feature in many serious illnesses. Perhaps the most impactful potential application of the MFS device in this setting is monitoring patients experiencing septic shock, the most severe subset of sepsis. Sepsis is characterised by profound circulatory, cellular, and metabolic abnormalities in response to an infection,[131] which leads to an inability to extract sufficient O_2 from the blood to meet the requirements of the tissues.[132,133] In 1998, the mortality rate for patients in septic shock was 50%.[134] A systematic review of 783 articles reporting mortality rates for septic shock between 2009 and 2019 found a mean septic shock 90-day mortality rate of 38.5%.[135] As mortality rates for sepsis and septic shock remain high, there is significant interest in identifying clinical indicators to guide treatment to improve patient outcomes.[135] For example, in the treatment of sepsis, targeting five indicators of the amount of oxygen delivered to the tissues ($\dot{D}_{O_2}$) has been shown to improve patient outcomes in what is known as Early Goal Directed Therapy.[136] It may therefore prove true that directly measuring the body's ability to use O_2, i.e. the rate of oxygen consumption, $\dot{V}_{O_2}$, offers a superior indicator to target, given suitable equipment to do so. Hirayama *et al.* found the rate of decline of a sepsis patient's $\dot{V}_{O_2}$ or $\dot{V}_{CO_2}$ (rate of CO_2 production) over time was significantly different between surviving and non-surviving participants in the study, with non-survivors declining at a higher mean rate.[137] However, the commercially available CCM Express device used by Hirayma *et al.* has an upper limit of 60% inspired O_2,[138] so would not be suitable for use in patients who require a higher fraction of O_2 - indeed 3 patients were excluded from the aforementioned study on this basis.[137] The MFS also offers a faster

response time (10 ms compared to 130 ms), greater accuracy for the O_2 measurements (0.45% compared to $< 1\%$) and significantly better volume accuracy (0.2% compared to 3%).[5,138]

Prior to the body of work presented in this thesis, the suitability of the MFS for patient monitoring in elective surgery had been demonstrated by Ciaffoni *et al.*.[5] However, the intensive care unit (ICU) presents a more challenging setting, due to the varying partial pressure of O_2 (PP_{O_2}) delivered to the patient and frequent therapeutic interventions. This chapter presents data from an observational study in the Adult Intensive Care Unit (AICU) at the John Radcliffe Hospital in Oxford, where patients were monitored using the MFS for the first time. Further details surrounding the motivations for a study using the device in this setting are provided, followed by the study design. Data collection for this study, which initially aimed to recruit 30 patients, began in February 2020. However, after the recruitment of just two ventilated ICU patients, who were each successfully monitored over a period of hours, the introduction of restrictions in response to the COVID-19 pandemic precluded further recruitment and data collection. The two sample datasets are used to illustrate the potential applications of the technique in this setting and its ability to provide clinically useful information to clinicians is discussed, as well as likely future avenues of research involving the MFS in an AICU.

3.1 Motivation for Study

Two quantities are vital to understanding the availability of oxygen to the body tissues. The first of these is the global oxygen delivery, $\dot{D}_{O_2}$, defined as the total amount of oxygen delivered to the tissues per minute irrespective of the distribution of blood flow.[139] This is the product of cardiac output ($\dot{Q}$) and the oxygen content of arterial blood, Ca_{O_2}.[140] The second is the global oxygen consumption, $\dot{V}_{O_2}$, which is the total amount of oxygen consumed by the tissues per minute. When respiration is aerobic this corresponds to the metabolic rate.[140] The relationship between these two quantities is illustrated in Figure 3.1. When a person's $\dot{D}_{O_2}$ is low, they are in a supply dependence regime, where their $\dot{V}_{O_2}$ is dependent on $\dot{D}_{O_2}$. Above a critical value of $\dot{D}_{O_2}$, $\dot{V}_{O_2}$ becomes supply independent and any increase in $\dot{D}_{O_2}$ will not increase the person's $\dot{V}_{O_2}$. A patient with severe pathology such as septic shock or respiratory failure may have increased metabolic needs,[141] as indicated in Figure 3.1 by the higher plateau value of $\dot{V}_{O_2}$ compared to the healthy baseline.

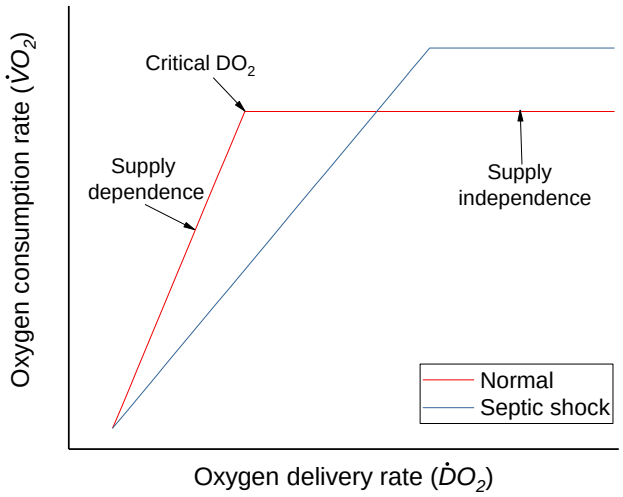


Figure 3.1: A simplified schematic demonstrating the relationship between rate of O_2 delivery, $\dot{D}_{O_2}$, and rate of O_2 consumption, $\dot{V}_{O_2}$ in a normal healthy person and a person in septic shock based on the review by Rocha *et al.*.[142]

In healthy subjects, a decrease in $\dot{D}_{O_2}$ can be compensated for by increasing the rate at which oxygen is extracted from the blood, so $\dot{V}_{O_2}$ remains unaffected. However, it has been proposed that this process is impaired in patients in critical care.[143] Therefore, these patients may require an abnormally high $\dot{D}_{O_2}$ in order to maintain an adequate $\dot{V}_{O_2}$, as shown in Figure 3.1.[142] Shoemaker *et al.* showed improved outcomes in high risk surgical patients when $\dot{Q}$ and hence $\dot{D}_{O_2}$ was increased,[144] and a later observational study showed that a patient's ability to increase their $\dot{Q}$ was associated with improved outcome.[145] In the study detailed in this chapter, cardiac output was not measured, but the potential to extend the capability of the device to measuring cardiac output through the use of trace gases in the future is discussed in Section 3.5. However, a direct measurement of $\dot{V}_{O_2}$ may be far more useful to clinicians, as currently they do not routinely have a direct measure of whether any increase in a patient's $\dot{D}_{O_2}$ causes a corresponding increase in $\dot{V}_{O_2}$. For example, in patients in cardiogenic shock, normalizing $\dot{Q}$ and $\dot{D}_{O_2}$ is insufficient to prevent mortality, suggesting a failure of $\dot{Q}$ and $\dot{D}_{O_2}$ to reflect dysfunction in the utilisation of O_2 at a cellular level.[146]

A range of treatment options are available to clinicians to increase $\dot{D}_{O_2}$. Examples include increasing a patient's inspired fraction of O_2, drug treatments to increase blood pressure (vasopressors such as noradrenaline and dopamine) or make the heart

pump blood harder (such as dobutamine), blood transfusions to increase the volume of oxygen rich blood delivered to the tissues and mechanical ventilation to increase the supply of oxygen to the blood.[147,148] However, these interventions sometimes provide no benefit and can even have some undesirable consequences. For example, higher doses of the vasopressor noradrenaline is posited to have an increasing adverse immunomodulatory effect.[149] A higher dosage of noradrenaline was not found to impact 28-day mortality, but did result in fewer ventilator free days.[150] Patients with septic shock who had been well fluid-resuscitated were treated with the drug dobutamine, an inotropic drug to increase cardiac contractibility and hence $\dot{Q}$ and $\dot{D}_{O_2}$, but showed no increase in tissue oxygen consumption.[151] Treating patients with a high inspired oxygen fraction for an extended period of time has been shown to cause severe hyperoxic acute lung injury (HALI) leading to permanent dysfunction.[152] Therefore, if patients are in a supply independent regime, as shown in Figure 3.1, any treatment to further increase $\dot{D}_{O_2}$ may cause increasing harm, yet with no increase in O_2 uptake.

Prior studies into the effect increasing $\dot{D}_{O_2}$ has on $\dot{V}_{O_2}$ have been limited by the technology available. As there is currently no satisfactory method for non-invasive monitoring of oxygen consumption on ICU wards,[36] studies have relied on indirect measurements, including arterial and venous blood gases and blood lactate concentrations.[153] Studies using these measures for early goal directed therapy (EGDT) have shown significant promise in improving outcomes when treating severe sepsis and septic shock in its early stages,[153,154] and accurate real-time assessment of $\dot{V}_{O_2}$ may provide a useful indicator in future studies.

Because the MFS simultaneously measures both $\dot{V}_{O_2}$ and $\dot{V}_{CO_2}$, the respiratory quotient (RQ) can easily be obtained. RQ measured using indirect calorimetry was shown to correlate with two useful clinical metrics, namely the length of stay in ICU and duration of mechanical ventilation in polytrauma patients with parenteral nutrition.[155] As RQ is determined by the macronutrients being metabolized, changes in RQ can indicate either under or overfeeding of the patient, both of which have adverse effects.[156]

Patients admitted to ICU require careful assessment of their energy expenditure (EE), such that appropriate levels of nutrition can be supplied. There are three ways of achieving this. The first and preferred method is indirect calorimetry,[157] where direct measurements of $\dot{V}_{O_2}$ and $\dot{V}_{CO_2}$ are used in conjunction with the Weir equation to calculate the energy expenditure in kcal/day:[158]

$$\text{EE} \;=\; 1440\,(3.94\,\dot{V}_{O_2} \;+\; 1.11\,\dot{V}_{CO_2} - 2.17\,TUN) \tag{3.1}$$

where $\dot{V}_{O_2}$ and $\dot{V}_{CO_2}$ are measured in L/min and TUN, the total urinary nitrogen, is measured in g/day. The urinary output is frequently excluded as it only contributes $\sim 1-2\%$ of the total EE.[159] However, the equipment to perform indirect calorimetry is not widely available. The second method uses measurement of $\dot{V}_{CO_2}$ without measurement of $\dot{V}_{O_2}$. The estimation of RQ (usually estimated to be 0.85 based on the standard proportions of macronutrients given to patients) can then be used alongside $\dot{V}_{CO_2}$ in place of $\dot{V}_{O_2}$ in the indirect calorimetry equations.[160] This showed better agreement with indirect calorimetry than the third method, the use of predictive equations, which is the least accurate method.[160,161] A range of different equations have been proposed, using some combination of a patient's age, weight, height, sex, respiratory minute volume (the volume of gas inhaled or exhaled per minute) and body temperature to predict EE, but these show poor agreement with indirect calorimetry.[161–164] A short period of measuring $\dot{V}_{O_2}$ and $\dot{V}_{CO_2}$ using the MFS could be a simple non-invasive way to improve estimations of patients' EE and hence more accurately predict their feeding requirements.

The aims of this study were manifold: to demonstrate the suitability of the technique for use in an intensive care setting, to establish a 'normal' range of oxygen consumption for ventilated patients in critical care and identify treatments that alter $\dot{V}_{O_2}$. This could then lead to future interventional studies where patients who fall below the normal range are identified and treatment could be tailored according to a patient's individual changes in $\dot{V}_{O_2}$ in response to interventions.

3.2 Methods

Two patients admitted to the Adult Intensive Care Unit (AICU) at the John Radcliffe Hospital were recruited to the study by Dr. Killian Donovan and Dr. Akshay Shah. Due to the COVID-19 pandemic, patient recruitment was paused indefinitely in March 2020, so the initial target of recruiting 30 patients could not be achieved. The research study's associated ethical application, "Oxygen consumption in critical illness", was approved by the National Research Ethics Service Committee East of England - Cambridge Central (REC reference 14/EE/0003).

Male and female patients aged 18 and over who were admitted to an Adult Intensive Care Unit with an expected duration of intubation and mechanical ventilation of 48 hours or more were eligible for the study. Any patients for whom the use of active humidification was indicated, such as those with heavy sputum production, were excluded from participating. As the critically ill patients recruited for this study lacked



Figure 3.2: A healthy volunteer demonstrating the set-up of the MFS connected in-line to a ventilator tubing system.

capacity to provide consent prior to enrolment, a suitable consultee was sought to advise on whether the patient would be likely to give consent. If the patient survived and regained capacity during their hospital admission, consent to use the data was sought from the patient.

As a purely observational study, no clinical interventions were performed. The only deviation from routine patient care was the addition of the MFS to the breathing circuit (as shown in Figure 3.2), adding approximately 80 ml of additional dead space to the ventilator circuit. This was accounted for when configuring the ventilator settings. In the AICU, active humidification is used for ventilated patients as routine (although other units do use passive humidification). However, at the point of obtaining ethical approval for the study, it was not possible to obtain highly accurate measurements of oxygen consumption in a patient under active humidification, due to measurement inaccuracies at high humidity levels. Therefore, for the duration of monitoring a patient with the MFS, the humidification system was changed to using an HME filter.

Although ethical approval allowed for gas exchange rates to be recorded by the MFS for up to 48 hours, the start and end points of the observational periods were determined by the clinical team. Any clinical interventions over this time period were recorded with their respective timestamps via the notes function of the LabVIEW software which controls data acquisition by the MFS. When a patient had to be turned, the MFS was briefly disconnected from the ventilator circuit then reattached after the patient had been moved.

3.3 Results

For both patients recruited to this study, gas exchange data was successfully recorded over the entire measurement period. Where patients had to be disconnected from the device due to clinical interventions, successful measurement recommenced upon reconnection in both cases. The addition of the device to the circuit caused no adverse effects to the patients and presented no difficulties to the clinical team providing patient care.

As only two patients were studied, it is not possible to perform any statistical analysis on the data collected about the response of patient groups to clinical interventions. However, for both patients, referred to henceforth as Patient A and Patient B, features of note are discussed to demonstrate the potential of this technique to provide clinically useful information and identify areas upon which future studies could focus.

3.3.1 Patient A

Patient A is a 43 year old female who was admitted with diabetic ketoacidosis, leading to vomiting, aspiration pneumonitis, severe acute respiratory failure and circulatory shock. The observational period began as the patient was recovering, immediately after a sedation hold and weaning from vasopressors. The ventilator was providing pressure support (PS), where each breath is initiated by the patient and both respiratory rate and tidal volume are determined by the patient, but the ventilator provides support by adding a driving pressure upon inspiration specific to the individual's needs.[165]

The MFS was connected in-line with Patient A's ventilator circuit for 2 hours and 35 minutes in total. An overview of the interventions while the patient was studied using the MFS is displayed in Figure 3.3, which shows the recorded gas fractions over the whole study period. Due to the long observation period, the individual breaths are not visible on the main plot, so an enlarged section of the plot is displayed to the right of the main graph, where the 14 breaths during the sample 1 minute period are clearly visible. The variable breath duration visible on this subplot is consistent with a patient managed with pressure support ventilation, where respiratory rate and tidal volume is determined by the patient.[166] Over the observational period the inspired fraction of O_2, F_{I,O_2}, was changed by clinicians multiple times: at the start the patient is being switched from 100% O_2 down to an F_{I,O_2} of 0.5 which was then lowered to 0.45 at 29 minutes. The F_{I,O_2} was then set to 1.00 for two further brief

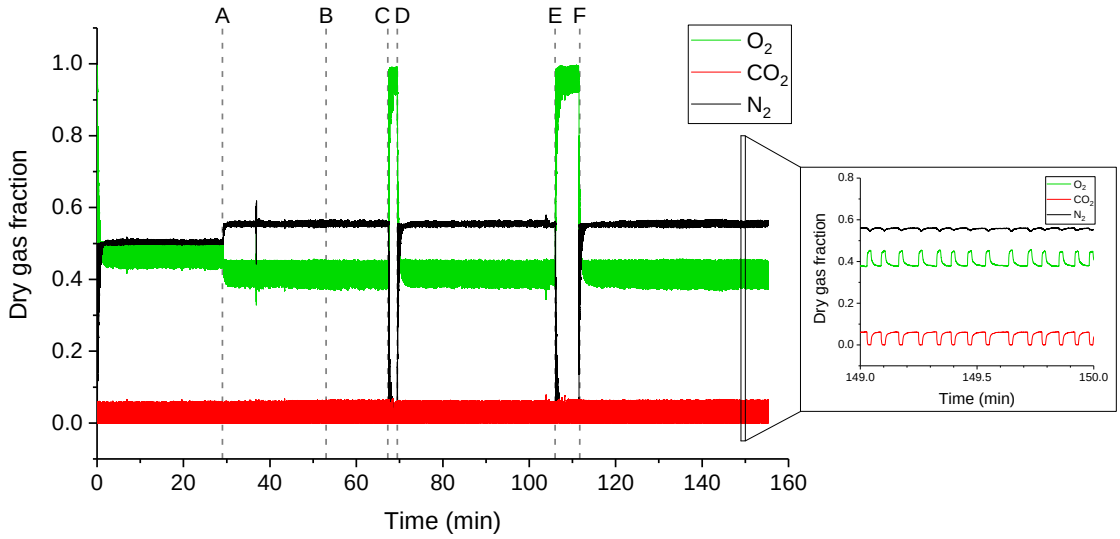


Figure 3.3: Recorded dry gas fractions of O_2, CO_2 and N_2 over the whole time that Patient A was studied using the MFS to the left, with an enlarged plot to the right showing the resolution of individual breaths over a selected 1 minute time period. Clinical interventions/observations at their respective time points during the study are illustrated by dashed lines. A: reduction in F_{I,O_2} from 0.50 to 0.45; B: bolused fentanyl during ward round to control tachypnoea, confluent bilateral infiltrates seen on CT thorax results; C-D: short burst of medical grade 100% O_2 during treatment by physiotherapists, then return to F_{I,O_2} of 0.45; E-F: temporary switch to 100% O_2 for desaturation during roll before again returning to an F_{I,O_2} of 0.45.

bursts for physiotherapy and to correct desaturation due to a roll. Although this is referred to by clinicians as 100% O_2 and hence referred to as such in this thesis, the actual percentage of O_2 would be expected to be slightly lower than this, as medical grade O_2 is supplied with a purity of at least 99.5%. This is consistent with the data recorded here where the actual F_{I,O_2} was found to be 0.995. Similarly the F_{I,O_2} when the ventilator was set to an F_{I,O_2} of 0.45, the measured F_{I,O_2} by the MFS was 0.447.

As described in the previous chapter, the dry gas fractions of O_2, CO_2 and N_2 are obtained by calculating the total number density of the gas passing through the MFS measurement plane using the barometric pressure and temperature measurements, then subtracting the spectroscopically measured water concentration from the total to give the total dry number density. Then the dry gas fractions can be simply calculated using the spectroscopic measurements for O_2 and CO_2 and the remainder can be used to deduce the concentration of N_2. Integrating the product of the gas fractions and the simultaneous measurement of flow gives the volume of a gas species

consumed or produced in a given time period. The MFS software can identify individual breaths and hence calculate the rate of gas consumption or production on a breath-by-breath basis. A sample section of data from Patient A taken at 1hr 6 min into the measurement period is shown in Figure 3.4, which shows the measured flow and dry gas fraction data alongside the calculated gas consumption or production rates for 10 breaths.

The averaged gas consumption rates over the 4 time periods with stable F_{I,O_2} are displayed in Figure 3.5, a cumulative volume uptake plot for O_2, CO_2 and N_2 over the entire measurement period. The gas consumption rates during these times are also indicated on the graph - the time periods immediately after a change of F_{I,O_2} were excluded from the calculations to account for the washin/washout of N_2. Overall the patient shows a general trend of decreasing rates of both O_2 consumption and CO_2 production and notably the highest $\dot{V}_{CO_2}$ and $\dot{V}_{CO_2}$ values correspond to the first time period, when F_{I,O_2} was at its highest maintained value of 0.50, compared to 0.45 for the other three periods. A rate of N_2 consumption of between 14.6 mL/min and 18.4 mL/min was measured across the 4 time periods, demonstrating excellent device stability. In a subject who is not changing position (and hence lung volume at FRC), a rate of N_2 consumption of zero would be expected, as N_2 is neither produced nor consumed in the body's metabolic processes. However, in this case a small consumption or production of N_2 may be expected aside from any measurement error by the MFS. At time point B on Figure 3.3, CT results were returned and showed evidence of bilateral infiltrates - changes in severity could contribute to the exchange rate of N_2 with an improvement leading to an apparent N_2 consumption or deterioration giving an apparent production of N_2 as the available lung volume for gas exchange reduces further. Unlike a volunteer breathing through the MFS in a fixed position during a short test in a lab or clinic, an ICU patient's lung physiology may change over the course of an ICU admission. However, this is not expected to be a major contributor to the rate of N_2 exchange.

The $\dot{V}_{O_2}$ and $\dot{V}_{CO_2}$ measured during these stable F_{I,O_2} time periods could be used to estimate the patient's EE using Equation 3.1, excluding the washout periods directly following a change in F_{I,O_2}. For the four time periods shown in Figure 3.5, the calculated EE would be 1646.2, 1569.0, 1536.7 and 1528.1 kcal/day respectively. Using Patient A's physical characteristics and the predictive equation for the energy expenditure for women, EE (F), proposed by Mifflin *et al.*:[162]

$$\text{EE (F)} = 10W + 6.25H - 5A - 161 \tag{3.2}$$

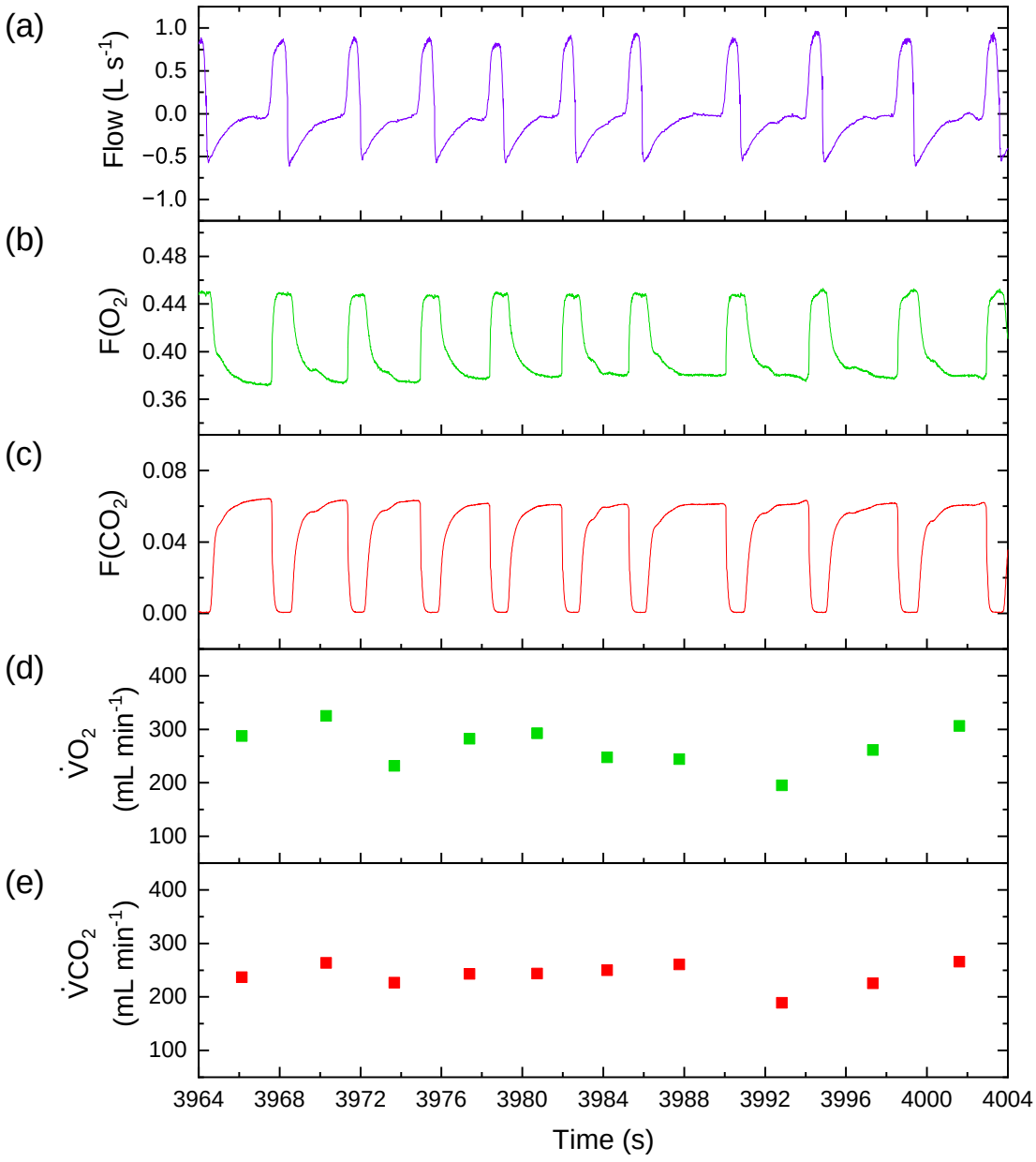


Figure 3.4: A sample 10 breath period showing how the flow (a) and dry gas fractions of O_2 (b) and CO_2 (c) can be used to calculate the gas exchange rates on a breath-by-breath basis: (d) $\dot{V}_{O_2}$ the rate of oxygen consumption and (e) $\dot{V}_{CO_2}$ the rate of CO_2 production.

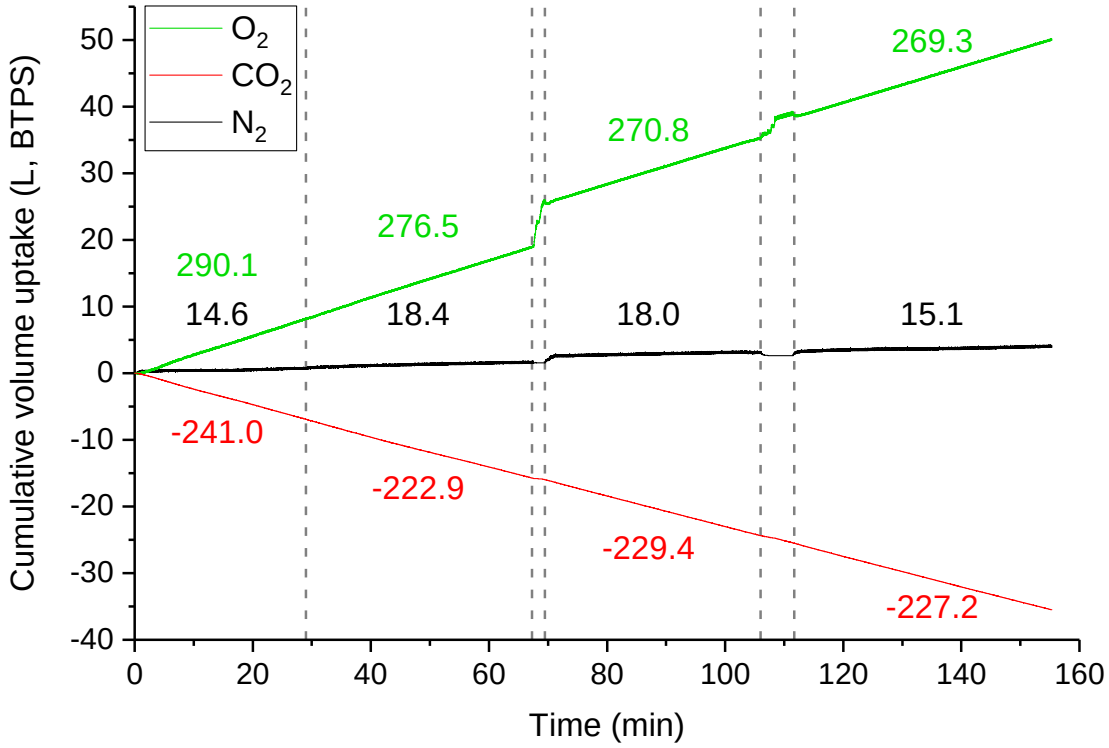


Figure 3.5: Cumulative volume plot showing the uptake of O_2, CO_2 and N_2 over the entire monitoring period. The rate of uptake of each gas species is also indicated for each of the 4 time periods where the patient received a constant F_{I,O_2}, with all consumption rates reported in mL/min. During the first time period, the F_{I,O_2} was 0.50 followed by 0.45 for the latter three sections of the plot. Both O_2 and N_2 show a positive rate of uptake, and hence are consumed, whereas for CO_2 this is negative as CO_2 is produced.

where W is weight in kg, H is height in cm and A is age in years, the estimated EE was 1406 kcal/day. All four MFS measurements indicate a higher than predicted EE for this patient. This difference would be expected for a patient in ICU, as ICU patients have been found to have an elevated EE across multiple studies, with these effects persisting in the weeks immediately following an admission to ICU.[159,167–170]

A simple example of how the MFS could monitor changes in the lungs in a ventilated patient is illustrated in Figure 3.6, which shows how an increase in F_{I,O_2} induces a washout of the N_2 in the lungs as the N_2 is replaced by O_2. In this example the F_{I,O_2} was increased from 0.45 to 1.00, instigating a washout of the N_2 from the patient's lungs. Because this washout data was collected incidentally rather than as a

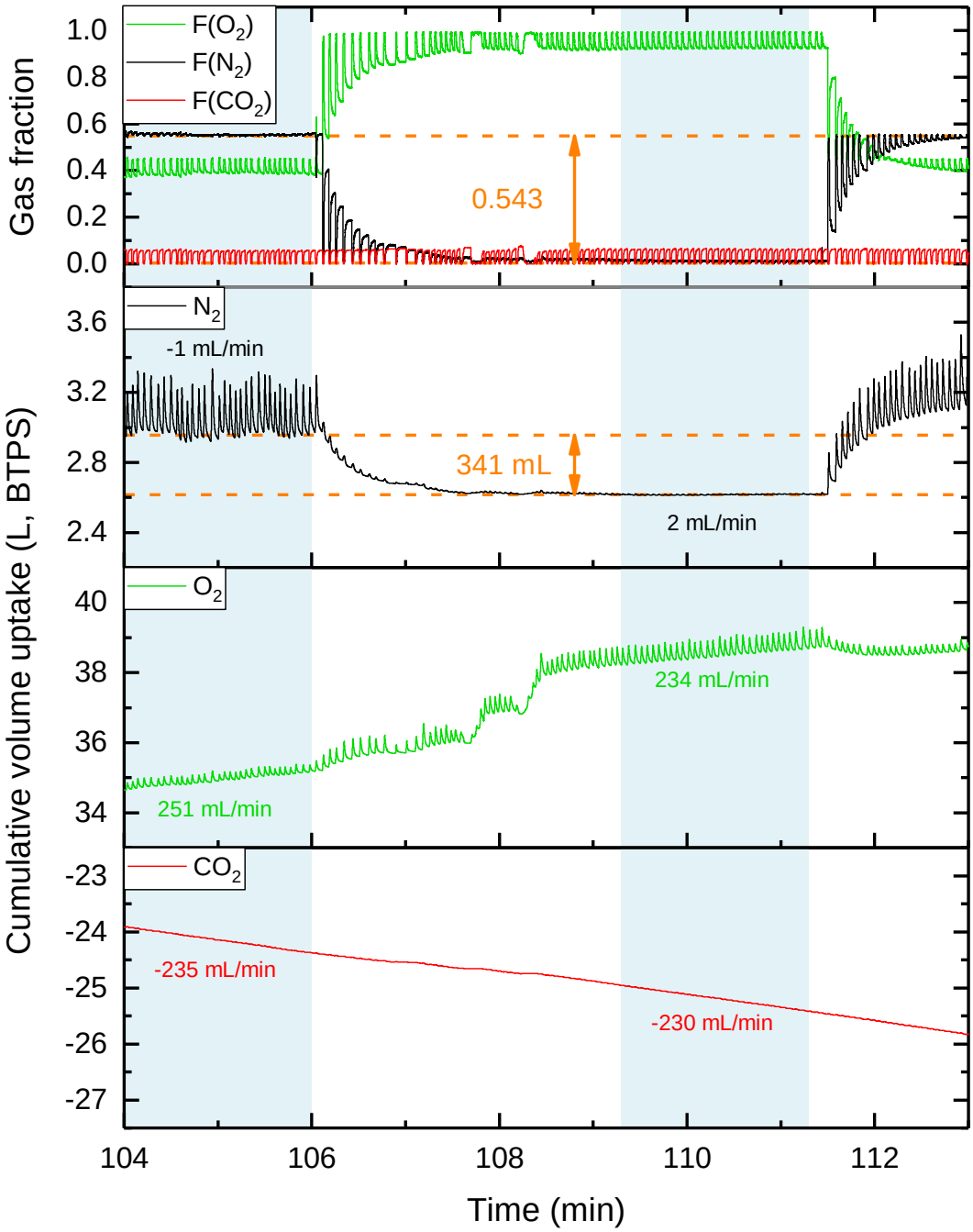


Figure 3.6: The measured dry gas fractions and cumulative uptake volumes of O_2, CO_2 and N_2 as the F_{I,O_2} is increased from 0.45 to 1.00 then lowered to 0.45 again. The orange labels on the upper plots show the measurements needed to estimate FRC, while the labels on the cumulative volume uptake plots show the measured gas exchange rates directly prior to the N_2 washout and at the end of the washout time once the $F_E N_2$ has stabilised.

planned MBW test, the patient was briefly disconnected twice during the washout period (seen as the two step changes in $\dot{V}_{O_2}$ seen on Figure 3.6 at times 107.7 min and 108.2 min). Although most of the N_2 had washed out of the lungs by the time of the first disconnection, this will introduce error into any calculations using this dataset. However, it still demonstrates how information about lung physiology could be obtained in a study that allowed interventions such that the patient could be given elevated F_{I,O_2} for a set period of time to allow a full undisturbed washout. As shown in Figure 3.6, the difference in $F_I N_2$ before and during the washout can be calculated (0.543 for this washout) as well as the difference in cumulative uptake of N_2 (341 mL for this washout) and from this the end-expiratory lung volume (EELV) can be estimated according to Equation 1.5. This quantity is analogous to FRC, as described in Figure 1.1, but while FRC refers to a person who is seated and breathing spontaneously, EELV better describes a mechanically ventilated patient whose end point of expiration may be determined by ventilator setting such as the addition of positive end-expiratory pressure (PEEP).[171] Based on these measurements, the EELV is estimated as 0.63 L. Based on Patient A's sex, age and height, their predicted FRC is 2.85 L in a seated position,[172] but this is decreased when a subject is supine; Lumb *et al.* measured an average decrease of 27.8% when healthy volunteers were supine instead of seated.[173] The supine predicted EELV is estimated as 2.06 L and thus Patient A has an EELV as a percentage of the predicted value of 30.6%. Such a low EELV would not be physiologically possible in a healthy individual, but low EELV values may be expected in the ICU population. In the case of patients with acute lung injury, ALI, or acute respiratory distress syndrome (ARDS), reduced lung volume is referred to as a patient having a 'baby lung', where an adult has an aerated lung volume close approximating that of a 5-6 year old child.[174] This phenomenon may be consistent with the low EELV and the observed bilateral infiltrates on Patient A's thoracic CT scan. Due to the uncontrolled nature of this washout and brief disconnections during the washout phase, this cannot be considered a reliable measure of this individual's EELV. However, it does provide evidence that in a future study where ethics permitted short-lived alterations to a patient's F_{I,O_2}, such measurements would be achievable in an ICU setting.

As the MFS measures both the rate of oxygen consumption, $\dot{V}_{O_2}$, and the rate of CO_2 production, $\dot{V}_{CO_2}$, it is possible to measure the respiratory quotient, RQ, according to:

$$\mathrm{RQ} = \frac{\dot{V}_{CO_2}}{\dot{V}_{O_2}} \tag{3.3}$$

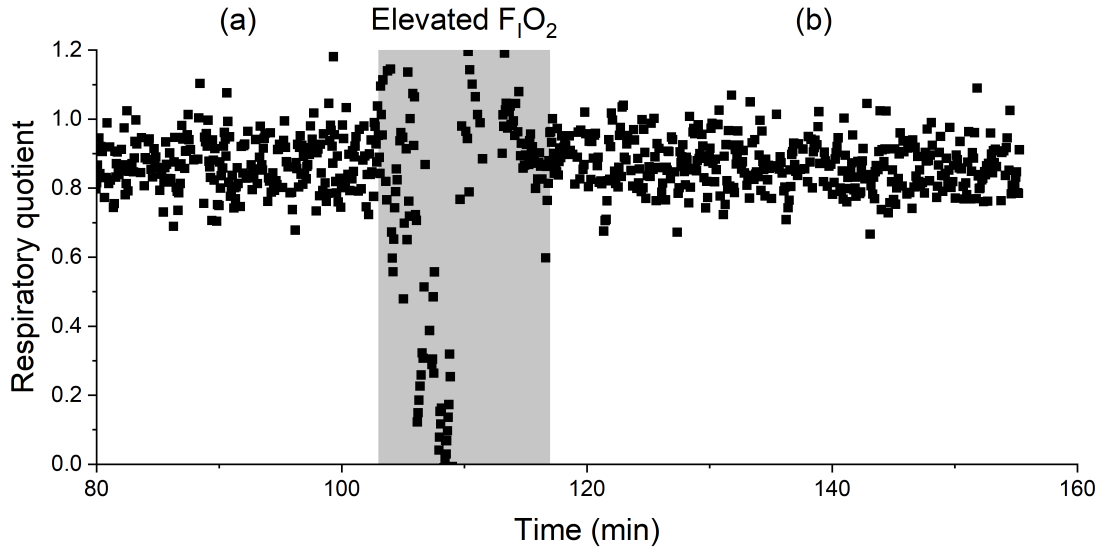


Figure 3.7: The respiratory quotient (RQ) for Patient A calculated on a breath-by-breath basis for two periods (a) and (b) when the patient did not receive any additional interventions from clinicians and had a consistent inspired fraction of O_2 (F_{I,O_2}) of 0.45. In between these two time periods for 5 minutes F_{I,O_2} was 0.998 - the grey shaded area includes this washin of O_2 period as well as the subsequent washout as F_{I,O_2} was returned to 0.45. The mean and standard deviation of the measured RQ during time (a) and time (b) were 0.875 ± 0.085 and 0.869 ± 0.076 respectively.

Figure 3.7 shows the calculated RQ for patient A on a breath-by-breath basis during a period where no interventions were performed apart from a brief switch to an F_{I,O_2} of 1.00 from 0.45. Prior to and after the switch the patient maintains a stable RQ, measured as an average of 0.875 (prior) and then 0.869 (after). In a mixed substrates diet, the RQ is approximately 0.8, due to contributions from protein (0.7), fat (0.8) and carbohydrates (1.0) and anaerobic respiration (0).[175] This is within the desired range - an RQ below 0.85 or above 1.00 may indicate under- or over-feeding respectively.[176,177]

3.3.2 Patient B

Patient B is a 26 year old male, who was admitted to the ICU with suspected meningoencephalitis (inflammation of the meninges and brain) with unknown aetiology and was both intubated and ventilated. At the beginning of the observational period in this study, the patient was sedated with propofol, midazolam, and fentanyl, and was assessed to have a Richmond Agitation and Sedation Score (RASS) of -5, the lowest possible score, which corresponds to a patient being unrousable, with no response to

voice or physical stimulation.[178] This patient's ventilation was entirely controlled by the ventilator, so unlike Patient A, the respiratory rate remained constant.

At the start of data collection for this patient, the F_{I,O_2} was reduced to 0.30 and changes in measured dry gas fractions over the 4 hour study period are displayed in Figure 3.8, along with the calculated breath-by-breath exchange rates of O_2, CO_2 and N_2. Clinical observations recorded as time-stamped notes via the MFS software are marked A-K on the plots. There was no detectable change in gas exchange rates in response to the delivery of a crystalloid bolus at point A. Following the disconnection at point B, the MFS was able to resume measurements, showing that monitoring using the MFS is feasible in ICU, even with the inevitable disconnections and reconnections that are typical during patient normal care. At point C, an increase in the inspiratory pressure was in response to arterial blood gas (ABG) test results showing that the patient was suffering from respiratory acidaemia was noted in the MFS record at 72 minutes. However, upon closer examination of the barometric pressure data collected by the MFS, the pressure was actually increased at 69.5 minutes from 747.1 mmHg to 750.4 mmHg. This corresponds to the time at which there was a notable increase in the rate of CO_2 production from 159.5 mL min^{-1} to 297.8 mL min^{-1} (averaged over 15 s, suggesting that this intervention was highly successful in increasing the rate at which CO_2 was removed from the body. This also indicates a limitation of the notes function in the software - there is some uncertainty as to the time alignment between observations/interventions and the recording of them in the software, depending on clinician availability. Upon further investigation, it was noted that a similar step change in $\dot{V}_{CO_2}$ from 108.8 mL min^{-1} to 148.9 mL min^{-1} was evident at 6 minutes which corresponded to an increase in P_I from 744.8 mmHg to 745.7 mmHg based on the MFS barometric pressure measurements. At point D another crystalloid bolus is given and gave rise to no observed changes in gas exchange rates, in keeping with the observation from Patient A. Following the sedation hold at E and subsequent shivering, rigors and suctioning then a period of disconnection of the patient for a roll, the gas exchange rate measurements did not stabilise again until the washin of N_2 was complete after the reduction in F_{I,O_2} to 0.21 at point H.

The delivery of metaraminol and noradrenaline indicated on Figure 3.8 at points I and J marks the first time the activity of these drugs in an ICU patient has been studied using the MFS and a change in $\dot{V}_{O_2}$ was observed in response to both drugs. The inspired fraction of O_2 remained constant over this time period, from 139 min (point H) until 220 min (just after point K). Figure 3.9 shows the O_2 consumption and CO_2 production rates in the time period during and shortly after delivery of

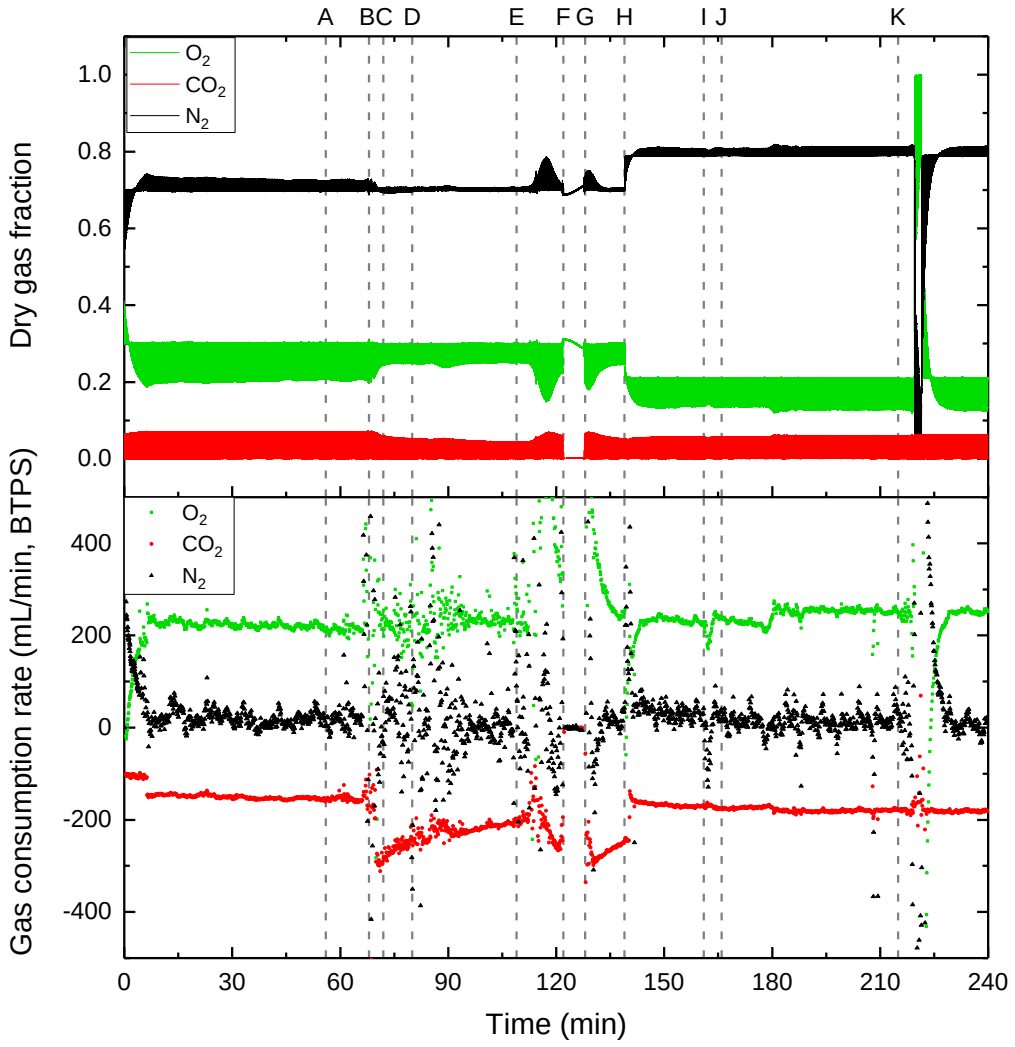


Figure 3.8: An overview of the time period over which MFS measurements were taken for patient B, with the upper plot displaying the dry gas fractions and the lower plot showing the calculated rate of consumption on a breath-by-breath basis for O_2, CO_2 and N_2. Clinical observations/interventions are labelled above the plot. A: 250ml crystalloid bolus starting (mean arterial pressure (MAP) of 55 mmHg); B: brief accidental disconnection; C: P_I increased, respiratory acidaemia on ABG (7.34, P_a, CO_2 6.76); D: further 250ml crystalloid bolus; E: sedation hold started (sedation remained off for remainder of the observational period although patient did not wake), followed by suctioning and shivering then shivering, rigors and seizures; F-G: disconnected for roll then reconnected; H: reduction in F_{I,O_2} from 0.30 to 0.21; I: 0.5mg metaraminol bolus (for MAP 54 mmHg); J: Noradrenaline started; K: Chest physiotherapy started - some suctioning and coughing.

drugs indicated at points I and J on Figure 3.8 on an enlarged scale. The data are presented in two ways: firstly with no averaging of the gas exchange rates calculated and plotted on an individual breath-by-breath basis and secondly with every data point calculated from averaging the gas exchange rate across the previous minute's whole breaths. Here 1 min was chosen for the averaging period as it is sufficient to make overall trends more visually distinct from the noise introduced by breath to breath variation, without obscuring short-lived fluctuations in exchange rates across the relatively short time window displayed.

In response to the delivery of a 0.5 mg metaraminol bolus, labelled as timepoint 1 on Figure 3.9, there was an immediate decrease in oxygen comsumption. This is consistent with the findings of Ciaffoni *et al.* who observed a decrease in oxygen consumption in response to receiving metaraminol in a patient undergoing an elective aortic aneurysm repair.[5] This fast response following delivery of the drug is expected as it has a reported onset of action of 1-2 minutes and a half-life of the order of minutes.[179] A reduction in O_2 consumption would also be expected, as metaraminol is an α-agonist, causing peripheral vasoconstriction, which would reduce blood flow to the tissues.[180] However, strikingly, there is little change in the rate of CO_2 production in response to administering metaraminol - this is different to the findings of Ciaffoni *et al.* when studying a surgical patient, where a simultaneous drop in $\dot{V}_{CO_2}$ was observed alongside the decrease in $\dot{V}_{O_2}$.[5] It may be expected that slowing the blood flow through the lungs would have a greater effect on $\dot{V}_{O_2}$ than on $\dot{V}_{CO_2}$, as while it is not possible to add more O_2 to fully saturated blood, more CO_2 can be removed per unit volume if the rate of blood flow is reduced.

The second drug delivered during this timeframe was noradrenaline, delivery of which was started intravenously from point 2 onwards on Figure 3.9, with flow rates of 8 mL/hr by point 3 which was increased to 10 mL/hr at point 4 before being reduced to 3.5 mL/hr at point 5. Noradrenaline, also referred to as norepinephrine, is a non-selective andrenergic drug whose use is indicated for patients in shock or with hypertension,[181] and due to its short half-life of 2.4 minutes it is usually administered continuously through an IV drip.[182] Clinical guidance indicates that blood pressure should be monitored every 2-3 minutes while determining the optimal maintenance dose, then every 5 minutes from then on.[182] Following 5 minutes of intravenous infusion a steady state plasma concentration should be reached,[182] and so the observed increase in $\dot{V}_{O_2}$ 12 minutes after the IV delivery of the drug was started may be longer than expected. However, it is possible that a change in $\dot{V}_{O_2}$ is only induced by a higher delivery rate; in this case the rate of transfusion wasn't increased to its maximum until

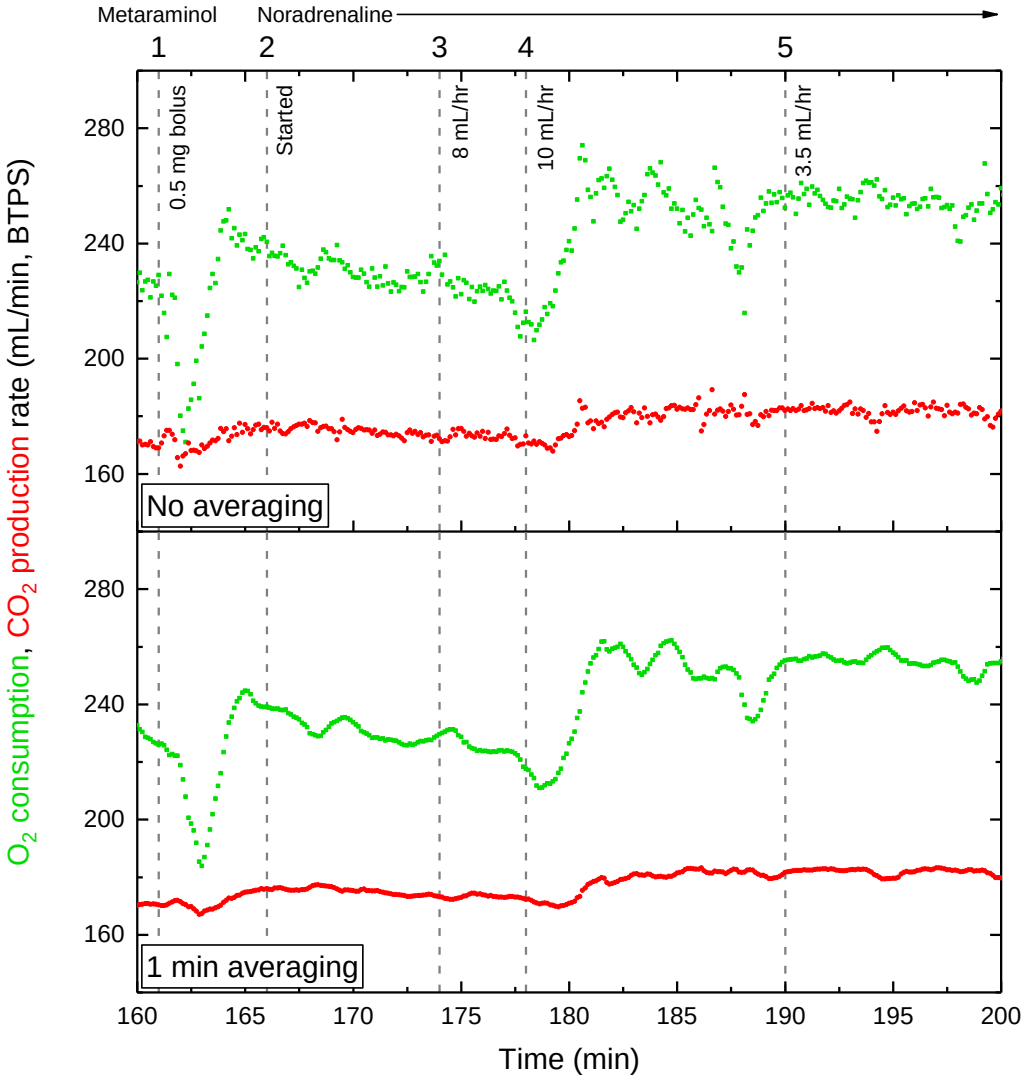


Figure 3.9: An enlarged section of the data collected from Patient B, showing the breath-by-breath O_2 consumption rate and CO_2 production rate with no averaging (above) and averaged over the breaths during the previous minute (below). Delivery of drugs was noted by clinicians. 1: 0.5mg metaraminol bolus (for MAP (mean arterial pressure) 54 mmHg), 2: Noradrenaline started, 3: noradrenaline delivered at 8 mL/hr of 4 mg noradrenaline in 50 mL glucose 5%, 4: noradrenaline increased to 10 mL/hr, 5: noradrenaline reduced to 3.5 mL/hr.

point 4. Indeed, it has been suggested that at lower concentrations of noradrenaline, the body's response may be dominated by agonistic activity at α_1 receptors, while at higher concentrations, activity at β_1 receptors may dominate.[182,183] As β_1 receptors have both chronotropic and inotropic effects on the heart (increasing both heart rate and atrial contractability),[184] activating these receptors may be expected to increase the rate of oxygen consumption. As α_1 agonists induce contractions of smooth muscle tissue leading to vascular constriction,[185] this may be inducing a competing effect of lowering oxygen consumption when noradrenaline is only present in the blood at lower concentrations. However, following the initial increase in $\dot{V}_{O_2}$ in response to noradrenaline, the elevated $\dot{V}_{O_2}$ was maintained even after a subsequent reduction in infusion rate, which may contradict this hypothesis.

The recorded RQ for Patient B over the 4 hour measurement period is shown in Figure 3.10, both on a breath-by-breath basis and also averaged over the whole breaths in the previous 5 minutes. Due to the longer time period of the data shown in Figure 3.10 compared to Figure 3.9, a longer averaging period is shown to make overall trends clearer. This highlights how, if this technique were used in the future as a tool for decision making, clinicians may wish to view the data averaged over different time periods depending on the duration of time over which they wish to examine the patient's response. The measured RQ during the stable periods (with consistent F_{I,O_2} and no disconnections) shown in Figure 3.10 is notably lower than that seen in Patient A, whose RQ was around 0.87. This could be due to underfeeding in Patient B, as this would lead to a reduction in RQ.[156] Another possible factor could be the effect of mechanical ventilation - if the ventilation is set a little lower, this results in increased CO_2 storage as not all the CO_2 produced metabolically is removed (and hence a lower RQ is measured).[186] A prolonged period of lowering CO_2 storage in the body once the ventilation is set a little higher could explain the gradual trend of increasing RQ during the first hour of measurement, when the RQ increases from approximately 0.60 to 0.72. At point B, there was an accidental disconnection causing temporary inaccurate RQ measurements. Following the increase in inspiratory pressure, P_I, the RQ appeared to stabilise briefly at a higher RQ of approximately 0.92 before the implementation of a sedation hold and disconnection for a roll. Once the patient had washed N_2 back into the lungs, following the decrease in F_{I,O_2} to 0.21 at point H, the RQ remained relatively stable at approximately 0.73, apart from a spike upon administration of the metaraminol, where the decrease in $\dot{V}_{O_2}$ was not matched by an decrease in $\dot{V}_{CO_2}$, as well as a decrease in RQ following the delivery of noradrenaline, which induced a proportionately bigger increase in $\dot{V}_{O_2}$ compared to $\dot{V}_{CO_2}$.

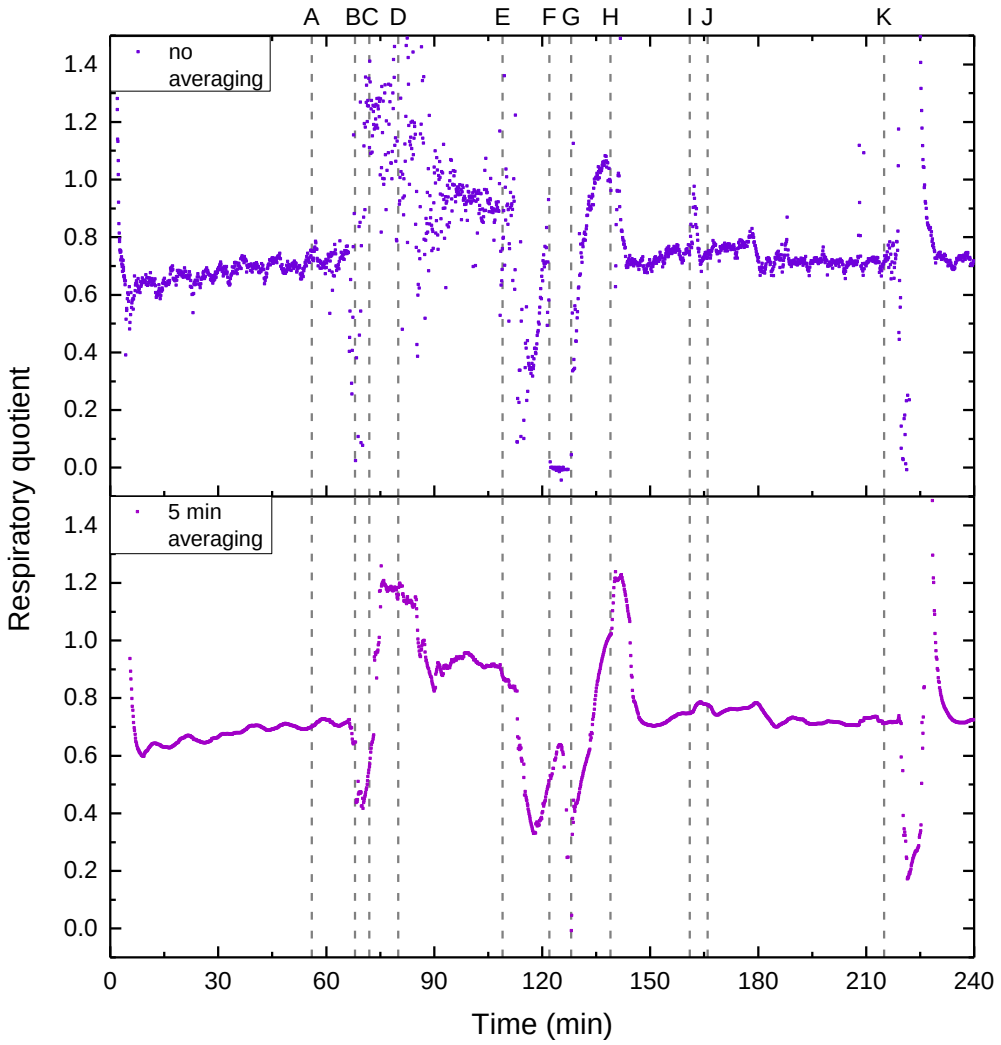


Figure 3.10: The measured respiratory quotient for Patient B on a breath-by-breath basis with no averaging (above) and averaged over the breaths during the previous 5 minutes (below). Clinical observations/interventions are labelled above the plot. A: 250ml crystalloid bolus starting (MAP 55); B: brief accidental disconnection; C: P_I increased, respiratory acidaemia noted on ABG results(PH = 7.34, P_{a,CO_2} = 6.76); D: further 250ml crystalloid bolus; E: sedation hold started (sedation remained off for remainder of the observational period although patient did not wake), followed by suctioning and shivering then shivering, rigors and seizures; F-G: disconnected for roll then reconnected; H: reduction in F_{I,O_2} from 0.30 to 0.21; I: 0.5mg metaraminol bolus (for MAP 54 mmHg); J: Noradrenaline started; K: Chest physiotherapy started - some suctioning and coughing.

3.4 Discussion

One of the primary goals of this initial study was to demonstrate the suitability of the MFS to monitor patients receiving varying F_{I,O_2} during their admission to ICU. Both nurses and doctors on the ward were satisfied that the presence of the additional equipment (both the measurement head and the MFS rack on a portable trolley) did not pose a risk to the delivery of patient care. Although the clinical team were satisfied that the presence of the MFS posed no risk to the patient nor obstructed patient care, it would be more practical if the measurement head and rack/trolley could be reduced in size (the current $\sim$ 1.8kg head requires support from a specialist Bytec arm). This is likely feasible should the device be commercialised, through investigating alternative materials and miniaturising the device electronics.[5]

The only, but insurmountable, barrier to recruiting further patients for this study was the implementation of restrictions imposed due to the COVID-19 pandemic. This means that given the presence of a clinician with available time to resume the study, further recruitment of patients would be feasible in the future.

Stable gas exchange rates were observed in both patients across a range of F_{I,O_2} values. As illustrated for Patient A, the MFS is also capable of measuring $\dot{V}_{O_2}$ when the patient is receiving 100% O_2, which previous commercial devices were unable to do.[138] For both patients, periods of disconnection were followed by successful reconnection and subsequent continuation of gas exchange measurements. Real time monitoring of ICU patients will always require periods of disconnection to maintain good circulation and prevent pressure ulcers,[187] as well as during other interventions such as performing chest physiotherapy and suctioning.[188,189] If a future study allowed for a controlled period before and after physiotherapy where F_{I,O_2} remained constant with no other interventions, the MFS could be used to compare gas exchange rates before and after physiotherapy, potentially comparing the effect of different techniques across multiple patients.

Similarly, this study showed how two drugs, metaraminol and noradrenaline induced a change in gas exchange rates in one patient that was measurable using the MFS. Observing the effect of these and other drugs across a range of patients would help establish whether the same trends are seen in all patients, or whether their effect varies and maybe even could be predicted based on a patient's diagnosis or other indicators. Provided that target $\dot{V}_{O_2}$ rates were well understood, a future interventional study could even titrate the delivery of a drug to give the desired change in gas exchange rates - whether acting upon this information improves patient outcomes

could then be investigated. As described in Section 3.1, at some point treatment may no longer be improving the health of the patient, yet the adverse effects from over-treating may persist.

In the case of increasing inspiratory pressure or varying F_{I,O_2}, the exact time point when the ventilator settings changed can easily be determined from the MFS data, as both barometric pressure and the dry gas fractions are measured every 10 ms for the duration of the observational period. This was helpful in interpreting the changes seen in Patient B in response to increasing P_I where the record in the notes was only added a few minutes after the change. However, the exact timing of drug delivery cannot be verified from the MFS data, so in order to better understand the response time for a drug to cause a change in gas exchange rates, an accurate record of the delivery time is required. Perhaps future users should be encouraged to also enter a time of intervention when entering it into the notes function instead of purely relying on the note timestamp - this would also allow for situations where it is not possible for the clinician to immediately log the observation/intervention, such as the presence of multiple clinical staff around the patient at the same time, preventing easy access to the MFS laptop.

Aside from the reduction in the scale of the study due to the implementation of COVID-19 restrictions in March 2020, the most significant limitation of the study is its purely observational nature. A prime example of this is the data in Figure 3.6, where the patient receives 100% O_2 for several minutes during chest physiotherapy, inducing a N_2 washout from the lungs. Although the figure illustrates how the MFS and specifically a N_2 washout can be used to provide information about a patient's lungs, the two disconnections introduce errors into the calculation of FRC and precludes further analysis of the washout. In the later chapters of this thesis, the use of the MFS in conjunction with a mathematical model of the lung is detailed and explored across multiple applications. This technique could also potentially be applied to ventilated patients in ICU, if the ethical approval for a study allowed researchers to increase the F_{I,O_2} for around 5 minutes during a time when no other interventions were being performed. Such data could then be analysed using the lung model to provide a snapshot of a patient's lung function and potentially with multiple tests over a period of a few days, how their lung health changes during their time in ICU.

3.5 Conclusions and Future Work

The successful data collection using the MFS to study patients in ICU demonstrates that it is possible to use the device in intensive care. Gas exchange rates were measured and remained stable during periods with no interventions and the respiratory quotients calculated at this time were within physiological limits. Changes to gas consumption rates were observed in response to interventions, such as the increasing of inspiratory pressure and the administration of drugs. This may offer valuable insights into the effect of these interventions. Since the initial trial of EGDT, subsequent studies have found alternative approaches may reduce mortality to a similar degree.[154] It is possible that this may in part be due to inadequate metrics for clinicians to target. Potentially the real-time, non-invasive measurement of oxygen consumption could provide a suitable target in the future.

In the first instance, a better understanding of the normal range of $\dot{V}_{O_2}$ in ICU patients should be sought through the recruitment of further patients to the study when it is possible to do so. As the study population would be fairly heterogenous, with varied physical characteristics, it may be useful to compare $\dot{V}_{O_2}$ between patients as a ratio to their predicted $\dot{V}_{O_2,max}$, which can be estimated based on sex, age and weight (for Patients A and B their predicted $\dot{V}_{O_2,max}$ would be 28.4 mL kg^{-1} min^{-1} and 49.3 mL kg^{-1} min^{-1} respectively).[190] As there is significant variation in $\dot{V}_{O_2}$ and $\dot{V}_{O_2,max}$ even within the healthy population, it may be the case that reporting $\dot{V}_{O_2}$ relative to an individual patient's measured $\dot{V}_{O_2}$ at an earlier stage during their admission may provide a more useful metric than absolute measurements. Collecting information on 30-day and 90-day mortality rates may also prove useful, as this may indicate whether a higher $\dot{V}_{O_2}$ was associated with improved outcomes. Further recruitment will also offer the chance to observe more patients' responses to drugs commonly used in the ICU and to see whether Patient B's responses to metaraminol and noradrenaline were typical or if inter-subject variability is seen. In a future study, the change in $\dot{V}_{O_2}$ upon changing the F_{I,O_2} (after a suitable period to allow the N_2 to washin/washout) could be measured across a larger sample of patients.

Improvements in the device measurement stability at increased humidity offer the possibility to extend patient monitoring using the MFS to a broader patient population, as there would be no requirement to restrict subject recruitment to those in whom passive humidification is not contraindicated.

Recent developments in the introduction of trace gas measurements of CH_4 and C_2H_2 to a molecular flow sensor has been shown by Smith *et al.* to offer real time

calculations of cardiac output ($\dot{Q}$).[191] Current techniques involve the use of an invasive pulmonary artery catheter (PAC) so this information is not routinely obtained for ICU patients, so a non-invasive technique for measuring $\dot{Q}$ could offer another useful metric which could be targeted by clinicians when deciding on interventions, as there is some evidence to suggest that increasing cardiac output leads to better outcomes.[145] This 5-gas version of the MFS is the same size and has identical external components as the 3-gas analyser used in this ICU study. Therefore, future studies may benefit from using this 5-gas analyser instead, as the same information regarding $\dot{V}_{O_2}$ and $\dot{V}_{CO_2}$ would be available, but with the additional benefit of collecting data on cardiac output. However, this would be more complicated than simply studying patients using the 3-gas MFS, due to the requirement to deliver trace gases to the patient, as opposed to simply delivering varying fractions of inspired O_2, which already forms part of routine patient care. Should delivery of CH_4 and C_2H_2 prove impossible in critical care due to safety concerns, an intriguing alternative possibility exists of using the ventilator to induce a small but measurable change in gas exchange rate along with simultaneous blood gas measurements to determine $\dot{Q}$.

As mentioned in the previous section, the successful use of the MFS in the ICU also opens up the possibility of inducing a nitrogen washout in a ventilated patient by increasing the inspired O_2 to 100% at a time when no other interventions such as physiotherapy, repositioning or a change in drug regimen are anticipated. This data could then be processed using a mathematical model of the lung (detailed in the next chapter) to provide potentially useful parameters describing lung volumes and degree of inhomogeneity. It may also be possible to compare lung mechanics under different ventilator settings, as a routine part of ICU care involves optimizing ventilator settings to maintain optimal pulmonary function.[192] The short term delivery of 100% O_2 would be quick, safe and is routinely given to patients as part of standard care so would be a non-invasive and safe intervention. With the exception of a study of people subjected to high G-forces while in a human centrifuge,[193] and a small scale study comparing the LNL model parameters in a prone, supine or seated position,[194] lung function testing with the device has primarily taken place with subjects in a seated position, so further studies would be required to establish normal lung parameters in subjects who are in a supine position for comparison. The parameters and potential information provided by this model of the lung is detailed in the next chapter, along with its application in pulmonary testing in conscious, seated patients with known or suspected risk of respiratory disease and healthy controls.

Chapter 4

Application of Molecular Flow Sensor to Assess Lung Inhomogeneity in Adults

At present the most common clinical tool for assessing lung function is spirometry, which provides multiple measurements, including the most commonly reported, FEV_1 (forced expiratory volume in 1 s). However, this technique is not sensitive to the early stages of declining function, and there is therefore a recognised need for superior techniques to assess respiratory health.[195] Lung inhomogeneity is an accepted marker of early stage lung disease, able to identify abnormal function at an earlier stage than spirometry in patients with chronic obstructive pulmonary disease (COPD) and cystic fibrosis (CF),[60,61,196,197] which are discussed in this thesis, as well as other lung diseases such as asthma,[198–200] and interstitial lung disease.[201] Although some degree of inhomogeneity is found in healthy lungs, the amount of inhomogeneity is elevated in people with lung disease. The current gold standard for assessing ventilation inhomogeneity is the multiple inert gas elimination technique (MIGET), where inert gases are delivered to the subject intravenously, then subsequent expired gas, arterial and venous samples are used to estimate the ventilation-perfusion distribution across the lung. However, due to the invasive nature of the procedure and complexity of operation, it is only suitable as a research tool and not for use in a clinical setting.

Analysis of multiple breath washouts (MBW) are the most commonly used clinical method to derive parameters which are believed to reflect the degree of lung inhomogeneity. The most common of these is the lung clearance index, which measures the number of lung turnovers required to reduce the expired fraction of nitrogen expired to 1/40th of its initial value, following a switch from air breathing to oxygen breathing. This chapter focuses on an alternative technique for analysing MBW data: the

lognormal lung (LNL) model.

The lognormal lung model is a mathematical model of gas exchange in the lung, developed by Mountain *et al.* to parameterise lung inhomogeneity. Multiple breath nitrogen washout data obtained using the molecular flow sensor (MFS) described in previous chapters is analysed using the measured respiratory flow rates as inputs to the model. The recovery of the LNL parameters (described later) was shown to be possible only due to the unparalleled accuracy of the molecular flow sensing technology,[202] so the potential of the LNL model is inextricably linked to the developments in laser gas analysis. An initial small scale study of young and old healthy control subjects and COPD patients showed significant differences between the LNL parameters obtained for the three subject groups,[115] and there remains great scope for exploring the clinical potential of this technique in this and other patient groups.

This chapter begins with an introduction to the lognormal lung (LNL) model, with a summary of the experimental protocol for data collection and an overview of the assumptions and fitting procedure of the LNL model. This is followed by a validation study conducted in collaboration with the Division of Physiology at the University of California, San Diego. The outputs of the LNL model were used to estimate the ventilation and perfusion distributions in patients with chronic obstructive pulmonary disease (COPD) to compare with MIGET measurements from the same subjects. Finally, the potential of the technique to identify abnormal lung physiology as a result of smoking is explored in a cross-sectional study of current young smokers in Oxford.

4.1 Assessing Lung Inhomogeneity with the Lognormal Lung Model

The process of obtaining LNL parameters to characterise subjects' lungs consists of two stages: performing an MBW experiment followed by analysis of the data using the Oxford advanced research computing (ARC) facilities. The washout may be performed in either a lab or clinical setting and the mobility of the device means it can be used in a variety of rooms within a hospital. The data can then be shared securely to be processed remotely and obtain the lung parameters. This section includes a description of both the data collection and an overview of the LNL analysis.

4.1.1 Multi-breath Nitrogen Washout Protocol

To perform the washout for analysis by the lognormal lung model, the subject is seated in an upright position, with back support. The measurement head can then be adjusted to a comfortable height for the subject. When the subject is comfortable, they are asked to begin breathing through a mouthpiece connected to an HME filter (Hans-Rudolph) affixed to the MFS measurement head, as demonstrated in Figure 4.1, with careful attention paid to ensure a tight seal with no leaks around the mouth and nose.

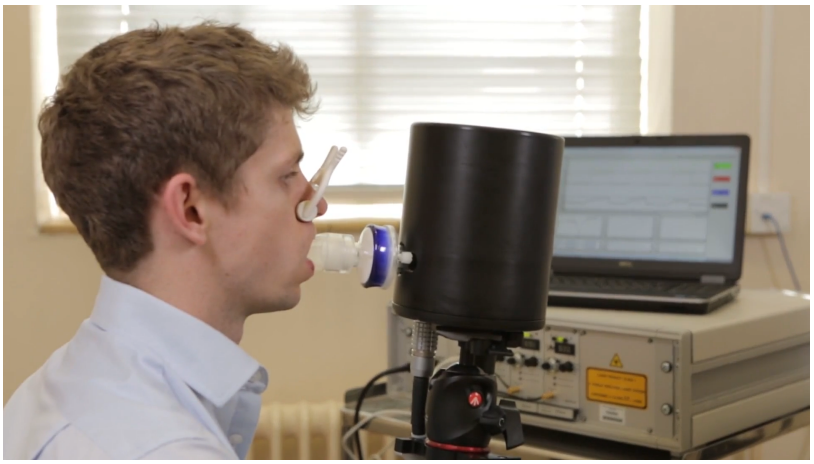


Figure 4.1: Set-up of the MFS in a clinic with the subject breathing through the measurement head while wearing a noseclip. Air followed by O_2 is then flowed through a T-piece connected to the other end of the measurement head.

Gas is supplied to the MFS head via a flow past system at a rate of approximately 50 mL min^{-1} - a sufficiently high gas flow rate to prevent re-breathing of expired gas by the subject. A two-way valve allows the operator to easily switch from air-breathing to oxygen-breathing at the beginning of the washout period. Subjects are allowed to breathe freely with no prescribed breathing pattern for the duration of the experiment. This is notably different from the requirements for traditional MBW analysis, where a constant tidal volume is needed. It is particularly noteworthy that, due to the lack of a prescribed breathing pattern for the LNL model method, a washout can still be analysed if a patient coughs during the experiment, provided that a good seal is maintained around the mouth and nose; this is particularly valuable for patients with a persistent cough.

The standard protocol for the MBW is 10 minutes of air breathing, followed by 5 minutes of breathing medical grade O_2, which has a specified purity of $> 99.5\%$. In the case of severe lung disease, a subject may have too high an expired N_2 fraction to

calculate an accurate FRC value after 5 minutes of breathing O_2. In these cases the subject is asked to continue breathing through the device for a few more minutes if the device is well tolerated. Performing a washout using the MFS is well tolerated by almost all subjects. The low resistance of the measurement head and lack of forced manoeuvres makes it suitable for use even in cases of more advanced respiratory disease.

The LabVIEW software described in Chapter 2 collects the washout data from the MFS. At the end of the washout the user can enter the subject number, age, height and weight, as well as details of the set- up used, such as the type of filter and mouthpiece, which will affect the total device deadspace. The user can also identify the start of the oxygen-breathing period and select the air breathing period to be used for analysis by the model. If any blood samples were taken during the experiment, this information can also be entered at this point to inform the modelling of blood gases, but the taking of blood samples does not form part of the routine clinical use of the technique. These files can then be directly uploaded to the ARC clusters to be analysed using the LNL model.

4.1.2 Lognormal Lung Model

The lognormal lung (LNL) model uses information from the gas exchange measured at the mouth by the MFS to estimate lung volume and assess the degree of inhomogeneity within the lungs. The reported volume is divided into two parts: the deadspace volume (V_D) and the alveolar volume (V_A). The LNL parameters also differentiate between the different factors contributing to ventilation inhomogeneity: the inhomogeneity of the deadspace path length to the site of gas exchange, the inhomogeneity of compliance (the ability of the lung to expand and contract), and the inhomogeneity of the vascular conductance (the ability of the circulation to perfuse lung tissue). These comprise the five core parameters determined by the model, as listed in Table 4.1.

The LNL model makes a number of simplifying assumptions about the structure of the lungs. It assumes that the lungs consist of N perfectly mixed compartments where gas exchange takes place. Each of these compartments will have an associated dead space and alveolar volume, as shown in Figure 4.2 for $N = 3$. For all the data contained in this thesis, N was set to 125, shown by Mountain to be sufficient to obtain accurate parameters, while maximising computational speed.[202] There also exists a common deadspace between the measurement plane within the measurement cell of the MFS and the subject's mouth, $V_{D,MFS}$, the volume of which is calculated for a given mouthpiece and HME filter set-up and entered into the model.

Parameter	Definition (Units)
V_A	Alveolar volume at FRC (litres, BTPS)
V_D	Deadspace volume (litres, BTPS)
σ_{CL}	Standard deviation for the natural logarithm of the standardized lung compliance
σ_{Cd}	Standard deviation for the natural logarithm of the standardized lung vascular conductance
σ_{VD}	Standard deviation for the standardized dead space
FRC	Functional residual capacity (litres, BTPS), i.e. the sum of V_A and V_D
FRC (% pred.)	Functional residual capacity expressed as a percentage of the predicted value
V_D/FRC	Ratio of the dead space volume to the total volume at FRC
Log SD$\dot{V}$	Standard deviation of the ventilation distribution
Log SD$\dot{Q}$	Standard deviation of the perfusion distribution
$\dot{V}_D/\dot{V}$	Fractional deadspace ventilation (proportion of the lung that is ventilated but not perfused)
$\dot{Q}_s/\dot{Q}$	Shunt fraction (proportion of the blood flow through the lungs that does not participate in gas exchange)

Table 4.1: Parameters estimated by the lognormal lung model: the first five are the primary parameters and the remaining seven parameters are calculated secondary to the fitting procedure. The final four parameters do not form part of the normal reporting of LNL parameters and are calculated specifically to allow direct comparison with the key parameters obtained from the multiple inert gas elimination technique (MIGET).

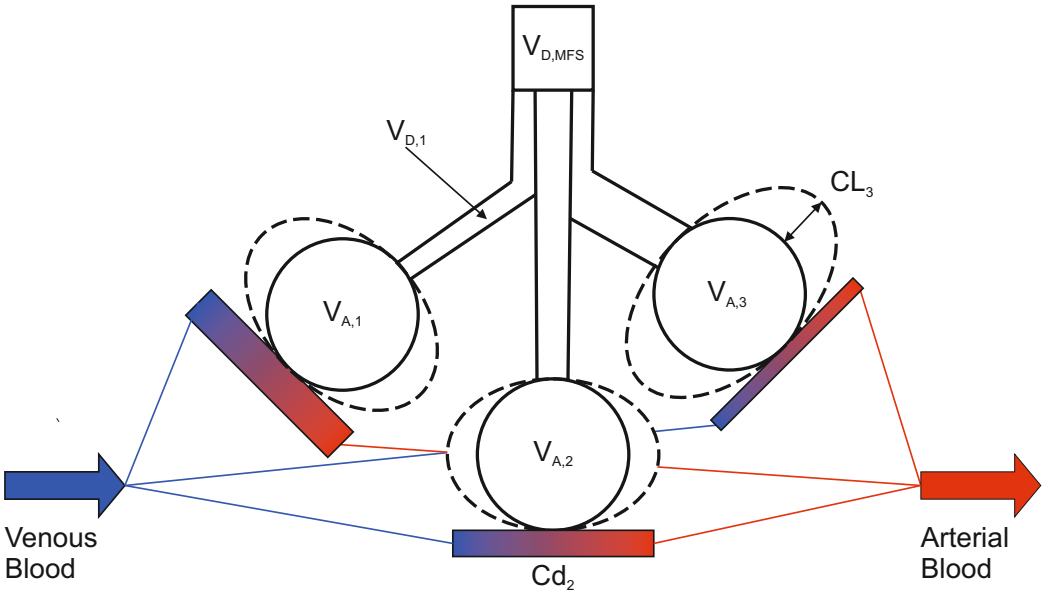


Figure 4.2: A simplified schematic of the LNL model for $N = 3$ compartments. The common deadspace from the HME filter and MFS measurement head between the mouth and the measurement plane is shown as $V_{D,MFS}$. Three alveolar compartments are shown, all with equal alveolar volume, $V_{A,i}$ but with unequal deadspace ($V_{D,i}$), conductance (Cd_i) and compliance (CL_i), as indicated above for compartments one, two and three respectively.

Each lung compartment will also have its own compliance (fractional alveolar volume change), CL_i and vascular conductance (fraction of the total perfusion of the lungs), Cd_i. Both of these are indicated in Figure 4.2. To restrict the number of model output parameters, the model assumes that compliance and vascular conductance can be fit to a bivariate lognormal distribution, based on previous washin studies by Wilson and Beck.[203,204] A normal distribution is used to approximate the distribution of the personal deadspace to provide a third parameter to describe the degree of inhomogeneity within the lungs. The standard deviations of these three distributions comprise the inhomogeneity parameters of the model: inhomogeneity of compliance (σ_{CL}), conductance (σ_{Cd}) and deadspace (σ_{VD}). A wider distribution and hence an increase in any of these parameters indicates a more inhomogeneous lung.

In addition to the five primary outputs of the LNL model, several secondary parameters which are calculated after the modelling is complete are also listed in Table 4.1. The first of these is the sum of V_A and V_D, giving the overall functional residual capacity (FRC), expressed either as an absolute volume or as a percentage

of the predicted FRC in L for that person based on their sex, age and height using the ERS regression equations determined by Quanjer *et al.*:[172]

$$\mathrm{FRC}_{pred,male} = 2.34H + 0.009A - 1.09 \tag{4.1}$$

$$\mathrm{FRC}_{pred,female} = 2.24H + 0.001A - 1.00 \tag{4.2}$$

where H denotes height in m and A is age in years. For ages between 18-25, an age of 25 years is substituted into the equations. Secondary to the estimate of the absolute deadspace volume, V_D, deadspace is also reported as a fraction of the summed lung volume at FRC to account for normal intra-subject variability in lung size.

LogSD$\dot{V}$ and LogSD$\dot{Q}$ are the estimated second moments of the ventilation and perfusion distributions respectively, to enable comparison with those calculated by the multiple inert gas elimination technique (MIGET). For a $\dot{V}/\dot{Q}$ distribution that is symmetrical about the mean this will be equivalent to the standard deviation of the distribution, hence the SD notation. Although these parameters can be estimated using the LNL model for the purposes of comparison with MIGET parameters, these do not form part of the usual reporting of the model parameters. It should be emphasized that there are significant differences between the LNL and MIGET approaches to assessing inhomogeneity. Both techniques use the principle of conservation of mass, but while the LNL model considers this in terms of gas volumes, MIGET relies only on concentrations and flux at steady-state. The broader range of the solubilities of the six gases used in MIGET compared with O_2 and CO_2 means that MIGET is sensitive to regions of higher and lower $\dot{V}/\dot{Q}$ than the LNL model. Furthermore, while the distributions obtained from the LNL model must necessarily be lognormal and hence unimodal, MIGET is able to identify multimodal distributions with up to three modes, although concerns have been noted about the level of detail that can be recovered.[205] This is discussed further in the validation study of the LNL model detailed in Section 4.2.

The LNL estimates are based on the distributions proposed by Wilson and Beck, where the experimentally determined ventilation-volume $\dot{V}/V$ and perfusion-volume $\dot{Q}/V$ distributions were assumed to be lognormal and linked to the MIGET ventilation-perfusion $\dot{V}/\dot{Q}$ distribution according to

$$\log\left(\frac{\dot{V}}{\dot{Q}}\right) = \log\left(\frac{\dot{V}}{V}\right) - \log\left(\frac{\dot{Q}}{V}\right) \tag{4.3}$$

and the standard deviations of these distributions are related to each other and the correlation between ventilation and perfusion, ρ, by

$$\sigma^2_{\frac{\dot{V}}{\dot{Q}}} = \sigma^2_{\frac{\dot{V}}{\dot{V}}} + \sigma^2_{\frac{\dot{Q}}{\dot{V}}} - 2\rho\sigma_{\frac{\dot{V}}{\dot{Q}}}\sigma_{\frac{\dot{V}}{\dot{Q}}} \tag{4.4}$$

As either the width of the $\dot{V}/V$ or $\dot{Q}/V$ distribution increases or the degree of correlation between the two decreases, the width of the $\dot{V}/\dot{Q}$ distribution will consequently increase. This relationship cannot however be used directly to determine the LogSD$\dot{V}$ and LogSD$\dot{Q}$ parameters from the LNL model parameters, as the LNL model assumes a lognormal distribution of the compliance and not the ventilation. Therefore, before estimating LogSD$\dot{V}$ and LogSD$\dot{Q}$, the alveolar ventilation ($\dot{V}_{A,i}$) of the compartments must first be estimated, i.e. the volume of fresh gas (excluding the volume of the deadspace gas, V_D, which does not participate in gas exchange) that enters a single alveolar compartment per unit time. This is achieved using the determined LNL parameter values for that washout and the final 5 minutes of the air-breathing part of the washout, where for a single breath:

$$\dot{V}_{A,i} = \sum_m \left(\frac{\dot{V}_i^m (V_T^m - V_{D,MFS}) - v_i V_D}{t_b^m} \right) \tag{4.5}$$

where $\dot{V}_i^m$ is the fractional ventilation of compartment i for breath m, V_T^m and t_b^m are the tidal volume and duration of that breath, and v_i is the fractional deadspace volume of compartment i. The ventilation-perfusion ratio of compartment i is then given by $\frac{\dot{V}_{A,i}}{\dot{Q}_i\dot{Q}}$, where the perfusion of that compartment is equal to $\dot{Q}_i\dot{Q}$, with $\dot{Q}_i$ representing the fractional perfusion of compartment i and $\dot{Q}$ the total blood flow or cardiac output. The standard deviation of the ventilation and perfusion distributions of $\log\frac{\dot{V}_{A,i}}{\dot{Q}_i\dot{Q}}$ will directly give the desired second moments to compare with MIGET. Because both the ventilation and perfusion are approximated as exactly lognormally distributed, unlike the MIGET values, LogSD$\dot{V}$ and LogSD$\dot{Q}$ calculated using this method will be equal, which is shown to be a good approximation in healthy subjects.[204]

Two other parameters reported by MIGET, the pulmonary shunt and deadspace ventilation, can also be estimated using the LNL model. The proportion of the lung which is perfused but not ventilated is described by the shunt fraction, estimated from the Berggren equation:[206]

$$\frac{\dot{Q}_s}{\dot{Q}} = \frac{C_{c,O_2} - C_{a,O_2}}{C_{c,O_2} - C_{v,O_2}} \tag{4.6}$$

where $\dot{Q}_s$ is the blood flow rate through the shunt, $\dot{Q}$ is the cardiac output, and C_{a,O_2} and C_{v,O_2} are the arterial and venous blood oxygen concentrations respectively and C_{c,O_2} is the pulmonary end-capillary oxygen concentration.

The proportion of the ventilation that does not participate in gas exchange (the fractional deadspace ventilation) can also be calculated through analysis of the expiratory CO_2 data from the MBW performed using the MFS. This is also known as the Bohr deadspace and is calculated according to:

$$\frac{\dot{V}_D}{\dot{V}} = \frac{F_{A,\mathrm{CO_2}} - F_{E,\mathrm{CO_2}}}{F_{A,\mathrm{CO_2}}} \tag{4.7}$$

where $F_{A,CO2}$ is the mean fractional alveolar CO_2 concentration based on the end expiratory CO_2 concentration measured by the MFS and the $F_{E,CO2}$ is the mean fractional CO_2 concentration for the entire exhaled breath,[207] both of which are calculated directly from MFS data.

The core LNL model parameters are derived using a non-linear least squares optimisation algorithm to find the set of parameters which most closely match the model output simulated expired gas fractions to those measured by the MFS during the MBW test described in Section 4.1.1. Sample expirograms displaying both measured and simulated data during the air and oxygen-breathing phases of the test are displayed in Figure 4.3. The corresponding cumulative volume plot over an entire MBW test for this subject is also shown in Figure 4.4 (a), alongside the cumulative volume estimated by the LNL model for each gas, with the residuals from the fitting shown below in Figure 4.4 (b). The small overall residuals indicate a good fit to the experimental data, although there is some misfit of the CO_2 plateaus in this volunteer. This misfit may arise because the individual was small (height 1.53 m, weight 47 kg) and breathed with small tidal volumes of ∼0.41 L. For example, in another small individual (height 1.58 m, weight 77 kg), but who breathed with a larger tidal volume (∼0.96 L), this misfit was not apparent.

It should be noted that in the initial version of the model proposed by Mountain *et al.* the concentration of dissolved gases in the blood delivered to the lungs is approximated and then arterial concentrations are derived as model outputs. This is the version of the model used in the early clinical studies detailed in this thesis: the study of young smokers (presented later in this chapter) and the initial pilot study of CF patients at the John Radcliffe Hospital (detailed in Chapter 5).

The development of the circulation and body gas stores (CBGS) model by Magor-Elliott *et al.* enables more sophisticated modelling of blood gas concentrations.[208]

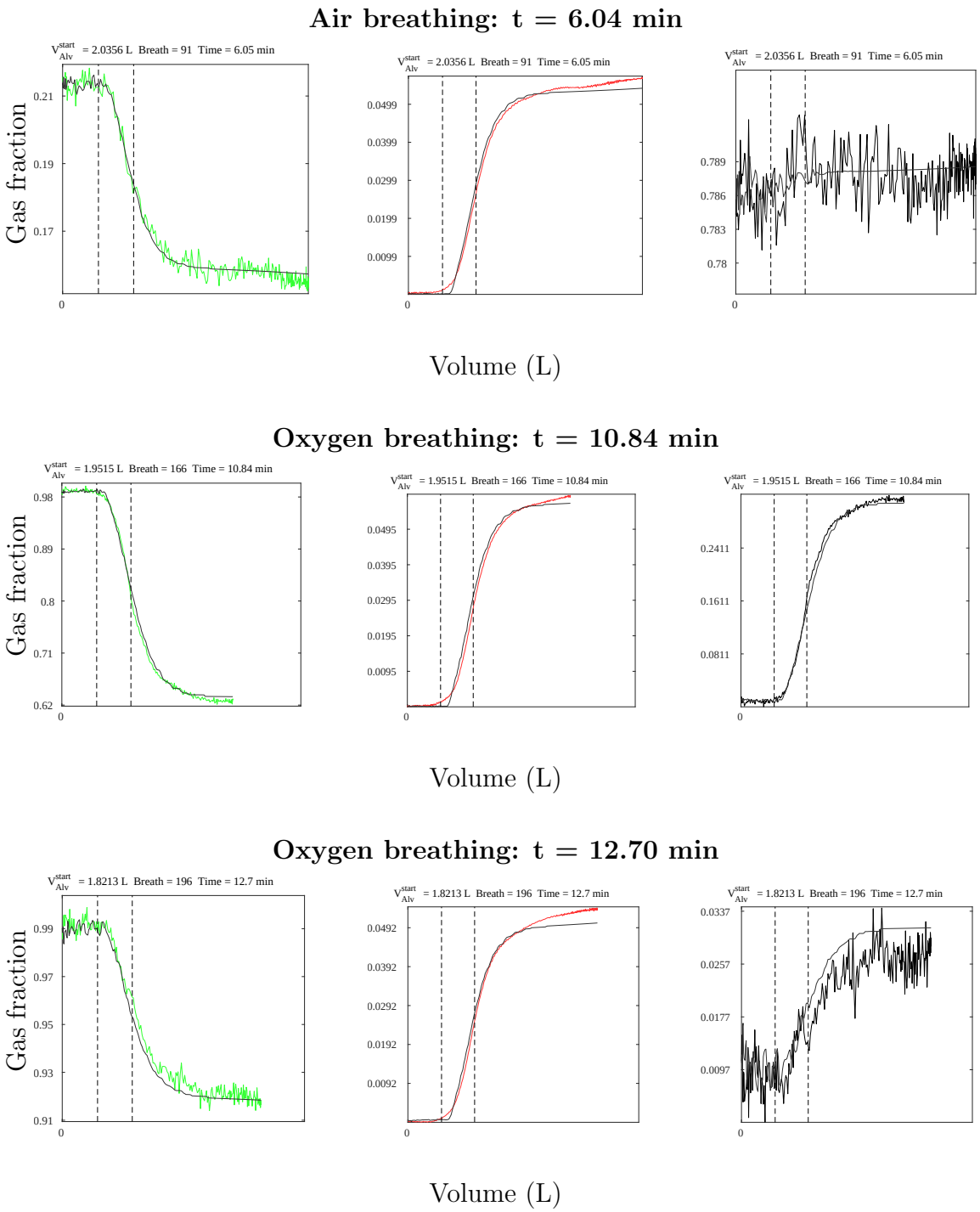
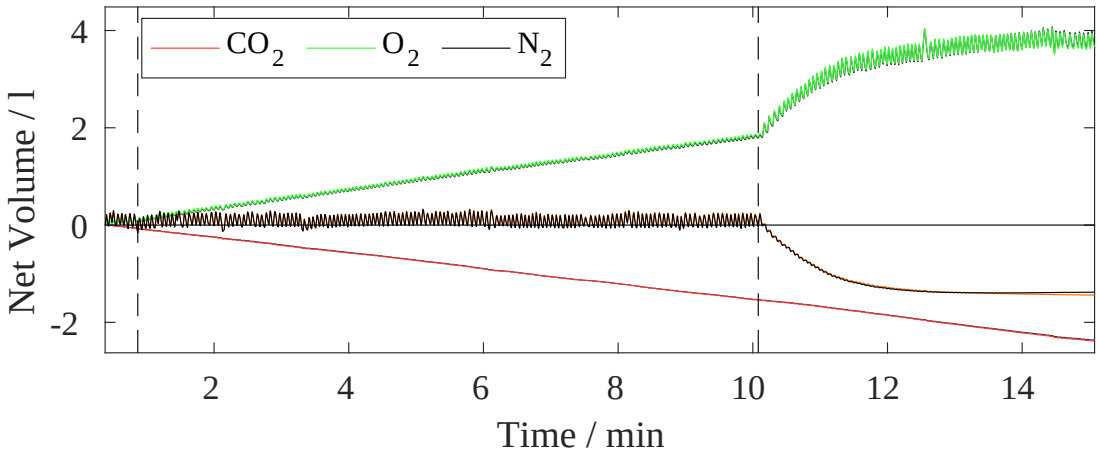


Figure 4.3: Fitted expiratory data from sample breaths during a MBW test on a healthy subject, plotting expired gas fraction against total volume of gas expired for a given breath. The first three figures show fitted expiratory breaths midway through the air breathing phase, the following three are selected from the start of the oxygen-breathing washout phase and the final three are from the end of the washout phase when the fraction of expired nitrogen is lower. The raw data recorded by the MFS for the O_2, CO_2 and N_2 fractions is shown in green, red and black at each time point and the corresponding fits by the LNL model are shown in black.

(a)



(b)

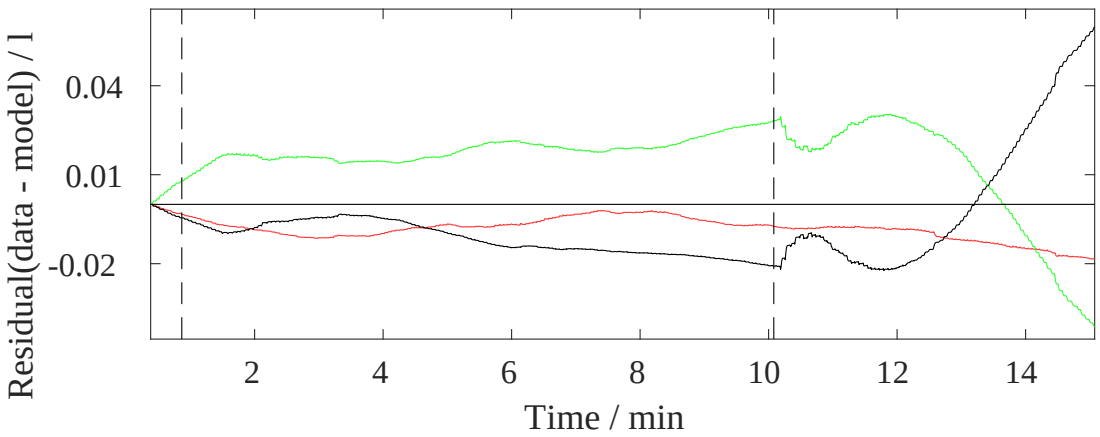


Figure 4.4: Sample data from a healthy subject's MBW with (a) showing the cumulative volume plot for the net volume measured by the MFS for O_2 (green), CO_2 (red) and N_2 as well as the corresponding simulated net gas volumes at the mouth simulated by the LNL model for each of the three gases. The residual net gas volumes (MFS data – LNL model) are shown for each gas in (b).

This model divides the body into compartments, the relative size and weight of which is defined for a "standard man" (25 years old, 1.8 m height and 70 kg mass). All these compartments are connected to the lungs by a series of separate circulatory vessels. This standard model can then be tailored to individual subjects by scaling their predicted body composition based on their sex, age, height and weight. The incorporation of the circulatory model into the LNL model allows the model outputs of arterial blood gas concentrations to be used as an input to determine the venous blood gas concentrations delivered to the lungs. This updated version of the LNL model is used for the later studies described in this thesis: the validation study comparing the LNL model with the multiple inert gas elimination technique (MIGET) and the second CF study performed in collaboration with the Royal Brompton Hospital.

4.2 Validation of Lognormal Lung Model by Comparison with MIGET

This section details a collaborative study performed at the University of California, San Diego (UCSD), where a comparison of parameters obtained using the multiple inert gas elimination technique (MIGET) and those derived from the lognormal lung (LNL) model was conducted for the first time. MIGET has been considered the gold standard for assessing lung inhomogeneity for almost 50 years, affording continuous distributions of the ventilation and perfusion of the lungs. In a perfectly homogeneous lung, all lung units would have the same $\dot{V}/\dot{Q}$ ratio, yet in reality the ventilation-perfusion ratio varies across even the healthy lung, due to factors such as gravity and deadspace. In the diseased lung, a greater degree of inhomogeneity in $\dot{V}/\dot{Q}$ is expected, with areas that are poorly perfused leading to areas of high $\dot{V}/\dot{Q}$, while areas which are poorly ventilated result in the low $\dot{V}/\dot{Q}$ regions of the lung. The most commonly reported parameters from the MIGET are the standard deviation of the ventilation and perfusion distributions, with elevated values expected in the presence of respiratory disease.

MIGET provided early evidence on the heterogeneity of the COPD patient population, who share no single unifying $\dot{V}/\dot{Q}$ distribution pattern.[209] The technique showed multiple $\dot{V}/\dot{Q}$ patterns depending on disease severity and phenotype, examples of which can be seen from the distributions in the UCSD study results, presented in Section 4.2.2.2. Historically COPD patients were termed "pink puffers" or "blue bloaters", classified as sufffering primarily from emphysema or chronic bronchitis respectively. In the case of patients with emphysema, patients unanimously presented



Figure 4.5: A photo of the research team from the University of Oxford and University of California, San Diego at the UCSD Radiology Imaging Laboratory prior to commencing the study comparing the LNL model results with the MIGET.

with a secondary peak at high $\dot{V}/\dot{Q}$, but no population of lower $\dot{V}/\dot{Q}$ regions, providing evidence for the theory of the destruction of the alveolar walls by emphysema and subsequent lack of perfusion. In the case of those suffering from chronic bronchitis, some but not all had a secondary $\dot{V}/\dot{Q}$ peak at low $\dot{V}/\dot{Q}$, likely due to mucus plugging, while others showed regions of high $\dot{V}/\dot{Q}$ or a combination of the two. Although the exact presentation varied between patients, $\dot{V}/\dot{Q}$ inequality was established as the major contributor to abnormal gas exchange in COPD patients and more significant than hypoventilation, shunt or diffusion limitation.[83] Both LogSD$\dot{V}$ and LogSD$\dot{Q}$ were found to correlate well with lung morphology,[210] and these parameters were shown to be more sensitive to early stage abnormalities in COPD patients than spirometry.[211] Increased $\dot{V}/\dot{Q}$ inequality was observed in patients suffering acute exacerbations, with a subsequent reduction upon recovery.[212] MIGET was also used to investigate the effect of multiple COPD drugs on $\dot{V}/\dot{Q}$ inequality, providing evidence for its course of action within the body - for example Melot *et al.* showed that almitrine bismesylate reduced $\dot{V}/\dot{Q}$ inequality through increasing the perfusion of better ventilated regions of the lung.[213,214]

This study allows a comparison between the degree of inhomogeneity observed using the LNL model and MIGET for the first time, and comparison between modelled and measured arterial blood values to validate the blood modelling which is incorporated into the LNL model.

Subject ID	Sex	Age/years	Height/m	Weight/kg	BMI
MIGET_1	M	64	1.78	102	32.2
MIGET_2	M	57	1.87	72	20.6
MIGET_3	M	67	1.78	104	32.8
MIGET_4	M	70	1.72	85	28.7
MIGET_5	M	55	1.58	45	18.0
MIGET_6	F	49	1.78	106	33.5
MIGET_7	M	53	1.59	88	34.8
MIGET_8	F	66	1.54	82	34.6
MIGET_9	M	69	1.78	77	24.3
Mean	-	61	1.71	85	28.8
Stdev	-	8	0.11	19	6.3

Table 4.2: Physical characteristics for all the participants recruited for the MIGET-LNL study.

4.2.1 Methods

All testing was conducted under ethical approval granted by the Human Subjects Research Protection Programme at UCSD and all experimental procedures were conducted at the UCSD Radiology Imaging Laboratory. In total, nine subjects with a COPD diagnosis were recruited for the study and their characteristics are listed in Table 4.2. Based on BMI, 4 patients would be classified as obese and one as overweight, which is common for the COPD population - approximately 65% of COPD patients are overweight or obese.[215]

Spirometry was performed on each subject using standard clinical practice prior to undergoing the MIGET procedure. Spirometry results were also converted to a percentage of the predicted value according to sex, age, height and ethnicity.

Each subject had an arterial and a venous line placed in opposite arms and the MIGET procedure was performed in a seated position. All the subject recruitment, spirometry, MIGET data collection and subsequent MIGET analysis was performed

by the research team of Professors Peter Wagner, Kim Prisk and Susan Hopkins. Following three sets of MIGET readings, the subjects were asked to perform two multiple breath washout experiments using the molecular flow sensor. Further details of the experimental method and subsequent analysis performed to obtain MIGET and MFS measurements are included in the following two subsections.

4.2.1.1 MIGET

The multiple inert gas elimination technique (MIGET) is a technique based on mass balance which relies on measurements of the retention and excretion of infused inert gases in the blood. The fraction of gas retained in arterial blood from the total amount delivered to the lung is a function of the inert gas partition coefficient λ and the $\dot{V}/\dot{Q}$ distribution. Hence the overall $\dot{V}/\dot{Q}$ distribution can be determined by measuring the retention for a range of 6 gases with varying solubility from $\lambda = 0.001$–100. Clearly, increasing solubility of a gas leads to increased retention of the gas. In order of least to most soluble, the infused gases used for the MIGET are sulphur hexafluoride, ethane, cyclopropane, isoflurane, diethyl ether and acetone.

To perform the technique, a radial arterial catheter was placed in one arm and a peripheral venous catheter in the other arm (to prevent any potential direct diffusion from the vein to the artery) with the subject in the supine position. A solution of the six inert gases in 0.9% saline was prepared which was then infused intravenously over a period of 40 minutes at a rate of 2-3 mL min^{-1}. Prior to obtaining the MIGET measurements for this study, the subject was moved to a seated position followed by a 20 minute break before commencing experiments to allow their respiratory system to equilibrate in the new position.

Retention is defined as the ratio of the systemic arterial partial pressure of a gas compared to the pulmonary arterial partial pressure, while excretion is the ratio of mixed expired to pulmonary arterial partial pressure. Hence three measurements of the partial pressure of the six inert gases are required. While the partial pressure of the systemic arteries and mixed expired gas can be easily obtained, direct measurement of pulmonary arterial blood would require a pulmonary arterial catheter, so is not generally used in MIGET studies in humans. Therefore, the pulmonary arterial pressure was instead estimated using the Fick Principle, utilizing mixed venous and arterial blood gas measurements and measured cardiac output.

For each set of MIGET measurements, mixed expired gas samples and arterial samples were taken physiologically simultaneously over the course of 2-3 breaths to allow for variability in tidal breathing. For the arterial samples, a sterile, untreated,

heparinised 30 mL syringe was used to collect a 6 mL sample. After a pre-determined delay to account for transit time from the mouth, a second researcher began collecting the 20 mL sample of expired gas in a sterile, ungreased glass syringe. The concentrations of inert gases in the blood and expired gas samples were determined using gas chromatography (Hewlett-Packard 5890) and cardiac output measurements were taken using impedance cardiography. The inert gas measurements from expired gas and blood samples were then entered into the MIGET software to determine the best fit $\dot{V}/\dot{Q}$ distribution to the data.

The function minimised to find the optimal solution for the 50 $\dot{V}/\dot{Q}$ units using the retention data from the 6 inert gases consists of 2 terms. The first of these accounts for the difference between the measured retentions of the 6 gases and the retentions calculated from a set of weightings for a 50 compartment $\dot{V}/\dot{Q}$ distribution. The second term is a smoothing function to afford stability of the distribution in the presence of experimental error. The weighting of the second term is determined by the scalar smoothing coefficient Z. For the data analysis for this study, the standard value of $Z = 40$ was used, which reflects a compromise between optimising the resolution of the derived distribution with acceptable stability of the results in the presence of experimental error. The residual sum of squares, RSS, indicates the quality of the fitting of the data to the 50 compartment model and is always quoted in the MIGET output files. It is calculated according to:

$$\text{RSS} = ||R - A.\dot{Q}|| + Z.||\dot{Q}||^2 \tag{4.8}$$

where R is the column vector containing the 6 retentions for the inert gases used, $\dot{Q}$ is a row vector of the blood flows of the 50 compartments and A is the 6×50 retention matrix where each element reflects the retention of an inert gas in one of the 50 $\dot{V}/\dot{Q}$ compartments according to:[83]

$$A = \frac{\lambda}{\lambda + \dot{V}/\dot{Q}} \tag{4.9}$$

Three sets of MIGET measurements were taken for each subject and the averaged values for Log$\text{SD}\dot{V}$, Log$\text{SD}\dot{Q}$, shunt and deadspace ventilation were compared with the LNL estimates.

4.2.1.2 MFS Washout and LNL Model

Following the completion of the MIGET measurements, each subject was asked to complete two washout tests as detailed in Section 4.1.1, with 10 minutes of air-

breathing followed by 5 minutes of breathing medical grade oxygen. Patients remained in the same upright position that they were in for the MIGET measurements.

For all the data in this study, the washouts were analysed using the updated version of the LNL model, which incorporates the CBGS blood modelling and allows the extraction of the modelled blood gas values at the timepoints when blood samples are taken. For each washout, the LNL non-linear least squares fitting routine was performed four times and the parameter set which returned the lowest overall residual (calculated by comparison between modelled and experimental data) was selected. Where a patient performed two washouts which successfully returned LNL parameters, an average of the two parameter sets was used in further analysis.

Due to the placement of an arterial line for the MIGET measurements, it was also possible to take samples during the washout procedure for comparison with the LNL model circulatory parameters. This does not form part of the routine clinical use of the MFS and LNL model and this study represents the first time that arterial samples could be directly compared with the LNL modelled values. During the air breathing phase of each washout, a 3 mL arterial blood sample was taken at approximately 5, 7 and 9 minutes, with the exact times recorded with a time stamp in the MFS LabVIEW software. These samples were then analysed using blood gas analysis and CO-oximetry. Arterial oxygen saturation was also continually measured using a pulse oximeter connected to the MFS. Therefore, in total three different estimates of blood oxygen concentration were obtained which could be used to estimate shunt.

4.2.2 Results

All but one of the nine subjects recruited for the study tolerated the MIGET protocol well and proceeded to the LNL section of the study. As no LNL washout data is available for comparison with MIGET data for this subject (MIGET_7), they are not included in the results and discussion. The data obtained from the remaining eight participants are presented in this section.

4.2.2.1 Spirometry

The spirometry data from the eight participants for whom both MIGET and LNL results were obtained are displayed in Table 4.3. Of the eight patients who completed at least one N_2 washout, seven displayed evidence of obstructive lung disease in their spirometry results, defined as having an FEV_1/FVC ratio below 0.7.[70] According to the Global Initiative for Obstructive Lung Disease (GOLD) staging system, only one

Subject ID	FEV_1/L	FEV_1/% pred	FVC/L	FVC/% pred	FEV_1/FVC
MIGET_1	0.8	23	2.00	43	0.40
MIGET_2	2.11	50	3.99	73	0.53
MIGET_3	1.55	52	2.29	59	0.68
MIGET_4	1.82	61	3.00	74	0.61
MIGET_5	2.14	75	3.37	91	0.64
MIGET_6	3.47	101	4.31	99	0.81
MIGET_8	1.90	92	2.52	92	0.75
MIGET_9	1.99	60	3.51	78	0.57
Mean	2.01	66	3.08	75.8	0.65
Stdev	0.71	24	0.78	17.4	0.14

Table 4.3: Spirometry data collected from the MIGET participants. FEV_1 is the forced expiratory volume in one second and FVC is the forced vital capacity. Absolute values in L are quoted at BTPS and % pred. describes the spirometry value as a percentage of the predicted value based on sex, age, height and ethnicity.

subject (MIGET_1) is classified as the most severe GOLD stage 4, due to having an FEV_1 of less than 30% of the predicted value for someone of their sex, age, height and ethnicity. No subjects are classified as GOLD stage 3 (defined as someone with an FEV_1 of 30–49% predicted). With FEV_1 values between 50% and 79% of their predicted value, five of the patients are classified as GOLD stage 2. The results of the remaining two participants, MIGET_6 and MIGET_8, display normal spirometry with FEV_1/FVC ratios above 0.7 and FEV_1 values exceeding 90% predicted.

4.2.2.2 MIGET

The values reported in this section are all calculated by averaging the results obtained from 3 sets of MIGET parameters. The residual sum of squares (RSS) values for fitting the 50 compartment model evaluates the quality of the fitting and the mean RSS values for nine participants are shown in Table 4.4. The low mean RSS of 3.87 ± 2.59

indicates good quality data (RSS should not exceed 5.3 in more than 50% of cases[83]). The fractional deadspace volume (ventilation at $\dot{V}/\dot{Q} = \infty$) and percentage shunt (perfusion at $\dot{V}/\dot{Q} = 0$) are also presented in this table. Due to the upper and lower limits of detectability, these will also include ventilation at $\dot{V}/\dot{Q} > 100$ and $\dot{V}/\dot{Q} < 0.005$ respectively.

Subject ID	RSS	Deadspace Ventilation	Shunt (%)	$\dot{V}/\dot{Q}$ distribution
MIGET_1	3.35	0.41	0.3	high $\dot{V}/\dot{Q}$ peak
MIGET_2	9.00	0.49	0.5	high $\dot{V}/\dot{Q}$ peak
MIGET_3	2.37	0.32	0.1	unimodal
MIGET_4	3.72	0.46	3.1	high $\dot{V}/\dot{Q}$ peak
MIGET_5	2.22	0.47	1.6	high $\dot{V}/\dot{Q}$ peak
MIGET_6	6.51	0.37	0.1	low $\dot{V}/\dot{Q}$ peak
MIGET_8	1.43	0.29	1.1	low $\dot{V}/\dot{Q}$ peak
MIGET_9	2.38	0.43	0.7	high $\dot{V}/\dot{Q}$ peak
Mean	3.87	0.40	0.9	-
Sd	2.59	0.07	1.0	-

Table 4.4: The residual sum of squares of the MIGET data for fitting the 50 compartment model. The shunt perfusion (the sum of all perfusion to regions of the lung with a $\dot{V}/\dot{Q}$ ratio of < 0.005) is presented as a percentage of the total perfusion. The deadspace ventilation (the sum of all ventilation to regions of the lung with a $\dot{V}/\dot{Q}$ ratio of > 100) is given as a fraction of the total ventilation. Also shown is a description of the shape of the $\dot{V}/\dot{Q}$ distribution.

In all subjects a proportion of total ventilation will correspond to regions of the lung that are not perfused, *i.e.* the deadspace ventilation, which has a $\dot{V}/\dot{Q}$ ratio of ∞ (a normal range for the deadspace ventilation is 20–40% of the total ventilation). In normal healthy subjects, with the exception of the deadspace ventilation, the populated compartments of the $\dot{V}/\dot{Q}$ distribution are confined to $\dot{V}/\dot{Q}$ values between 0.3 and 3.[83,216] None of the COPD patients in this study had a $\dot{V}/\dot{Q}$ distribution confined to this range, so this group displayed a mismatch between the ventilation

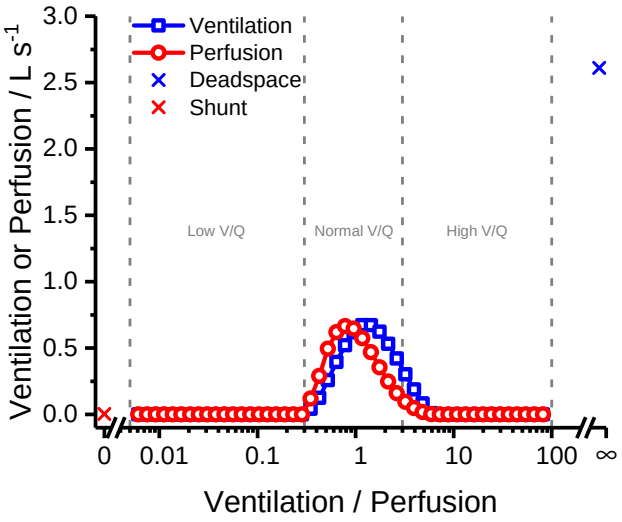


Figure 4.6: The $\dot{V}/\dot{Q}$ distribution determined by MIGET for the sole participant who displayed a unimodal distribution (MIGET_3). The shunt perfusion and deadspace ventilation determined by MIGET are also included on the same scale, corresponding to the perfusion and ventilation of the lung compartments where the $\dot{V}/\dot{Q}$ ratio is zero and infinity respectively.

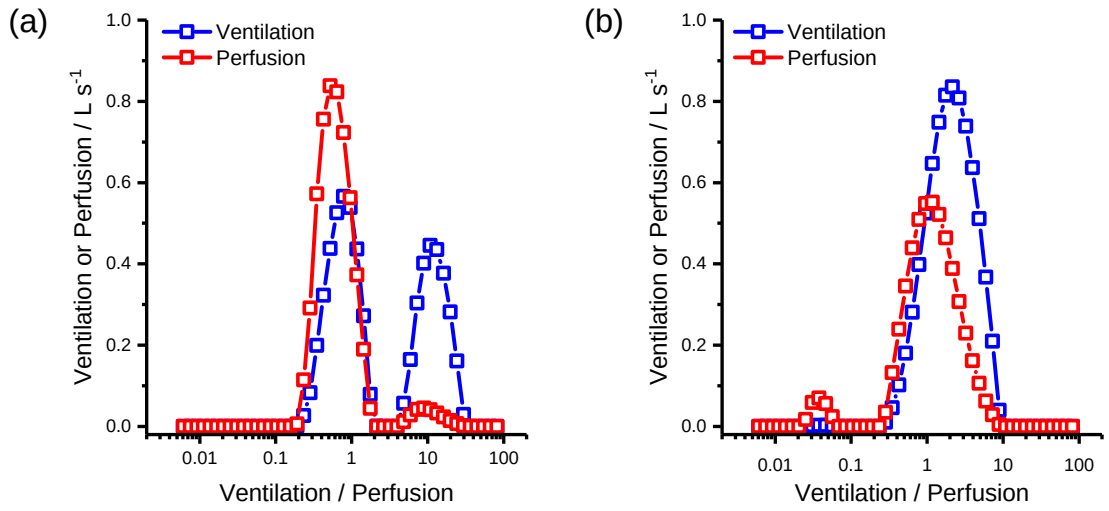


Figure 4.7: Sample bimodal $\dot{V}/\dot{Q}$ distributions resolved by the 50 compartment MIGET model with (a) displaying a second peak at high $\dot{V}/\dot{Q}$ (MIGET_2) and (b) showing a second peak at low $\dot{V}/\dot{Q}$ (MIGET_6).

and perfusion of the lungs compared to healthy individuals - this results in reduced pulmonary gas exchange efficiency. A unimodal distribution was observed for only one of the subjects (MIGET_3) and this is displayed in Figure 4.6, with the normal range of healthy individual's $\dot{V}/\dot{Q}$ distribution also indicated for reference. Bimodal distributions were resolved for the remaining eight subjects. Two subjects showed a peak at low $\dot{V}/\dot{Q}$, corresponding to poorly ventilated regions of the lung, while the remaining five displayed a peak at high $\dot{V}/\dot{Q}$, reflecting poorly perfused compartments (individual assigments are included in Table 4.4). Sample bimodal distributions from two of the subjects are presented in Figure 4.7.

Table 4.5 shows the first three moments of the $\dot{V}/\dot{Q}$ distribution on a logarithmic scale for the 48 compartments with a $\dot{V}/\dot{Q}$ ratio between 0.005 and 100. Elevated

Subject	Perfusion Moments			Ventilation Moments		
	$\dot{Q}_{mean}$	LogSD$\dot{Q}$	$\dot{Q}_{skew}$	$\dot{V}_{mean}$	LogSD$\dot{V}$	$\dot{V}_{skew}$
MIGET_1	1.06	0.82*	0.54	2.65**	1.02*	-0.10
MIGET_2	0.68*	0.73*	0.86	2.43**	1.44*	0.65
MIGET_3	0.97	0.55	0.07	1.35*	0.59	0.00
MIGET_4	0.80	0.75*	0.36	1.68*	0.94*	0.09
MIGET_5	0.61*	0.89*	0.91	2.61**	1.43*	0.18
MIGET_6	1.12	0.80*	-0.81	1.85*	0.67*	0.07
MIGET_8	1.50	1.08*	-3.63**	2.70**	0.64	-0.11
MIGET_9	0.57**	0.79*	0.39	1.29*	1.00*	0.16
Mean	0.91	0.80	-0.16	2.07	0.97	0.12
Sd	0.32	0.15	1.50	0.59	0.33	0.24

Table 4.5: The first ($\dot{Q}_{mean}$ and $\dot{V}_{mean}$), second (LogSD$\dot{Q}$ and LogSD$\dot{V}$) and third ($\dot{Q}_{skew}$ and $\dot{V}_{skew}$) moments of the perfusion and ventilation distributions. Where these values fall outside the normal range reported by Hopkins and Wagner,[83] this is denoted by * for moderately abnormal and ** for severely abnormal.

second moments, LogSD$\dot{Q}$ and LogSD$\dot{V}$, reflect greater dispersion of the distributions and hence increased lung inhomogeneity. This is observed for seven of the subjects with moderately abnormal LogSD$\dot{Q}$ values and six of the subjects with moderately abnormal LogSD$\dot{V}$ values.

In a previous study of seven healthy subjects aged 23-63, the MIGET measurements for LogSD$\dot{V}$ and LogSD$\dot{Q}$ reported by Sá *et al.* were strongly correlated (Pearson's r = 0.975, p < 0.001).[217] By contrast, Figure 4.8 shows there was little concordance between LogSD$\dot{V}$ and LogSD$\dot{Q}$ measured by MIGET for the COPD patients in the MIGET-LNL study, with only the unimodal subject MIGET_3 lying close to the line of identity. The two with a secondary high $\dot{V}/\dot{Q}$ peak have a higher degree of ventilation inhomogeneity, while those with a low $\dot{V}/\dot{Q}$ peak have greater perfusion inhomogeneity. The two low $\dot{V}/\dot{Q}$ peak subjects, MIGET_6 and MIGET_8, were the only two subjects with normal spirometry, which is consistent with the findings of Rodrìguez-Roisin *et al.* that in the earliest stages of COPD, greater abnormality was seen in LogSD$\dot{Q}$ than LogSD$\dot{V}$ due to the presence of low $\dot{V}/\dot{Q}$ peak, posited to reflect the presence of poorly-ventilated but well-perfused small airways, which spirometry cannot sensitively detect.[86]

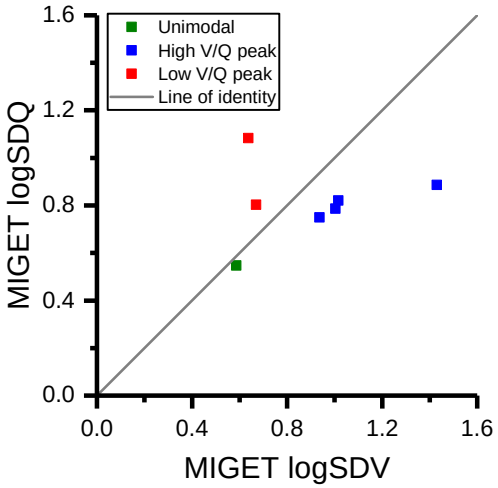


Figure 4.8: Intra-subject comparison of LogSD$\dot{V}$ and LogSD$\dot{Q}$ values determined by MIGET. The correlation between the two parameters for these subjects was found to be non-significant (Pearson's r = 0.711, p = 0.17).

4.2.2.3 Lognormal Lung

Of the eight subjects who progressed to the LNL part of the study, seven consented to performing two washouts, while one subject (MIGET_4) only performed a single washout. For one subject (MIGET_3), a significant leak from the noseclip on the first washout meant that this dataset had to be excluded from further analysis. Analysis of the end tidal nitrogen fraction at the end of the washout is shown in Figure 4.9. An average of the final three breaths of the washout phase was used to account for variability due to participants' unrestricted tidal breathing. In order to obtain a good estimate of the lung parameters, the LNL model requires the cumulative expired volume of nitrogen to reach an asymptote, which is not possible if there remains a high expired N_2 fraction at the end of the washout period. As shown in Figure 4.9, the two washouts for subject MIGET_2 were clearly incomplete and hence have not been included in further analysis. Therefore, there remain seven subjects with LNL parameters to compare to the MIGET measurements. For the five participants for whom two sets of LNL parameters were obtained, the two sets of values were averaged to provide the values used in subsequent analysis.

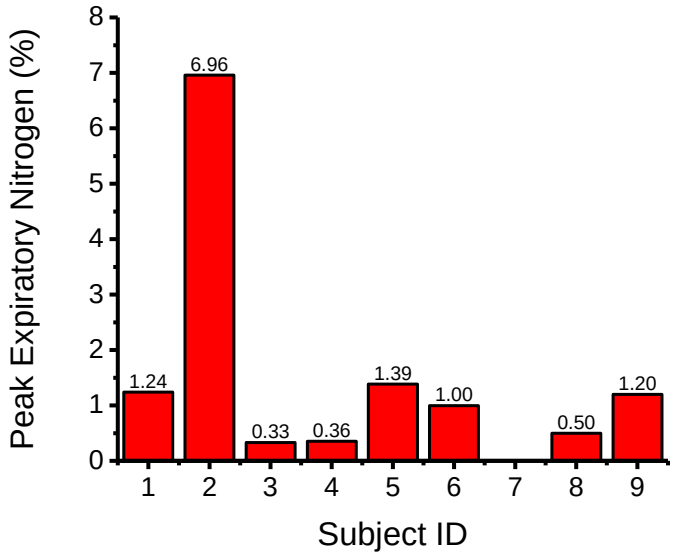


Figure 4.9: Averaged end-tidal peak expiratory nitrogen fraction for the final three breaths of the washout phase. Where two washouts were successfully completed by a subject, the average of the two datasets is shown.

The five core LNL parameters for the seven participants are presented in Table 4.6, alongside the standard deviations if two washouts were successfully analysed. For

five of the subjects, the σ_{CL} and σ_{Cd} values lie well above the upper end of normal observed in a healthy control group of comparable age to these subjects.[218] Taking into account normal change with age, two of the participants (MIGET_6 and MIGET_8) display σ_{CL} values within the observed range of values for healthy controls of a similar age, although towards the upper limits of normal.[115,218,219] For MIGET_8, σ_{Cd} also lies towards the upper end of the range of healthy controls, while for MIGET_6 σ_{Cd} greatly exceeds the healthy control range. In a cross-sectional study of 32 COPD patients ranging from stage 1-4 COPD, Smith *et al.* observed a single patient with stage 2 COPD who had a σ_{CL} value within the normal range,[218] so these two subjects represent potentially interesting outliers within the COPD population. Notably these two subjects are the only volunteers in this study who do not show evidence of obstructive spirometry according to their FEV_1/FVC ratio. The inhomogeneity of deadspace, σ_{VD} values for all participants in this study lie above 0.34, the mean of the healthy population studied by Smith *et al.*, with σ_{VD} for MIGET_1, MIGET_3 and MIGET_8 exceeding the upper limit of normal observed in the same study.[218,219] It is however consistent that many subjects in this study fall within the healthy range for this parameter, as it has been shown to be less sensitive than the other two LNL

Subject ID	V_D (L)	V_A (L)	σ_{VD}	σ_{CL}	σ_{Cd}	FRC (% pred.)
MIGET_1	0.34 ± 0.02	6.97 ± 0.18	0.51 ±< 0.01	1.03 ±< 0.01	2.57 ± 0.01	200.1 ± 5.5
MIGET_3	0.14	2.11	0.48	0.87	1.43	61.1
MIGET_4	0.14	3.26	0.44	0.85	2.13	95.5
MIGET_5	0.15 ±< 0.01	3.30 ± 0.01	0.45 ± 0.01	0.86 ± 0.03	2.14 ± 0.07	111.2
MIGET_6	0.10 ±< 0.01	1.82 ± 0.03	0.41 ± 0.06	0.58 ± 0.06	1.45 ± 0.14	63.4 ± 0.8
MIGET_8	0.11 ± 0.02	1.83 ± 0.16	0.46 ± 0.01	0.61 ± 0.01	0.92 ± 0.01	77.1 ± 7.2
MIGET_9	0.13 ± 0.02	3.49 ± 0.07	0.39 ± 0.01	0.82 ± 0.03	1.49 ± 0.06	97.9 ± 1.5
Average	0.16	3.25	0.45	0.80	1.73	100.9
St. Dev.	0.08	1.79	0.04	0.16	0.57	44.0

Table 4.6: The core parameter values output by the LNL model analysis. The deadspace and alveolar volumes (V_A and V_D) are expressed as litres at body temperature, ambient pressure and gas saturated with water vapour (BTPS). For the five participants who successfully completed two washouts, the standard deviation of the values obtained is shown to two decimal places.

model inhomogeneity parameters in discriminating between healthy controls and patients with diagnosed asthma and COPD.[200,218,219]

The alveolar volume for MIGET_1 is significantly larger than the other participants with reasonable agreement between the two washouts performed. Summing the alveolar and deadspace volumes and comparing with the predicted volume at FRC based on age, sex and height shows this subject has an FRC of 200% of the predicted value. This suggests significant lung hyperinflation/air-trapping at rest in this patient, a pattern of disease which is often observed in COPD.[220] Normal values of FRC (% pred.) were observed for four individuals - a normal value (95% confidence interval) was defined as 75-120% of the predicted value.[69] Two subjects, MIGET_3 and MIGET_6, had FRC (% pred.) values of 61% and 63% respectively, which is below the normal range. Although obstructive lung disease is characterised by elevated lung volumes, obesity may be a confounding factor in these subjects. Based on their BMI values (Table 4.2), both subjects would be classified as mildly obese, which in subjects with no diagnosis of lung disease was associated with a 22% reduction in FRC.[221,222]

In addition to the LNL parameters presented in Table 4.6, an estimate of LogSD$\dot{V}$, LogSD$\dot{Q}$, % shunt, and fractional deadspace ventilation were all calculated secondary to the LNL fitting procedure as described in Section 4.1.2. A comparison between these values and those obtained using the MIGET is included in the following section.

As part of the LNL model fitting procedure, the arterial blood gas concentrations of O_2 and CO_2 are estimated and can be output at a given point in the washout. As arterial lines were already in place for the MIGET protocol, it was possible to take arterial blood samples for comparison with the model values. Three samples were taken during the air breathing phase of each washout and the modelled partial pressure of O_2 and CO_2 is compared with the values obtained from blood gas analysis in Figures 4.10 and 4.11 respectively. The model outputs modelled gas concentrations with lag times from 0-60 s to account for the time taken to collect the sample for a given experiment. In this analysis a lag time of 10 s is used to approximate the time taken to collect the sample. With the exception of MIGET_3, the model predicted a higher arterial partial pressure of O_2, PaO_2, than the measured arterial samples. On average across all 12 washouts the LNL model predicted a PaO_2 value 13.9% higher than the measured blood gas analyser values. Meanwhile the modelled arterial partial pressure of CO_2, $PaCO_2$, was higher for five of the washouts and lower for the remaining six, predicting on average a $PaCO_2$ 2.5% higher than the experimentally determined values.

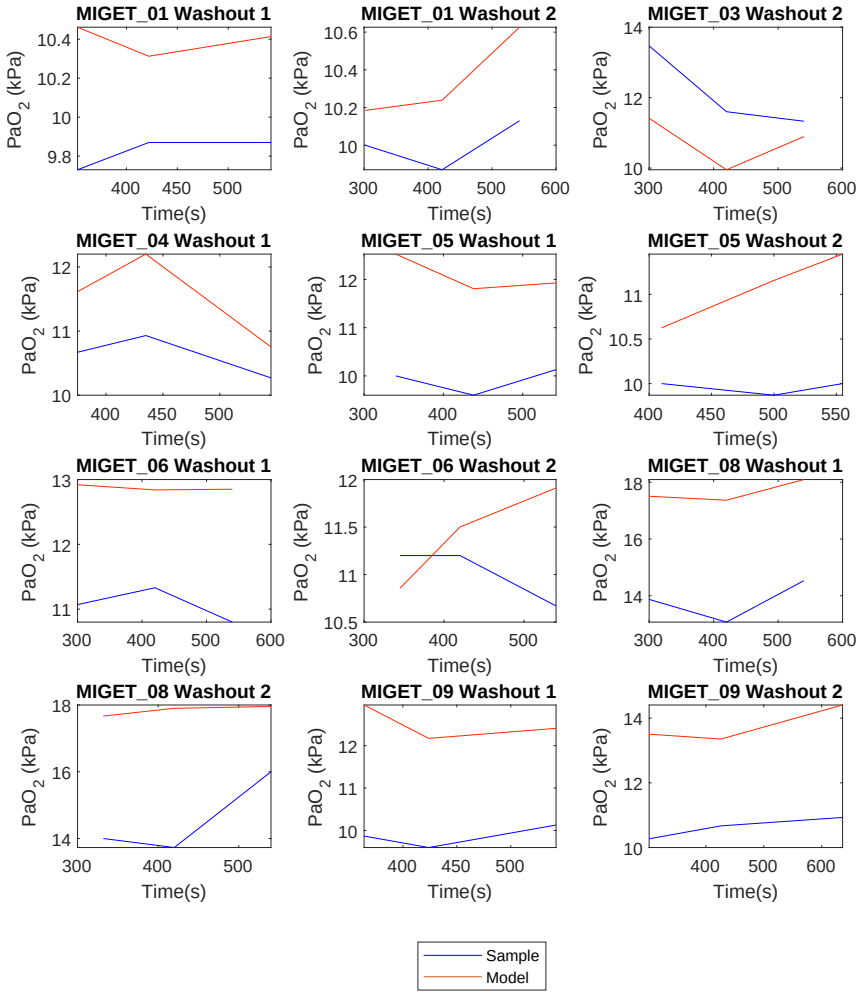


Figure 4.10: A comparison between the measured arterial oxygen content at three intervals during the air breathing phase of the washout and the LNL modelled arterial oxygen content at the same time point with a 10 s lag time. Measurements were obtained through arterial blood samples analysed using a blood gas analyser.

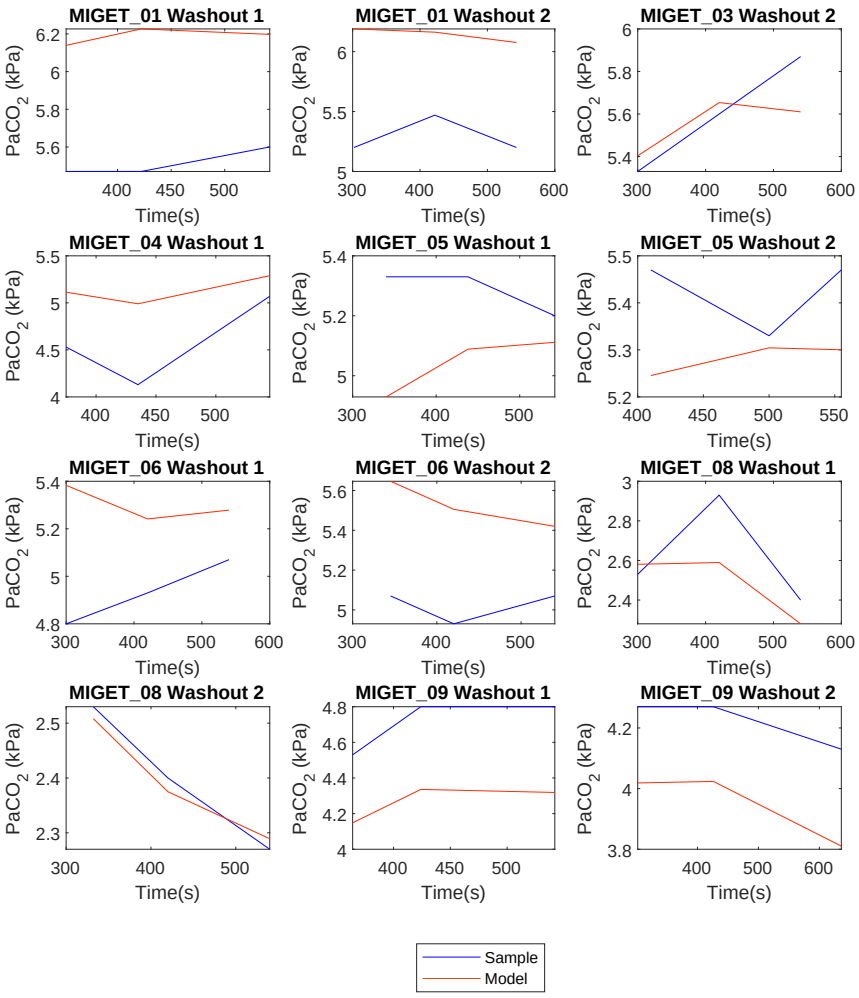


Figure 4.11: A comparison between the measured arterial carbon dioxide content at three intervals during the air breathing phase of the washout and the LNL modelled arterial carbon dioxide content at the same time point with a 10 s lag time. Measurements were obtained through arterial blood samples analysed using a blood gas analyser.

4.2.3 Discussion

The comparison between the measured partial pressure of O_2 in arterial blood samples and the modelled LNL values showed a general trend of the model overestimating the blood oxygen content. This is consistent with the blood modelling of the LNL model, as the LNL model does not include all possible mechanisms to lower the oxygen content. In particular, regions of shunt (or very low $\dot{V}/\dot{Q}$) are not incorporated within the model, so venous blood that effectively bypasses the lungs as it perfuses under-ventilated regions will be returned unchanged to the arterial blood. The single exception is MIGET_3, for whom a lower O_2 content was predicted. Notably the MIGET measured shunt of 0.1% was very low for this participant and this subject is the only one without significant population of low $\dot{V}/\dot{Q}$ regions of the lung, as shown by their $\dot{V}/\dot{Q}$ distribution (Figure 4.6).

The reverse may be expected of the CO_2 concentrations, but in fact little bias is seen between the measured and modelled values for the participants in this study. The discrepancies seen for CO_2 may reflect some limitations of the blood modelling of tissue solubilities for CO_2 within the blood model. For two subjects, MIGET_5 and MIGET_9, the measured CO_2 content exceeded the modelled at all three timepoints across both washouts. This could result from a high $\dot{V}/\dot{Q}$ peak (which both patients had), whereby the ventilation of a bulla (an alveolar sac with no blood flow, *i.e.* alveolar deadspace) is attributed in the model to the more effective univariate $\dot{V}/\dot{Q}$ distribution where it would act to lower the model arterial CO_2.

As discussed in Section 4.1.2, four parameters can be estimated from the LNL model, secondary to the fitting procedure: the second moments for the ventilation and perfusion distributions (LogSD$\dot{V}$ and LogSD$\dot{Q}$), the deadspace ventilation and pulmonary shunt. In addition to a direct comparison between the parameter values estimated by the two methods, Bland-Altman analysis is also shown in Figures 4.12 and 4.14. First proposed by Bland and Altman in 1983, the technique seeks to overcome the limitations of using correlation coefficients where a high correlation coefficient does not necessarily confirm sufficient agreement between techniques that they could be used interchangeably in a clinical setting.[223] The technique instead investigates the difference between the measured values through plotting the mean of the two values against the difference between them, illustrating a confidence interval within which 95% of the differences would fall.[224] These plots are used to evaluate the level of agreement between two techniques and identify the presence of systemic bias or outliers within the population studied. For the four parameters where Bland-Altman plots were used, Shapiro-Wilk tests for normality of the distributions found that they

were significantly drawn from normal distributions (for deadspace ventilation, shunt, LogSD$\dot{V}$ and LogSD$\dot{Q}$, p = 0.282, 0.268, 0.996 and 0.533 respectively). Therefore, it is acceptable to plot the difference between measured values against the mean without taking logarithms for the Bland-Altman analysis.[224]

Considering first the deadspace ventilation in Figure 4.12 (a), strong correlation was observed between the values obtained for the two techniques (Pearson's r = 0.798, p = 0.031). However, Figure 4.12 (b) shows clear bias, with the LNL model estimating a lower deadspace ventilation than MIGET. This finding is consistent with the LNL model only including anatomical deadspace in its estimate, while the MIGET deadspace also incorporates physiological deadspace resulting from unperfused lung volume. Although the Bland-Altman analysis does not identify them as outliers, three of the participants with a high $\dot{V}/\dot{Q}$ peak identified by MIGET show the greatest discrepancy between the techniques. The high $\dot{V}/\dot{Q}$ peak indicates the presence of poorly perfused areas of the lung and therefore the presence of alveolar deadspace, which would be excluded from the LNL model's estimation of solely anatomical deadspace. For the three subjects with a unimodal distribution or low $\dot{V}/\dot{Q}$ peak, the presence of alveolar deadspace would not be expected and correspondingly close agreement between MIGET and the LNL model is observed.

Figure 4.12 (c) compares the percentage shunt calculated by the two methods and shows very little concordance between the two methods (Pearson's r = 0.537, p = 0.214). This is further confirmed by the Bland-Altman plot in Figure 4.12 (d) which shows that on average the LNL model significantly overestimates shunt. There exists an intrinsically higher uncertainty in the LNL model's estimation of any circulatory parameters compared with airways parameters, due to the limited information encoded within the expired gas concentrations. In the case of shunt, this is blood which does not participate in gas exchange at all and hence is not directly 'seen' by the model. Mountain *et al.* theorized that the inability of the LNL model to resolve multimodal $\dot{V}/\dot{Q}$ distributions may result in an overestimation of shunt by the model.[115] However, this would be expected to result from misattributing regions of low $\dot{V}/\dot{Q}$ to shunt, whereas in this study the model overestimated the shunt by the largest margin for the subjects with secondary high $\dot{V}/\dot{Q}$ peaks.

Directly measuring arterial blood samples afforded two additional LNL model estimates of the shunt, in addition to the estimate based on pulse oximetry readings recorded by the MFS as part of the standard MBW protocol. Figure 4.13 (a) shows a significant bias in the measurement of arterial oxygen saturation by the CO-oximeter, a device that uses spectrophotometry to measure the concentration of different forms

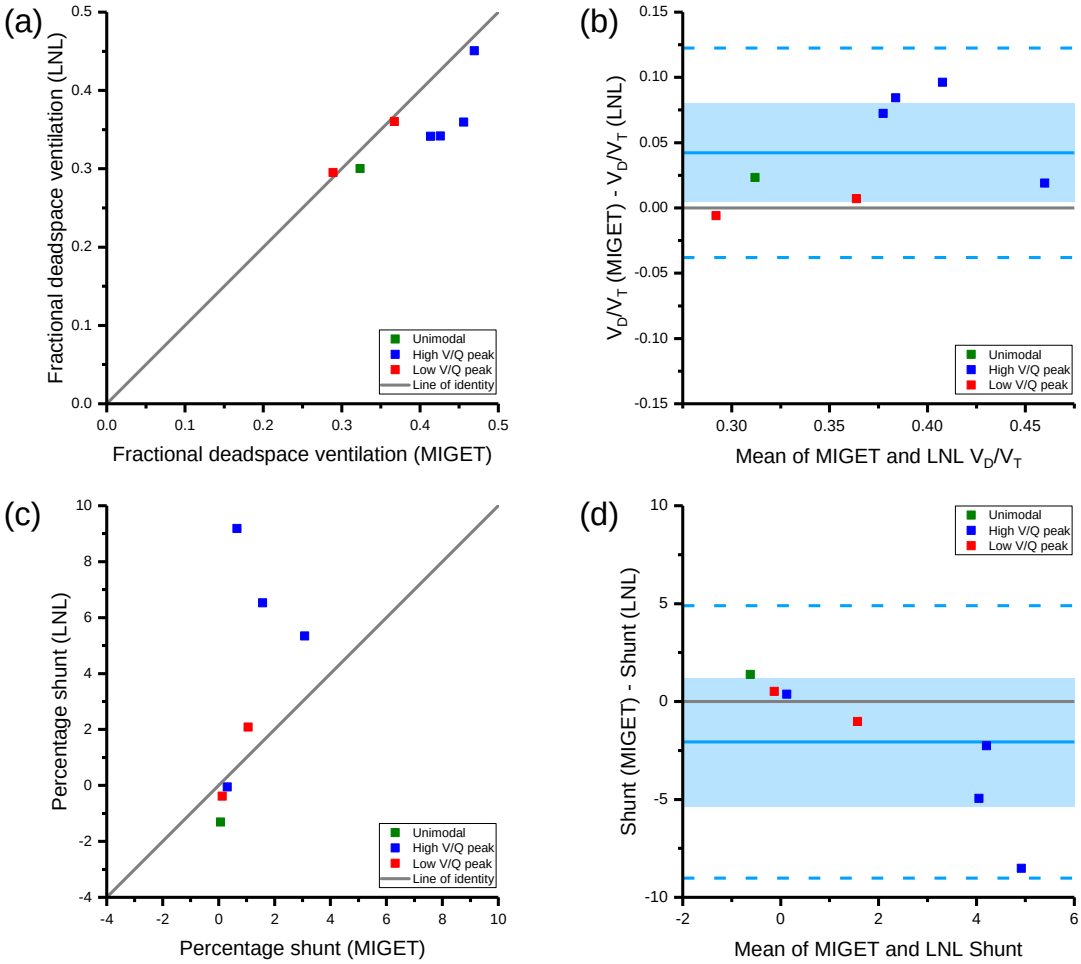


Figure 4.12: A comparison between the estimated fractional deadspace ventilation V_D/V_T (a) and percentage shunt (c) obtained from MIGET analysis and LNL modelling. The single participant with a unimodal $\dot{V}/\dot{Q}$ distribution is shown in green, the four with a second peak at high $\dot{V}/\dot{Q}$ in blue and the two with a second peak at low $\dot{V}/\dot{Q}$ are shown in red. A line of identity is displayed on each plot for reference. The agreement between the values of fractional deadspace ventilation and percentage shunt estimated by the two techniques are also compared using Bland-Altman analysis, displayed in (b) and (d) respectively. The plots are centred around the line of identity (grey) and comparison between the points and this line indicates the bias between the values for the two methods. The complete blue line shows the mean difference between the measurements with the shaded blue area representing the 95% confidence interval for the mean value. The dashed blue lines denote ±1.96SD from the mean, the range within which 95% of the data points are expected to fall.

of haemoglobin in the blood. The higher measurements of oxygen saturation from the CO-oximeter resulted in physiologically impossible values of less than 0% shunt in all but one participant, as seen in Figure 4.13 (b). The higher SpO_2 measured

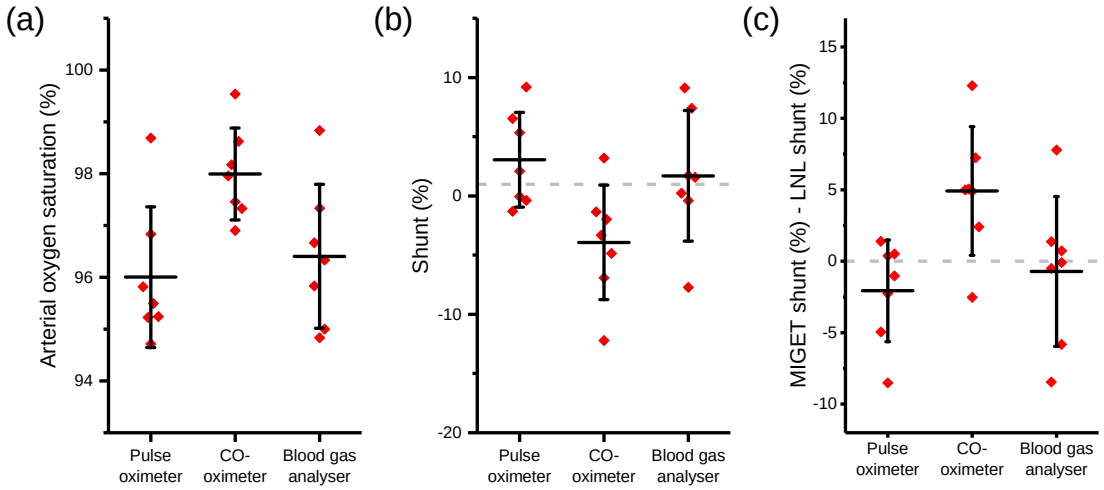


Figure 4.13: The arterial oxygen saturation values obtained for the participants during the air breathing phase of the washout (a) measured using the pulse oximeter integrated into the MFS data acquisition software and analysis of three arterial blood samples using a CO-oximeter and a blood gas analyser with mean ± 1SD displayed for each. The corresponding calculated percentage shunt values using the three different measurements are displayed in (b) with the mean ± 1SD indicated. The mean percentage shunt obtained using the MIGET is also displayed for reference using a dashed grey line.

by CO-oximetry could potentially result from a left shift in the oxygen dissociation curve due to the presence of carboxyhaemoglobin. In the case of CO preferentially binding to haemoglobin, O_2 binds more strongly to the remaining vacant Hb sites, resulting in less O_2 being released to the tissue.[225] However, most subjects had ceased smoking and the HbCO measured by the CO-oximeter was within the expected range for non-smokers for all subjects apart from MIGET_4 and MIGET_6.[226] A more likely explanation for the bias in the SpO_2 CO-oximeter measurements may be poor calibration of the device.

Figure 4.14 compares the estimated LogSD$\dot{V}$ and LogSD$\dot{Q}$ for the two techniques. The LNL model considerably underestimates both parameters, with the notable exception of the single subject, MIGET_3, who has a unimodal $\dot{V}/\dot{Q}$ distribution. Unlike MIGET, which can identify up to three modes, the LNL model assumes that the compliance and perfusion is lognormal and hence the estimates of LogSD$\dot{V}$ and LogSD$\dot{Q}$ are necessarily based on a unimodal distribution. Estimating the second moments for the ventilation and perfusion distributions using a lognormal (and therefore uni-

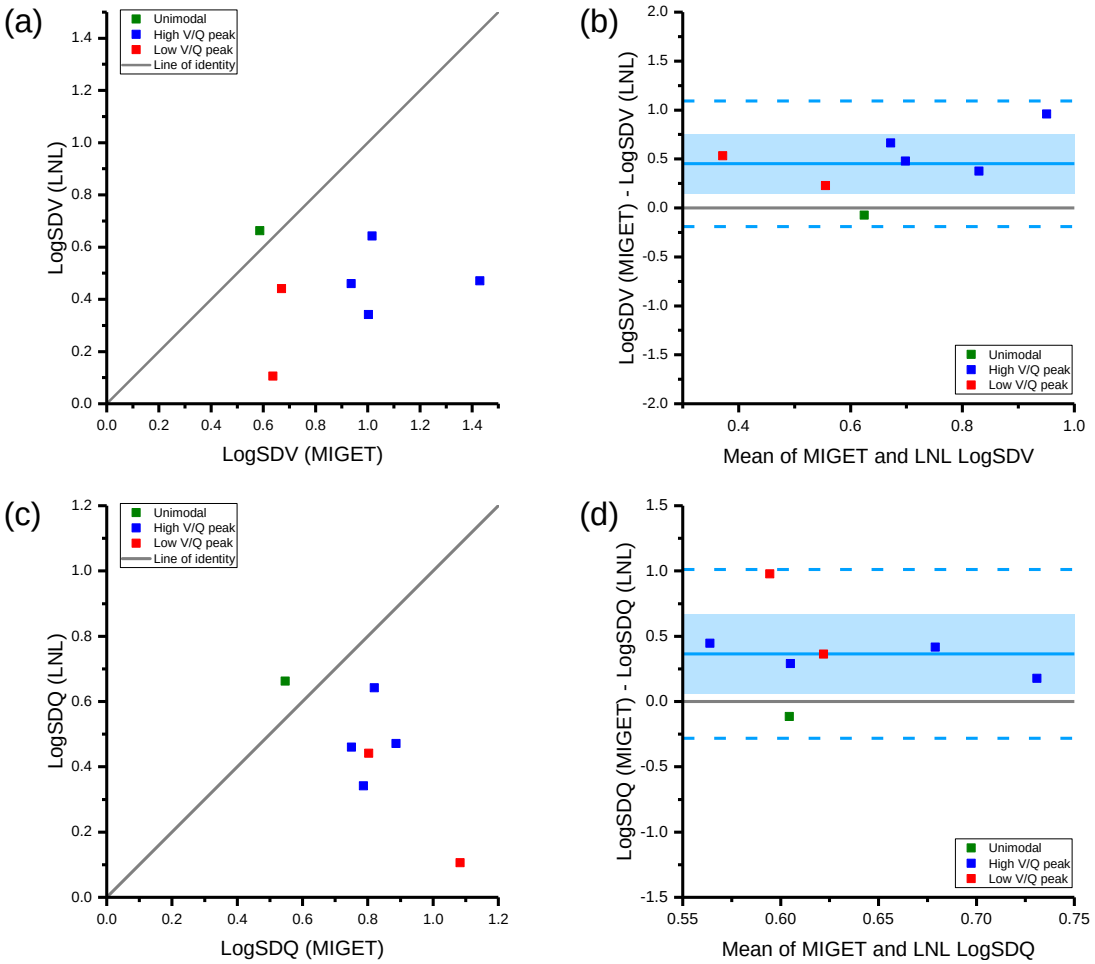


Figure 4.14: A comparison between LogSD$\dot{V}$ (a) and LogSD$\dot{Q}$ (c) obtained from MIGET analysis and LNL modelling. The single participant with a unimodal $\dot{V}/\dot{Q}$ distribution is shown in green, the four with a second peak at high $\dot{V}/\dot{Q}$ in blue and the two with a second peak at low $\dot{V}/\dot{Q}$ are shown in red. A line of identity is displayed on each plot for reference. The agreement between the values of LogSD$\dot{V}$ and LogSD$\dot{Q}$ estimated by the two techniques are also compared using Bland-Altman analysis, displayed in (b) and (d) respectively. The plots are centred around the line of identity (grey) and comparison between the points and this line indicates the bias between the values for the two methods. The complete blue line shows the mean difference between the measurements with the shaded blue area representing the 95% confidence interval for the mean value. The dashed blue lines denote ±1.96SD from the mean, the range within which 95% of the data points are expected to fall.

modal) fit to the MIGET $\dot{V}/\dot{Q}$ distribution (Figure 4.15) shows deviation from the line of identity, which explains some of the discordance between MIGET and the LNL model values. In particular, a lognormal fit to the MIGET perfusion distribution underestimates LogSD$\dot{Q}$ for all subjects apart from the unimodal subject, MIGET_3.

Poor agreement in the case of COPD patients with multimodal $\dot{V}/\dot{Q}$ distributions may also indicate that some assumptions of the LNL model may break down in the presence of more advanced disease. For example, the LNL model assumes that compliance remains constant over each breath cycle - this may not be true in a very obstructed lung, where regions of low $\dot{V}/\dot{Q}$ empty before regions of high $\dot{V}/\dot{Q}$. It is important to note that the LNL model was initially conceptualized to target early evidence of lung abnormalities, so a lack of agreement in the case of the patients with well developed lung disease should not preclude the utility of the technique in identifying lung disease at an early stage.

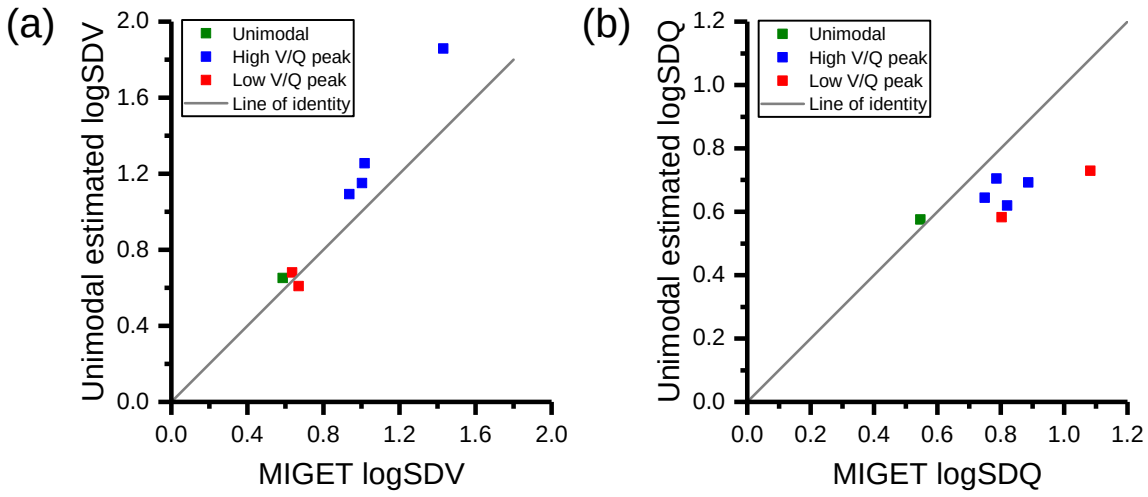


Figure 4.15: Comparison of Log$\text{SD}\dot{V}$ (a) and Log$\text{SD}\dot{Q}$ (b) determined directly by MIGET with the values obtained from a lognormal fit to the ventilation and perfusion distributions.

Although it is possible to estimate some of the MIGET parameters from the LNL model fit, the two techniques do not aim to quantify the same aspects of lung function. Consequently, it is possible that the LNL model parameters could offer new information that MIGET does not. For example, for MIGET_3 the LNL model parameters σ_{CL} and σ_{Cd} show evidence of abnormal lung physiology, while both Log$\text{SD}\dot{V}$ and Log$\text{SD}\dot{Q}$ lie within the normal range. MIGET_8 is also interesting, as they have a normal Log$\text{SD}\dot{V}$ and moderately abnormal Log$\text{SD}\dot{Q}$, while σ_{CL} and σ_{Cd} both lie towards the upper end of the normal range reported by Smith *et al.*.[219]

Exploring the correlations between Log$\text{SD}\dot{V}$ and Log$\text{SD}\dot{Q}$ measured by MIGET and the three LNL model inhomogeneity parameters found no significant linear correlation between the two, although the small sample size limits statistical analysis of

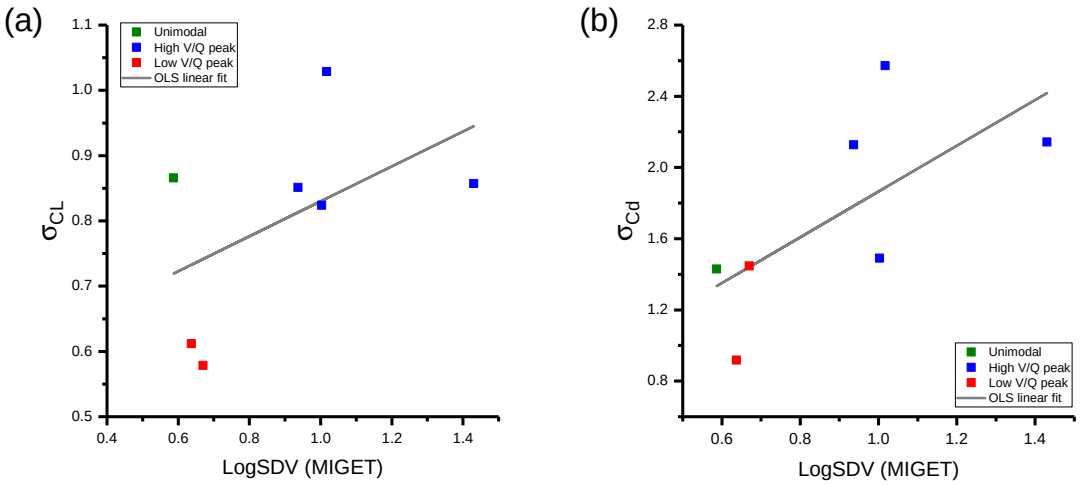


Figure 4.16: Comparison between the LogSD$\dot{V}$ measured by MIGET with the LNL model inhomogeneity parameters (a) σ_{CL} and (b) σ_{Cd}, with an OLS linear fit shown for each (σ_{CL}: intercept $= 0.562 \pm 0.192$, gradient $= 0.268 \pm 0.205$, σ_{Cd}: intercept $= 0.579 \pm 0.591$, gradient $= 1.286 \pm 0.630$).

the relationships between parameters. Figure 4.16 appears to show potential moderate positive correlation between LogSD$\dot{V}$ and the parameters σ_{CL} and σ_{Cd}. Pearson's correlation coefficient was not significant for either (σ_{CL}: Pearson's r = 0.505, p = 0.248; σ_{Cd}: Pearson's r = 0.674, p = 0.097). Spearman's correlation coefficient, which is sensitive non-linear monotonic relationships, suggested significant correlation for σ_{Cd} ($\rho = 0.893$, p = 0.007) but not σ_{CL} ($\rho = 0.321$, p = 0.482). As noted before the small sample size limits the comparison of these parameters, but this could be an interesting area for further research in any future comparative studies of the two techniques.

4.2.4 Conclusion

This study represents an important milestone in research using the MFS: for the first time the device was transported internationally, demonstrating its robustness to travel via international freight, opening up the possibility of future international collaboration. The MBW test was well tolerated by the participants and was easy to incorporate into the MIGET study, being significantly less demanding to perform than MIGET for both participants and researchers.

The non-invasive nature of performing an MBW test with the MFS makes it suitable for use in a clinical setting, whereas MIGET remains an invaluable tool for physiology research, but is too invasive and complex to form part of routine clinical

assessment. The LNL model may even have the ability to identify abnormalities in patients in whom LogSD$\dot{V}$ and LogSD$\dot{Q}$ appear normal, as evidenced by the subject for whom the MIGET parameters were normal while the LNL model identified abnormal inhomogeneity of complicance and conductance.

The estimates of MIGET parameters by the LNL model showed good agreement for the participant with a unimodal $\dot{V}/\dot{Q}$ distribution, but significant differences for the subjects with bimodal $\dot{V}/\dot{Q}$ distributions, potentially highlighting the LNL model assumptions being more applicable to people with early stage rather than advanced lung disease. This would align with the technique aiming to identify early evidence of lung disease.

The conclusions of this study are limited due to the small sample size. In the future it would be interesting to compare the MIGET and LNL parameters in other patient groups. In particular it would be valuable to compare values in people with less advanced lung disease, for example young smokers or CF patients with preserved FEV_1 and further explore the relationship between inhomogeneity assessed by MIGET and the inhomogeneity parameters of the LNL model. The study presented in the following section, comparing young smokers with no respiratory symptoms to healthy controls, demonstrates the potential of the LNL model to identify abnormalities in individuals with normal spirometry.

4.3 Cross-sectional Study of Lung Inhomogeneity in Young Smokers

Smoking increases the risk of developing multiple lung diseases, including lung cancer and interstitial diseases and it is the primary causative factor for the development of COPD, with 50 % of lifelong smokers going on to develop the disease.[227] COPD was the fourth leading cause of death worldwide in 2019,[70] and a recent Lancet commission noted significant deficiencies in the early identification, stratification and treatment of COPD patients, with the level of research funding this condition has attracted being described as "woefully inadequate" when compared with other diseases of comparable morbidity/mortality. One of the six core strategies proposed to aid their goal to work towards the elimination of COPD was the "implementation of a more inclusive diagnosis of COPD, allowing for the detection of mild disease before irreversible pathological changes have occurred".[228] This study explores the potential value inhomogeneity testing using the MFS and LNL model could offer as a technique which is potentially sensitive to early-stage lung abnormalities.

Diagnosis of COPD still relies on post-bronchodilator spirometry, where the presence of COPD is defined as having an FEV_1/FVC ratio below 0.7, as diagnosis based on symptoms alone is acknowledged as unreliable.[229] Staging of the disease is determined by FEV_1 as a percentage of the predicted value, with stages 1 to 4 indicating mild to severe disease. Misdiagnosis remains a significant problem, with this method under diagnosing younger patients and over diagnosing older patients, in whom a decline in spirometry is expected regardless of the presence of disease.[230]

Spirometry primarily identifies disease in the large airways as seen in the later stages of COPD, although at this stage any changes identified are likely irreversible.[228] Initial lung damage due to smoking and in the early stages of COPD involves changes to the small airways in the lung,[231] but spirometry cannot reliably detect parenchymal changes and destruction.[232] Normal spirometry should therefore not be considered conclusive evidence of the absence of lung disease.[233] In addition to its inadequacy in detecting clinical findings observed in imaging, spirometry is also a poor predictor of symptoms, exercise capacity, and overall quality of life and does not capture the heterogeneity of the disease.[234] The inadequacy of spirometry to detect changes to the small airways means that there is an identified clinical need for improved tools to assess lung damage at an earlier stage.[235]

This study investigates whether inhomogeneity testing could offer a non-invasive method to detect early changes in the lungs of young smokers with a greater degree of sensitivity than spirometry.

4.3.1 Methods

4.3.1.1 Experimental Methods

Twenty-three current smokers aged 18-35 were recruited in two ways. Some were recruited from advertising in and around the University of Oxford and subsequently underwent testing at the Department of Physiology at the University of Oxford. Others were recruited as part of their participation in a post-recovery study of primary spontaneous pneumothorax and participated in testing in clinic. Subject characteristics for the smoking and control groups are displayed in Table 4.7. Age and sex-matched controls were taken from an existing database of control subjects, including never-smoking participants in the post-recovery study of primary spontaneous pneumothorax patients.

Ethical approval for the post-pneumothorax study was granted by NHS Research Ethics Committee (REC reference 16/SC/0412) and the study of the remaining young

smokers and healthy controls was approved by South Central Oxford A Research Ethics Committee (REC reference 17/SC/0172) and Scotland A Research Ethics Committee (REC reference 1/SS/0091). Prior to participating in the study, all participants were given a Participant Information Sheet (PIS) and signed an informed consent form. The subjects' smoking history was recorded and the number of pack years of smoking was calculated for each subject, defined as:

$$\text{Pack years} = \frac{\text{Years smoked} \times \text{Daily cigarettes}}{20} \tag{4.10}$$

Any use of vaping products was also recorded - two of the subjects reported vaping in addition to smoking cigarettes.

Volunteers were then asked to perform forced spirometry to an acceptable standard, as defined by the British Thoracic Society, with the two highest recorded values of FEV_1 and FVC being within 150 mL or 5 % of each other, whichever is greater.[236] They were then asked to perform two nitrogen washout experiments, consisting of 10 mins of breathing air then 5 mins of breathing oxygen using the MFS. A 15 minute interval between the two washouts allowed the subject to rest and for their lungs to expel the oxygen from the previous washout. Where two sets of parameters were found by the model the average of the two washouts was used for the subject.

4.3.1.2 Statistical Analysis

Two different approaches to analysing the data were considered for this study. The first of these simply aimed to compare the smoking group with the age and sex matched control group, then investigate correlations between parameters within the smoking group. While this method is simpler, it does not account for difference in physical characteristics which may contribute to the difference between groups. Although the two populations are well-matched in terms of sex, age and height, the mean BMI for the two groups is shown to differ significantly (Table 4.7). The second approach explored the relationship between lung parameters and pack years controls for any confounding physical characteristics by including physical characteristics in the multiple linear regression. Both methods for analysis are detailed in this section and presented in the results.

Shapiro-Wilk tests were performed to test for normality for FEV_1 (% pred.) and the model parameters in both the smoking and control groups as well as F-tests to test for a difference in variance between groups. Based on the results of these tests, Welch's t-test was subsequently selected to compare mean parameter values between

Characteristic	Controls	Smokers
M:F ratio	14:9	14:9
Age	25.0 ± 5.1	25.0 ± 4.5
Height (cm)	175 ± 9	174 ± 8
Weight (kg)	65 ± 11	72 ± 13
BMI	21.3 ± 2.5	23.6 ± 3.7

Table 4.7: A comparison of participant characteristics in the smoking group and age and sex matched control group (reported as Mean ±1 S.D.). The variance does not differ significantly between the two groups for any characteristics ($p > 0.05$, F-test). The difference in mean between the two groups differs significantly from zero for BMI ($p = 0.023$, student t-test). No significant difference was found for age, height and weight ($p > 0.05$, student t-test).

the smoking and control groups. The relationship between FEV_1 (% pred.) and the model parameters was investigated using Pearson correlation coefficients.

Multiple linear regression analysis performed in MATLAB on all participants was used to investigate the predictive power of pack years on the model parameters while controlling for the difference due to age, sex, height, BMI. This was also performed for FEV_1 (% pred.) and FRC (% pred.) but with the predictor variables age, sex and height excluded, as these are already controlled for through comparison with the predicted value. The fitted regression model was:

$$y = \beta_0 + \beta_1 x_1 + \beta_2 x_2 + \beta_3 x_3 + \beta_4 x_4 + \beta_5 x_5 \tag{4.11}$$

where y is the parameter being fit to the regression model and x_{1-5} represent the predictor variables in the model: x_1 is sex (M=0, F=1), x_{2-4} are the natural logarithm of each subject's age, height and BMI divided by the mean of all 46 subjects, and x_5 is number of pack years (pack years = 0 for the control group). The coefficient β_0 is the offset, while β_{1-5} are the regression coefficients determined for the respective variables. The final regression coefficients are obtained through successive regressions, each time excluding the least significant variable until only the term for pack years and any physical characteristics for which $\beta \neq 0$, $p < 0.05$ remain. The same multiple linear regression analysis was also performed on the dataset with the four smokers with 10 or more pack years excluded to investigate the predictive power of pack years

in subjects with less than 10 pack years of smoking history. All 23 control subjects were included in this secondary regression analysis.

If subjects expressed an interest in smoking cessation, they were asked to make contact to arrange a follow up visit after two weeks of quitting.

4.3.2 Results

A comparison between the FEV_1 (% pred.) and LNL parameter values for the smoking (S) and non-smoking (NS) groups is displayed in Figure 4.17. Data points within each group are arbitrarily offset horizontally for clarity. The mean was found to differ significantly between the two groups for all LNL parameters except for σ_{VD} and V_D. However, when deadspace volume is expressed as a fraction of the lung volume at FRC, a significant difference between smokers and non-smokers is evident.

There existed a moderately strong positive correlation between the number of pack years of smoking amongst the smoking group and the inhomogeneity of compliance (σ_{CL}). Figure 4.18 shows moderate positive correlation and the coefficient of determination, $R^2 = 0.429$ for the linear fit, implying a significant portion of the variability in σ_{CL} within the smoking group can be explained by their cumulative smoking history. The subject with 16 pack years of smoking looks like a potential outlier, although the lack of other volunteers with such a high pack year history means that it is not conclusive - notably this subject reported smoking less cigarettes compared to previously (1 per day on average), but did also vape 3 mL of vape fluid per day. No significant correlation was found between pack years and FEV_1 or any of the other LNL parameters. The number of cigarettes smoked per day at the time of participating in the study was recorded for all but the three smokers recruited as part of the post-pneumothorax study. No significant correlation was found between the number of cigarettes smoked per day and the FEV_1 (% pred.) or LNL parameters for the remaining 20 smokers.

The results for FEV_1 (% pred.) and the core model parameters for all participants are presented in Figure 4.19, with the smoking group separated into three groups based on pack year history. Figures 4.19 (b) and (c) illustrate an apparent increase in inhomogeneity of compliance (σ_{CL}) and conductance (σ_{Cd}) with increased smoking history. Multiple linear regression was performed to determine whether the physical characteristics sex, age, height and BMI were significant regressors for any of these six parameters. FEV_1 (% pred.), σ_{CL} and σ_{Cd} were not significantly predicted by any of the physical characteristics in the regression models ($p > 0.05$). σ_{VD} was only

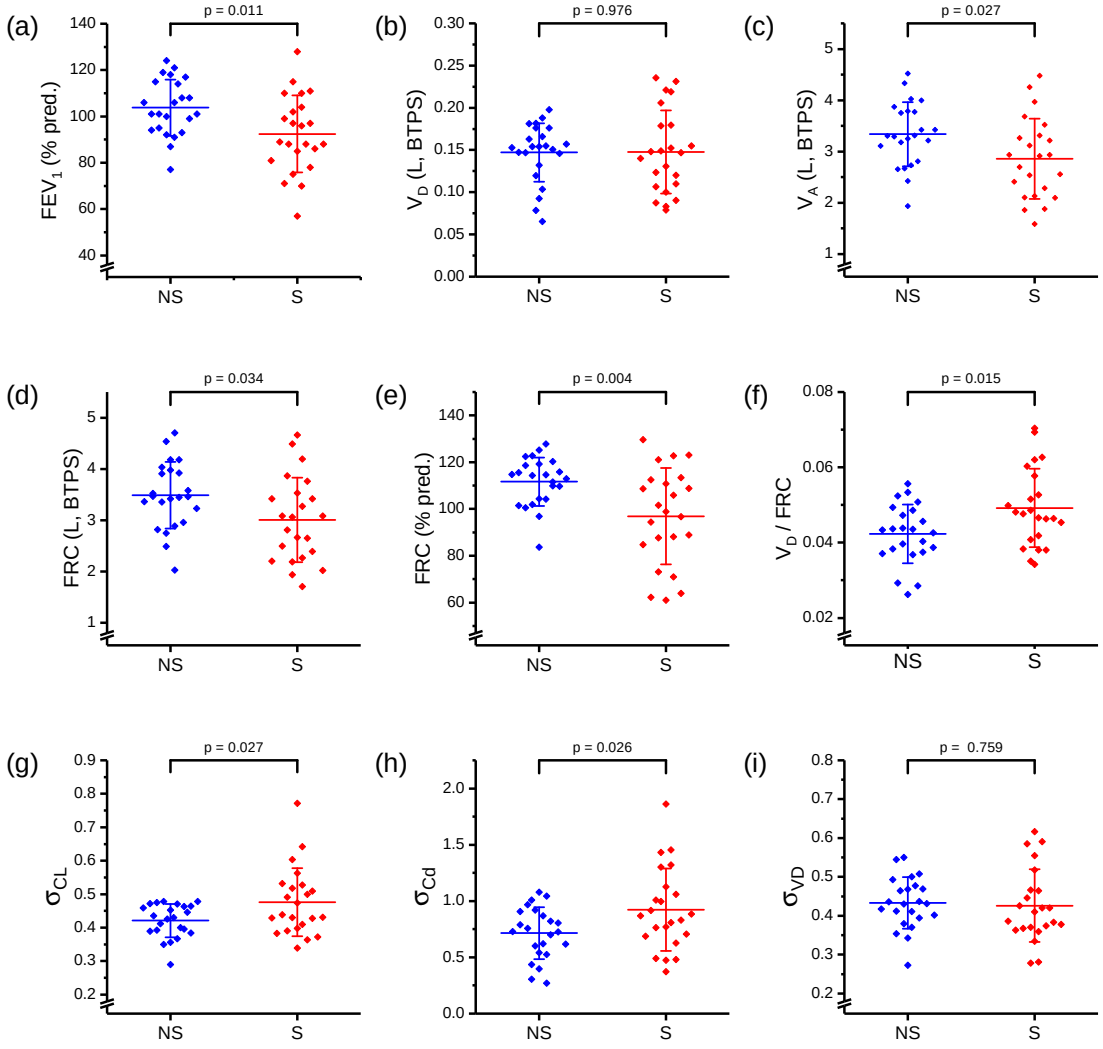


Figure 4.17: Comparison between the smoking (S) and never-smoking (NS) control group (a) FEV_1 (% pred.), (b)-(f) LNL model volume parameters, and (g)-(i) LNL model inhomogeneity parameters, with p-values for Welch's t-test comparing the two groups displayed above each plot. There was a significant difference in the group means ($p < 0.05$ for FEV_1 (% pred.), V_A, FRC (L, BTPS), FRC (% pred.), V_D/FRC, σ_{CL}, and σ_{Cd} while there was no significant difference between the smoking and never-smoking group means for V_D and σ_{VD} ($p > 0.05$).

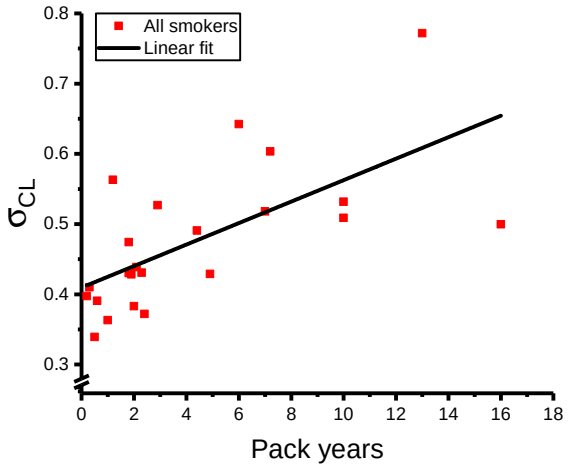


Figure 4.18: The LNL inhomogeneity parameter σ_{CL} vs. pack years for all 23 smoking subjects. A simple linear fit to the data is also shown (intercept = 0.410 ± 0.023, and gradient = 0.015 ± 0.004, $R^2 = 0.429$). The correlation is significant (Pearson's r = 0.655, $p < 0.001$).

significantly predicted by sex. FRC was significantly predicted by height and BMI, while V_D was significantly predicted by sex and height.

The smoking group had a pack year history of 0.2-16 pack years with a mean of 4.3 pack years. Following the removal of all non-significant physical characteristics from the regression model, the number of pack years did not significantly predict FEV_1 (% pred.), σ_{VD}, FRC or V_D (p = 0.12, 0.73, 0.34, and 0.71 respectively). Number of pack years was only a significant predictor of σ_{CL} ($\beta_5 = 0.0285, p < 0.00001$, Adjusted $R^2 = 0.401$) and σ_{Cd} ($\beta_5 = 0.0143, p = 0.023$, Adjusted $R^2 = 0.091$). Notably, when the four smokers with ≥ 10 pack years were excluded and the multiple linear regression model analysis was repeated, this result remained significant for both σ_{CL} ($\beta_5 = 0.0201, p < 0.0001$, Adjusted $R^2 = 0.324$) and σ_{Cd} ($\beta_5 = 0.0599, p = 0.017$, Adjusted $R^2 = 0.113$). Subjects in this reduced smoking group ranged from 0.2 to 7.2 pack years with a mean of 2.7 pack years.

Two of the secondary parameters derived from the LNL model, the FRC as a percentage of the predicted value and the fractional deadspace volume were also analysed using multiple linear regression and a comparison between the values for the controls and the smokers stratified by pack years is shown in Figure 4.20. BMI was found to significantly predict FRC (% pred.), while no physical characteristics significantly predicted V_D/FRC. Neither parameter was significantly predicted by pack years.

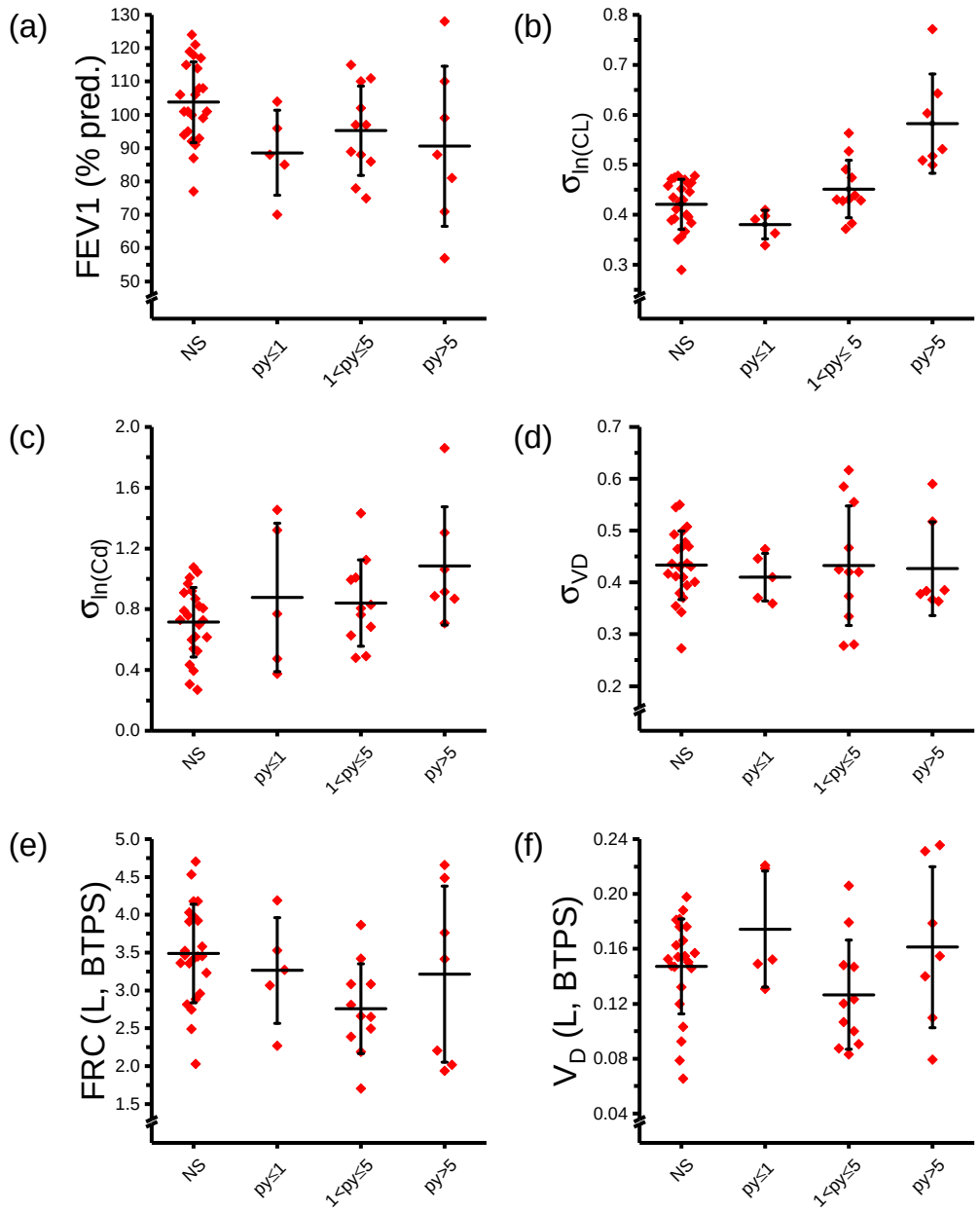


Figure 4.19: (a) FEV_1 (% pred.), (b)-(d) the lognormal lung model inhomogeneity parameters σ_{CL}, σ_{Cd} and σ_{VD} and (e)-(f) the lognormal lung model FRC (L, BTPS) and V_D (L, BTPS) for the controls and smokers (divided into three groups passed on pack year (py) history). Mean ± 1 S.D. is indicated for each subgroup. Multiple linear regression performed on all six of these parameters with age, sex, height, BMI and pack year history as predictor variables found that number of pack years was only a significant predictor of σ_{CL} ($\beta_5 = 0.028, \mathrm{p} < 0.00001$) and σ_{Cd} ($\beta_5 = 0.014, \mathrm{p} = 0.023$).

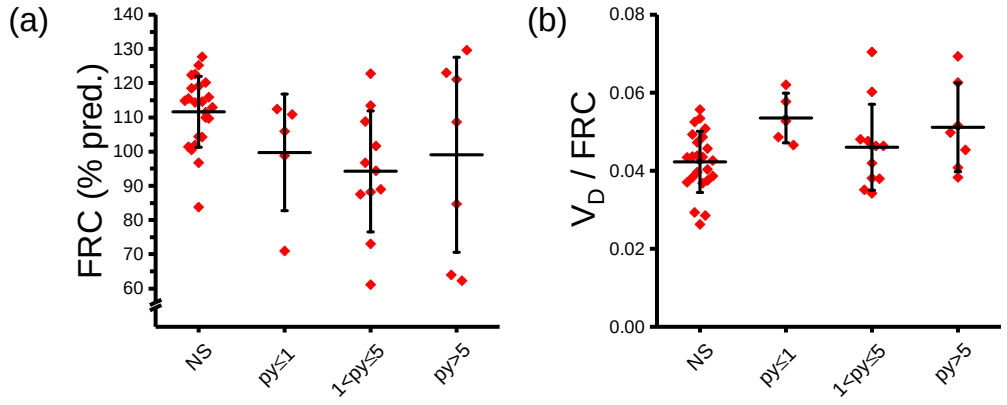


Figure 4.20: Secondary derived LNL model volume parameters (a) FRC (% pred.) and (b) the fractional deadspace volume V_D/FRC for the controls and smokers (divided into three groups passed on pack year (py) history). Mean ±1 S.D. is indicated for each subgroup. Multiple linear regression performed on FRC (% pred.) with BMI and pack year history as predictor variables found that BMI was a significant predictor of FRC (% pred.) ($\beta_4 = -54.6, \mathrm{p} = 0.002$), but number of pack years was not a significant predictor of FRC (% pred.) ($\beta_5 = -0.816, \mathrm{p} = 0.211$). For V_D/FRC age, sex, height and BMI were not significant predictors and number of pack years was not a significant predictor of V_D/FRC ($\beta_5 = 0.0007, \mathrm{p} = 0.056$).

4.3.3 Discussion

Greater inhomogeneity of compliance and conductance was found in young smokers, as both σ_{CL} and σ_{Cd} were elevated in the smoking group compared with controls. However, σ_{VD} was not significantly different between the two groups, implying that a broadening of the deadspace distribution is not associated with early changes in the lungs as a result of smoking. This is consistent with the findings of a cross-sectional study of COPD patients using the LNL model technique: compared to healthy controls, σ_{CL} and σ_{Cd} were significantly elevated in stage 1 COPD patients, while no significant increase in σ_{VD} was seen until stage 3 COPD.[219] Therefore, σ_{CL} and σ_{Cd} appear to offer greater potential as clinical markers for early lung abnormalities than σ_{VD}.

Pack years was not found to significantly predict spirometric values or the volume measurements afforded by the LNL. Notably, both σ_{CL} and σ_{Cd} were significantly predicted by pack years. That pack years remained a significant predictor of both σ_{CL} and σ_{Cd} even when the smoking group was restricted to subjects with less than 10 pack years shows that these parameters are considerably more sensitive to the effects of a lower cumulative smoking history in otherwise healthy subjects than existing techniques. For example, despite traditional MBW analysis being acknowledged as

more sensitive to early abnormalities than spirometry, the MBW parameters S_{acin} and S_{cond} (described briefly in Section 1.3.6) were only found to be significantly elevated in subjects with more than 10 pack years.[237] This suggests that the LNL model parameters σ_{CL} and σ_{Cd} represent an exciting development in the detection of early stage lung damage due to smoking in the absence of any respiratory symptoms.

Smoking has been linked to the presence of respiratory bronchiolitis based on autopsy findings of young smokers (mean age of 25) who died of non-pulmonary causes.[238] It may be the case that elevated σ_{CL} at least partially reflects inflammation due to current smoking, with oedema in the small airways resulting in a temporary increase in stiffness in parts of the lung and hence a broadening of the compliance distribution. If this is the mechanism by which σ_{CL} is increased, this could be reversed upon smoking cessation. Alternatively, if it is found that for some smokers there is no change in σ_{CL} or their σ_{CL} value remains above that of the healthy control range, this may be indicative of some degree of irreversible structural changes to the small airways.

Despite efforts to partner with a smoking cessation clinic to recruit current smokers and follow up with repeat measurements post-quitting, this was not successful due to the restructuring of NHS smoking cessation in Oxfordshire and limitations due to the COVID-19 pandemic. However, two subjects who expressed an interest in quitting were asked to return for a second study visit. One returned 2 weeks after quitting and the second after 6 weeks (delayed due to a broken leg). While it is not possible to perform meaningful statistical analysis on a sample of two subjects, it is noteworthy that both subjects saw a decline in σ_{CL} upon quitting. A decrease in σ_{CL} of 13.0% (from $\sigma_{CL} = 0.54$ to $\sigma_{CL} = 0.47$) and 8.5% (from $\sigma_{CL} = 0.47$ to $\sigma_{CL} = 0.43$) for the two subjects respectively. Smoking cessation was confirmed in both by an expired CO test. It is particularly interesting that both showed a decreased σ_{CL} despite the second subject's initial σ_{CL} falling within the normal range of the control group. However the change in σ_{Cd} was not consistent between the two subjects – the first saw a decrease of 38.2% from 1.28 to 0.79, while the second showed no change and σ_{Cd} remained at 0.81.

Early detection of lung abnormalities due to smoking on an individual basis and communication of this to smokers could prove to be a powerful tool in aiding smoking cessation. While the measured FEV_1 (% pred.) only falls outside the normal range for two of the seven smokers with over 5 pack years, all 7 would be identified as having an abnormal value of σ_{CL}. Reporting spirometry results to smokers as a 'lung age' based on regression analysis of healthy individuals is associated with improved success rates

of smoking cessation.[239] It is possible that performing a similar regression analysis on a large sample of healthy control subjects across a broad age range could offer a similar estimated 'lung age' based on the LNL model lung volumes and inhomogeneity parameters. Although age was not found to significantly predict the inhomogeneity parameters across the narrow age range of participants in this study, Mountain *et al.* found that both σ_{CL} and σ_{Cd} were higher for subjects aged 70–79 years old compared to subjects aged 20-24 years old.[115] Similarly, in a larger recent analysis of 179 healthy volunteers aged between 18 and 80, Bithell found that σ_{CL} increases with age, even in the absence of respiratory disease.[240]

While current or former smokers comprise the majority of diagnosed COPD cases, of all people with a history of smoking, only about 20% are estimated to go on to develop the disease.[241] It is therefore of particular clinical interest to achieve early identification of those at higher risk.

Several factors, including but not limited to smoking history, have been linked to susceptibility of developing COPD:[228] current smoking, number of pack years of smoking history, exposure to biomass smoke,[242] a genetic deficiency in the production of alpha-1 antitrypsin,[243] or a diagnosis of childhood or adult asthma.[244,245] However, at present there is no clinical measure of lung function which adequately detects early signs of COPD or predicts which currently symptom-free smokers will develop COPD. Ascertaining whether the LNL model has this capability would require its inclusion as a measurement tool in a large longitudinal study of smokers.

At present many countries have screening programmes for lung cancer in high risk groups and it has been suggested that these programmes should be expanded to identify those at high risk of progressing to COPD.[246] If elevated σ_{CL} was shown to significantly predict a later diagnosis of COPD, this technique could offer a relatively cheap, non-invasive additional test to perform which involves no ionising radiation.

4.3.4 Conclusions and Future Work

This study shows increased lung inhomogeneity in young smokers compared to never-smoking controls. Specifically the parameters σ_{CL} and σ_{Cd}, reflecting the inhomogeneity of compliance and conductance, were elevated in the smoking group and show promise as tools to detect early stage lung abnormalities resulting from smoking.

Sex, age, height and BMI were not found to significantly predict either parameter, so the parameters seem to be fairly insensitive to these physical characteristics in this age range. This could simplify the use of both of these in clinical settings. Further study would be required to determine if this holds true across a larger population,

especially if a wider age range were considered, as some degree of broadening of these inhomogeneity parameters has been observed due to normal ageing.[240]

A higher number of pack years of smoking was associated with both increased σ_{CL} and σ_{Cd} and importantly this was still true even when participants with ≥ 10 pack years were excluded from the regression analysis. Therefore, both parameters appear to be sensitive to changes in the lungs as a result of a relatively small smoking history. In particular, σ_{CL} demonstrates potential as a parameter that can identify specific individuals as showing signs of lung abnormalities: every member of the smoking group with more than 5 pack years had a σ_{CL} value above the range for the healthy control group.

If the detected increase in inhomogeneity does indeed reflect changes to the small airways as a result of smoking, this could also prove clinically useful in identifying early signs of COPD before the disease has progressed to the large airways and is detected by spirometry. A further area for future research is looking at the association between elevated parameters such as σ_{CL} and a propensity to develop COPD. This would require the inclusion of this inhomogeneity test as part of a longitudinal study of active smokers.

A greater numbers of smokers pre- and post-quitting would be needed to determine whether the decrease in σ_{CL} seen in the two volunteers studied pre- and post-quitting is consistently observed across a larger sample size. However, the observed reduction of σ_{CL} in response to smoking cessation in these two participants does highlight the exciting potential for the model to detect acute changes in an individual's lung physiology. This may be of great use to clinicians within smoking cessation clinics, as well as more widely in respiratory clinics where quantifying the effect of clinical interventions on lung physiology would be of great importance. In this particular instance the changes may reflect a reduction in inflammation or a reversal of changes to the lung caused by smoking, implying that the increased inhomogeneity in these two patients may be at least partially reversible.

Future work should be centred around identifying whether elevated inhomogeneity parameters is a result of permanent airway remodelling or temporary inflammation. This could be investigated through a trial integrated within a smoking cessation clinic where volunteers could be studied prior to quitting and then again at intervals during the course of their smoking cessation programme. Smoking cessation clinics serve a wide age range of patients, so it may also be possible to determine whether any response of the LNL model parameters to smoking cessation is consistent across all age ranges.

Chapter 5

Investigation of Lung Inhomogeneity in Adults with Cystic Fibrosis

Cystic fibrosis (CF) is a multisystem genetic condition which affects the lungs, pancreas, liver, and intestines,[247] but it is the decrease in lung function which is the primary cause of morbidity, with 90% of patients dying from respiratory complications.[248]. Significant progress has been made in treating CF, leading to a greatly improved life expectancy for patients today compared with previous generations. The median survival of CF patients born post—2000 is now predicted to exceed 50 years.[8] With reduction in lung function as the primary cause of death, monitoring patients and developing new and effective treatments requires sensitive measures to assess treatment efficacy and/or disease progression. As people are living longer with better lung health, there is a clinical need for more sensitive methods for identifying reduced lung function at an earlier stage.

Cystic fibrosis is a recessive disease and the most prevalent inherited disease in Caucasians with over 10,000 people living with CF in the UK today and more than 70,000 worldwide.[249,250] The disease is caused by a mutation in the cystic fibrosis transmembrane conductance regulator (CFTR) gene, which codes for the production of the CFTR protein responsible for regulating the transport of salt and fluids into and out of cells. In people who inherit a mutated copy of the CFTR gene from each parent, this process is impaired, leading to the build-up of a thick mucus in the airways. This thickened mucus is difficult to clear from the lungs, leading to progressive airway damage and an increasing predisposition to chronic lung infection: in the UK 41% of CF patients have chronic Pseudomonas aeruginosa, 7% have non-tuberculous mycobacterium (NTM) and 9% of people are infected with aspergillus.[249]

A range of different treatment modalities are used to delay progression of the disease. Airway clearance forms an important part of disease management, including the use of breathing techniques and airway clearance devices at home and treatment by specialist physiotherapists in the clinic. Inhaled drug therapies are widely used to thin the mucus, dilate the airways or treat an infection - in 2018 79.4% of patients in the UK received at least one form of inhaled therapy. Infections are also frequently treated with antibiotics – in 2018, 44.7% of patients received at least one course of intravenous (IV) antibiotics.[249] The range of antibiotics available for use in the CF population has increased, as well as novel methods of delivery, such as intelligent nebulisers and dry powder devices.[251] When lung disease is advanced, a patient may be referred for a lung transplant, which can extend and improve the quality of a patient's life but does not provide a cure for CF.

The introduction of drugs that directly modulate the CFTR protein (CFTR modulators) has induced a paradigm shift in the treatment of CF patients, treating the cause of the disease instead of focussing on managing symptoms for the first time. CFTR modulator drugs such as ivacaftor provide a novel approach for targeting certain variants of the gene mutation responsible for CF directly, by regulating the flow of chloride ions across the cell membrane. CFTR monotherapy became available in 2013, reaching 4% of the CF population.[252] The later introduction of dual therapy and then triple therapy means that up to 90% of patients may be eligible for treatment with CFTR modulators.[253] There is currently a great deal of interest in clinical trials assessing the therapeutic value of different combinations of CFTR modulators.[254]

People with CF are closely monitored for their entire lives, with regular monitoring and treatment as well as a more in-depth assessment at annual reviews. FEV_1 remains the primary tool for assessment of lung function in CF patients and has been shown to act as a reliable predictor for life expectancy, as well as being a primary endpoint in many pivotal clinical trials. FEV_1 is also one important indicator used to determine whether a patient would be a good candidate for a lung transplant – in patients with an FEV_1 below 30% or an FEV_1 that is rapidly declining despite optimal treatment, evaluation for a transplant is indicated.[255] However, there are still concerns with FEV_1 as a clinical endpoint. Szczesniak *et al.* highlighted the significant variability in the reporting of FEV_1 endpoints in clinical trials for chronic CF therapies.[256]

The lung clearance index (LCI) is emerging as a preferred technique, due to its increased sensitivity to early stage lung damage. However, as noted in Chapter 1, the LCI measurement is limited by the lack of standardisation of equipment, experimental protocol and accepted parameter range.

Computerised tomography (CT) scans allow clinicians to diagnose a range of morphological abnormalities such as bronchiectasis (abnormal widening of the airways), peribronchial thickening (bronchial wall thickening) and mucus plugging (the exclusion of parts of the lung from gas exchange by mucus).[257] However there is concern that numerous CT scans lead to a CF patients receiving a cumulative effective dose (CED) of radiation above that of the general population, which should be minimised where possible.[258]

The novel analysis of an N_2 multi-breath washout (MBW) obtained using the MFS and subsequent analysis with the lognormal lung model detailed in Chapter 4 has the potential to provide a more sensitive technique for monitoring patients and assessing treatment efficacy than is currently available. This chapter presents two studies of adult patients with cystic fibrosis. Firstly a pilot study looking at a diverse group of CF patients is presented: patients are compared with healthy controls, intra-group comparisons are made with the aid of imaging history, and intra-subject comparisons look at the effect of physiotherapy on an individual's LNL parameters. Building on the success of the LNL model at sensitively distinguishing even early stage CF from healthy controls, the second study presented in the chapter investigates the potential of the lognormal lung parameters as a marker of early lung disease in patients with preserved FEV_1. In this study measurements were also made using a commercially available device, the Exhalyzer D, which measures the lung clearance index, a parameter that has been shown to be more sensitive to early stage abnormalities than spirometry. This represents the very first comparison between the LCI and the LNL parameters in any patient group.

5.1 Preliminary Study of the Utility of the Lognormal Lung Model in the CF Population

Previous work has noted the potential of the LNL model to provide a more sensitive assessment of early stage lung disease in COPD patients than spirometry, with particular interest in σ_{CL}, a parameter reflecting inhomogeneity of lung compliance.[219] An investigation of patients with asthma also found that σ_{CL} showed promise as a marker for disease activity and control, by comparison with a healthy control group, assessment pre- and post bronchodilator therapy and comparison with symptom severity.[200] This study marks the first use of this technique in CF patients.

Despite its ubiquitous use as a primary endpoint in clinical trials involving CF patients, the failure of FEV_1 to reflect early changes in lung function, even when irre-

versible lung damage is visible on CT scans, is well documented.[259] Lung damage in CF patients is characterised by an accumulation of sticky mucus, leading to bacterial colonisation and frequent episodes of infection and inflammation.[260] Parts of the lung become obstructed by mucus-plugging and the lungs are damaged by the destruction of the lung parenchyma and diffuse bronchiectasis.[261] This study investigates the potential of σ_{CL} and other LNL parameters to provide a useful metric to evaluate lung disease in CF patients without the need for expensive equipment, ionising radiation or the use of scarce isotopes.

5.1.1 Methods

5.1.1.1 Patient Recruitment

In total, 14 patients with CF volunteered to take part in this study at the John Radcliffe Hospital. They were opportunistically recruited by clinical members of the research team when they were attending outpatient appointments for annual reviews, or during their stay for inpatient treatment, some of whom were studied before and after physiotherapy. Fourteen age- and sex-matched controls were selected from an existing database of previously studied healthy subjects. Of the 14 CF patients, 7 had preserved FEV_1 (defined as an $FEV_1 > 70\%$) and the corresponding subset of the 7 age- and sex-matched controls matched with these patients were used to test the ability of the LNL analysis of an MBW to discriminate between healthy control subjects and CF patients with preserved lung function based on spirometry. Healthy control subjects were all recruited from in and around the University of Oxford and studied at the Department of Physiology, Anatomy and Genetics. All subjects were recruited under the ethical approval granted by the South-Central Oxford A Research Ethics Committee (Reference: 17/SC/0172) and provided informed written consent.

5.1.1.2 Experimental Protocol

Patients who consented to take part in the study performed a single MBW, using the adult MFS described in Chapter 2. Washouts were conducted with the same protocol described in Chapter 4: 10 minutes of air breathing followed by 5 minutes of breathing medical grade O_2. Subjects whose exhaled N_2 concentration exceeded 2% after 5 mins of O_2 breathing were allowed to continue breathing until this point was reached if the device was well tolerated by the patient. The data from these washouts were processed as described in Chapter 4 to give the 5 primary model

outputs: alveolar volume V_A, deadspace volume V_D and the standard deviations of the compliance, conductance and deadspace volume, σ_{CL}, σ_{Cd} and σ_{VD} respectively.

Spirometry was carried out using standard procedures. Each patient or healthy control subject repeated a forced maximal expiration 3 times or until a participant recorded 3 attempts differing by less than 150 mL or 5% from each other (whichever is greater), from which the maximum value was selected, as per the BTS recommendations.[63] The FEV_1 and FVC values were recorded, as well as the FEV_1 and FVC as a percentage of the predicted values for that patient, based on their age, sex, height and ethnicity, according to the BTS guidelines.[236] For the purposes of identifying patients with preserved FEV_1, an FEV_1 above 70% was considered to be within the acceptable normal range.

If available in a patient's medical records, prior CT scans from between January 2011 and June 2019 were accessed. Two experienced clinicians, who were blinded to the LNL parameters obtained, viewed these images and used their clinical judgement to categorise the degree of bronchiectasis as mild, moderate or severe. For those patients where no CT scans had been performed, the clinicians viewed other imaging and medical history to judge the likely level of bronchiectasis.

Four of the patients studied were receiving physiotherapy as a routine part of their inpatient clinical care following an exacerbation and completed a washout prior to and after their physiotherapy session. The physiotherapy techniques employed for each patient were determined by the patient and treating clinician and included a variety of airway clearance strategies, such as the use of positive pressure devices and inhaled nebulisers. Patients undergoing physiotherapy were asked to put a mark on a visual analogue scale (VAS), to indicate their current level of chest discomfort in response to the question "How does your chest feel" with 0 at the start of the scale described as "As clear as you could imagine" and 10 at the end of the 10 cm line corresponding to "As congested as you can imagine", both before and after physiotherapy. This measured distance along this line is hence referred to as the VAS score. Spirometry measurements were obtained before and after treatment and the mass of sputum produced during and in the 2 hours immediately after physiotherapy was also recorded as a potential measure of the degree of airway clearance.

5.1.1.3 Statistical Analysis

Normality was assumed for demographic information such as age and spirometry measurements. Based on the results of F-tests of variance, student t-tests were used to test for a difference in mean between two groups. The Shapiro-Wilks test was

employed to test for deviations from normality for any variables for which the distribution was unknown to test the suitability of using parametric tests to analyse the results. The assumption of normality was rejected for p-values below 0.05. As nonparametric testing was indicated, the Mann-Whitney test was used instead to test for stochastic equality between the control and CF groups.[262] The degree of correlation between different parameters was tested using Spearman's rank correlation. Correlation coefficients take values between -1 and +1, but correlation is determined based on rank and the method is suitable for monotonically increasing and decreasing relationships as well as linear correlation.

5.1.2 Results

In total 14 CF patients completed 20 washouts. Eighteen of these washouts returned parameters on the lognormal lung model and one was rejected for poor fit quality. For one subject it was not possible to obtain LNL model parameters for the single washout performed, so this subject was excluded from further analysis. Six of the remaining 13 patients recruited had preserved FEV_1, allowing additional analysis of this subset of the CF population. Previous imaging was available for 12 of the CF patients and four patients were studied pre- and post-physiotherapy. For two of these subjects, only the pre- or post-physiotherapy washout returned LNL model parameters, so only two subjects are included in the analysis.

5.1.2.1 Comparison between CF Patients and Healthy Controls

A comparison of the physical characteristics of the CF patients studied and the age- and sex-matched controls is presented in Table 5.1 and demonstrates that the two groups are well matched, with no statistically significant difference in the variance or mean of age, height, weight and BMI for the two groups.

Figure 5.1 compares the spirometry results for the entire CF group with the healthy controls. The mean FEV_1 and FVC as a percentage of individuals' predicted values for the control population both exceed the expected value of 100% for a healthy population, with sample means of 107% and 110% respectively. Based on a one-sample t-test it cannot be concluded that the sample mean FEV_1 (% pred.) differs significantly from 100% ($p = 0.056$), while the mean FVC (% pred.) was found to differ significantly from 100% ($p = 0.007$). As the control subjects were primarily recruited from the student body and researchers at the university, this may be due to the correlation between a higher level of education and greater participation in sport,[263] which is associated with increased spirometric volumes.[264,265]

	CF Patients	Healthy controls
Males:Females (n)	5:8	5:8
Age (years)	27.8 ± 10.0	28.2 ± 8.9
Height(cm)	165 ± 13	172 ± 8
Weight (kg)	63.0 ± 18.0	63.0 ± 11.7
BMI (kgm^{-2})	22.7 ± 3.1	21.1 ± 2.9

Table 5.1: Physical characteristics for the CF patient and healthy controls groups, displayed as mean $\pm$ 1 S.D.. There is no statistically significant difference between the variance ($p > 0.05$, F-test) or mean ($p > 0.05$, student t-test) of the two groups for any of the above physical characteristics.

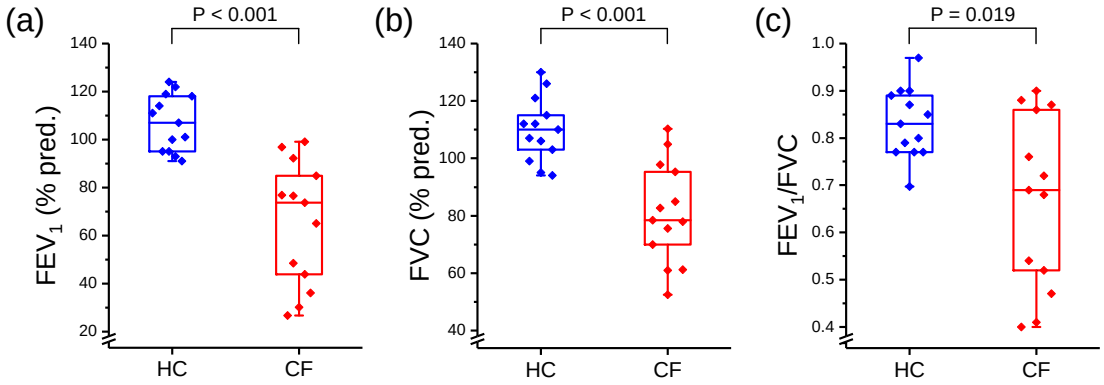


Figure 5.1: Spirometry measurements for healthy controls (HC) vs. cystic fibrosis patients (CF) with the volume as a percentage of its predicted value for FEV_1 (a) and FVC (b) and the absolute ratio of FEV_1 to FVC (c). Mann-Whitney U-test p-values comparing the distributions of the two groups are displayed above each plot.

As would be expected for people with CF, there is significant variation in spirometry values within the study showing an extremely heterogenous group, with FEV_1 (% pred.) values ranging from 27% to 99%. Although there is a clear difference between the two groups' spirometry, the significant degree of overlap between the two groups means that many of the CF patients cannot individually be identified as having abnormal lung function based on spirometry measurements alone. There is evidence of obstructive lung disease based on the spirometry measurements for seven of the CF subjects, for whom an FEV_1/FVC ratio below 0.7 was observed. Notably, the absolute FEV_1/FVC ratio was the only spirometry value from the FEV_1, FVC and the resulting ratio (both absolute and as a percentage of the predicted value) that correlated with age (Spearman's $\rho = -0.593$, p = 0.033), showing the expected increased degree of obstructive lung disease as CF patients age. However, increased age was also associated with a reduced FEV_1/FVC ratio in the control group (Spearman's $\rho = -0.657$, p = 0.015).

The first three plots of Figure 5.2 show a comparison between the lung volumes measured by the LNL model for the two groups. Although the absolute deadspace volumes for the two groups were not found to be drawn from significantly different distributions, V_D values for 6 of the CF patients exceeded those observed for the healthy control group. However, the alveolar volume, V_A, which dominates the summed lung volume at FRC, was significantly reduced in the CF patients. The reduced lung volumes of the CF patients was also observed with the lower mean FRC (% pred.). Therefore when the deadspace volume was instead normalised to give V_D/FRC (Figure 5.2 (g)), the difference between the two groups is far more apparent and the measured values for 8 CF subjects clearly exceed the normal range.

While both airways parameters σ_{VD} and σ_{CL} differ between the two groups, with an increase in inhomogeneity in the people with CF, the parameter σ_{CL} shows particular promise as a sensitive measurement in the CF population, as the value for every single CF patient exceeds the observed range in the healthy control group (Figure 5.2 (f)). By scaling these inhomogeneity parameters by the normalised deadspace, the difference between the groups is enhanced: the final two plots of Figure 5.2 show the product of the fractional deadspace and σ_{VD} and σ_{CL} respectively show a strikingly skewed distribution for the CF group. Both $\sigma_{VD} * V_D/\text{FRC}$ and $\sigma_{CL} * V_D/\text{FRC}$ clearly separate the CF group into two distinct groups, with the same five participants displaying an σ_{CL}*V_D/FRC and σ_{VD}*V_D/FRC value significantly above the rest of the CF patient group. The parameters σ_{VD} and σ_{CL} are positively correlated within the CF group (Spearman's $\rho = 0.593$, p = 0.033), suggesting the increased airways

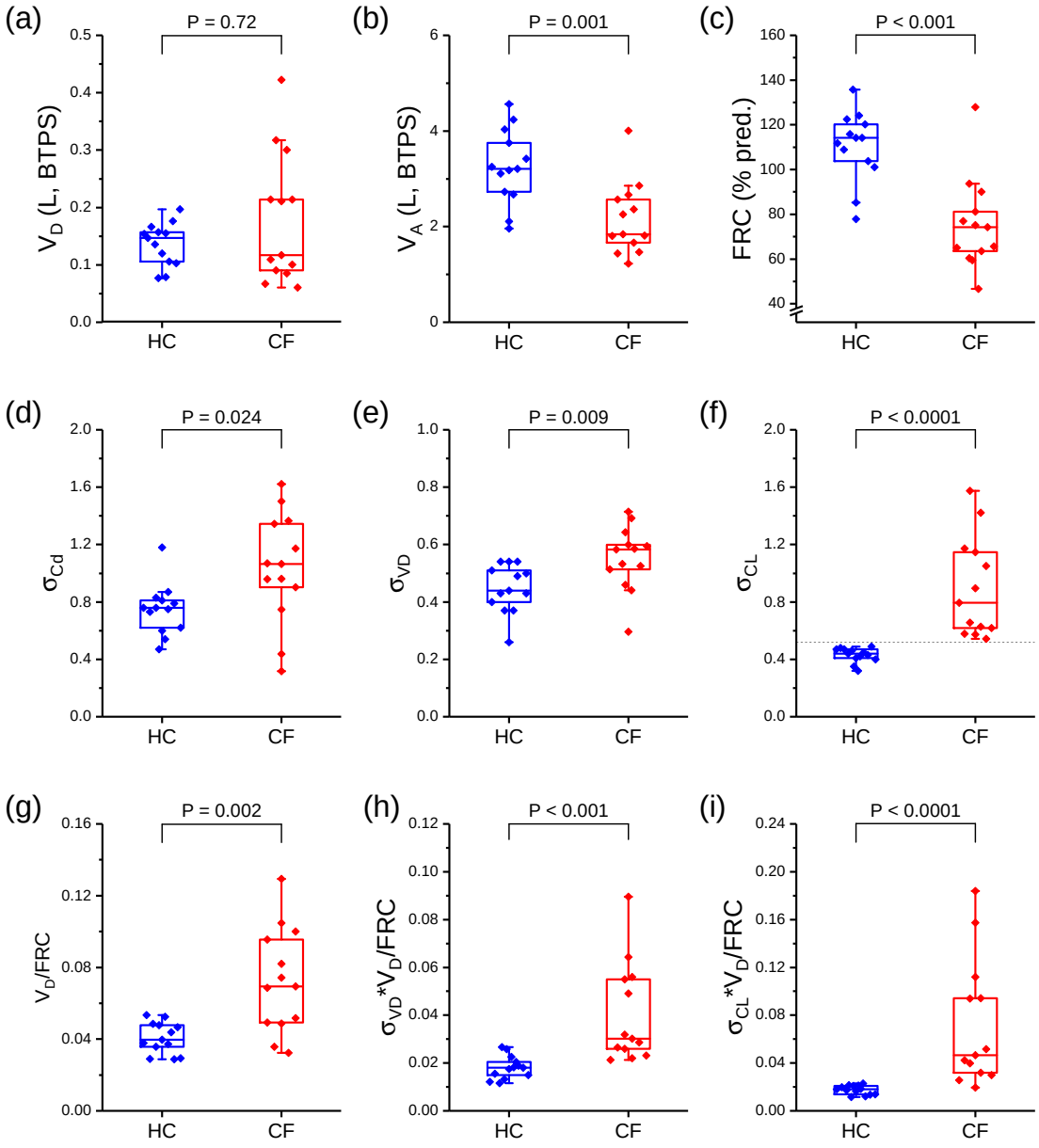


Figure 5.2: A comparison between all LNL parameters for the entire CF group with healthy controls. The core volume parameters for deadspace and alveolar volume are given in (a) and (b) with the sum as a fraction of the predicted FRC in (c). The inhomogeneity parameters σ_{Cd}, σ_{VD} and σ_{CL} are shown in (d)-(f) and secondary derived parameters, the fractional deadspace and its product with σ_{VD} and σ_{CL} are shown in (g)-(i). P values given are for the Mann-Whitney U-test. On figure (f) a dashed grey line at $\sigma_{CL} = 0.51$ illustrates the complete separation between the two groups, with all healthy controls lying below the line while the values for all CF patients exceed it.

Parameter	Age		Height		Weight		BMI	
	HC	CF	HC	CF	HC	CF	HC	CF
V_D	0.56*	0.80**	0.78**	0.81***	0.51	0.86***	0.04	0.89***
V_A	0.65*	0.49	0.88***	0.84***	0.75**	0.81***	0.2	0.6
σ_{VD}	-0.59*	0.07	-0.87***	0.09	-0.64*	-0.05	-0.09	-0.09
σ_{CL}	-0.29	0.59*	-0.43	0.44	-0.18	0.45	0.15	0.55*
σ_{Cd}	0.39	0.48	0.11	0.50	0.15	0.47	0.12	0.40
V_D/FRC	0.07	0.78**	0.04	0.62*	0.03	0.67*	0.08	0.77**
FRC (% pred.)	0.59*	0.45	0.76**	0.84***	0.57*	0.82***	0.12	0.65*
$\sigma_{VD} * V_D$/FRC	-0.48	0.57*	-0.60*	0.38	-0.58*	0.37	-0.22	0.53
$\sigma_{CL} * V_D$/FRC	0.01	0.76**	-0.18	0.56*	-0.01	0.62*	0.23	0.74**

Table 5.2: Spearman's correlation coefficients between the primary and secondary LNL model parameters and the physical characteristics. The significance of the correlation coefficients is denoted as * for $p < 0.05$, ** for $p < 0.01$, and *** for $p < 0.001$.

inhomogeneity in terms of deadspace and compliance occurs concurrently. However, it should be noted that $\sigma_{CL} * V_D$/FRC shows a much narrower range of normal and subsequently identifies more subjects in the CF group that are abnormal. Further discussion of this observation will continue in the subsequent section investigating a possible relationship between bronchiectasis observed on imaging with these and other LNL parameters.

The degree of correlation between model parameters and physical characteristics was analysed for both the CF patients and the healthy controls, with the resulting Spearman's rank correlation coefficients displayed in Table 5.2. For both LNL parameters σ_{CL} and V_D/FRC, significant positive correlation with age was observed within the CF group, while no significant correlation was seen in the healthy controls, implying that these parameters reflect the progression of the disease and declining lung function beyond normal ageing. This data is represented graphically in Figure 5.3. One individual with CF has a σ_{CL} value that is noticeably lower than other CF patients of a similar age, suggesting unusually healthy lungs for someone with CF - this subject is highlighted in Figure 5.3 (a). This finding is supported by the classification according to imaging in the following section, as this subject was the only person with CF above 25 who was classified as having only 'mild' bronchiectasis in this study. This implies that it may be possible to use this parameter to identify

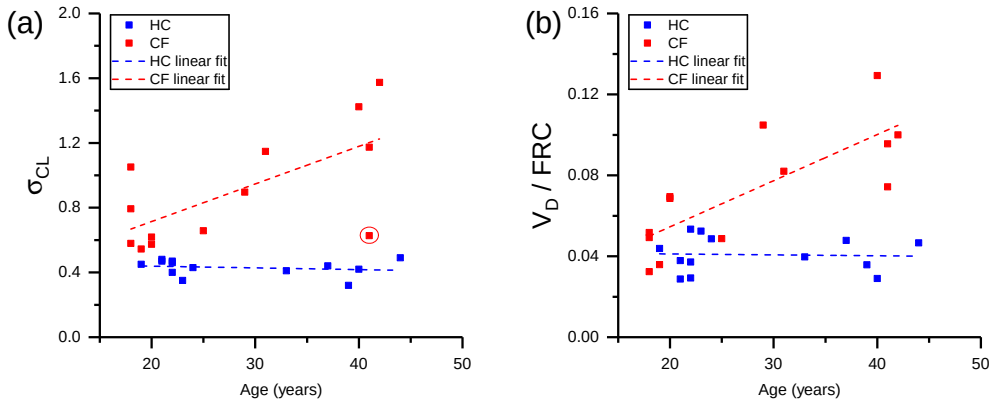


Figure 5.3: The variability of (a) σ_{CL} with age for the two groups with linear fits to the healthy control HC group (slope = -0.00108 ± 0.00168, intercept = 0.460 ± 0.049) and cystic fibrosis CF group (slope = 0.023 ± 0.0078, intercept = 0.250 ± 0.228) and similarly in (b) V_D/FRC with age for the healthy controls (slope = $-4.46 \times 10^{-5}2.951 \times 10^{-4}$, intercept = 0.0420 ± 0.0087) and CF patients (slope = 0.00228 ± 0.00054, intercept = 0.00889 ± 0.01598). One subject on the σ_{CL} plot is highlighted using a circle to denote a potential outlier, but this was not considered conclusive due to the small sample size and hence this subject was not excluded from the linear fit.

CF patients who are seeing a lesser or greater decline in lung function than expected for their age, perhaps as a metric of how well the disease is being managed. This subject was also notably the subject with the highest FEV_1 and FVC as a percentage of their predicted value out of the entire CF group at 99% and 110% respectively. Despite the lower value of σ_{CL} compared to other CF patients of a similar age, it still lies above the normal healthy range, so unlike spirometry this metric may be able to identify abnormal lung function while still distinguishing them from those with more significant abnormalities.

The lung volumes V_D and V_A both showed the expected positive correlation with height, with larger lung volumes observed in taller individuals. However, the significant positive correlation between height and FRC (% pred.) was not expected, as a subject's height is accounted for when the predicted FRC volume for each individual is calculated. For the healthy controls, height also correlated positively with σ_{VD}.

Higher BMI was correlated with higher values of σ_{CL} and V_D/FRC, amongst CF patients, which may seem unexpected, as previous studies have found that higher BMI is associated with better lung function,[266] with a significant increase in the probability of having severe lung disease with a lower than normal BMI.[267] However, this study is limited by the small sample size - no patients recruited for this study

Parameter	FEV_1 (L)		FEV_1 (% pred.)		FVC (L)		FVC (% pred.)		FEV_1/ FVC	
	HC	CF	HC	CF	HC	CF	HC	CF	HC	CF
V_D	0.42	-0.32	-0.06	-0.45	0.63*	0.37	0.21	-0.30	0.31	-0.81***
V_A	0.75**	-0.088	0.15	-0.28	0.82***	0.61*	0.21	-0.11	-0.08	-0.65*
σ_{VD}	-0.59*	-0.47	0.1	-0.43	-0.78**	-0.28	-0.17	-0.46	-0.15	-0.34
σ_{CL}	-0.1	-0.63*	0.01	-0.67*	-0.24	-0.05	0.00	-0.52	-0.26	-0.79**
σ_{Cd}	-0.18	-0.18	-0.25	-0.28	-0.04	0.42	0.21	-0.17	0.11	-0.62*
V_D/FRC	-0.04	-0.30	0	-0.41	0.01	0.19	0.15	-0.32	0.15	-0.68*
FRC (% pred.)	0.66*	-0.13	0.29	-0.31	0.68*	0.52	0.31	-0.13	-0.06	-0.7**
$\sigma_{VD} * V_D$/FRC	-0.46	-0.58*	-0.03	-0.64*	-0.53	-0.07	-0.13	-0.56*	0.16	-0.69**
$\sigma_{CL} * V_D$/FRC	-0.05	-0.58	0.05	-0.63*	-0.03	0.01	0.27	-0.52	0.11	-0.81***

Table 5.3: Spearman's correlation coefficients between the primary and secondary LNL model parameters and the spirometry measurements. The significance of the correlation coefficients is denoted as * for $P < 0.05$, ** for $P < 0.01$, and *** for $P < 0.001$.

had a BMI below the normal healthy range (the lower limit was a BMI of 20.2) and the two patients with the highest BMI values (31.7 and 26.1), were two of the oldest patients in the study at 41 years old, which is likely a confounding factor.

The correlation coefficients investigating the relationship between spirometry and LNL measurements are presented in Table 5.3. The alveolar volumes recorded for the healthy subjects were found to correlate strongly with both the absolute FEV_1 and FVC volumes. However this same trend was not observed for the CF patients, as no correlation was found with FEV_1 and only moderate correlation with FVC. This is likely explained by the presence of obstructive lung disease greatly reducing a patient's ability to forcibly exhale, but having a much lesser effect on the LNL derived measurement of lung volume at FRC, as this test involves no forced manoeuvres.

Declining pulmonary function as a feature of CF pathology is diagnosed based on both the FEV_1 (% pred.) and the FEV_1/FVC ratio and in fact the ratio of FEV_1/FVC is the spirometry parameter which shows the strongest correlation with all the LNL parameters except for σ_{VD}, which shows only weak negative correlation with FEV_1/FVC. A lower FEV_1/FVC ratio was associated with a higher σ_{VD}, σ_{VA}, σ_{CL}, σ_{Cd}, FRC (% pred.), V_D/FRC, $\sigma_{VD} * V_D$/FRC and $\sigma_{CL} * V_D$/FRC.

5.1.2.2 Comparison with Severity of Bronchiectasis

Of the 13 CF patients included in this study, 12 had imaging available in their medical notes to enable assessment of the degree of bronchiectasis by two experienced clinicians who were both blinded to the LNL parameter values. It was determined that there was evidence that the degree of bronchiectasis was severe for 4, moderate-severe for 2, moderate for 2 and mild for 4 of the patients. Where possible, CT scans were used for this assessment, with 8 subjects having available chest CT scans. The four patients judged to have severe bronchiectasis were all diagnosed using chest CT scans. One subject was determined to have mild bronchiectasis at the lung bases based on an incidental finding from an abdominal and pelvic CT. The remaining 3 subjects were assessed using chest X-rays, with moderate-severe bronchiectasis judged likely for two of the subjects and mild bronchiectasis for the remaining subject. The most up to date imaging ranged from 2011 to 2019 for these patients, while testing for this study took place in 2018-19, so the severity of bronchiectasis may have worsened since these images were taken.

The spirometry data for these 12 patients is presented in Figure 5.4, with the assessed severity of bronchiectasis indicated by the data point colour. A Spearman's rank correlation coefficient test was performed for each parameter, assigning a numer-

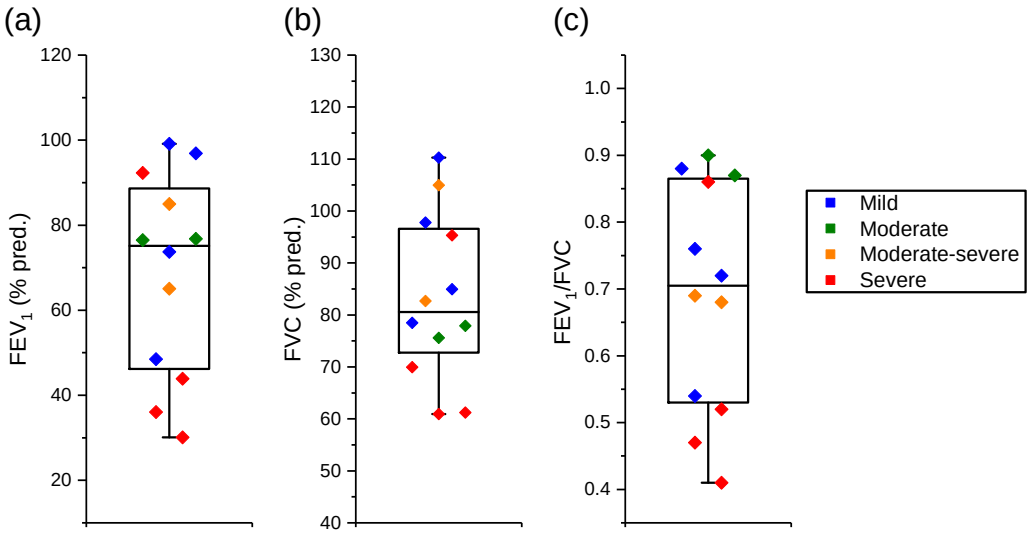


Figure 5.4: A comparison of the measured spirometry values for CF patients with varying degrees of bronchiectasis, with the severity of bronchiectasis denoted by data point colour. (a) FEV_1 and (b) FVC are presented as a percentage of the predicted value for each subject alongside (c) the absolute FEV_1/FVC ratio.

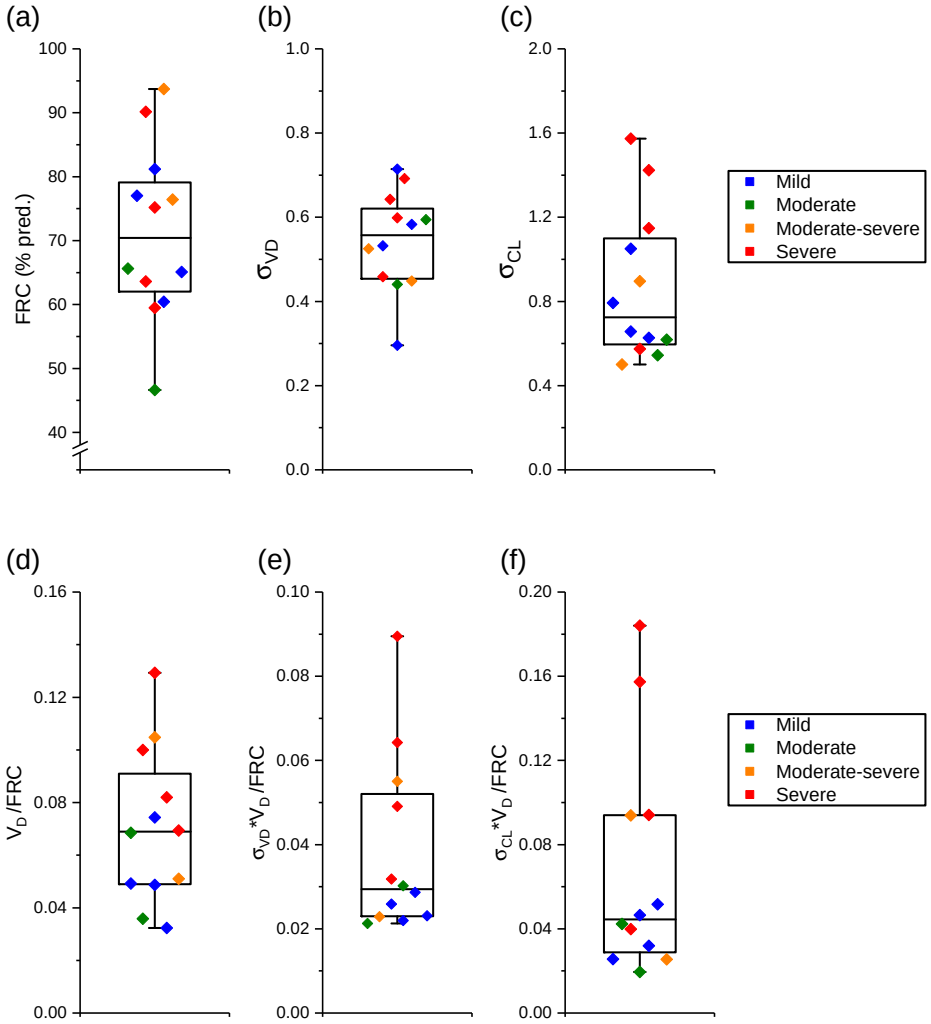


Figure 5.5: A comparison of airways LNL parameters for CF patients with severity of bronchiectasis denoted by colour: (a) the FRC as a percentage of a subject's predicted value and the inhomogeneity parameters for (b) the deadspace distribution σ_{VD} and (c) the compliance distribution σ_{CL}. A comparison of the LNL deadspace parameters values for CF patients with varying degrees of bronchiectasis. The only parameters for which Spearman's rank correlation was significant were V_D/FRC ($\rho = 0.699, \mathrm{p} = 0.011$) and $\sigma_{VD}{}^{*}V_D$/FRC ($\rho = 0.706, \mathrm{p} = 0.010$)

ical value to the degree of bronchiectasis: mild (1), moderate (2), moderate-severe (3) and severe (4). The Spearman's rank correlation coefficients were all negative (i.e. a greater degree of bronchiectasis associated with poorer spirometry values). The correlation coefficients determined for FEV_1 (% pred.), FVC (% pred.) and FEV_1/FVC were -0.502 (p = 0.096), -0.546 (p = 0.066) and -0.459 (p = 0.134) respectively, although the p-values were too high to reject the null hypothesis that no correlation

exists. However, visual inspection of the data shows that the same three subjects with the lowest spirometry values all had severe bronchiectasis.

The LNL model airways parameters FRC (% pred.), σ_{VD} and σ_{CL} are presented in Figure 5.5 (a)-(c). Although none of these parameters were found to significantly correlate with degree of bronchiectasis, the same three subjects with severe bronchiectasis and the lowest spirometry values were the same three subjects with the highest values of σ_{CL}. Unlike the spirometry measurements obtained using forced manoeuvres, the FRC values for the three patients who appear to have the most obstructed lungs were not the lowest in the group.

Figure 5.5 (d)-(f) compares the parameter values V_D/FRC and the product of the fractional deadspace with the airways inhomogeneity parameters σ_{VD} and σ_{CL}. Both V_D/FRC and $\sigma_{VD}{}^*V_D$/FRC were found to correlate significantly with severity of bronchiectasis with Spearman's rank correlation coefficients of 0.699 (p = 0.011) and 0.706 (p = 0.010) respectively, while no significant correlation was found for $\sigma_{CL}{}^*V_D$/FRC ($\rho = 0.495$, p = 0.102).

As noted in the comparison with healthy control subjects in Section 5.1.2.1, the product of deadspace and compliance inhomogeneity parameters with the fractional deadspace results in a significantly skewed distribution. The three patients with the lowest spirometry values and severe bronchiectasis ranked amongst the top four highest V_D/FRC, $\sigma_{VD}{}^*V_D$/FRC and $\sigma_{CL}{}^*V_D$/FRC values (Figure 5.5 (d)-(f)). Every subject determined to have severe bronchiectasis had a $\sigma_{VD}{}^*V_D$/FRC value above any of the patients with mild or moderate bronchiectasis. It is also interesting to note that the subject designated 'moderate' with the next highest value for $\sigma_{VD}{}^*V_D$/FRC had the most out of date imaging, with the classification of moderate being determined from their last CT scan 7 years prior to the study.

5.1.2.3 CF Patients with Preserved FEV_1

Of the 13 CF patients in this study, seven had preserved FEV_1 (defined as > 70% of the predicted value) and this section considers this subgroup separately from the whole group, as there is particular clinical interest in providing a more sensitive assessment of pulmonary function in patients with less advanced disease. The subjects from the control group who were selected based on age and sex to match with these individuals comprise the control group for this section. As shown in Table 5.4, the two groups contain equal numbers of males and females and are well matched in terms of age, height, weight and BMI.

	CF Patients	Healthy controls
Males:Females (n)	1:6	1:6
Age (years)	24.6 ± 8.2	24.7 ± 6.4
Height(cm)	160 ± 11	172 ± 7
Weight (kg)	59.0 ± 21.1	59.4 ± 8.9
BMI (kgm^{-2})	22.5 ± 4.1	19.8 ± 2.1
FEV_1 (% predicted)	85.8 ± 10.5	105.9 ± 14.0

Table 5.4: A comparison between the physical characteristics of the CF patients with preserved FEV_1 (defined as $> 70\%$) with the corresponding subgroup of healthy controls matched to these patients. There is no statistically significant difference between the variance ($p > 0.05$, F-test) or mean ($p > 0.05$, student t-test) of the two groups for any of the above physical characteristics.

The spirometry values for these subgroups are compared in Figure 5.6 (a)-(c). Although Mann-Whitney U-tests suggest a significant difference between the distribution of both FEV_1 (% pred.) and FVC (% pred.), there remains significant overlap between the subjects with CF and the healthy controls. Meanwhile for the FEV_1/FVC ratio, no significant difference between the two distributions was found. Indeed only one of the subjects with preserved FEV_1 had a FEV_1/FVC ratio below 0.7 that would indicate the presence of obstructive lung disease.

As noted in Section 5.1.2.1 when comparing the entire CF group and healthy controls, the superior ability of σ_{CL} to distinguish between controls and CF patients is highlighted again in Figure 5.6 (d). Every single CF patient was found to have a σ_{CL} value higher than the range of the control group, despite having spirometry values within the normal range, implying that this parameter may provide a more sensitive assessment of pulmonary abnormalities in patients with early stage CF. In the analysis of this subgroup, there was also complete separation between the controls and CF patients for FRC (% pred.) as well. However, this is likely due to the fact that the control group is not representative of the general population - amongst these healthy controls every single subject exceeded 100% FRC (% pred.), while a mean of 100% is expected for the population as a whole. For V_D/FRC, no significant difference was found between the two distributions, although four of the seven CF patients were found to have a V_D/FRC value well outside the normal healthy range.

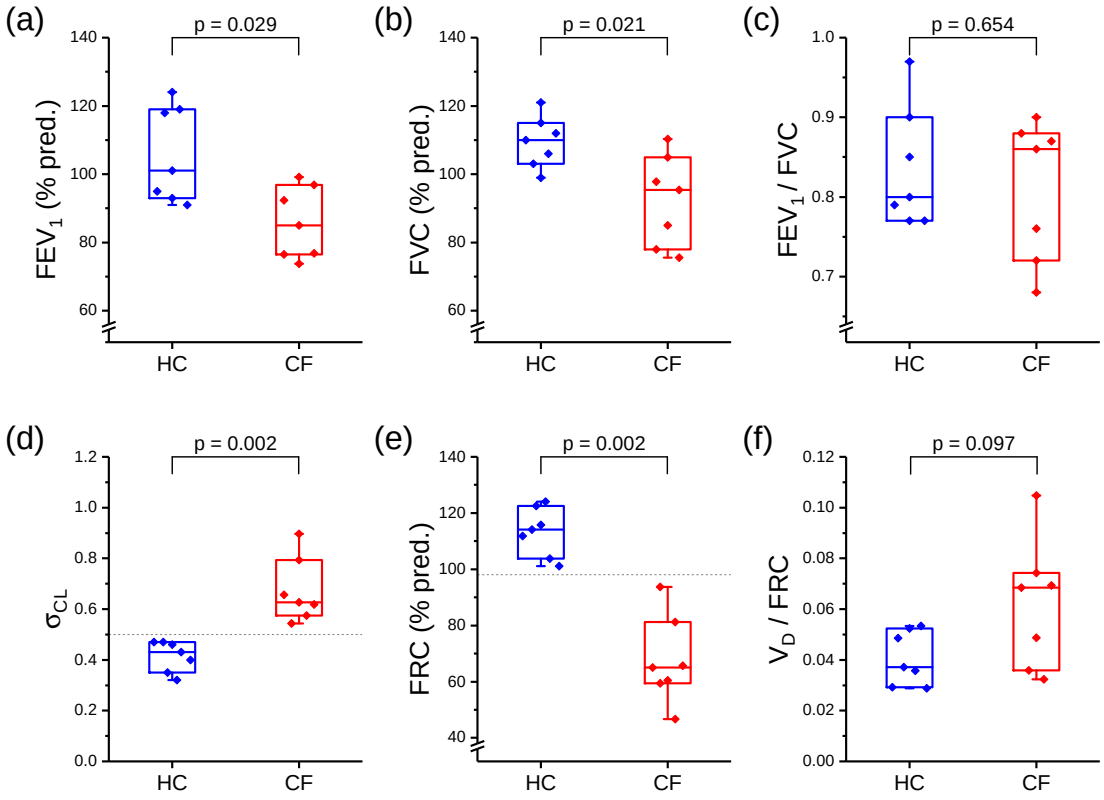


Figure 5.6: A comparison of the spirometry measurements (a)-(c) and selected LNL parameters (d)-(f) for the subset of CF patients with preserved FEV_1 and their respective controls. The complete separation between the range of values for the two groups for both σ_{CL} and FRC (% pred.) is highlighted by a grey dashed line on each plot. P-values calculated from Mann-Whitney U-tests comparing the distributions of the two groups are displayed above each plot.

5.1.2.4 Assessing the Effect of Physiotherapy

Two of the four patients studied pre- and post-physiotherapy performed washouts for which LNL model parameters could be adequately fitted to the data, denoted CF_1 and CF_2 in this section. Both subjects expectorated sputum in the two hours post-physiotherapy and both reported that their chest felt clearer following the intervention according to their self-reported level of congestion on the VAS, although for CF_2 this was from a lower baseline level of discomfort. Both of these results are displayed in Figure 5.7 (a) and (b) respectively. As shown in Figure 5.7 (b), the response in FEV_1 to the physiotherapy differed, with CF_1 showing a decrease in volume of 4.5% while for CF_2 FEV_1 increased by 12.7% post-physiotherapy. Figure 5.7 (d) shows an increase in FVC for both patients, by 4.0% and 10.6% respectively.

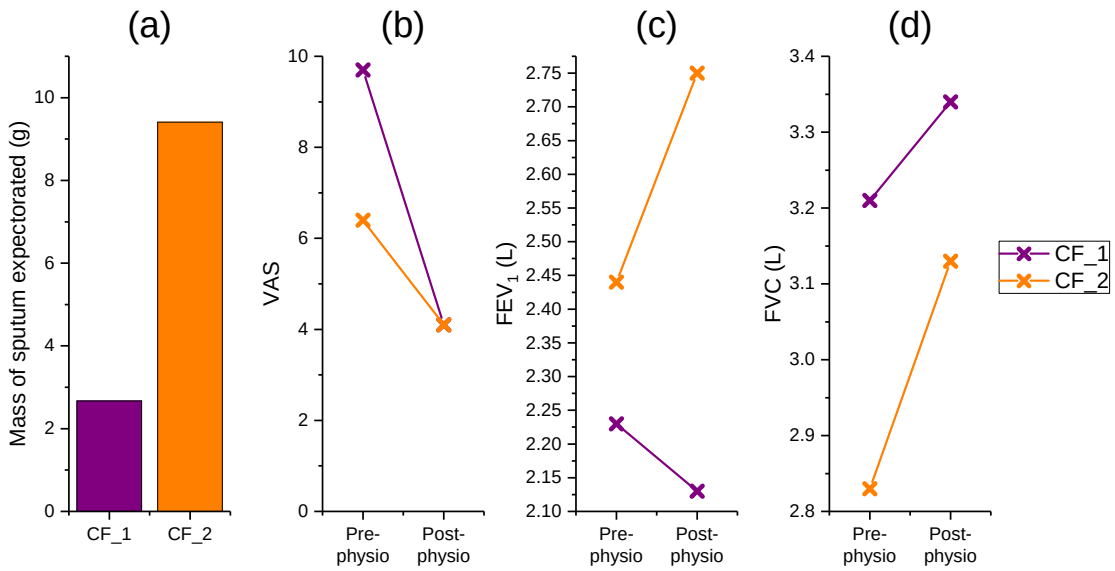


Figure 5.7: (a) The mass of sputum expectorated in the two hours following physiotherapy and (b) the change in level of discomfort as marked by the patient on a visual analogue scale (VAS) from 0 to 10 where an increased score represents greater discomfort. The spirometry measurements (c) FEV_1 and (d) FVC are expressed as the absolute value in litres.

The change in the various LNL model parameters following physiotherapy is shown in Figure 5.8 - the percentage change in each parameter is displayed in a heatmap alongside the absolute change in the parameters V_D/FRC and σ_{CL}. Both V_D/FRC and σ_{CL} were lower than the mean value for the whole CF cohort, even prior to physiotherapy. Despite this, σ_{CL} was still seen to decrease in both subjects. Indeed, a decrease in all three inhomogeneity parameters was observed following physiotherapy, suggesting that physiotherapy may at least temporarily decrease lung inhomogeneity.

For the LNL model lung volume measurements the results are more discordant. The alveolar volume V_A increased in CF_1 but decreased in CF_2 and because FRC is dominated by V_A, this led to an overall decrease in FRC for CF_2. Increased absolute deadspace volume post-physiotherapy was observed for both subjects, although this effect was much greater for CF_2, for whom V_D increased by 23.9% (from 67 mL to 83 mL), resulting in a significantly increased fractional deadspace V_D/FRC. However, due to the proportionately greater increase in V_A compared to the decrease in V_D, CF_1 instead saw a small decrease in V_D/FRC.

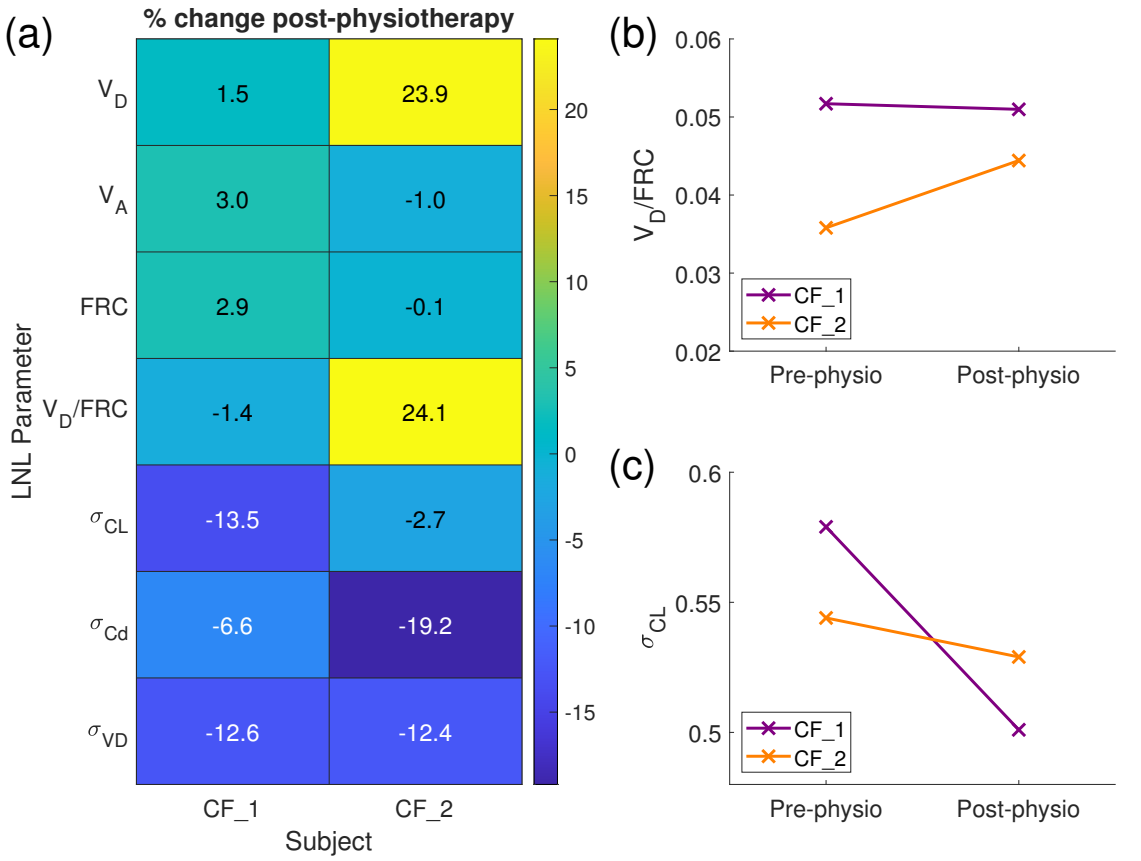


Figure 5.8: The percentage change in LNL model parameters for each of the subjects following a session of physiotherapy with the magnitude and direction of the change indicated by colour in (a) alongside (b)-(c), the absolute change in the parameters V_D/FRC and σ_{CL}.

5.1.3 Discussion

This study marks the first time that the technique of analysing an MBW with the LNL model has been used in patients with cystic fibrosis. The comparison of the spirometry results for the CF patients and healthy controls highlights the well-documented limitation of FEV_1 in identifying early stage lung disease in CF. Although there is a statistically significant difference between the distributions of the two groups, there remains a significant overlap between the two groups.

Of all the LNL parameters, σ_{CL} as a parameter seems especially promising, showing evidence of abnormality in every single CF patient. Indeed, every single CF patient was found to have a σ_{CL} value above the maximum value observed in the control group, including patients with preserved FEV_1. With the small sample of 7 individuals with CF and preserved FEV_1, a key focus for future work should be

on recruiting more patients with spirometry values within the normal range. This is in fact the focus of the following section which details a study of patients with early stage CF, looking at comparisons between CF patients and healthy controls using the metrics of spirometry, the LNL model and the lung clearance index, which is believed to be more sensitive in the early stages of disease progression.

Considering other parameters of the LNL model, the other two inhomogeneity parameters σ_{VD} and σ_{Cd} were also elevated in CF patients, although without the clear separation offered by the parameter σ_{CL}. The alveolar volume was smaller for CF patients and so was the total lung volume at FRC as a percentage of their predicted FRC, as has previously been observed in the CF population.[268] The reduced alveolar volume could be a result of mucus plugging in CF patients. Although absolute deadspace was not found to be significantly higher in CF patients, the proportion of their lungs not contributing to gas exchange was higher than healthy controls. This could be a result of bronchiectasis, a mechanism in which the conducting airways of CF patients are enlarged.

Both the fractional deadspace and the inhomogeneity of compliance were found to correlate strongly with age in CF patients, yet showed no such correlation in the controls. This could indicate that these parameters would prove useful as a tool for clinicians in monitoring decline in lung function over time as patients deviate further from normal values as their disease progresses. Interestingly, a similar investigation into the correlation between FEV_1 (% pred.) and age found that the correlation was non-significant ($\rho = -0.35$, $p = 0.238$), implying less sensitivity to change over time than σ_{CL} and V_D/FRC.

Multiple LNL parameters were found to correlate strongly with other physical characteristics, highlighting the need for a larger scale study of normal values for the healthy population to ascertain the weighting of different factors that influence a person's LNL parameter values. In particular, the volume measurements V_A and V_D were strongly correlated with height, which is unsurprising given the predictive empirical equations derived for estimating an individual's total FRC. For the healthy controls, height also correlated positively with σ_{VD}. While a larger sample size would be necessary to confirm this correlation, it could result from how the deadspace is modelled. If a taller person had longer large airways, these would be shared equally between all the model compartments, leading to a narrower distribution of deadspace volumes and hence smaller σ_{VD}.

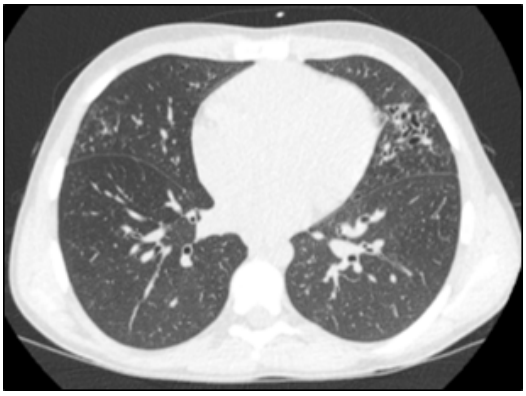
As well as comparing the LNL parameters to the physical characteristics of the participants in this study, it is also of particular interest to clinicians to be able to

connect parameters to structural abnormalities in the lung. For example at present the presence and severity of bronchiectasis is determined by imaging, the use of which is limited due to the radiation dose from CT[269] and cost of equipment and operation of an MRI scanner.[270]

Two example patients are presented in Figure 5.9 to illustrate the potential ability of this technique to distinguish between different clinical features of the disease. These patients both have low FEV_1 values, but very different levels of bronchiectasis found on chest CT scans taken 7 months prior to their involvement in this study. Subject (a) was found to have mild bronchiectasis, while the level of bronchiectasis in subject (b) was judged by clinicians to be severe - the increased airway diameter is clearly visible on the CT scan shown in Figure 5.9 (b). In terms of σ_{CL}, both (a) and (b) lie not just above the range for the healthy population, but also well above the median value of 0.79 for the CF patients recruited for this study, with values of 1.15 and 1.05 respectively. However, this is not the case for the parameter V_D/FRC. In patient (b) with severe bronchiectasis, a significantly higher fractional deadspace above the median value for the CF group was observed, while a markedly lower value of V_D/FRC was seen for the patient (a) with mild bronchiectasis that was in fact just below the lower limit of normal based on the healthy control group.

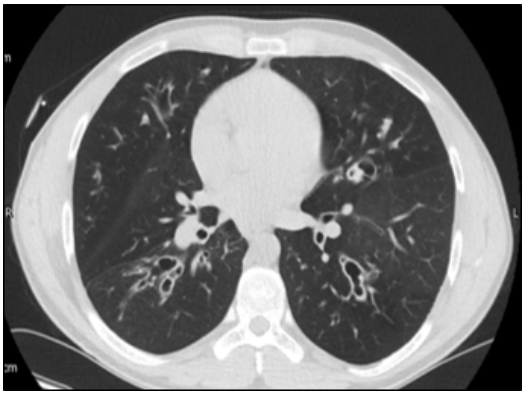
A similar trend was observed for both composite parameters $\sigma_{VD}{}^{*}V_D$/FRC and $\sigma_{CL}{}^{*}V_D$/FRC, although for both of these parameters both patients exceeded the maximum value observed in the control population. It would seem plausible that the widening of the conducting airways through bronchiectasis would lead to an increased proportion of the lung volume that does not contribute to gas exchange and hence greater V_D/FRC. It was noted that subject (a) had a history of suffering from particularly frequent infections. Recurrent infection could lead to a stiffening of the alveolar walls in the most affected regions of the lung and hence an increased variability in the ability of parts of the lung to expand and contract, potentially causing the elevated σ_{CL} seen in subject (a). A significantly larger sample size would be needed to provide concrete evidence for correlation between disease presentation and the LNL parameters, but this comparison does provide a glimpse of the exciting potential for a technique which is able to distinguish between the different contributing factors to a decline in lung function in individual patients.

(a) Mild bronchiectasis



$FEV_1 = 48\%$
$\sigma_{CL} = 1.05$
$V_D/\text{FRC} = 0.049$
$\sigma_{VD}{}^{*}V_D/\text{FRC} = 0.029$
$\sigma_{CL}{}^{*}V_D/\text{FRC} = 0.052$

(b) Severe bronchiectasis



$FEV_1 = 30\%$
$\sigma_{CL} = 1.15$
$V_D/\text{FRC} = 0.082$
$\sigma_{VD}{}^{*}V_D/\text{FRC} = 0.049$
$\sigma_{CL}{}^{*}V_D/\text{FRC} = 0.094$

Figure 5.9: Sample CT scans from CF patients in this study with the degree of bronchiectasis judged by clinicians to be (a) mild and (b) severe. Both subjects' scans were taken 7 months prior to their participation in this research study. The subject with severe bronchiectasis has an FEV_1 (% pred.) 38% lower than the subject with mild bronchiectasis and a higher σ_{CL}, V_D/FRC, $\sigma_{VD}{}^{*}V_D/\text{FRC}$ and $\sigma_{CL}{}^{*}V_D/\text{FRC}$ by 10%, 67%, 69% and 81% respectively.

Meaningful statistical analysis linking the severity of bronchiectasis to LNL parameters obtained in this study is limited, due to the small sample size, heterogeneity of the available imaging and subjective methodology of the assessment of severity. Nevertheless, this pilot study suggests there may be potential for the LNL parameters to provide insight into structural abnormalities such as bronchiectasis. Since the earliest use of CT scans to observe CF patients in the 1980s, multiple systems for providing a score to quantify the degree of abnormality detected have been proposed.[256,271–278] High resolution computerised tomography (HRCT) scores have been found to correlate better with frequency of exacerbations than FEV_1, so have been proposed as a potential endpoint in clinical trials.[277] However, there are clear issues with increasing the use of CT scanning. Most significantly, the overuse of CT scans introduces unnecessary exposure to radiation and associated increased risks of inducing cancer in exposed cells.[279] It is also increasingly recognised that the discovery of incidental findings from imaging can have negative outcomes from patients in terms of increased anxiety, subsequent unnecessary testing and overtreatment.[280] As a non-invasive test involving no radiation, the LNL model could provide a useful alternative

if found to correlate well with HRCT scores. A future study would need to assess the patient close in time to receiving a CT scan, suggesting the point for recruitment should be at the time of referral for a scan. A larger sample size would also be needed and eventually a longitudinal study would be needed to determine whether any of the LNL parameters are sensitive enough to identify the development of abnormalities over time on an individual level.

The final section of the data collected for this study focussed on patients receiving in-patient physiotherapy. Physiotherapy remains a core part of routine clinical management of CF, aiming to both improve patient quality of life and reduce the loss of pulmonary function as the disease progresses. Specifically, it seeks to reduce associated symptoms including cough, excessive sputum production, dyspnoea, exercise intolerance, and reduced quality of life.[281] Physiotherapy has been shown to improve mucus transport in CF patients in the short term.[282]

However there is limited evidence to recommend one technique or protocol over others,[281] and this may in part result from a lack of suitable clinical endpoints available to adequately access the efficacy of interventions, as the accuracy, reliability, sensitivity and validity of current metrics is questionable.[74] Current common clinical endpoints such as FEV_1, patient satisfaction surveys and quality of life scores have failed to distinguish between the success of different airway clearance techniques, although numbers of pulmonary exacerbations has been shown to distinguish between the effectiveness of two different airway clearance techniques: Positive expiratory pressure (PEP) and high frequency chest wall oscillation (HFCWO).[283] In another study, this time comparing postural drainage with percussion (PD) and autogenic drainage (AD) for airway clearance, McIlwaine *et al.* found no statistically significant difference in any spirometric values, despite patients expressing a preference for AD as it "worked the best" and they expectorated more sputum.[284] It is however important to note that measuring sputum production following physiotherapy is not always a good measure to assess airway clearance, as patients may swallow their sputum (this was the case for one patient studied but not included in the analysis for this study due to a failed washout).

Patient reporting is a valuable but subjective assessment of a technique so there would be great clinical value in an objective measure, which could potentially be offered by the LNL model. The sample size of two is too small for statistical analysis, but demonstrates the potentially useful information that the technique could provide. It was noted in both patients that all three inhomogeneity parameters were seen to decrease post-physiotherapy, suggesting that the intervention reduced overall

inhomogeneity of the lung. Taking the inhomogeneity of compliance for example, it is plausible that encouraging the expectoration of sputum clears the most severely congested regions, improving their ability to expand and contract and hence reducing the variability of compliance across the lung. This could explain the reduction in the parameter σ_{CL}, which was observed in both patients in the study. To investigate the potential of the LNL parameters to detect changes in pulmonary function resulting from physiotherapy, a larger sample size would be needed, with standardization of the airway clearance techniques performed. A follow up washout at 24 hours and then 1 week after physiotherapy could offer interesting insight into whether any changes observed as a result of the treatment persist beyond the time immediately after the session.

5.2 Comparison of Lognormal Lung Model and Lung Clearance Index

Based on the success of the preliminary study at the John Radcliffe Hospital, a second study was designed in collaboration with the Royal Brompton Hospital (RBH), focusing on people with CF with preserved FEV_1. The RBH is one of the leading centres for CF research in Europe, with extensive experience in performing MBW tests and researching the LCI and other MBW parameters. This study enabled a comparison between the LNL parameters obtained from an MBW using the MFS with standard MBW parameters measured by a commercial device for the first time, including the most commonly used $LCI_{2.5}$.

It has been demonstrated across multiple studies that the LCI is a more sensitive measure of early stage CF than spirometry,[248,285–288] and is therefore becoming increasingly important in clinical management of CF, given concerns that by the time abnormal spirometry is observed, the changes to the lung may be irreversible due to the self-perpetuating cycle of infection and inflammation.[248,289,290] Although early recognition of this problem was focussed on the paediatric CF population, with the great strides in early treatment and disease management, this lack of sensitivity is likely to become more significant in the adult patient population as well. The LCI has been shown to be well tolerated in both children and adults, distinguishing CF patients from healthy controls across multiple studies.[196,291–294] It is also thought to reflect the degree of inhomogeneity in the lung[295] and provide information about the 'silent zone' of the lung,[248,295] i.e. the small airways which pathology studies have shown are involved in early stage deterioration of the lungs.[296,297] Although FEV_1

remains the primary pulmonary function test used as a clinical endpoint in clinical trials, LCI is increasingly being used as an additional endpoint,[298] showing greater sensitivity than FEV_1 across multiple trials.[299] $LCI_{2.5}$ has also been used in clinical trials of various CFTR modulator therapies, showing improved lung function in response to the treatment.[300–302]

There are, however, still several problems with the LCI. The LCI does not describe a well defined physiological quantity, such as lung volume - it is an arbitrary parameter representing the number of lung turnovers required to reach an arbitrary concentration of expired gas. The LCI is purported to represent ventilation inhomogeneity, but could in fact produce a wide range of values for a series of completely homogeneous lungs, as many different factors contribute to an elevated LCI, such as deadspace and tidal volumes. When a subject performs an MBW test, there will always be breath to breath variation in end-expiratory lung volume and tidal volume, which is of neurological origin. To mitigate this, LCI tests are repeated 3 times on each patient and values within 10% of each other are accepted. LCI values are commonly obtained through either a N_2 or SF_6 MBW. In comparative studies of N_2 washouts using an Exhalyzer D device with SF_6 washouts using an Innocor device, the measured LCI values varied considerably between the two methods, with the N_2 washout calculating a higher LCI.[96,303] In this study, an Exhalyzer D was used to allow a more direct comparison with the results of an N_2 washout using the MFS.

Based on the initial pilot study, the parameter σ_{CL} shows particular promise as an alternative measure of early stage lung disease in detecting an increase in the inhomogeneity of lung expansion, providing a more sensitive metric than FEV_1 in patients with early stage CF. Recruitment of more patients with preserved FEV_1 offers the opportunity to further explore the utility of this and other LNL parameters in this subgroup of CF patients. With its analysis of different aspects of inhomogeneity, comparison between the LNL parameters and LCI values also offers the potential to evaluate the significance of inhomogeneity as a mechanism responsible for elevated LCI values observed in individuals with CF.

5.2.1 Methods

A molecular flow sensing device was transported to the Royal Brompton Hospital in London, which was added to the ethical approval 17/SC/0172 as an additional trial site. In June 2019, five healthy subjects were recruited by members of Professor Jane Davies' research group at the Royal Brompton Hospital/Imperial College London and the use of the molecular flow sensor was demonstrated to them to prepare them

for future subject recruitment. Further volunteers were recruited by the team in February-March 2020, determined by the availability of clinical staff to conduct the experiments. Subsequent subject recruitment was then delayed indefinitely by the COVID-19 pandemic from mid-March 2020 onwards.

Cystic fibrosis patients with preserved FEV_1, defined as ordinarily having an FEV_1 of $> 70\%$, were recruited, as well as additional healthy control subjects with no known lung disease or smoking history. All participants gave informed written consent prior to taking part in the study and were recruited under the same ethical approval 17/SC/0172.

In total, 12 people with CF and 18 healthy control subjects were recruited. The initial 5 subjects all performed a single MBW and the remaining 25 subjects performed two MBWs using the MFS. All subjects performed spirometry on the same day as their MBW tests on the MFS. Spirometry measurements were standardised by comparison with expected values for a volunteer's age, sex, height and ethnicity in order to report FEV_1 and FVC as a percentage of the predicted value. All but two subjects performed up to three MBW tests using the Exhalyzer D device. These two subjects were unable to perform MBW tests during their visit due to a lack of availability of the device during their visits.

5.2.1.1 Conventional Multiple Breath Washout Parameters

The Exhalyzer D (Eco Medics) is a commercial instrument which is widely used to carry out nitrogen washout tests in pulmonary function clinics and has been used extensively in clinical trials.[304] The Exhalyzer D multiple breath washouts were analysed using the specialist Spiroware software (Eco Medics). FRC is estimated from the ratio of the measured exhaled volume of N_2 over the washout period to the change in inhaled N_2 concentration between the start and end of the washout, as shown in equation 1.5. The lung clearance index is then calculated by dividing the cumulative expired volume over the course of the washout by the calculated FRC, (Equation 1.6), giving the number of lung turnovers required to reach the final N_2 concentration. The Spiroware software calculates the number of lung turnovers to reach both 1/40th and 1/20th of the initial starting concentration, giving $LCI_{2.5}$ and LCI_5 respectively.

Two parameters derived from analysis of the Phase III slopes of the washout breaths are also calculated by the Spiroware software: S_{cond} and S_{acin}. These are calculated from the gradient and the intercept of the graph plotting the gradient of the phase III slope against lung turnover between 1.5 and 6 lung turnovers.[305] Moment ratios were also determined from the Exhalyzer D washout tests, with the

Spiroware software reporting both the first and second moment ratios, M_1/M_0 and M_2/M_0. The zeroth moment, M_0 is found by plotting the normalised end tidal N_2 concentration, C_{net}, against lung turnovers, TO. M_0 is the integrated area under the curve between the washout start and the point at which $F_{N_2,insp}$ reaches 1/40th of its starting concentration. The first moment, M_1, is the integral of C_{net}*TO, equivalent to the centre of gravity of the area under the curve, while the second moment M_2 is equal to the integral of $C_{net} * TO^2$, which gives a higher weighting to later breaths in the washout. An elevated moment ratio, M_1/M_0 or M_2/M_0, is associated with poorer ventilation to a greater proportion of the lung and increased ventilation inhomogeneity.[306]

5.2.1.2 Lognormal Lung Model Parameters

The washout data collected from the MFS was securely transferred via OneDrive to allow analysis by the lognormal lung model on the Oxford advanced research computing (ARC) system. The LNL model analysis is detailed in Chapter 4 and affords the 5 primary outputs: V_D, V_A, σ_{CL}, σ_{VD}, σ_{Cd}. FRC can then be derived from the sum of the model's calculated V_A and V_D. To report the FRC as a percentage of the expected value, the measured FRC was compared to the ERS regression equations determined by Quanjer *et al.* given in Equations 4.1 and 4.2.[172]

Personal deadspace volume, V_D, was also calculated as a normalised deadspace, V_D/FRC, to estimate the proportion of the lung which does not participate in gas exchange. When two washouts successfully returned parameters, an average of the two values was taken for each parameter. A coefficient of variation was calculated for each of these volunteers by taking a ratio of the difference between the two measurements to the mean parameter value for that subject.

5.2.1.3 Statistical Analysis

Based on the results of Shapiro-Wilks tests for deviations from normality and F-tests for unequal variance, an unpaired two-sample t-test, assuming unequal variances (Welch's t-test), was used to assess whether the mean value of a physical characteristic or a parameter differed significantly between the CF group and the healthy control group.[307] A one sample t-test was used to determine whether the mean FRC as a percentage of the predicted FRC differed significantly from 100% in the healthy control group at the 0.05 significance level.

The degree of correlation between different parameters was determined using the Pearson product-moment correlation coefficient, denoted by r, which takes values

between -1 and +1. In the case of the assessment of the degree of bronchiectasis, Spearman's rank correlation was used as the more appropriate tool to explore any potential relationship between the rank of bronchiectasis severity and various parameters.

5.2.2 Results

In total 12 patients with preserved FEV_1 were recruited. Preserved FEV_1 was defined as ordinarily having an FEV_1 greater than 70%, based on recent medical history. Two of these volunteers were unable to perform an MBW using the Exhalyzer D instrument, due to a lack of device availability, and for one subject the lognormal lung model was unable to return parameters for either washout test. Therefore 9 people with CF are included in this analysis comparing the LNL model results with conventional MBW parameters, including the LCI. Six of these nine CF patients had two washouts successfully return LNL parameters, so only these six subjects were included when calculating the coefficient of variation (CoV) for each parameter.

One person in the control group was studied in both the 2019 and 2020 data collection periods, so only one of these sets of results was included when obtaining the mean, significance and correlations of the lung parameters. The second set of results were used as here two MFS washouts were performed, so a mean of the two sets of LNL parameters could be used and a CoV could be calculated. All 18 healthy control subjects successfully performed MBW tests on the MFS and Exhalyzer D, so there are 18 subjects to include in the control group. Of these 18 people, 12 performed two washouts using the MFS which produced LNL parameters, so 12 subjects are included in calculations of the CoVs for the control group.

A comparison of the demographic data for the control and CF groups is displayed in Table 5.5. No statistically significant difference between the mean age, height, weight or BMI of the two groups was found and hence the two groups can be considered well matched. Ideally additional female volunteers would be recruited for the control group, but this was not possible because of restrictions due to the COVID-19 pandemic.

All 27 volunteers attempted to perform spirometry, but one healthy volunteer was unable to perform spirometry to the required standard. Therefore the mean values for the control group were obtained from the other 17 volunteers. The spirometry results are summarised in Table 5.6. The measured FEV_1 for one volunteer with CF was 66%, but this subject was still included in further analysis as they met the inclusion criterion of ordinarily having an FEV_1 above 70% and a measurement in

	Healthy controls	CF Patients
Male:Female ratio	11:7	4:5
Age (years)	24.7 (±6.4)	29.8 (±11.9)
Height(cm)	171 (±10)	166 (±9)
Weight (kg)	67.7 (±12.7)	67.0 (±12.9)
BMI (kgm^{-2})	23.0 (±3.1)	24.2 (±3.8)

Table 5.5: Physical characteristics for the 18 healthy control subjects and 9 subjects with cystic fibrosis for whom both LNL parameters and MBW parameters from the Exhalyzer D were available. The values are presented as Mean±1SD. Welch's t-tests show that the difference between the means of the two groups is not statistically significant for age ($p = 0.261$), height ($p = 0.245$), weight ($p = 0.903$) or BMI ($p = 0.453$).

	Healthy controls	CF Patients
FEV_1 (L, BTPS)	3.61 (±0.84)	2.98 (±0.76)
FEV_1 (% predicted)	95.6 (±11.3)	87.2 (±11.0)
FVC (L, BTPS)	4.39 (±1.15)	3.72 (±0.99)
FVC (% predicted)	99.4 (±14.5)	91.7 (±11.4)
FEV_1/FVC	0.83 (±0.07)	0.80 (±0.06)

Table 5.6: The mean FEV_1 and FVC measurements for the healthy control group and the CF group are presented as both absolute values and as a percentage of a volunteers predicted value based on sex, age and height. Results are displayed as Mean ± 1S.D.. No significant difference was found between the mean FEV_1 ($p = 0.066$), FEV_1 % pred. ($p = 0.083$), FVC ($p = 0.135$), FVC % pred. ($p = 0.152$) or FEV_1/FVC ($p = 0.379$) based on Welch's t-tests.

this study which differed from this limit by less than the expected degree of within subject variability.[308] The mean FEV_1 and FVC for the CF group was lower than the healthy controls in terms of both the absolute value and the measurement expressed as a percentage of the predicted value. However, Welch's t-test found that there was not a significant difference in FEV_1 or FVC between the CF patients and healthy control subjects ($p > 0.05$). None of the participants with cystic fibrosis had an FEV_1/FVC ratio below 0.7, so the spirometry results do not indicate the presence of obstructive lung disease in these patients.[309]

5.2.2.1 MBW Volume Measurements

The lung volume estimated by the LNL model analysis of the MBW performed using the MFS device is divided into two parts: the alveolar volume V_A, and deadspace volume, V_D, displayed in Figures 5.10 (a) and (b) respectively. The alveolar volume was lower in the volunteers with cystic fibrosis compared to the healthy volunteers, but there is no significant difference between the absolute deadspace volumes for the two groups. However, the deadspace volume normalised to total lung volume, shown in Figure 5.10 (c), was elevated in the CF group.

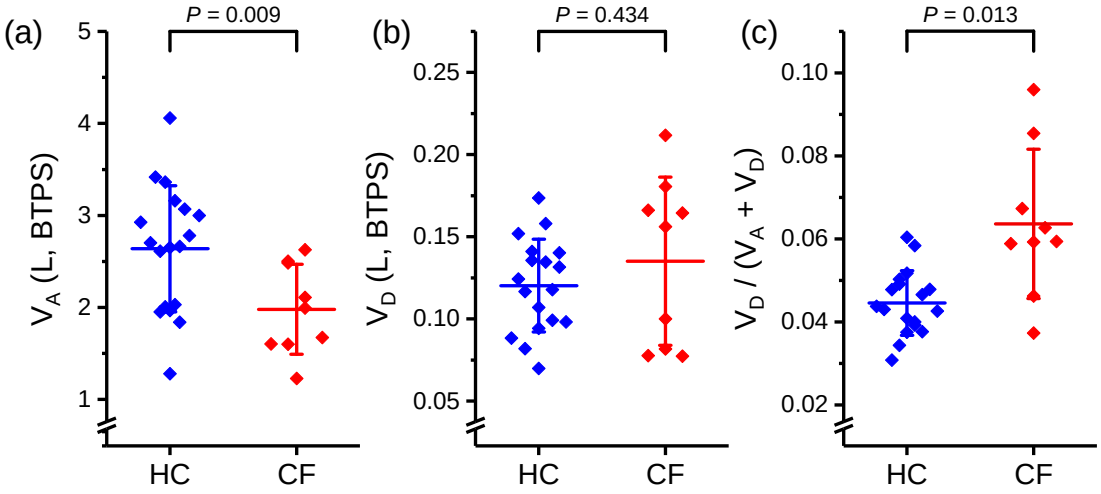


Figure 5.10: Comparison of the LNL model outputs for the Cystic Fibrosis patients (CF)with the healthy control subjects (HC). The LNL model outputs of alveolar volume (V_A) and deadspace volume (V_D) are shown in plots (a) and (b) respectively. The deadspace volume as a fraction of FRC (calculated from $V_A + V_D$) is shown in (c). P-values calculated using Welch's t-test are displayed above the plots.

As observed in the previous pilot study, Pearson's correlation coefficients showed strong correlation with height for both V_D and V_A in both the CF and control groups. Unlike the findings for the more heterogenous group of CF patients studied in the pilot study (which included patients with much more severe lung disease based on spirometry), no significant correlation was found between the fractional deadspace V_D/FRC and age ($r = 0.531$, p = 0.142) for the subjects with preserved FEV_1 in this study.

The sum of V_D and V_A constitutes the volume of the lung at FRC, shown as an absolute volume in Figure 5.11 (a) and as a percentage of the predicted FRC for each individual in Figure 5.11 (b). Both plots show that the FRC is lower in the CF group than the healthy control group in terms of both absolute and predicted values. The mean FRC (% pred.) for the control group is 90.8%, so is lower than the expected mean FRC of 100% (p = 0.023, one sample t-test) based on regression equations and a control group representative of the entire population of healthy normals.

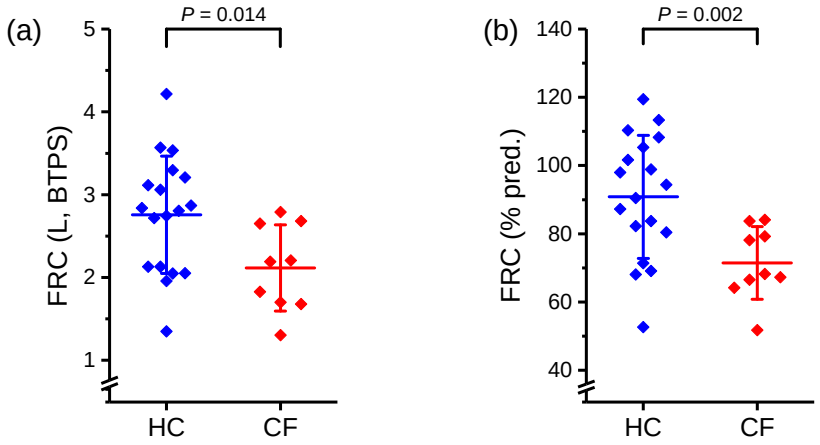


Figure 5.11: Comparison of the LNL model FRC measurements for the Cystic Fibrosis patients (CF) with the healthy control subjects (HC). The absolute volume of the lung at FRC is shown in (a), while the FRC as a % of a subjects predicted FRC based on sex, height and age is shown in (b). The mean FRC is significantly lower for the volunteers with CF both in terms of absolute volume (2.12 ± 0.52L vs. 2.76 ± 0.71L, $p < 0.05$ Welch's t-test) and percentage of the predicted volume ($71.5 \pm 10.7\%$ vs. $90.8 \pm 18.1\%$, $p < 0.01$ Welch's t-test).

The repeatability of the lung volume measurements calculated by both the Exhalyzer D and the LNL model were very good, as illustrated in Table 5.7, although the CoV was lower for the Exhalyzer D than the LNL for the FRC measurement.

Parameter	Coefficient of Variation (%)	
	Healthy Control (n=12)	Cystic Fibrosis (n=6)
V_A	3.9	4.2
V_D	4.4	6.3
V_D/FRC	5.3	6.8
FRC (LNL)	3.8	4.0
FRC (ExD)	2.8	2.2

Table 5.7: Coefficients of variation for the LNL model volume parameters (V_A, V_D, V_D/FRC and FRC) and the FRC measured by the Exhalyzer D device for both the healthy control and cystic fibrosis groups.

The FRC measurements derived from the LNL model analysis are compared with the FRC measurements obtained from the MBW performed using the Exhalyzer D device in Figure 5.12. The measurements are similar, but visual inspection of the data points in Figure 5.12 against the line of identity shows that the FRC measurements obtained from the LNL model are consistently lower than those measured using the Exhalyzer D. As shown in Table 5.7, the error in FRC measurements obtained from the two techniques are comparable. Hence the regression line fit to the data in Figure 5.12 was calculated using reduced major axis regression instead of ordinary least squares fitting, as this technique is most suitable for comparing techniques with similar uncertainties.[310] This fit shows that the difference between the measurements of FRC by the two techniques can primarily be attributed to an offset effect rather than a large deviation from the gradient of 1.

However, it should be emphasized that the smaller FRC measured by the LNL model is not unexpected, due to the difference in how the two techniques calculate FRC. Not all the nitrogen exhaled during the washout will have been residing in the lungs at the start of the washout. Over the course of the washout period, N_2 will be output by the circulatory system as nitrogen is cleared from the blood and body stores.[315,316] The LNL model does account for this in its modelling of the circulatory system,[208] while the Exhalyzer D software does not. Hence a greater volume of exhaled N_2 would be attributed to lung volume by the Exhalyzer D than the LNL model.

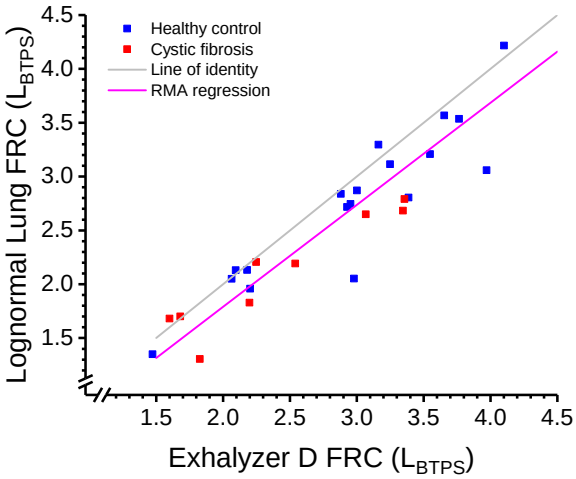


Figure 5.12: A comparison of the measured FRC by the Exhalyzer D device and the MFS device and LNL analysis for the CF patients and healthy controls. The line of identity is shown for reference. A linear fit of the data using reduced major axis regression in MATLAB is also shown.[311] A gradient of 0.948 (0.809, 1.111) and an intercept of -0.106 (-0.563, 0.284) was found, with 95% confidence intervals calculated according to the procedure outlined by Jolicoeur, Mosimann and McArdle.[311–313] No outliers were identified through analysis using a bagplot in R.[314]

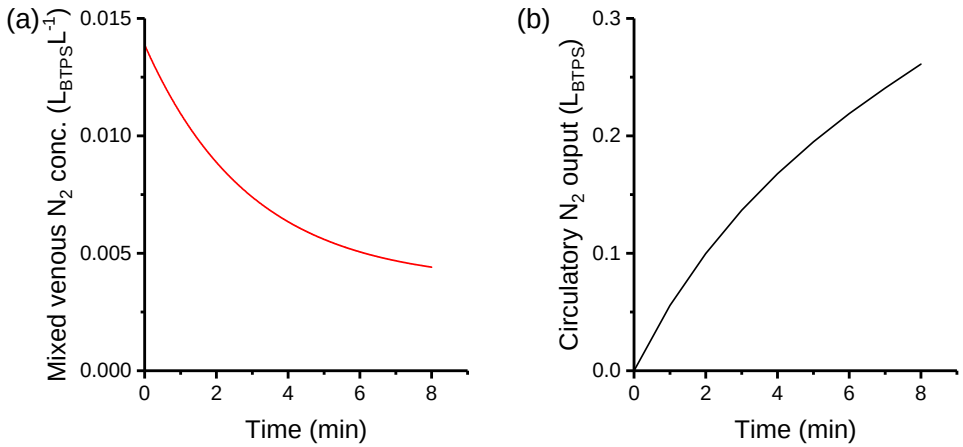


Figure 5.13: The mixed venous concentration of N_2 during a N_2 MBW predicted by the circulation and body gas stores (CBGS) model is shown in (a). The figure is reproduced from the paper by Magor-Elliott *et al.*.[208] The estimated N_2 volume output by the circulatory system during an MBW is shown in (b), with the simplifying assumptions of no recirculation of circulatory N_2 and a constant cardiac output of 4.5 L min^{-1}.

To emphasize this point, the modelled venous concentration of N_2 as a function of washout time by the circulation and body gas stores (CBGS) model developed by Magor-Elliott *et al.* is displayed in Figure 5.13 (a). If it is assumed that the cardiac output is constant and all the N_2 is removed from the mixed venous blood, the volume of N_2, V_{N_2}, output by the circulatory system by time t of the washout can be calculated according to:

$$V_{N_2}(t) = \int_0^t C_{v,N_2}(t) \cdot \dot{Q}(t)dt \tag{5.1}$$

where $\dot{Q}(t)$ is the cardiac output and $C_{v,N_2}(t)$ is the mixed venous concentration of N_2 at time t. If a constant cardiac output of 4.5 L min^{-1} is assumed, the N_2 output

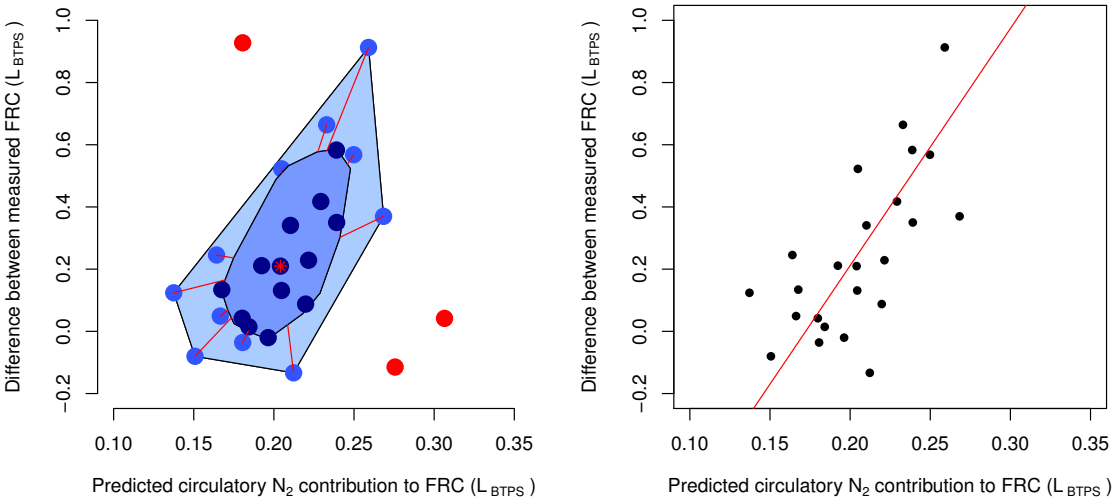


Figure 5.14: A bagplot comparing the predicted contribution to the FRC measured by the Exhalyzer D due to N_2 output by the circulatory system during the washout time with the difference between the FRC measured by the Exhalyzer D and the FRC measured using the MFS and LNL model. The central red asterisk represents the depth median, which is surrounded by a darker blue polygon, the bag, which contains n/2 data points with the greatest depth. The bag is multiplied by a factor of 3 to create a fence (not plotted) and a polygon is drawn to form a loop enclosing all data points between the bag and the fence. Identified outliers which lie outside this fence are shown in red. To the right, a reduced major axis regression line calculated following the exclusion of the identified outliers is displayed. A gradient of 7.6225 (5.5491, 10.4705) and an intercept of -1.3131 (-1.8961, -0.8887) was found, with 95% confidence intervals calculated according to the procedure outlined by Jolicoeur, Mosimann and McArdle.[311–313]

by the circulatory system as a function of washout time can be estimated, as shown in Figure 5.13 (b). The contribution to the observed FRC can then be estimated by dividing V_{N_2} by the change in inspired fraction of N_2 on beginning the washout.

The Exhalyzer D reports the time period for each washout, and this was used to estimate the total N_2 output by the circulatory system that contributes to the observed FRC for each subject. This is plotted against the observed difference in FRC calculated by the Exhalyzer D and the LNL model in a bagplot (Figure 5.14), a technique for identifying and displaying outliers in bivariate datasets proposed by Rousseeuw *et al.* as the bivariate alternative to the boxplot.[314] Three outliers were identified and excluded from further analysis. Reduced major axis regression was used to fit the regression line to the data, to account for the comparable errors in both variables. This linear fit was calculated in MATLAB and is also shown in Figure 5.14.[311] Although the prediction works well for the median washout time, as evidenced by the red asterisk (the depth median) on the bagplot in Figure 5.14 (a) lying close to the line of identity, Figure 5.14 (b) shows that the predicted contribution to FRC as a result of N_2 being removed from the circulatory system does not fully explain the difference in measured FRC between the methods.

5.2.2.2 Lung Inhomogeneity Parameters

The three LNL parameters describing the width of the deadspace, compliance, and conductance distributions are displayed in Figure 5.15. The standard deviation of the compliance distribution (σ_{CL}) is significantly elevated in the group of volunteers with CF, while the standard deviation of the deadspace (σ_{VD}) and conductance (σ_{Cd}) distributions showed no significant difference between the means of the two groups.

In both the healthy group and the CF group, none of the three inhomogeneity parameters correlated strongly with age (Pearson's correlation coefficient, $p < 0.05$). The inhomogeneity of compliance σ_{CL} was found to correlate negatively with height in this study within the control group ($r = -0.550$, p = 0.018), but the correlation with height in the healthy population was not deemed significant for either σ_{VD} ($r = -0.424$, p = 0.079) or σ_{Cd} ($r = -0.389$, p = 0.110). Similarly no correlation was found between the three inhomogeneity parameters and height in the CF group. The parameters σ_{CL}, σ_{VD} and σ_{Cd} were also not found to correlate significantly with weight or BMI for either the patient group or the control group.

The mean coefficient of variation (CoV) for each of the parameters is shown in Table 5.8. The two parameters assessing inhomogeneity in the airways showed comparable repeatability, with mean CoVs for the healthy controls and CF patients re-

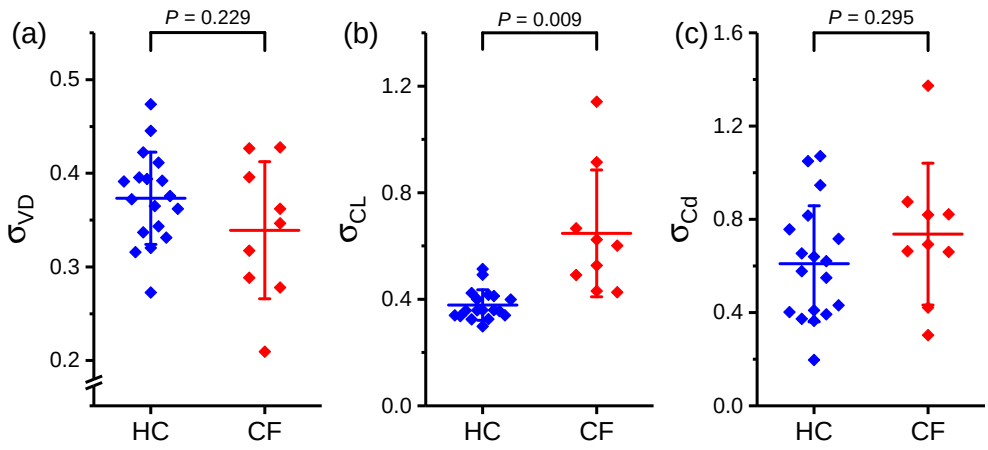


Figure 5.15: LNL parameters for the standard deviation of the (a) deadspace, (b) compliance, and (c) conductance distributions for the healthy control (HC) and cystic fibrosis (CF) groups. The mean value of σ_{CL} was higher for the cystic fibrosis group (0.647 ± 0.238 compared with 0.378 ± 0.057, $p < 0.01$ Welch's t-test). No significant difference was observed between the two groups for σ_{VD} and σ_{Cd}.

spectively of 4.1% and 3.5% for σ_{VD} and 4.9% and 4.1% for σ_{CL}. As expected, more substantial variability was seen for σ_{Cd}, a circulatory parameter which describes the standard deviation of the logarithm of the vascular conductance distribution, with a CoV of 37.2% and 17.3% for the two groups.

The six conventional MBW parameters obtained using the Exhalyzer D are presented in Figure 5.16, with the CoV for each displayed in Table 5.8. All parameters apart from S_{acin} show a significant difference in mean value between the CF and healthy control populations. In particular, the parameter S_{cond} shows near complete separation between the CF patients and healthy controls, with S_{cond} lying within the CF range for only one healthy control. However, the parameter displays poor repeatability, seen here by the CoVs for the two groups in Table 5.8, which has been noted as a limitation to its clinical use across multiple studies.[317–319]

The degree of correlation between the two LNL parameters which were found to differ significantly between the CF group and the control group (σ_{CL} and V_D/FRC) and the MBW parameters from the Exhalyzer D was evaluated and is presented in Table 5.9. Positive correlation was seen between σ_{CL} and the LCI values in the CF group. However, as illustrated in Figure 5.17 for $LCI_{2.5}$, a stronger correlation was observed between the $LCI_{2.5}$ values and V_D/FRC, implying that the fractional deadspace may be a greater contributor to increased LCI values than the inhomo-

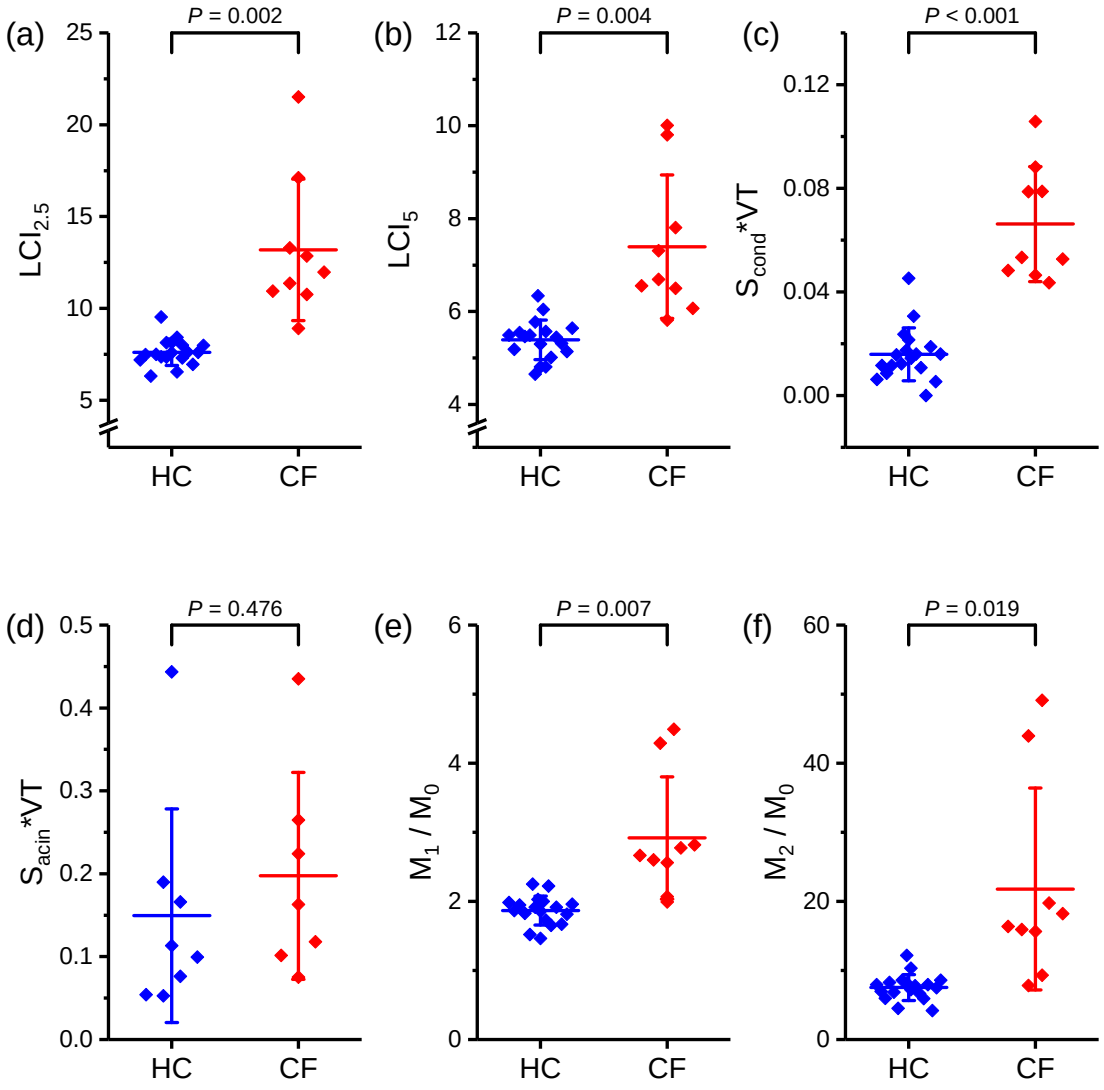


Figure 5.16: MBW parameters obtained from the Exhalyzer D device, all of which are considered to assess aspects of inhomogeneity within the lungs. (a)-(b) The lung clearance indices, $LCI_{2.5}$ and LCI_5, measure the number of lung turnovers required to reach 1/40th and 1/20th of the starting N_2 concentration respectively. (c)-(d) S_{cond} and S_{acin} are derived from phase III slope analysis and represent the gradient and offset of the plot of the lung turnover versus phase III slope gradients for each breath of the washout. (e)-(f) M_1/M_0 and M_2/M_0 are the first and second moment ratios calculated over the washout period. The mean value for every parameter except for S_{acin} was higher in the CF group compared to the healthy control group ($p < 0.05$, Welch's t-test). The Exhalyzer D was only able to evaluate S_{acin} for 8 of the 18 control subjects and 7 of the 9 CF subjects. All other parameters could be measured for all participants.

Parameter	Coefficient of Variation (%)	
	Healthy Control (n=12)	Cystic Fibrosis (n=6)
σ_{VD}	4.1	3.5
σ_{CL}	4.9	4.1
σ_{Cd}	37.2	17.3
$LCI_{2.5}$	2.5	2.4
LCI_5	1.8	2.4
S_{cond}	62.2	8.4
S_{acin}	19.3*	18.8
M_1/M_0	3.1	3.8
M_2/M_0	6.9	12.8

Table 5.8: The mean coefficients of variation for the three LNL model distribution parameters (σ_{VD}, σ_{CL}, and σ_{Cd}) and the six conventional MBW parameters obtained from the Exhalyzer D (LCI, S_{cond}, S_{acin} and the moment ratios). *For the S_{acin} CoV for the control group n=5, as the Exhalyzer D device was only able to calculate S_{acin} for 5 of the 12 volunteers in the control group with two sets of LNL parameters.

geneity parameter σ_{CL}. A multiple linear regression was performed to test whether σ_{CL} and V_D/FRC could significantly predict $LCI_{2.5}$ across the 27 subjects, including all controls and CF patients for whom both Exhalyzer D and LNL model parameters were available using the following model:

$$LCI_{2.5} = \beta_0 + \beta_1 V_D/\text{FRC} + \beta_2 \sigma_{CL} \tag{5.2}$$

where β_{0-3} were coefficients to be determined. The overall regression was statistically significant ($R^2 = 0.801$, $F(2, 24) = 88.7$, $p < 1 \times 10^{-11}$), with the $LCI_{2.5}$ significantly predicted by both V_D/FRC ($\beta_1 = 142.59$, $p = 3.8737 \times 10^{-7}$) and σ_{CL} ($\beta_2 = 7.855$, $p = 6.1835 \times 10^{-5}$), with a non-significant intercept $\beta_0 = -1.4627$ ($p = 0.10825$). Multiplying the mean V_D/FRC and σ_{CL} values by the respective regression coefficients finds a mean contribution of 3.68 from σ_{CL} and 7.26 from V_D/FRC, demonstrating again the larger contribution to $LCI_{2.5}$ from the parameter V_D/FRC, a parameter which does not reflect inhomogeneity of the lungs.

MBW Parameters	σ_{CL}		V_D/FRC	
	Healthy Control (n=18)	Cystic Fibrosis (n=9)	Healthy Control (n=18)	Cystic Fibrosis (n=9)
$LCI_{2.5}$	-0.038	0.661	0.261	0.934
LCI_5	-0.046	0.441	0.216	0.953
S_{cond}	0.559	0.702	-0.059	0.441
S_{acin}	-0.524*	0.177**	0.123*	0.782**
M_1/M_0	-0.083	0.637	0.464	0.866
M_2/M_0	-0.014	0.681	0.558	0.860

Significance level

p>0.05

p<0.05

p<0.01

p<0.001

Table 5.9: Pearson's correlation coefficients assessing the degree of linear correlation between MBW parameters measured by the Exhalyzer D and the LNL parameters with significant variation between CF and healthy participants, σ_{CL} and V_D/FRC. The significance of the Pearson's r values assessed by a t-test is displayed using a colour gradient. The strongest correlations found were between the $LCI_{2.5}$ and LCI_5 and V_D/FRC for the CF group. *n=8 for the healthy controls and **n=7 for the CF patients for measurements of S_{acin}.

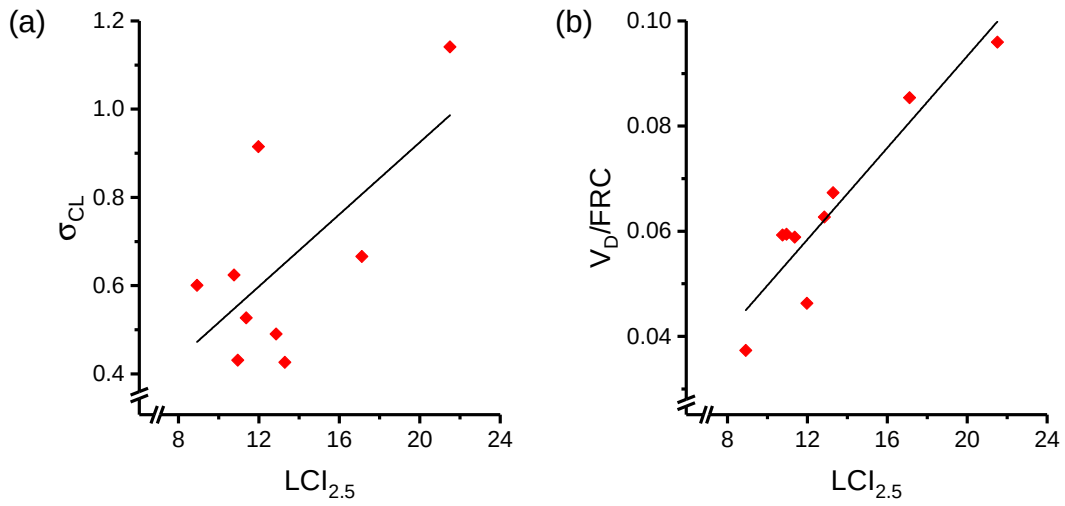


Figure 5.17: Comparison between the $LCI_{2.5}$ and σ_{CL} in (a) and between the $LCI_{2.5}$ and V_D/FRC in (b) for the nine CF patients with parameters from both the LNL model and the Exhalyzer D. Ordinary least-squares fits are shown for reference.

5.2.2.3 Severity of Bronchiectasis

Where available the medical notes of participants were checked for any previous diagnosis of bronchiectasis based on CT imaging and grouped into one of three categories: no imaging/no evidence of bronchiectasis, mild bronchiectasis and severe bronchiectasis. For the control subjects, imaging was available for only one of the subjects, for whom an incidental finding of mild bronchiectasis was observed. Of the 11 CF patients, the degree of bronchiectasis was judged to be severe in 6 subjects and mild in 2 of the subjects. For the remaining 3 subjects there was no imaging available and bronchiectasis was considered by clinicians to be unlikely in two and no bronchiectasis was observed on prior imaging for one subject. The parameters identified in the previous pilot study as potentially interesting are compared for the three groups in Figure 5.18.

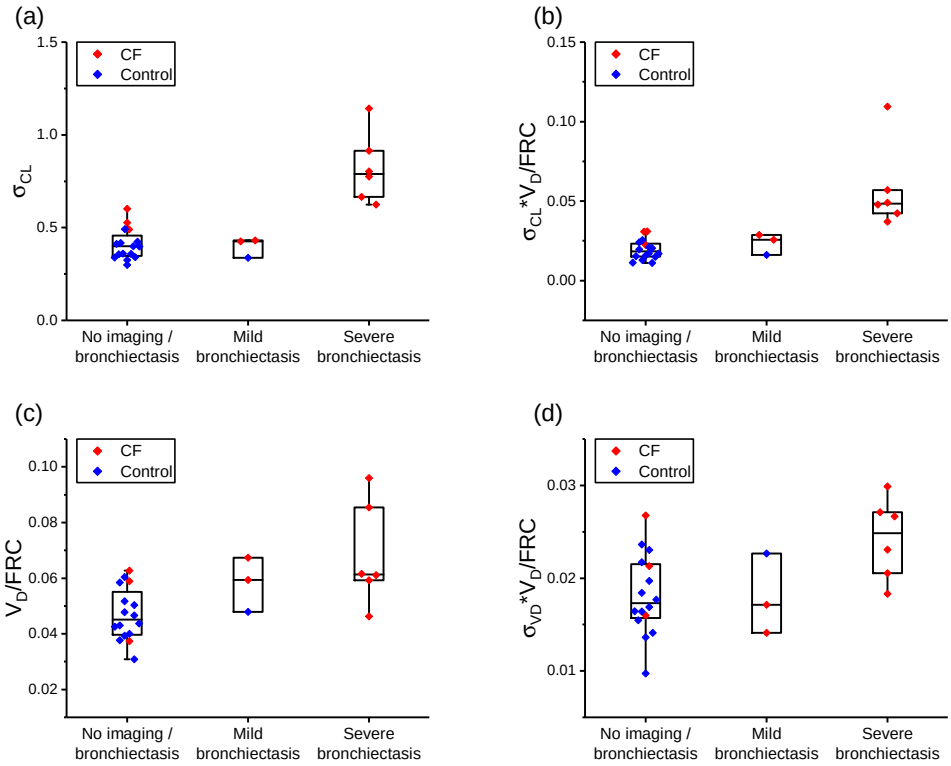


Figure 5.18: A comparison between the LNL parameters of interest (a) σ_{CL}, (b) σ_{CL}*V_D/FRC, (c) V_D/FRC and (d) σ_{VD}*V_D/FRC for the patients grouped by severity of bronchiectasis if imaging was available and no imaging/bronchiectasis if not. All subjects were included with CF patients shown in red and controls in blue.

By assigning each of the three categories a rank (no bronchiectasis/imaging = 1, mild = 2 and severe = 3), a Spearman's rank correlation was performed on all

25 subjects, including all CF patients and controls. Significant positive correlation was found for all four of the parameters presented in Figure 5.18: σ_{CL} ($\rho = 0.662$, $p < 0.001$), V_D/FRC ($\rho = 0.601$, $p = 0.001$), σ_{CL}*V_D/FRC ($\rho = 0.730$, $p < 0.0001$) and σ_{VD}*V_D/FRC ($\rho = 0.438$, $p = 0.029$). When the same test was repeated but just looking at the CF group, only σ_{CL} ($\rho = 0.754$, $p = 0.007$) and σ_{CL}*V_D/FRC ($\rho = 0.804$, $p = 0.003$) were found to be significantly correlated with the ranked severity of bronchiectasis. FEV_1 (% pred.) was not found to correlate significantly with rank for either the entire study group ($\rho = -0.372$, $p = 0.067$) or the subset of participants with CF ($\rho = -0.494$, $p = 0.123$). Of the 25 subjects for whom LNL parameters were compared with severity of bronchiectasis, 23 had LCI values available and LCI was found to correlate with severity using the same ranking system ($\rho = 0.6229$, $p = 0.002$). However, when control subjects are excluded from this analysis, leaving just the 9 CF patients with both LCI and LNL parameters, no significant correlation was observed between severity of bronchiectasis and LCI ($\rho = 0.39198$, $p = 0.297$).

5.2.3 Discussion

In this study, CF patients with preserved FEV_1 and healthy control subjects performed N_2 MBW tests using the molecular flow sensor, which was subsequently analysed using the lognormal lung model. The same volunteers also performed N_2 MBW tests using an Exhalyzer D device, allowing comparison between conventional MBW parameters and LNL parameters for the first time. The device and procedure were well-tolerated by patients and this study also marks the first time the device has been used in a clinical setting outside of the Oxford University Hospitals sites, showing the feasibility of training new users and the potential for multi-centre trials.

For the version of the Exhalyzer D software used at the point of data collection for this study and subsequent analysis, on average a lower FRC was found using the LNL model compared to the Exhalyzer D. Further investigation of the effect of the LNL model accounting for the N_2 output from the blood over the washout period was shown to potentially account for some of this difference, but showed poorer agreement as the washout time deviated from the mean value. However, since this analysis was completed, Wyler *et al.* reported inaccuracies in the measurement of O_2 by the Exhalyzer D device and the manufacturer subsequently issued a correction to the software to reprocess the data to account for the effect of the 'cross-talk' between the O_2 and CO_2 measurements.[320] The reanalysed data is shown in Figure 5.19. Although there is now excellent agreement between the two methods, this is somewhat surprising, as we believe that the Exhalyzer D technology does not account

for modelled circulatory N_2 so would not expect perfect agreement between the two techniques, although the calculations used in the Exhalyzer D software are not open access. Discrepancies between FRC measured by different commercial devices have been noted before, such as a comparison between Innocor (which uses an SF_6 washout) and the Exhalyzer D by Bayfield *et al.* who found that the FRC values could not be directly compared between devices.[114] The Innocor measured FRC was found to be lower than for Exhalyzer D (prior to the discovery of the measurement inaccuracy of the Exhalyzer D),[114] suggesting that post-correction there may be an even greater difference.

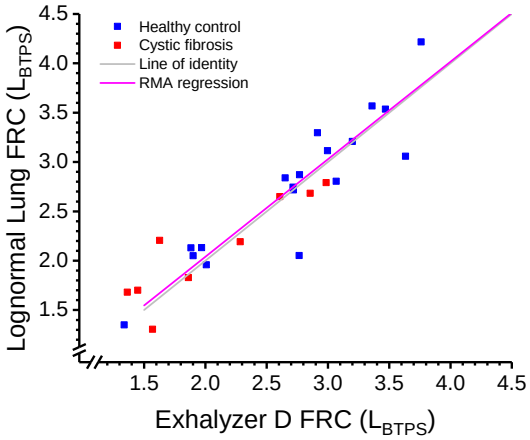


Figure 5.19: A comparison of the FRC after applying the correction to the Exhalyzer D measurements and the LNL calculated values for the CF patients and healthy controls. The line of identity is shown for reference. A linear fit of the data using reduced major axis regression in MATLAB is also shown.[311] A gradient of 0.988 (0.843, 1.159) and an intercept of 0.065 (-0.364, 0.430) was found, with 95% confidence intervals calculated according to the procedure outlined by Jolicoeur, Mosimann and McArdle.[311–313]

For the early stage CF patients recruited in this study, spirometry was unable to distinguish between the CF and control groups. This is consistent with FEV_1 reflecting obstruction in the large airways, which commonly does not become apparent until later stage lung disease.[195] Parameters derived from MBW tests have the potential to detect changes in the small airways and hence detect early-stage lung disease.[248] For the participants in this study the CF patients were found to have a higher mean $LCI_{2.5}$, LCI_5, both moment ratios and S_{cond} compared to the healthy control subjects with good reproducibility. S_{cond} showed an exceptional ability to discriminate between the CF and control groups. However, as has been observed before, this parameter demonstrated poor repeatability.[321]

In agreement with the subset of the pilot study with preserved FEV_1, the early-stage CF group in this study also showed significantly elevated values for σ_{CL}, indicating increased inhomogeneity of lung compliance compared to healthy controls. Unlike the pilot study, there was some overlap between the CF patients and controls. The σ_{CL} values determined for three of the CF patients fell below 0.5, while σ_{CL} exceeded 0.5 for all CF patients in the pilot study, including those with preserved FEV_1. With a value of 0.51, σ_{CL} for one healthy control subject was above the maximum value for the control groups in both the CF pilot study and the young smokers study. This highlights the need for a future study and retrospective analysis of previously recruited healthy control subjects to establish the normal range of values for healthy people with no history of respiratory disease, which has recently been attempted by Bithell.[240]

No statistically significant difference was observed between the two groups for the mean values of σ_{VD} and σ_{Cd}. In a previous study of another patient group with obstructive lung disease, even in stage 1 COPD ($FEV_1 > 80\%$) σ_{Cd} was significantly elevated,[200,219] and a higher σ_{Cd} was also found for young smokers compared to never-smokers in the study detailed in Chapter 4. However, although the mean σ_{Cd} was found to be higher in the CF group in this study, the difference was non-significant. This may be a result of the difference in the underlying physiology between the two diseases or a reflection on the inadequate sample size in this study to detect the difference. No significant difference was found between the mean σ_{VD} for the patient and control groups.

The repeatability of the airways parameters calculated by the LNL model were very good, while the circulatory parameter σ_{Cd} showed a much higher intra-subject variability. Recent work on introducing tracer gases to the MBW protocol shows the potential for improved estimation of cardiac output and hence more reliable modelling of the circulatory parameters in the future.[191]

An elevated fractional deadspace was also seen in the CF group in the study, in agreement with the findings from the pilot study. Stronger correlation was found between a patient's LCI value and V_D/FRC than between the LCI and σ_{CL}. Historically, the LCI has been considered to provide an assessment of the degree of inhomogeneity within the lungs. However, the results of this study suggests that the effect on the LCI inhomogeneity in the lung is highly convolved with the total deadspace within the lungs. Hence, an increased LCI may be largely due to an increased total deadspace rather than being primarily driven by increased inhomogeneity.

The contribution from the deadspace volume to the LCI has been suggested previously by Gonem *et al.*. Using a simple two compartment model of the lungs, they attributed elevated LCI values in CF patients to increased deadspace and ventilation inhomogeneity, deriving the parameters LCI_{vent} and LCI_{dead} to estimate the significance of the two factors.[321] The results of this study using the LNL model not only provides further evidence against the hypothesis that elevated LCI is primarily driven by increasing inhomogeneity, it also highlights the potential strength of the LNL parameters over the LCI. It may give more detailed insight into the physiological processes that are taking place in a single patient rather than just a single number that encapsulates an overall deterioration in pulmonary function due to multiple factors.

If the LNL parameters were able to distinguish between multiple diagnoses seen on imaging, such as bronchiectasis, this could further increase the utility of the LNL model parameters. Previous studies comparing HRCT scores and pulmonary function tests found that the LCI was superior to FEV_1 in sensitively detecting abnormal lung structure in patients with CF and non-CF bronchiectasis.[248,322,323] This study also found that LCI correlated with the groupings of participants based on severity of bronchiectasis, while FEV_1 did not. The analysis of the severity of bronchiectasis in this study also suggests that σ_{CL}, V_D/FRC, σ_{VD}*V_D/FRC and σ_{CL}*V_D/FRC may differentiate between no, mild and severe bronchiectasis with greater sensitivity than LCI. The rating of the severity of bronchiectasis in this study was however lacking in sensitivity and a priority for future research of CF patients should be a study specifically designed to make this comparison. This would involve recruiting a larger sample size, performing an MBW test at the point of referral to or shortly after a CT scan and using an objective metric such as a HRCT score to assess the severity of bronchiectasis.

The LNL model may also offer the potential for a more sophisticated alternative metric: an *idealised* lung clearance index, i-LCI. While retaining the connection to the LCI, which clinicians are increasingly familiar with using in clinics and trials, this has the potential to both improve standardization of the LCI measurement and provide additional information about the source of an elevated LCI. Using the determined LNL parameters, it is possible to simulate breathing with a fixed tidal volume. This could eliminate variability caused by different device deadspaces and differing breathing patterns. It may also be possible to quantify the relative contributions to the LCI from the baseline expected for a homogeneous lung, personal deadspace and inhomogeneity of the deadspace, compliance and conductance.

As well as the potential for a more sophisticated calculation for an idealized lung clearance index, the LNL parameters themselves and in particular σ_{CL}, also show promise as early indicators of abnormal lung function. As the protocol for an MFS washout for LNL analysis does not require a fixed tidal volume, this could make the MBW test more appropriate for use in younger children. However, the deadspace volume for the adult device is too large to use in children and so a smaller device would be necessary. The miniaturization of the MFS for use in paediatric patients is detailed in the following chapter.

5.2.4 Conclusions and Future Work

Both studies presented in this chapter show that it is feasible to conduct MBW tests on CF patients using the MFS and then subsequently analyse the data using the LNL model. The device was well-tolerated by both patients and healthy controls and successful data collection was achieved both with and without the presence of non-clinical researchers to assist clinicians with the data collection.

A heterogeneous group of CF patients were recruited for the first pilot study detailed at the beginning of the chapter, with spirometry ranging from severely obstructed to within the normal range. All three inhomogeneity parameters were elevated in the CF group compared to healthy controls. As observed in the study of young smokers detailed in the previous chapter, the parameter describing the inhomogeneity of compliance σ_{CL} showed particular promise as a sensitive measure of early-stage lung abnormalities in patients with normal spirometry, with all CF patients in the pilot study having values above the maximum observed for the healthy controls.

Based on this pilot study, a second study of the CF population, this time at the Royal Brompton Hospital, was devised to focus on recruiting patients with 'preserved FEV_1', which again found that σ_{CL} was elevated in CF patients, although with some overlap of values with the control group. This second study also allowed comparison of the LNL model parameters with conventional MBW parameters, including the LCI, for the first time. It has frequently been asserted that the LCI is a measure of ventilation inhomogeneity.[324] However the results of the second study of this chapter show that while there is in fact positive correlation between inhomogeneity of compliance and the LCI, there is in fact also a significant contribution to increased LCI as a result of increased deadspace relative to overall lung volume.

In both studies, imaging reports were accessed in patients' medical notes to investigate possible correlation between LNL model parameters and structural abnormalities, namely the severity of bronchiectasis. Although the two studies are not directly comparable due to different grading of the degree of severity of bronchiectasis, both found that certain LNL model parameters correlated with degree of bronchiectasis. In particular the parameters σ_{CL}, V_D/FRC, σ_{CL}*V_D/FRC and σ_{VD}*V_D/FRC would merit further investigation.

The LNL parameters before and after physiotherapy were compared in two patients and both showed a decrease in all three inhomogeneity parameters after the treatment. Further recruitment of patients pre- and post- physiotherapy should be resumed when possible in order to have sufficient statistical power to identify which LNL parameters, if any, show a significant change in response to the intervention. It would also be of great interest to test whether any changes correlate with other metrics such as patient discomfort level and whether the response varies depending on the techniques used during the physiotherapy session.

In addition to extending the study of patients' response to physiotherapy, other patient responses to interventions should also be investigated – for example patients could be studied prior to commencing and while undergoing treatment with antibiotics in response to an exacerbation. This in particular may help distinguish between the LNL model parameters' responses to short term inflammation versus permanent structural lung abnormalities. If the LNL parameters are sensitive to patient response to IV antibiotics this could be of great use to clinicians. At present the length of treatment is determined by FEV_1 and patient symptoms, but a more sensitive pulmonary function test could enable clinicians to better balance the risk of under-treating and exacerbating symptoms vs. the risk of complications from extended use of antibiotics.[325]

In general the recruitment of more patients with CF is required, including longitudinal studies to see how parameters change as the disease progresses. Studying the response to interventions such as physiotherapy and IV antibiotics as well as comparison with structural abnormalities observed in imaging all provide areas for future study.

Chapter 6

Development of a Paediatric Molecular Flow Sensor

Cystic fibrosis is now most commonly diagnosed at birth, due to the introduction of the UK-wide newborn screening programme in 2006,[326] with patients then receiving pulmonary monitoring and care throughout their childhood. The advent of CFTR modulator therapies has resulted in many children with CF reaching adulthood with normal spirometry and so more sensitive techniques for assessing lung function in children are needed.

The previous chapter explored the potential for using MFS technology in combination with the LNL model to assess lung inhomogeneity as a more sensitive measure of lung disease. In particular, the superior ability of the σ_{CL} parameter to distinguish CF patients with preserved FEV_1 from healthy controls indicates that a similar test in children at a very early stage of lung disease may prove informative. However, the adult device is not suitable for paediatric patients, due to its large instrument deadspace. Therefore this chapter is concerned with the development of a new paediatric MFS based on the same molecular flow sensing principles as the adult MFS, but with design modifications for this new application.

Firstly, miniaturisation of the measurement cell was required, the design of which is described in Section 6.2. Furthermore, due to the limited concentration span of children, it would be preferable to eventually be able to use a shorter test than the 15 minute protocol used in the studies of adults detailed in Chapters 4 and 5. Extending the capability of the device to measuring the concentration of CH_4 and C_2H_2 may allow the determination of LNL model parameters through a trace gas washin as an alternative to the N_2 washout.

Section 6.3 therefore gives an overview of the spectroscopic transitions employed for the trace gas measurements as well as the necessary additional terms in the flow

calculations. This is followed in Section 6.4 by details of the modelling required to design a pair of multipass mirrors with laser diodes and photodetectors placed to achieve optical paths of sufficient length to enable the required measurement sensitivity.

Following the successful design and calibration of this paediatric molecular flow sensor (MFS-P), it is currently being used to study paediatric CF patients at the Royal Brompton Hospital and an early dataset from this study is presented in Section 6.5 to illustrate the potential value of this technique in paediatric clinics. This chapter concludes with discussion of the future work of this study and other avenues of research within the paediatric population that could be explored using this novel technology.

6.1 Motivation

The median age of a diagnosis of cystic fibrosis is 2 months old,[327] usually via newborn screening (NBS) programmes. Following a positive sweat chloride test and/or the discovery of two CF causing CFTR mutations, a newly diagnosed patient is immediately referred to a CF specialist centre,[328] where they will be closely monitored throughout their lives. As respiratory failure is the primary cause of morbidity from CF, early management to slow the progression of lung disease is a key objective for clinicians. This includes daily management of the condition and prompt treatment of exacerbation and infections, as well as new therapies involving CFTR modulators which target the underlying gene mutation directly. There is a recognised clinical need for better methods of assessing the effectiveness of these treatments in children with CF. The potential of more sensitive technologies is twofold: improved targeting of existing treatment options in individual management of paediatric patients and the ability to better assess the effect of early intervention of novel therapeutics in young children in longitudinal clinical trials.

Spirometry is still the most widely used tool in assessing lung function over a CF patient's life. The observed decline in FEV_1 amongst CF patients starts in childhood before decreasing more rapidly in adulthood.[267] However, spirometry has long been recognised as an unsatisfactory metric within the paediatric population - even in 2012, prior to the widespread use of CFTR modulator therapies, 66% of patients aged 6-15 had normal FEV_1.[329]

MBW testing and particularly the LCI has shown to provide a more sensitive measure of changes in pulmonary function - multiple-breath washout detects abnormal lung function in children with CF more readily than either plethysmography or

spirometry.[330] The lack of forced manoeuvres also eliminates issues around discomfort experienced by patients - this may be particularly important during exacerbations, when performing spirometry may provoke painful coughing. Multiple-breath washout outcomes are sensitive to inflammation and infection in children with cystic fibrosis.[331] Dornase alfa was found to significantly improve LCI[332] and, unlike spirometry, the LCI was able to detect a treatment effect from hypertonic saline (HS) inhalation in patients with CF with mild disease.[333] Therefore the LCI may be a suitable tool to assess early intervention strategies in this patient population. LCI is a more sensitive indicator than FEV_1 or FEF_{75} (maximal expiratory flow when 75% of forced vital capacity was expired) for detecting structural lung disease in CF, and a normal LCI almost excludes HRCT abnormalities.[293]

The important role of the LCI in the clinical management of CF is increasingly recognised, but the exact applications of the test in monitoring CF lung disease is still uncertain.[334] This may in part be due to the convolution of different aspects of lung function contained within the single LCI measurement. As evidenced in the previous chapter, the LCI does not primarily offer a measurement of lung inhomogeneity, as the LNL model parameter V_D/FRC was found to correlate more strongly with LCI than σ_{CL} does with LCI. This conclusion is further supported by the work of Gonem *et al.*, who also determined that deadspace was a significant contributer to an elevated LCI.[321]

As discussed in the previous chapter, there are several other limitations to conventional MBW testing, with possibly the most significant in the paediatric CF population being the requirement for a patient under investigation to perform the test under strict limits to their tidal volume. While this may present some difficulties in the adult population, this is much more likely to pose problems in the paediatric age range, as some children are unable to complete the test or it may require multiple attempts. There also exist discrepancies between LCI values obtained from SF_6 vs. N_2 washout procedures,[335] with both being considered to have drawbacks in paediatric lung function testing. SF_6 is a potent and persistent greenhouse gas, with a 100-year Global Warming Potential (GWP_{100}) of 23,700;[336] therefore its use should be limited where possible. There is also concern that medical grade O_2 (99.5% purity), which is used in N_2 washouts, may significantly perturb lung function, in particular the distribution of both ventilation and pulmonary blood flow in very young children.[337] This is thought to account for some of the differences seen between SF_6 washin and N_2 washouts.[337] Therefore, alternatives to this may be welcome, and this was one of the driving forces in introducing an additional optical channel in MFS-P to measure

the concentration of the tracer gas CH_4. As noted previously, this also offers the possibility that in the future the time taken to conduct a test may be shortened by the use of a washin test rather than a washout test. The LNL model analysis also includes modelling of the circulatory system, accounting for the effect of the body stores of the gases being used in the calculation of MBW parameters. Therefore, it may be expected that LNL model parameters may show better agreement when calculated using different trace gases than a similar analysis using only standard LCI calculations.

6.2 Miniaturisation of the Molecular Flow Sensor

Designing a device and experimental protocol suitable for use in paediatric patients presents additional challenges, namely achieving a low enough instrument deadspace while retaining measurement sensitivity and a short enough experimental protocol for young children.

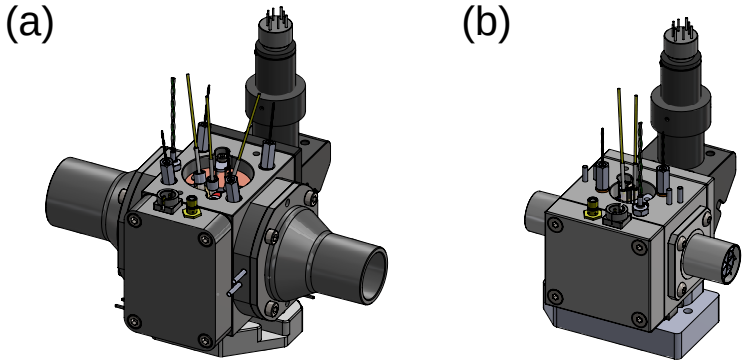


Figure 6.1: A comparison of the schematics of the (a) adult and (b) paediatric MFS measurement cells, with dead space volumes of 50 mL and 16 mL respectively.

The total equipment deadspace for the device was restricted to <2 ml kg^{-1} body-weight in accordance with the European Respiratory Society (ERS) recommendations for young children, as outlined in their 2013 consensus statement.[60] The target age group for the use of this device ranges from 5 years old, so using the mean of the 15th percentile of weights for 5 year old girls and boys of 15.9 kg,[338] the upper limit for total device dead space was set at 31.8 ml. This is inclusive of the 15 ml volume of an HME filter (Medisize Hygrovent Child HME) as well as the equipment deadspace. Consequently, the upper limit of the measurement cell deadspace was set at 16.8 ml and the final design shown in Figure 6.1 has a device deadspace of 16.1 ml.

The basic design of the device remains the same as the adult MFS: every 10ms pressure and temperature measurements are taken to calculate total number density alongside simultaneous measurements of the concentrations of the respiratory gases of interest. When combined with space and time-aligned measurements from the Lilly-type pneumotachograph that converts the pressure drop across a pair of wire meshes to the flow rate, this enables the bidirectional measurement of the flux of each gas as a subject breathes through the device. As with the adult device, a single barometric pressure sensor (HCA0811ARH8, First Sensor AG) is placed into the gas flow through the measurement cell from above. Two custom made K-type thermocouples of the same type as those used in the adult MFS are are exposed to the gas flow within the measurement cell to measure temperature. The calibration procedures for both the barometric pressure sensor and thermocouples are same as those detailed in Section 2.2.

The reduction in bore radius necessitated some changes to the flow sensing system. The wire mesh used to induce the pressure drop in the adult device with 36 µm wire diameter and 75 µm aperture width (111 µm pitch) would not produce a sufficient pressure drop across the smaller bore of the MFS-P. Initially two wire meshes with wire thickness 65 µm and spacing 140 µm (205 µm pitch) and wire thickness 90 µm and spacing 180 µm (270 µm pitch) were trialled. A custom program for driving the mechanical pump was written to test the maximum measurable flow rate with various different meshes to test the flow rate at which the HCLAs would become saturated. Some sample data for the first of these meshes are illustrated in Figure 6.2 (a). This clearly shows the variability in saturation limits between the HCLAs, but the maximum measurable flow rate is limited by the HCLA that saturates at the lowest flow rate. For the 205 µm pitch mesh, some HCLAs were saturated at a pump speed of 120 ms^{-1}, which corresponds to a flow rate of 56.7 L/min, while the 270 µm pitch mesh resulted in HCLA saturation at 115 ms^{-1} or 54.3 L/min.

The maximum measurable flow rate was too low with this iteration of the paediatric MFS design, and crucially the total resistance with this configuration was deemed too high for a child to breathe through comfortably. As a result it was determined that the light traps should be redesigned to reduce resistance. This new design had an altered configuration of the vanes to produce a more laminar flow at each end. As with the adult device, these new light traps were also 3D printed in steel to provide good thermal contact with the gas flow. Following changes to the light traps (from a miniaturised version of the adult light traps shown in Figure 6.2 (b) to the variable pitch design shown in Figure 6.2 (c)) it was possible to reduce the total resistance to

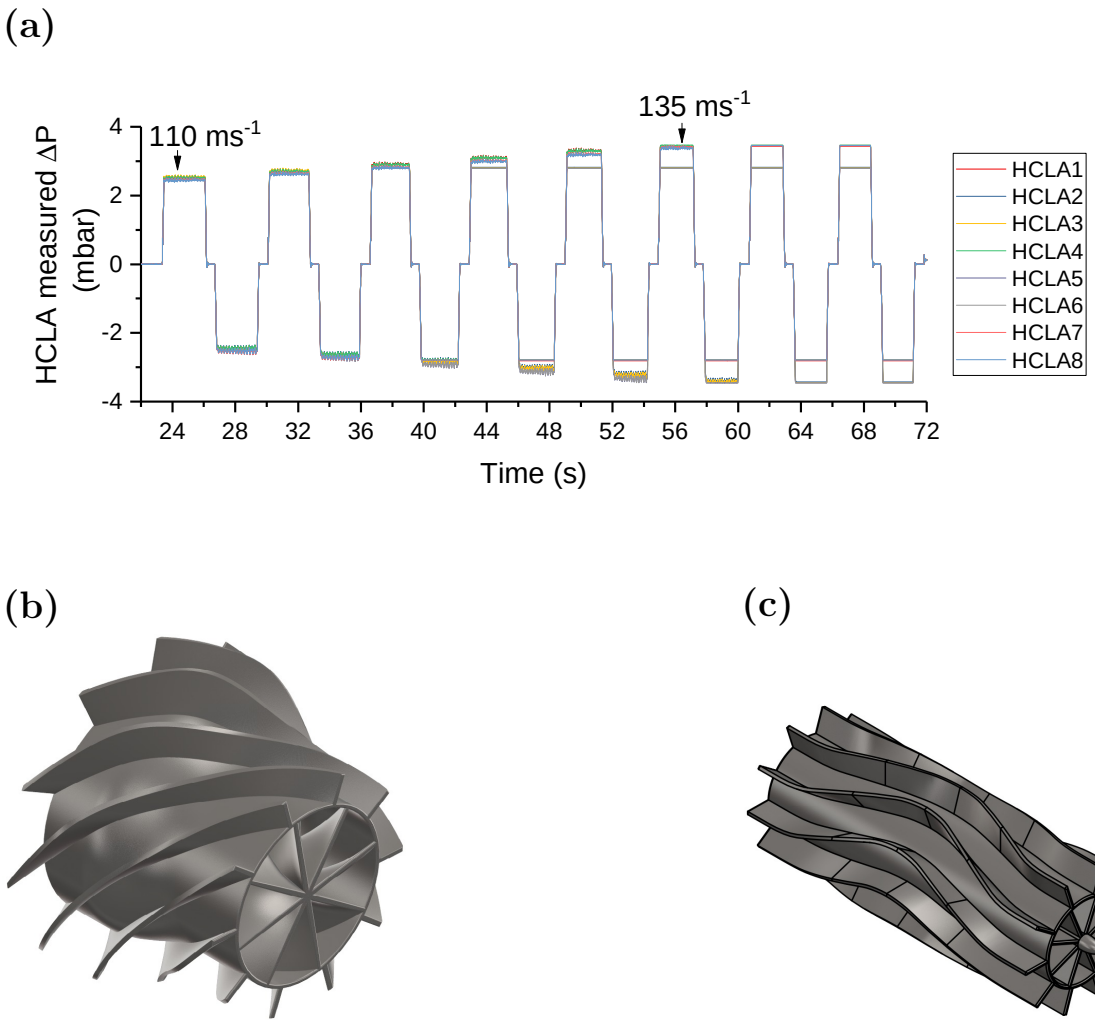


Figure 6.2: (a) Sample data of the initial MFS-P configuration prior to a redesign of the light traps, with wire thickness 65 µm and spacing 140 µm (205 µm pitch). The pump programme instructs the pump to move at constant velocity in one direction then the other, increasing in increments of $5\,\mathrm{ms}^{-1}$ to determine the speed and corresponding flow rate at which individual HCLAs become saturated. As a part of the redesign based on these findings, the light trap design was changed from a miniature version of the conical pitch design for the light traps used in the adult MFS (b) to a variable pitch design (c), reducing the overall resistance of the paediatric MFS.

an acceptable level. This modification did result in a small increase in deadspace but the total deadspace was still below the acceptable limit. The maximum measurable flow rate of this new configuration was found to be ∼120 L/min using a wire mesh with 63 µm wire diameter and 239 µm aperture width (302 µm pitch). The flow sensors were also changed from the HCLAs used in the adult device to SM9336 sensors (TE Connectivity), due to their better resolution, stability and signal to noise ratio. The flow calibration procedure used was the same as described in Section 2.4 for the adult MFS, except with the pump flow program appropriately scaled to reflect the lower maximum flow rate.

Due to the addition of trace gas measurements in MFS-P, the design of the measurement head requires two optical paths for direct laser absorption spectroscopy: one for the CH_4/C_2H_2 measurements (described in further detail in Section 6.3) and one that replicates the CO_2/H_2O channel described previously in the adult device, as well as a comparable optical cavity for the measurement of O_2 concentrations. The same spectroscopic transitions used in the adult MFS (detailed in Section 2.3.1) were used to measure the concentration of O_2 and CO_2 in the paediatric device. For H_2O the transition at 1369 nm was selected over that at 1854 nm due to the lower cost of the appropriate laser. The spectroscopic parameters used were therefore the same as those detailed in Table 2.1 and the procedure used to calibrate the device and the equations used to calculate gas concentrations were the same as those detailed in Section 2.3. However, halving the diameter of the measurement cell did require design changes for both the optical channels to retain measurement sensitivity. For the CO_2 and H_2O measurements, which employ direct laser absorption spectroscopy, the two-pass V-shaped path used in the adult device was doubled to create a four-pass W-shaped path within the cell. The modelling used for designing the multipass mirrors, which includes this W-path, is detailed in Section 6.4. Based on the modelling the expected path length was 64.6 mm. Some deviation from this value would be expected based on the assembly so the exact distance specific to this device was calculated to be 65.436 mm, using the same calibration procedure against reference gravimetrically certified CO_2 gas mixtures detailed in Section 2.3.2 for the adult device. Sample transmission and absorption spectra for CO_2 and H_2O displayed in Figure 6.3 demonstrate excellent fitting with small residuals.

The effects of reducing the length of the optical cavity used to measure O_2 (by a factor of two) had to be addressed during the design process for the MSF-P, in terms of sensitivity and optical stability. The optical cavity mirrors are made of fused silica ($n = 1.452$ at 760 nm), the same material as for the adult device, and are

manufactured by Layertec to the desired specification. The mirror diameter, 12.5 mm, is approximately half that of the adult device.

To compensate for the shortened cavity length, a mirror coating with a specified mirror reflectivity of 99.9% (increased from 99.8% in the adult device) is desirable, and so the closest available coating, with a specified reflectivity of $99.90 \pm 0.02\%$ at a wavelength of 770 nm was selected. Following assembly within the device, the actual apparent reflectivity as determined in the standard calibration of the O_2 channel (section 2.3.3) was found to be 99.843%, corresponding to an effective pathlength enhancement factor within the optical cavity of 637.

When selecting an appropriate radius of curvature for the concave cavity mirrors, it is important to consider the optical stability condition for the cavity (the condition that informs the design about detrimental diffraction losses in the cavity – a situation to be avoided). To this end, two useful dimensionless parameters, known as the g parameters, can be defined for any (linear) optical cavity, thus:

$$g_1 = 1 - \frac{L}{R_1} \text{ and } g_2 = 1 - \frac{L}{R_2} \tag{6.1}$$

with g_1 and g_2 calculated from the respective radii of curvature of the two mirrors, R_1 and R_2, and the optical distance, L, between the reflective surfaces of the cavity mirrors. Stable resonators must satisfy:

$$0 < g_1 g_2 < 1 \tag{6.2}$$

For example, for a calculated optical distance between the reflective surfaces of the mirrors of 31.6 mm, a mirror radius of curvature of 30 mm would only be marginally within the stability criterion, close to being a confocal condition, and is therefore determined not to be sufficiently opto-mechanically robust for this application.

To mitigate against residual mode noise in the cavity, the relative cavity transmission frequencies must be considered. The resonant frequencies for any cavity mode can be specified by the integers l, m, and n, where l and m denote the variation in electric field in the transverse direction while n specifies variation in the longitudinal direction:

$$v_{lmn} = \frac{c}{2L}\left(n + \frac{m + l + 1}{\pi} \arccos\left(\pm\sqrt{g_1 g_2}\right)\right) \tag{6.3}$$

where c is the speed of light. Halving the mirror radius of curvature from 200 mm in the adult device to 100 mm was considered, but leads to a frequency spacing ratio between transverse cavity modes (Δv_{lmn}) to the free spectral range (FSR $= c/2L$) of close to 0.5 and hence introduces coincidences in frequency between high and low

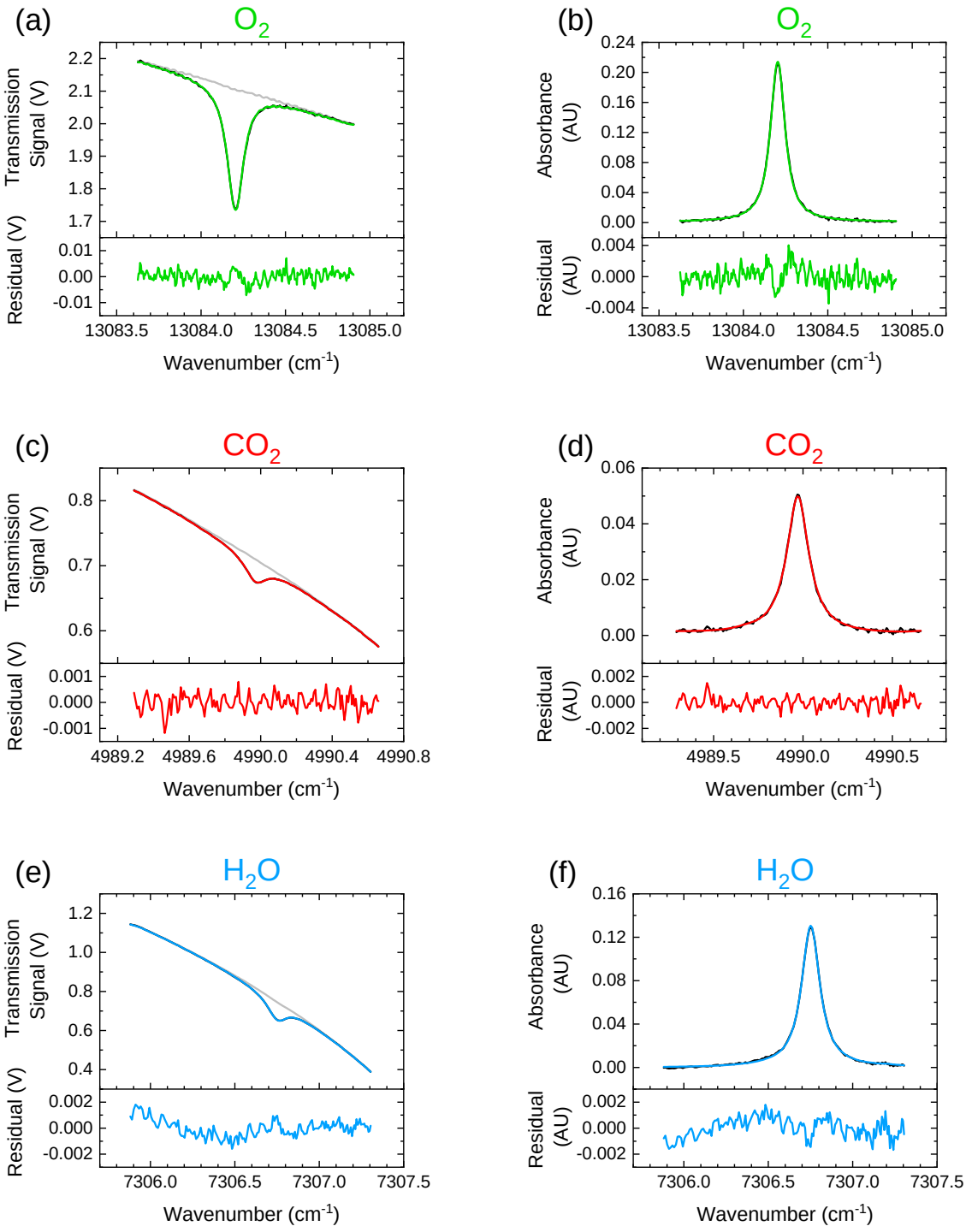


Figure 6.3: Sample transmission and corresponding absorption spectra for (a)-(b) O_2 at a calculated concentration of 5.06×10^{18} molec cm^{-3} (20.93% of dry gas volume), (c)-(d) CO_2 at 1.40×10^{18} molec cm^{-3} (5.83% of dry gas volume) and (e)-(f) H_2O at 2.26×10^{17} molec cm^{-3}. The baselines are shown on the transmission spectra in grey, the raw spectra in black and the best fit Voigt profiles in green/red/blue.

order modes, reinforcing residual mode noise. Therefore, a slightly smaller radius of curvature of 75 mm was selected to be more optimal.

The final design of the optical cavity exhibited excellent transmission characteristics and a sample O_2 transmission spectrum and corresponding absorption spectrum, recorded during a paediatric washout, is displayed in Figure 6.3, demonstrating the excellent fitting and small residuals.

6.3 Methane and Acetylene Trace Gas Detection

The paediatric MFS design incorporates the ability to measure the trace gases CH_4 and C_2H_2 via an additional optical path within the measurement head. The reasons for this are twofold: firstly, the possibility for a shortened washout procedure, and secondly, for improved modelling of the LNL model's circulatory parameters.

CH_4 is recognized as a suitable inert exogenous tracer gas for use in MBW test in the consensus statement by Robinson *et al.*[60], as it does not participate in gas exchange, is fairly insoluble in blood (Bunsen solubility coefficient of 0.0405) and other tissues and is safe at concentrations suitable for MBW testing. Other possible inert gases which fulfil these criteria are N_2 (which is already used in MBW tests using the MFS), Ar, He and SF_6.[60] Argon has previously been used as a tracer gas in MBW experiments with Ar concentrations monitored using rapid-responding mass spectrometers.[83] However, neither Ar nor He would be potential candidates for incorporation into the MFS due to their lack of IR activity. In earlier experiments, mass spectrometry was used to monitor the concentration of the inert trace gas SF_6 during an MBW, but this is not currently favoured due to the high purchase and maintenance costs,[291] so has been supplanted by the commercially available gas analyser Innocor, which employs photoacoustic infrared spectroscopy to monitor the inspiration of 0.2% SF_6. However, the release of SF_6 should be kept to a minimum due to its IR activity resulting in a significant contribution to the greenhouse effect (20 times that of CO_2). Methane is also IR active, but contributes less to the greenhouse effect (4 times that of CO_2), so CH_4 is the clear choice for an inert exogenous trace gas for use in the MFS-P.

In contrast to CH_4, C_2H_2 has a high solubility in blood (Bunsen solubility coefficient 0.889) so would take longer to reach equilibration in the lungs. The relative uptake of the two gases provides additional information for estimating the relative widths of the compliance and conductance distributions (σ_{CL} and σ_{Cd}). Both gases

Molecule	CH_4	CH_4	CH_4	C_2H_2
Wavelength (nm)	1653.72	1653.73	1653.73	1530.37
Wavenumber (cm^{-1})	6046.96	6046.95	6046.94	6534.36
Vibrational band	$0020 \leftarrow 0000$	$0020 \leftarrow 0000$	$0020 \leftarrow 0000$	$101 \leftarrow 000$
Rotational assignment	$4, A_1 \leftarrow 3, A_2$	$4, F_1 \leftarrow 3, F_2$	$4, F_2 \leftarrow 3, F_1$	P(8)
Cross section ($cm^2\,cm^{-1}$)	1.46×10^{-21}	9.28×10^{-22}	7.88×10^{-22}	1.21×10^{-20}
γ_{self} ($cm^{-1}atm^{-1}$)	0.079	0.079	0.079	0.158
γ_{air} ($cm^{-1}atm^{-1}$)	0.058	0.077	0.065	0.082

Table 6.1: Parameters for the additional spectroscopic transitions employed in the paediatric molecular flow sensor. The wavelength is defined as the transition wavelength in a vacuum. Cross section is defined as the integrated collisional cross section at 296 K. The vibrational band originates in the ground vibrational state, with the quanta of energy in the excited state in each vibrational mode given in the form $v_1v_2v_3v_4$. The rotational assignment is reported as J, K, where J is the angular momentum quantum number and K is the symmetry.[122,339]

are safe for humans to breathe at the intended concentrations of 0.2% and 0.6% respectively, a gas composition in air that can be produced and certified for medical use by BOC.

The two lasers used to measure the two trace gases are multiplexed together and follow the second optical path within the multipass cell, which is also used for the measurement of CO_2 and H_2O, as described in the previous section. A 10 mW distributed feedback (DFB) laser (NTT Electronics, NLK1U5EAAA) was used to probe the 3 overlapping R(3) transitions in the first overtone of the vibrational band at 1654 nm corresponding to the v_3 C-H stretch. For the measurement of acetylene a second 10 mW DFB laser (NTT Electronics, NLK1C5EAAA) was used, this time operating at a wavelength of 1530 nm, to probe the P(8) transition within the combination $v_1 + v_3$ band, which comprises the symmetric and asymmetric C-H stretching modes. The CH_4 and C_2H_2 absorption features were selected due to having sufficiently high absorption cross sections and the absence of any nearby overlapping features in the CO_2 and H_2O absorption spectra. The assignments of the four relevant spectroscopic transitions and their respective absorption cross sections and pressure broadening parameters are given in Table 6.1.

The paediatric MFS measurement cell has a bore diameter of 14 mm, compared to 24 mm in the adult devices. To accommodate the smaller diameter of the paediatric device and retain measurement sensitivity, a design that increased the length of the optical paths was necessary. In the case of the multiplexed CO_2 and H_2O channel, the number of passes through the cell needed to be doubled from the 2-pass V-path to a 4-pass W-path. Although the cross section of the 3 overlapping CH_4 transitions is comparable to that of the CO_2 and H_2O lines, the concentration range for the trace gas measurements means that a much greater path length is required and this is provided by a Herriott cell arrangement.

The final design used custom-made nickel mirrors with a gold finish, with a diameter of 7.3 mm and a radius of curvature of 43.78 mm, with custom holes bored to allow insertion of the photodiodes and corresponding detector at the calculated positions for each channel. A 3D CAD visualisation of the two optical paths within the Herriott cell is shown in Figure 6.4 and the modelling used to ensure adequate positioning of the spots in relation to the laser diode and photodetectors is explained in detail in the following section. The successful incorporation of the trace gas channels into the device is illustrated in Figure 6.5 which shows excellent fitting of both the CH_4 and C_2H_2 spectra at the required trace gas concentrations (0.6% and 0.2% respectively).

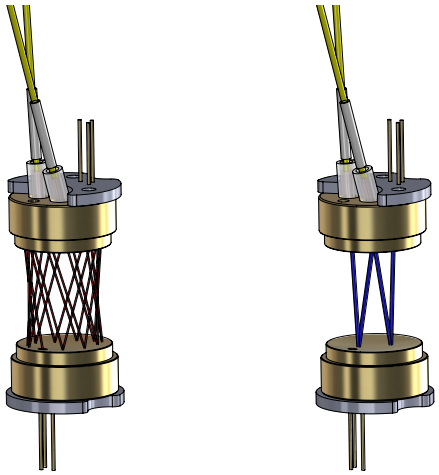


Figure 6.4: Schematic of the Herriott cell design within the paediatric MFS measurement head, showing the 21-pass CH_4/C_2H_2 optical path (left) and the 4-pass CO_2/H_2O optical path (right).

The addition of the trace gases must also be accounted for when calculating the flow rate in the MFS-P. The density, viscosity and Sutherland constants used in the

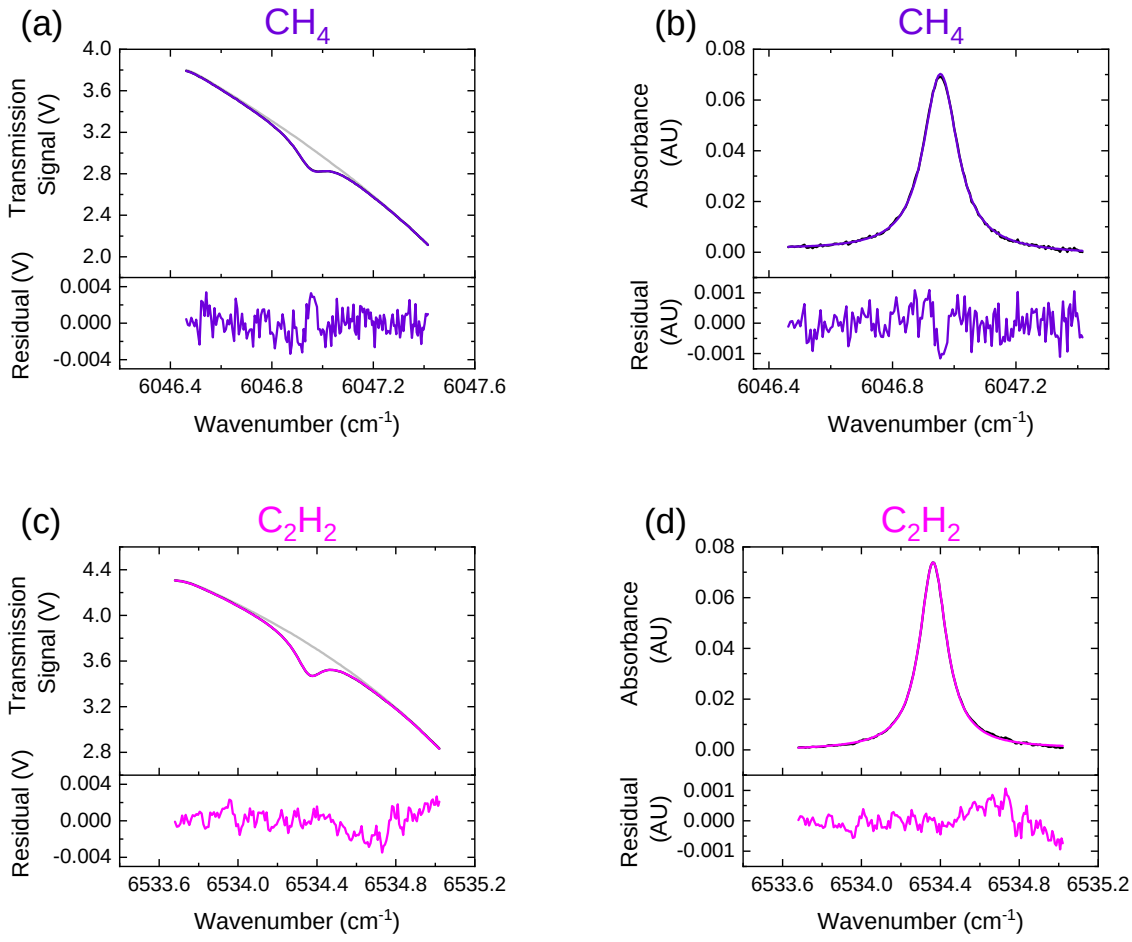


Figure 6.5: Sample transmission and corresponding absorption spectra for (a)-(b) CH_4 at a calculated concentration of 1.46×10^{17} molec cm^{-3} (0.599% of dry gas volume) and (c)-(d) C_2H_2 at 4.96×10^{16} molec cm^{-3} (0.203% of dry gas volume). The q_1 adjusted baselines are shown on the transmission spectra in grey, the raw spectra in black and the best fit Voigt profiles in pink/purple.

Molecule	Density (kg m^{-3})	Viscosity (µPa s)	Sutherland constant (K)
CH_4	0.717	10.25	175.84
C_2H_2	1.17	9.36	285.89

Table 6.2: Literature values for density, viscosity and Sutherland constants, all at 273.15 K and 1 atm for CH_4 and C_2H_2.[126] All other density and viscosity values used are the same as those listed in Table 2.4.

flow calculations for the paediatric flow sensor for O_2, CO_2, H_2O, N_2 and Ar are the same as those in Table 2.4. The corresponding values for CH_4 and C_2H_2 must also be used when determining flow rate and are given in Table 6.2.

6.4 Modelling Optical Paths of the Multipass Cell

As described in the previous section, the smaller bore diameter of the paediatric MFS and the addition of trace gases with their smaller absorption cross sections and lower concentration ranges necessitated a more complex design than the simple V-path used to measure CO_2 and H_2O in the adult device. The addition of optical channels to measure the concentration of CH_4 and C_2H_2 also required a secondary optical path with a longer path length to measure these trace gases at concentrations of less than 0.6% and 0.2% respectively. In order to successfully design the multipass cell with the laser diodes and photodetectors in suitable positions for the final pass to hit the active area of the photodetector, it was necessary to calculate the size and position of the spots for each optical path. In this section the multiplexed CH_4 and C_2H_2 21-pass optical path will henceforth be referred to as Channel 1 and the 4-pass CO_2 and H_2O path as Channel 2.

The ray-tracing used for the initial estimates in this modelling relies on the paraxial approximation, which assumes small reflection angles such that $\theta \approx \sin\theta \approx \tan\theta$. This approximation holds for mirrors with large radii of curvature, but becomes less appropriate when the radius of curvature is comparable to the mirror separation (as is the case for the multipass cell in the paediatric MFS, where the radius of curvature of the mirrors is 43.78 mm and the separation is 14 mm).

The incident ray, $\mathbf{r}$, can be described by its x and y coordinates, r_x and r_y and

the angles of incidence from the z axis in the x and y directions, θ_x and θ_y:

$$\mathbf{r} = \begin{bmatrix} r_x \\ \theta_x \\ r_y \\ \theta_y \end{bmatrix} \tag{6.4}$$

The transformation of this vector by propagation through space or interaction with an optical component can be represented by a ray transfer matrix, $\mathbf{T}$, to produce the ray **r'**:

$$\mathbf{r'} = \mathbf{Tr} \tag{6.5}$$

Propagation by a distance d through free space or through a medium with a constant refractive index, such as traversing the distances between the Herriott cell mirrors, is given by:

$$\mathbf{T}(d) = \begin{bmatrix} 1 & d & 0 & 0 \\ 0 & 1 & 0 & 0 \\ 0 & 0 & 1 & d \\ 0 & 0 & 0 & 1 \end{bmatrix} \tag{6.6}$$

To account for the curvature of the mirrors and hence the difference between the closest and furthest separation of the mirrors at 14 mm and 15.23 mm, the distance travelled, d, was approximated to be 14.61 mm for this model. Reflection off a concave curved surface, with focal lengths f_x and f_y in the x and y directions, can be described by:

$$\mathbf{T}(f) = \begin{bmatrix} 1 & 0 & 0 & 0 \\ \frac{-1}{f_x} & 1 & 0 & 0 \\ 0 & 0 & 1 & 0 \\ 0 & 0 & \frac{-1}{f_y} & 1 \end{bmatrix} \tag{6.7}$$

For a spherical mirror the focal length is half the radius of curvature, and so f_x and f_y were set to 21.89 mm.

The resulting ray following propagation through space then subsequent reflection by a curved mirror can be described by multiplying the two transformation matrices together, according to:

$$\mathbf{T} = \mathbf{T}(f)\ \mathbf{T}(d) \tag{6.8}$$

This resulting transformation matrix describes a single pass through the measurement cell. In order to model the entire optical path, this can be extended to the result of n passes through the cell:

$$\mathbf{T}^n = (\mathbf{T}(f)\ \mathbf{T}(d))^n \tag{6.9}$$

where $n = 21$ for Channel 1 and $n = 4$ for Channel 2. For the n^{th} spot the position and angle of any reflected light is given by $\mathbf{T}^n\mathbf{r}$ and this was used to obtain an initial estimate of spot position. The elements of the matrix $\mathbf{T}^n$ can also be used to estimate the spot diameter, where A, B, C and D in the following equations correspond to the matrix elements t_{11}, t_{12}, t_{21} and t_{22} respectively. As the multipass mirrors used in this application are spherical, this is equivalent to using the matrix elements t_{33}, t_{34}, t_{43} and t_{44}.

The initial beam width, w, as the lasers enter the multipass cell was estimated to be 0.6 mm, based on the laser diode aperture. The complex beam parameter, q, which describes the evolution of a Gaussian beam as it propagates along the z axis, is related to the beam width according to:

$$\frac{1}{q} = \frac{1}{R_w} - \frac{i\lambda}{\pi\omega^2} \tag{6.10}$$

where λ is the wavelength of light and R_w is the wave's radius of curvature.[340] If the beam enters the system with a complex beam parameter q_0, transformation by a given ABCD matrix, such as propagation through the cell (Equation 6.6) or reflection by one of the cell mirrors (Equation 6.7) will result in a change in q given by:

$$q = \frac{Aq_0 + B}{Cq_0 + D} \tag{6.11}$$

The new beam width can therefore be determined through considering the imaginary part of Equation 6.10 according to:

$$w = \sqrt{\frac{\lambda}{-\pi\ \mathrm{Im}(q^{-1})}} \tag{6.12}$$

and hence an estimate of the spot size can be estimated for each reflection through the cell. These calculations were used to predict the spot sizes displayed in Figure 6.6 (a). Based on this calculation, the proposed design was deemed suitable, as the predicted beam width across all passes was below the upper acceptable limit determined by the 1 mm active area of the photodetectors.

Although there is some tolerance in terms of errors in spot size, the inaccuracies introduced by the paraxial approximation breaking down (due to the mirror separation being only 5 times greater than the mirror radius of curvature) meant that a more accurate model was required to determine spot position. Hence a vector model written in MATLAB was used to estimate the position of each reflection and crucially the final reflection onto the photodetector. This geometric model considered the incident ray as a vector beginning at the point of the laser diode and passing through the

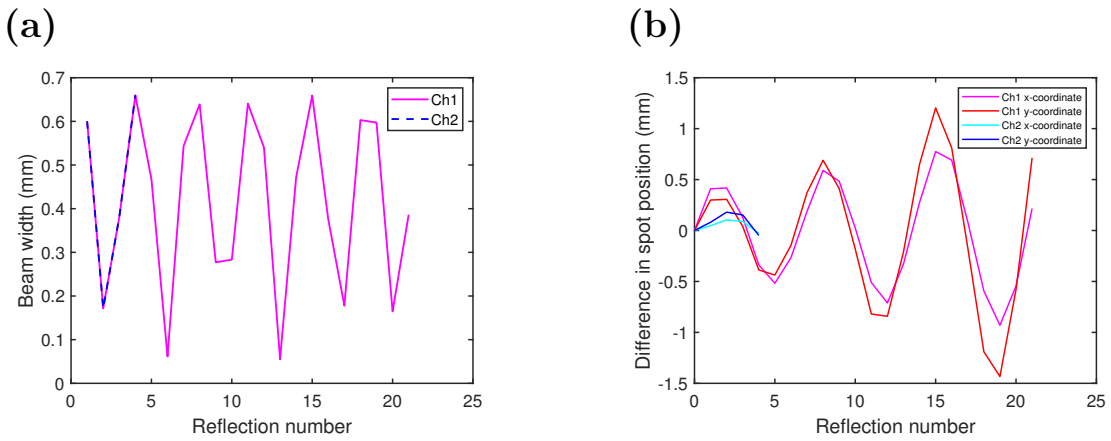


Figure 6.6: (a) The calculated spot size for each reflection for all reflections of the 21-pass CH_4 and C_2H_2 channel (Ch1) and the 4-pass CO_2 and H_2O channel (Ch2) and (b) comparison between the calculated spot position using the ray transfer matrix and vector methods.

cell to strike the opposite mirror surface, constructed in MATLAB using the equation of a sphere of radius equal to the radius of curvature of the cavity mirrors. The angle of reflection was then calculated using the normal to the calculated tangent of the curved mirror surface at the point of reflection. This was repeated until the beam hit coordinates within the photosensitive region of the detector on the final pass. The inadequacy of the ray transfer matrix estimate in predicting the position of each spot is demonstrated in Figure 6.6 (b), which shows the difference in the x and y coordinates of each spot position as calculated by the vector and ray transfer models. In the case of the 4-pass channel the difference between the final spot position calculated by the two models is negligible, but for the 21-pass system, the error of 0.71 mm in the ray transfer matrix estimate would result in little overlap with the detector and hence an unstable measurement.

The position of the spots for both the CO_2/H_2O and CH_4/C_2H_2 optical paths is shown in Figure 6.7, with the positions calculated according to the vector calculations and the spot sizes as calculated using ray transfer matrix analysis. The modelling was successful as no further modification was needed when the multipass cell was assembled inside the measurement head. A 3D diagram showing the optical paths between the multipass mirrors is shown in Figure 6.4. Suitable modelling of the position of the final spot facilitated the acquisition of the trace gas spectra shown in Figure 6.5 and sufficiently sensitive concentration measurements.

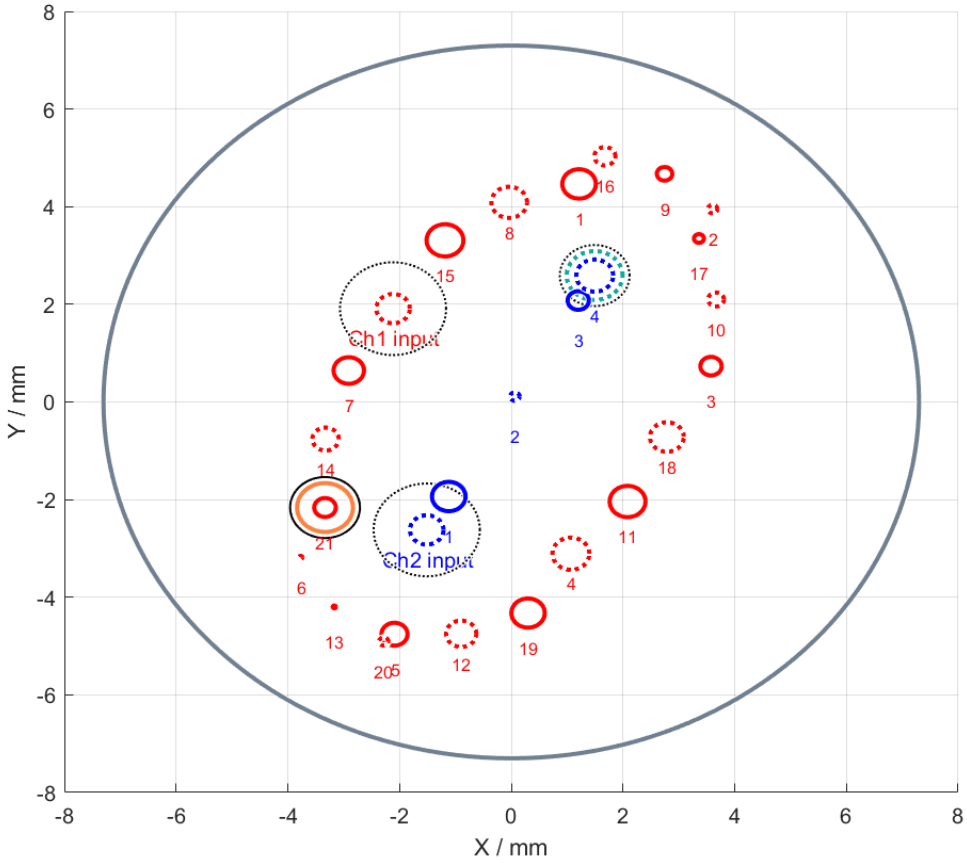


Figure 6.7: Calculated spot positions for the Herriott cell design for the CO_2, H_2O, CH_4 and C_2H_2 measurements using a vector model. The black circle shows the diameter of the pair of gold plated mirrors. The CH_4 and C_2H_2 channel (Ch1) is shown in red and the multiplexed CO_2 and H_2O channel (Ch2) is shown in blue. All positions corresponding to the upper mirror are represented by a dashed line and all lower mirror positions are indicated by a solid line. The numbers below each spot correspond to the reflection number for that channel. Spot size is calculated using the paraxial approximation and ray tracing matrices. The photodiode inputs are indicated: the black circles show the dimension of the bore hole and the inner red/blue circles represent the beam width when the beam enters the cell. The photodetector receive hole diameter is shown in black for both outputs and the orange/green circles represent the active area of the photodetector.

6.5 Sample Patient Data

The paediatric molecular flow sensor is currently being used at the Royal Brompton Hospital in the first trial in children, where the device is used to perform a washin/washout protocol followed by subsequent data analysis using the LNL model.

Paediatric CF patients are being recruited by the research group of Professor Jane Davies with ethical approval from HSC REC B (REC reference 17/NI/0046). To illustrate the successful use of the technique in the clinic, a sample data set is shown in this section, taken from a 17 year old CF patient with well-controlled CF. The patient performed two tests with a break between tests and the device was well-tolerated.

The experimental protocol for this study involves the patients breathing through the MFS-P for approximately 12 minutes while wearing a nose clip, with unrestricted tidal breathing. The one exception to this is at the end of the test where they are asked to perform a large inhalation then exhalation before returning to tidal breathing in order to assess gas trapping. This section of the test was not used in the modelling of the washouts by the LNL model. The measured dry gas fractions for one of the tests are displayed in Figure 6.8. Following a period of acclimating to the seated

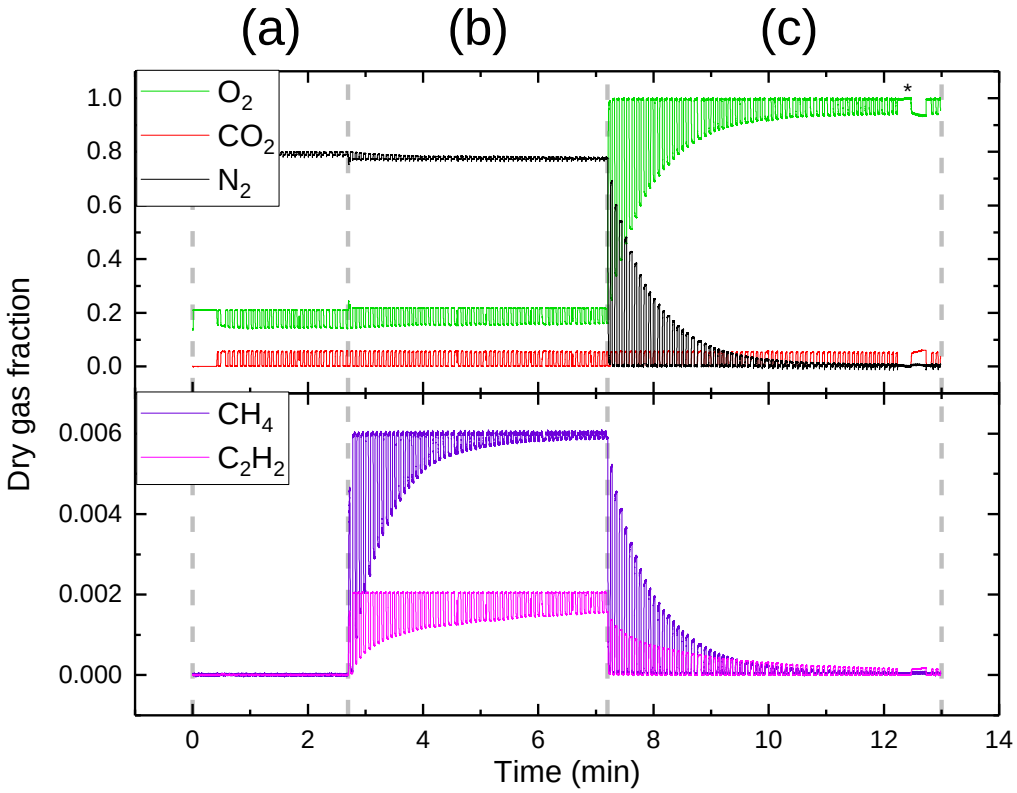


Figure 6.8: Sample dataset from a 17 year old CF patient, showing the dry gas fraction of the respiratory gases during the three phases of the experiment where the inspired gases were: (a) air, (b) air with 0.6% CH_4 and 0.2% C_2H_2 by volume and (c) medical grade O_2 with $> 99.5\%$ purity. At the end of phase (c) the gas trapping test portion of the experiment can clearly be seen by the large cumulative volume change in the O_2 plot during the maximal inhalation followed by maximal exhalation, denoted by $\star$.

position to attain a steady state, the patient puts on the nose clip and begins the test with breathing air with no trace gases 30 s into the recorded data allowing for the zeroing of the HCLAs used in the flow sensing system. After 2 minutes of air breathing the patient is switched to breathing air containing 0.6% CH_4 and 0.2% C_2H_2 by volume and the washin of these trace gases continues for 5 minutes. At this point the patient is switched to breathing medical grade O_2 and the simultaneous washout of N_2 and the trace gases CH_4 and C_2H_2 commences.

The corresponding cumulative volume plots for this dataset is shown in Figure 6.9. An excellent near zero N_2 balance of 1.5 ml min^{-1} was measured during the air breathing, indicating a well-calibrated device and a good seal around the patient's nose and mouthpiece precluding any leaks. The N_2 plot also shows that an asymptote was reached by the end of the washout period, as is required for reliable LNL model

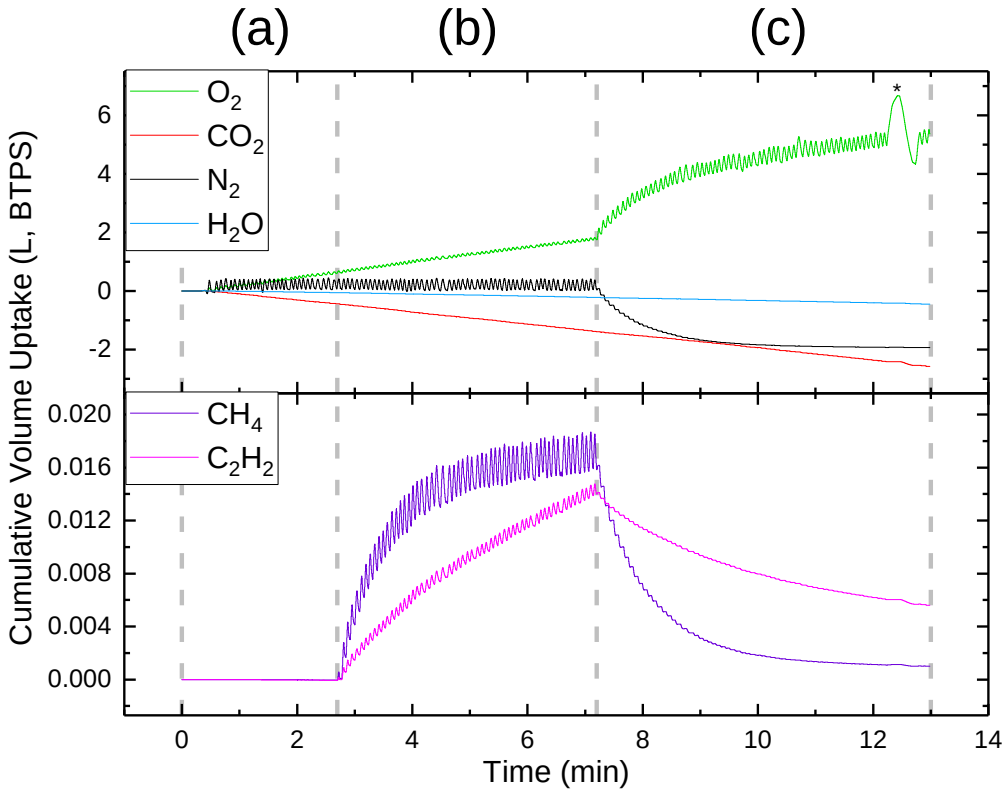


Figure 6.9: Sample dataset from a 17 year old CF patient, showing the cumulative volume uptake of the respiratory gases during the three phases of the experiment where the inspired gases were: (a) air, (b) air with 0.6% CH_4 and 0.2% C_2H_2 by volume and (c) medical grade O_2 with $> 99.5\%$ purity. At the end of phase (c) the gas trapping test portion of the experiment can clearly be seen by the large cumulative volume change in the O_2 plot during the maximal inhalation followed by maximal exhalation, denoted by $\star$.

analysis.

During the trace gas washin phase it is clear that the cumulative volume uptake of CH_4 rose more rapidly than C_2H_2 at the start of the washin, as a result of the higher inspired fraction of CH_4, before plateauing towards the end of the washin. However, the cumulative volume uptake of C_2H_2 continued to rise with a near constant rate of consumption of 2.2 mL min^{-1}. This can be explained by the higher solubility of the C_2H_2 in blood. The Bunsen solubility coefficient in blood, given as the volume of gas absorbed per unit volume of blood at 1 atm and 37 °C, is 0.889 for C_2H_2 compared to 0.0405 for CH_4.[341] Therefore after 5 minutes a patient's blood is not near saturation so their consumption of C_2H_2 has not plateaued. During the washout phase, CH_4 was observed to washout more slowly than N_2 and does not completely washout during this time period. Again this can be explained by the difference in gas solubility in blood, as N_2 has the lowest of all the gases used in this test, with a Bunsen solubility coefficient in blood of 0.012.[342]

To analyse the data using the LNL model, the test is split into two phases: the air breathing phase and the washin/washout phase. During the air breathing period (shown as (a) and (b) on the Figures 6.8 and 6.9) the model applies non-linear least squares regression to best fit the expiratory gas flow for O_2, CO_2 and N_2. The experimental protocol in this study offers three ways of analysing the washin/washout phase:

1. N_2 washout: as with the standard adult protocol described in Chapters 4 and 5, the expiratory N_2 flow is fit during the O_2 breathing phase (c).

2. CH_4 washout: the expiratory CH_4 flow is fit during the O_2 breathing phase (c).

3. CH_4 washin: the expiratory CH_4 flow is fit during the trace gas breathing phase (b).

This third method benefits from the fact that the two analysis periods occur simultaneously, so offers the possibility of shortening the protocol in the future by removing the O_2 breathing phase.

For each of these three methods, the fitting was repeated four times and the parameter set with the lowest total residual was selected. This was repeated for the patient's second dataset and the calculated mean and standard deviation is shown for each parameter and method in Table 6.3. This patient was described as having well-managed CF and this appears to be borne out by the LNL model parameters, in contrast to even the CF patients with preserved FEV_1 described in Chapter 5. The

Parameter	N_2 washout	CH_4 washout	CH_4 washin
V_D	0.089 ± 0.014	0.093 ± 0.008	0.085 ± 0.004
V_A	2.83 ± 0.09	2.75 ± 0.08	2.71 ± 0.09
FRC	2.92 ± 0.11	2.84 ± 0.08	2.80 ± 0.09
FRC (% pred.)	105 ± 4	102 ± 3	101 ± 4
V_D/FRC	0.030 ± 0.003	0.032 ± 0.002	$0.030 \pm < .001$
σ_{VD}	$0.26 \pm < .01$	0.23 ± 0.02	0.18 ± 0.01
σ_{CL}	0.33 ± 0.02	0.34 ± 0.01	0.42 ± 0.01
σ_{Cd}	0.63 ± 0.02	0.64 ± 0.01	0.72 ± 0.01

Table 6.3: Parameters determined from two experiments performed on MFS-P by a 17 year old CF patient using three different methods of analysis. All values are presented as mean ± 1S.D..

patient's FRC is slightly above the predicted value for their age and height and the low measured V_D/FRC would be toward the lower end of the range of healthy adult controls studied in Chapter 5. This patient's σ_{CL} value is similarly low compared to the adult CF patients. However, the recruitment of paediatric controls for direct comparison would be necessary in order to more accurately assess this patient's LNL parameters. Good intra-method repeatability was demonstrated for all the parameters across the three methods for this patient. The agreement between methods is reasonably good, particularly between the two washout methods. The alveolar volume determined using the two CH_4 methods was higher than for the N_2 washout analysis and particularly in the case of the CH_4 washin. This may in part be due to the previously noted incomplete washin/out of CH_4 due to its greater blood solubility compared to N_2. The effect of incomplete washin/out could be investigated in the future by introducing a longer washin phase then repeating the LNL model analysis while varying the time period over which the washin phase is fit. It is also possible that this difference arises due to the model incorrectly accounting for the transfer of CH_4 between the blood and body stores, so in the future more work may need to be done to develop the CH_4 body stores model. As may be expected for a young patient

with well-managed CF, gas trapping observed from the large breaths at the end of the protocol was considered to be non-significant for this individual.

Although this device is still in the very early stages of usage in the clinic, it is extremely promising that the device is well tolerated in children and is operating in a clinical setting with an excellent N_2 balance during the air breathing phase with good intra-subject repeatability for the determined LNL model parameters. The future potential for a shorter protocol is highlighted by the ability to determine parameters using just the 2 minutes of air breathing followed by 5 minutes of trace gas in air, which would be highly desirable to allow use for younger or less compliant patients who cannot tolerate longer experimental protocols.

6.6 Conclusions and Future Work

This chapter has detailed the development and initial implementation in a clinical setting of a new clinical tool: the paediatric MFS. This offers the possibility of investigating the utility of LNL model analysis in the paediatric population for the first time. As shown by the sample patient data, the addition of a new optical channel to measure trace levels of CH_4 and C_2H_2 also introduces the capability to estimate LNL model parameters in three different ways: the N_2 washout used in the adult device, the washin of CH_4 and the subsequent washout of CH_4. Due to its high solubility in the blood, C_2H_2 does not reach an asymptotic cumulative uptake within a feasible time period to use this as a washin or washout gas alone, but its greater solubility will provide additional information to improve the blood modelling and hence improve the estimate of the inhomogeneity parameter σ_{Cd}.

The development of the paediatric molecular flow sensor introduces the potential for new avenues of research and applications of this technology. The ongoing clinical trial of the device in the paediatric CF population at the Royal Brompton Hospital will provide the first opportunity to compare the lognormal lung parameters of children with CF with those of the non-CF population. There are multiple research questions to be explored within this study. The first and most obvious one is the analogue of the comparisons made between adult CF patients with preserved FEV_1 and non-CF controls in Chapter 5. In the adult population σ_{CL} was elevated in CF patients, so it must be determined whether this observation is also seen in paediatric patients. Although the one patient shown in the previous section appeared to have LNL parameters within a normal range, on a population level elevated LNL model parameters may seem likely, as in adults there was correlation between σ_{CL}

and LCI values, and the finding of an elevated LCI value in paediatric CF patients is well-documented.[343,344]

Studying patients at the same time as they undergo a CT scan will also form part of this study. This will address a major limitation of the investigation of the relationship between imaging and LNL model parameters in the adult CF studies detailed in Chapter 5, where it was not possible to obtain the imaging assessment at the same point in time as the MFS washout, introducing uncertainty about whether their imaging still provided an accurate assessment of structural abnormalities at the time of performing their washout tests.

The novel ability to obtain multiple estimates for each LNL model parameter from the same patient dataset due to the incorporation of trace gas measurements into the MFS-P design offers the opportunity to explore discrepancies between the three estimates and further improve the modelling of the trace gases. The single dataset shown in Section 6.5 is too small a sample size to draw conclusions about the level of agreement between the three analyses, but it is promising that there is good agreement between the N_2 and CH_4 washout parameters. If borne out amongst a larger study group, the observed discrepancy between the two sets of washout values and the CH_4 washin parameter values would merit further investigation. This may involve performing a series of washouts with a longer washin/washout phase then analysing each dataset with the LNL model multiple times, truncating the data at different points to investigate the effect of an incomplete washout on the determined parameters.

In later studies using the device, changes to LNL model parameters in response to different clinical interventions may also be studied. The proposed investigations in the adult CF population involving response to physiotherapy and antiobiotics could also be extended to the paediatric age range as a result of the development of MFS-P.

This technology may also have useful clinical applications beyond the paediatric CF population. For example, performing a N_2 washout using the adult MFS and subsequent LNL model analysis showed promise in adult asthma patients, finding that asthma patients had a higher σ_{CL} than healthy controls and a decrease in the σ_{CL} value following the delivery of the bronchodilator salbutamol.[200] Due to the lack of sensitivity of spirometry to small airways disease, it has been suggested that MBW testing alongside the standard spirometry tests may provide clinicians with useful information about disease activity in children.[337] However, elevated LCI values have only been found in paediatric patients with mild-severe asthma, with most patients still falling within the range for healthy non-asthmatic children.[337,345] The study of

adult CF patients in Chapter 5 found correlation between the LCI and the LNL model parameters V_D/FRC and σ_{CL}, so it would be interesting to explore whether either of these parameters could better distinguish asthma patients from controls.

A second potential application of this new technology could be in investigating air pollution related respiratory symptoms in children. Amongst adolescents, proximity of a motorway to their home is associated with a substantial reduction in lung function determined by spirometry.[346] In younger children no correlation was found between exposure to increased traffic pollution near the home and lung function measured by spirometry, LCI and plethysmography.[347] It would be interesting to investigate which, if any, LNL model parameters would be affected by air pollution in children across a range of ages.

In conclusion, the development of the paediatric MFS constitutes an exciting technological advance which provides intriguing opportunities to expand the application of molecular flow sensing and hence LNL model analysis to younger patient groups. In diseases such as cystic fibrosis which involve monitoring and intervention throughout childhood, this could potentially provide a more sensitive assessment of pulmonary function in the form of a technique that is easy and safe to perform with paediatric patients, as it requires no forced manoeuvres or prescribed breathing patterns and involves no ionising radiation.

Chapter 7

Conclusions and Future Work

The work presented in this thesis provides tantalising evidence for the potential utility of the molecular flow sensor (MFS) across a range of clinical applications. The study presented in Chapter 3 demonstrates that the instrument can safely be used in a critical care setting and provide reliable measurements over an extended period of several hours without recalibration. As noted previously, the scale of this study was greatly reduced as a direct result of the COVID-19 pandemic, but the early data collected from the two patients recruited prior to the implementation of COVID-19 restrictions make a compelling case for the importance of future work in this area. Using the MFS to provide stable and accurate monitoring of $\dot{V}_{O_2}$ across a range of F_{I,O_2} may provide valuable information on the success of a clinical intervention for patients experiencing shock, potentially allowing clinicians to maximise improvements to $\dot{V}_{O_2}$, while avoiding unnecessary side effects from over-treatment in the future. Interesting responses were observed as a result of a patient being administered the drugs metaraminol and noradrenaline, as well as changes in gas exchange rates following a change in ventilator settings. Certainly further work would be needed to see if similar effects were observed across multiple patients. A future interventional study could offer the opportunity to study the lung function of patients in ICU through their breathing 100% O_2 for around 5 min and hence performing a N_2 MBW. As demonstrated with an interrupted washout in one of the patients already studied, this could be used to estimate the end-expiratory lung volume (EELV). Indeed, this may be a method by which the effectiveness of recruitment manoeuvres may be assessed. In combination with the lognormal lung (LNL) model described in Chapter 4, this could be extended to provide a more thorough assessment including measuring deadspace volume and lung inhomogeneity. In the case of patients with acute lung injury/acute respiratory distress syndrome (ALI/ARDS) with significantly reduced end expiratory lung volume (commonly referred to as the 'baby lung'), it is extremely challenging

to tailor ventilator settings to an individual's needs so as to minimise the risk of ventilator-induced lung injury (VILI), as basing tidal volume on a patient's weight alone has been insufficient.[348] Both EELV measured by a N_2 MBW and other parameters such as σ_{CL} and changes in these parameters due to clinical interventions may eventually be used to guide the treatment plan for a given patient so as to maximise the recruitment of atelectatic lung tissue, while minimising the risk of VILI.

Chapter 4 presents two initial studies of lung inhomogeneity. The LNL model analysis was compared for the first time with MIGET, the accepted premier method for assessing lung inhomogeneity and a valuable research tool, despite its impracticality in a clinical setting. Although the LNL model does not aim to reproduce the parameters obtained from MIGET, the parameters LogSD$\dot{Q}$ and LogSD$\dot{V}$ were able to be estimated as secondary parameters after the fitting procedure. Notably, excellent agreement was shown between these values and the MIGET measured LogSD$\dot{Q}$ and LogSD$\dot{V}$ for the single patient with a unimodal $\dot{V}/\dot{Q}$ distribution. Poorer agreement was shown in the other subjects, which is perhaps to be expected for patients with more advanced lung disease for whom the LNL model is a less appropriate descriptor of their lungs. In particular, the underlying assumption of the LNL model that both the compliance and conductance distributions are unimodal may not apply to the advanced stages of lung disease. In this first study involving international collaboration, the MFS was safely transported to the USA and performed well in this new location, opening up the possibility of future global collaborations. For example, should the opportunity arise to compare MIGET distributions and LNL model parameters in healthy controls or patients with early stage lung disease, this could be explored further.

In the study of young smokers with no symptoms of respiratory disease, the LNL model parameter σ_{CL} successfully identified all smokers with a pack year history exceeding 5 pack years as being outside of the healthy control range. Similarly, the parameter was found to be significantly predicted by pack year history in this group, even when the group was restricted to those with less than 10 pack years. This illustrates one of the potential strengths of the technique: the ability to identify abnormalities at an individual level, even when spirometry values remain within the normal range. However, the question as to the nature of the abnormalities identified is still unclear. The increase in the inhomogeneity of lung compliance may result from short term inflammation or it could arise primarily from long term structural changes to the lung. To this end, a future study of young smokers before smoking cessation and at multiple time points after is the most pressing future work to be undertaken in

this area. With the significant rise in the prevalence of vaping, particularly amongst young people, the comparison between the lungs of vapers with both healthy controls and smokers is also an important avenue for future research as the medical community seeks to quantify the potential risks of vaping to future lung health.

The use of the MFS in combination with the LNL model also showed great promise in the two studies involving CF patients. In particular, the ability of the parameter σ_{CL} to differentiate between healthy controls and CF patients whose FEV_1 values lie within the normal range may have important implications for monitoring patients in the early stages of the disease. The comparison between the LNL parameters and the lung clearance index, LCI, found that both σ_{CL} and V_D/FRC, measures of compliance and deadspace respectively, correlated with LCI values, challenging the idea that the LCI primarily measures the degree of inhomogeneity in the lung. A key advance in lung inhomogeneity testing of CF patients is the possibility to obtain measurements from the paediatric cohort and this is achieved with the development of a miniaturised paediatric version of the device, MFS-P. By adding the ability to measure the concentration of CH_4 and C_2H_2 in this device, MFS-P introduces intriguing possibilities in terms of shortening the washout protocol, improving the reliability of the LNL circulatory parameters, and informing the further development of the blood modelling within the LNL model. As noted previously, future studies involving both adult and paediatric devices should focus on recruiting more patients with preserved lung function, investigating the relationship between LNL parameters and assessment via CT scan, and studying the changes in LNL parameters as a result of interventions, such as physiotherapy, a course of antibiotics or changes in drug regimens.

The observed changes in LNL model parameters in response to interventions in a small number of individuals in this thesis offers a glimpse of the wider potential of the device in clinical practice in identifying changes to an individual's lung physiology. In the case of smokers studied before and after smoking cessation, any reduction in inhomogeneity assessed by the LNL model may quantify the degree to which any lung damage caused by smoking has been reversed. Further longitudinal studies may even allow clinicians to predict the likelihood of further pulmonary problems based on both acute and long-lasting changes, allowing better targeting of resources to monitor individuals at greater long-term risk of COPD. In the case of patients undergoing physiotherapy, it can be difficult to assess the success of a treatment session, as this can be highly subjective and relies on a patient's ability to self-report. An objective metric which is sensitive to acute changes may be useful in evaluating

a management strategy for a particular patient or in cross-sectional studies into the effect of physiotherapy across the CF population.

If, for example, a change in one of the LNL model parameters were also found to correlate well with favourable long-term patient outcomes, this may be a promising candidate as an endpoint in clinical trials. If a parameter were also more sensitive to small but clinically significant changes in lung physiology than current endpoints, this could reduce the number of volunteers required to detect a significant effect from a new drug in clinical trials.

Beyond the scope of the patient groups studied in this thesis, there exists a wide range of other potential clinical applications for this technique. For example in the case of patients with asthma, Smith *et al.* found that some patients with normal spirometry were found to have σ_{CL} values exceeding the normal range.[219] Interestingly, in this study a patient's σ_{CL} but not FEV_1 was found to significantly predict whether a clinician would escalate therapy on the basis of the asthma being judged poorly controlled. This again highlights the potential value of a new objective metric in the management of respiratory disease. The development of the paediatric MFS offers the chance to extend this to children with asthma, a patient group in which an objective metric may be even more desirable, as self-reporting of symptoms may be less reliable.

The technique may also have potential in understanding the effect of new and emerging respiratory diseases in the future. Magor-Elliott *et al.* observed elevated inhomogeneity parameters in patients following infection with COVID-19.[349] The progression of the LNL parameters in individuals may show the ability of the lung to recover from damage caused by the disease and, as hypothesised for smokers, it may be possible to predict the probability of future complications.

A currently unstudied patient population who may eventually benefit from this technique is pregnant and post-partum women, who are at increased risk of pulmonary embolism. At present, excluding a diagnosis of pulmonary embolism relies on computerised tomography pulmonary angiograms, which involve ionizing radiation and have an associated increased lifetime breast cancer risk to the mother.[350] If LNL model parameters within a normal range were found to indicate the absence of a pulmonary embolism, this could potentially form part of clinical decision making to exclude these individuals from further testing to reduce unnecessary exposure. More generally, the LNL model parameters may offer interesting insights into changes in lung physiology in pregnancy, even in the absence of pathology, and the effect of

pregnancy on the parameters would have to be well understood before further clinical studies in this group.

There may also be exciting applications for the device in studying the healthy population. For example, the MFS may be a useful tool to accurately assess how $\dot{V}_{O_2}$ in healthy individuals changes with altitude and in studies of hypoxia. Analysing a N_2 washout may also offer interesting insight into changes in the healthy lung in response to increased altitude, as well as potentially providing an interesting insight into adaptations in pulmonary physiology amongst groups who live at high altitude.

At present, any interpretation of the model parameters requires an understanding of the normal range of values for each parameter. However, as work to better define the normal range of model values within the healthy population progresses, the ability of the model to output parameters as a Z-score in addition to the absolute values may make this a more attractive technique for wider clinical practice,[240] as less knowledge of the physiology underpinning the model would be required to interpret an individual's LNL model parameter set.

The work in this thesis has concentrated on the further development of the adult MFS and the design of a new paediatric device, as well as exploring its potential use within a few clinical settings. The possible clinical applications of the device in paediatric and adult populations are manifold and it is hoped that the novel measures offered by the device can help to inform clinical decision making and improve patient outcomes across a range of settings in the future.

References

[1] Life sciences vision. Technical report. https://www.gov.uk/government/publications/life-sciences-vision, date accessed 2023-08-08.

[2] Out in the cold: lung disease, the hidden driver of NHS winter pressure. Technical report. https://www.asthmaandlung.org.uk/out-cold-lung-disease-hidden-driver-nhs-winter-pressure, date accessed 2023-08-09.

[3] Ian Hall, Samantha Walker, and Stephen T Holgate. Respiratory research in the UK: investing for the next 10 years. *Thorax*, 77(9):851–853, September 2022.

[4] Prescribing Costs in Hospitals and the Community - England 2021/22 | NHSBSA. https://www.nhsbsa.nhs.uk/statistical-collections/prescribing-costs-hospitals-and-community-england/prescribing-costs-hospitals-and-community-england-202122, date accessed 2023-08-09.

[5] Luca Ciaffoni, David P. O'Neill, John H. Couper, Grant A. D. Ritchie, Gus Hancock, and Peter A. Robbins. In-airway molecular flow sensing: A new technology for continuous, noninvasive monitoring of oxygen consumption in critical care. *Science Advances*, 2(8), 2016.

[6] NICE. Sepsis: the recognition, diagnosis and early management (NG51) Putting NICE guidance into practice. Technical report, National Insititute for Health and Care Excellence, 2016. https://www.nice.org.uk/guidance/ng51, date accessed 2023-10-04.

[7] Sharon R. Rosenberg and Ravi Kalhan. Recent advances in the management of chronic obstructive pulmonary disease. *F1000Research*, 6, 2017.

[8] J. A. Dodge, P. A. Lewis, M. Stanton, and J. Wilsher. Cystic fibrosis mortality and survival in the UK: 1947-2003. *European Respiratory Journal*, 29(3):522–526, March 2007.

[9] Pamela B. Davis. Cystic fibrosis since 1938. *American Journal of Respiratory and Critical Care Medicine*, 173(5):475–482, March 2006.

[10] I. M. Balfour-Lynn and J. A. King. CFTR modulator therapies – Effect on life expectancy in people with cystic fibrosis. *Paediatric Respiratory Reviews*, 2020.

[11] William McNulty and Omar S. Usmani. Techniques of assessing small airways dysfunction. *European Clinical Respiratory Journal*, 1(1):25898, January 2014.

[12] Created with BioRender.com.

[13] Nakisa Kia'i and Tushar Bajaj. *Histology, Respiratory Epithelium*. StatPearls Publishing, July 2019. `http://www.ncbi.nlm.nih.gov/pubmed/31082105`, date accessed 2021-01-09.

[14] Smita Pakhale, Zoheir Bshouty, and Theodore K. Marras. La comparaison des prévisions en pourcentage et des valeurs percentiles pour interpréter l'exploration fonctionnelle respiratoire. *Canadian Respiratory Journal*, 16(6):189–193, 2009.

[15] D. E. O'Donnell and P. Laveneziana. Physiology and consequences of lung hyperinflation in COPD. *European Respiratory Review*, 15(100):61–67, December 2006.

[16] Nina Saxena. Restrictive lung disease. In *The Perioperative Medicine Consult Handbook*, pages 199–202. Springer International Publishing, January 2015.

[17] Tae Rim Shin, Yeon Mok Oh, Joo Hun Park, Keu Sung Lee, Sunghee Oh, Dae Ryoung Kang, Seungsoo Sheen, Joon Beom Seo, Kwang Ha Yoo, Ji Hyun Lee, Tae Hyung Kim, Seong Yong Lim, Ho Il Yoon, Chin Kook Rhee, Kang Hyeon Choe, Jae Seung Lee, and Sang Do Lee. The prognostic value of residual volume/total lung capacity in patients with chronic obstructive pulmonary disease. *Journal of Korean Medical Science*, 30(10):1459–1465, 2015.

[18] Michael Quinn and Alessandra Rizzo. *Anatomy, Anatomic Dead Space*. StatPearls Publishing, October 2019.

[19] Sal Intagliata and Alessandra Rizzo. *Physiology, Lung Dead Space*. StatPearls Publishing, September 2018.

[20] Amir Sharafkhaneh, Nicola A. Hanania, and Victor Kim. Pathogenesis of emphysema: From the bench to the bedside. *Proceedings of the American Thoracic Society*, 5(4):475–477, May 2008.

[21] Johan Petersson and Robb W. Glenny. Gas exchange and ventilation-perfusion relationships in the lung. *European Respiratory Journal*, 44(4):1023–1041, October 2014.

[22] T.S. Walsh. Recent advances in gas exchange measurement in intensive care patients. *British Journal of Anaesthesia*, 91(1):120–131, July 2003.

[23] Daren K. Heyland, Deborah J. Cook, Derek King, Philip Kernerman, and Christian Brun-Buisson. Maximizing oxygen delivery in critically ill patients: A methodologic appraisal of the evidence. *Critical Care Medicine*, 24(3):517–524, March 1996.

[24] P. Jolliet, J. B. Thorens, L. Nicod, C. Pichard, U. Kyle, and J. C. Chevrolet. Relationship between pulmonary oxygen consumption, lung inflammation, and calculated venous admixture in patients with acute lung injury. *Intensive Care Medicine*, 22(4):277–285, 1996.

[25] Jack W. Kern and William C. Shoemaker. Meta-analysis of hemodynamic optimization in high-risk patients. *Critical Care Medicine*, 30(8):1686–1692, 2002.

[26] Rodney M. Durham, Kathy Neunaber, John E. Mazuski, Marc J. Shapiro, and Arthur E. Baue. The use of oxygen consumption and delivery as endpoints for resuscitation in critically ill patients. *Journal of Trauma - Injury, Infection and Critical Care*, 41(1):32–40, July 1996.

[27] Kent Lundholm, Anders Hyltander, and Rolf Sandström. Nutrition and Multiple Organ Failure. *Nutrition Research Reviews*, 5(1):97–113, January 1992.

[28] C.J.K. Henry. Basal metabolic rate studies in humans: measurement and development of new equations. *Public Health Nutrition*, 8(7a):1133–1152, October 2005.

[29] D. C. Hunter, T. Jaksic, D. Lewis, P. N. Benotti, G. L. Blackburn, and B. R. Bistrian. Resting energy expenditure in the critically ill: Estimations versus measurement. *British Journal of Surgery*, 75(9):875–878, September 1988.

[30] Elizabeth C. Weekes. Controversies in the determination of energy requirements. *Proceedings of the Nutrition Society*, 66(3):367–377, August 2007.

[31] Christophe Faisy, Nicolas Lerolle, Fahmi Dachraoui, Jean François Savard, Imad Abboud, Jean Marc Tadie, and Jean Yves Fagon. Impact of energy deficit calculated by a predictive method on outcome in medical patients requiring prolonged acute mechanical ventilation. *British Journal of Nutrition*, 101(7):1079–1087, 2009.

[32] Hui Chen Lo, Ching Hsiung Lin, and Ling Jang Tsai. Effects of hypercaloric feeding on nutrition status and carbon dioxide production in patients with long-term mechanical ventilation. *Journal of Parenteral and Enteral Nutrition*, 29(5):380–387, September 2005.

[33] Pierre Singer, Claude Pichard, Claudia P. Heidegger, and Jan Wernerman. Considering energy deficit in the intensive care unit. *Current Opinion in Clinical Nutrition and Metabolic Care*, 13(2):170–176, March 2010.

[34] Lee anne S. Chapple, Luke Weinel, Emma J. Ridley, Daryl Jones, Marianne J. Chapman, and Sandra L. Peake. Clinical Sequelae From Overfeeding in Enterally Fed Critically Ill Adults: Where Is the Evidence? *Journal of Parenteral and Enteral Nutrition*, 44(6):980–991, August 2020.

[35] Claudia Paula Heidegger, Mette M. Berger, Séverine Graf, Walter Zingg, Patrice Darmon, Michael C. Costanza, Ronan Thibault, and Claude Pichard. Optimisation of energy provision with supplemental parenteral nutrition in critically ill patients: A randomised controlled clinical trial. *The Lancet*, 381(9864):385–393, February 2013.

[36] C. Black, M. P.W. Grocott, and M. Singer. Metabolic monitoring in the intensive care unit: A comparison of the Medgraphics Ultima, Deltatrac II, and Douglas bag collection methods. *British Journal of Anaesthesia*, 114(2):261–268, February 2015.

[37] Karen K.Y. Koo, Jack C.J. Sun, Qi Zhou, Gordan Guyatt, Deborah J. Cook, Stephen D. Walter, and Maureen O. Meade. Pulmonary artery catheters: Evolving rates and reasons for use. *Critical Care Medicine*, 39(7):1613–1618, 2011.

[38] Monica R. Shah, Vic Hasselblad, Lynne W. Stevenson, Cynthia Binanay, Christopher M. O'Connor, George Sopko, and Robert M. Califf. Impact of the pulmonary artery catheter in critically ill patients: Meta-analysis of randomized clinical trials. *Journal of the American Medical Association*, 294(13):1664–1670, October 2005.

[39] Sujanthy S. Rajaram, Nayan K. Desai, Ankur Kalra, Mithil Gajera, Susan K. Cavanaugh, William Brampton, Duncan Young, Sheila Harvey, and Kathy Rowan. Pulmonary artery catheters for adult patients in intensive care. *Cochrane Database of Systematic Reviews*, 2013(2), February 2013.

[40] G. Guyatt. A randomized control trial of right-heart catheterization in critically ill patients. *Journal of Intensive Care Medicine*, 6(2):91–95, 1991.

[41] Mauricio G. Cohen, Robert V. Kelly, David F. Kong, Venu Menon, Monica Shah, Jorge Ferreira, Karen S. Pieper, Douglas Criger, Rosana Poggio, E. Magnus Ohman, Joel Gore, Robert M. Califf, and Christopher B. Granger. Pulmonary artery catheterization in acute coronary syndromes: Insights from the GUSTO IIb and GUSTO III trials. *American Journal of Medicine*, 118(5):482–488, 2005.

[42] James Dean Sandham, Russell Douglas Hull, Rollin Frederick Brant, Linda Knox, Graham Frederick Pineo, Christopher J. Doig, Denny P. Laporta, Sidney Viner, Louise Passerini, Hugh Devitt, Ann Kirby, and Michael Jacka. A Randomized, Controlled Trial of the Use of Pulmonary-Artery Catheters in High-Risk Surgical Patients. *New England Journal of Medicine*, 348(1):5–14, January 2003.

[43] James A. Hill, Daniel F. Pauly, Debra R. Olitsky, Stuart Russell, Christopher M. O'Connor, Beth Patterson, Uri Elkayam, Salman Khan, Lynne W. Stevenson, Kimberly Brooks, Lynne Wagoner, Ginger Conway, Todd Koelling, Carol Van Huysen, Joshua Hare, Elayne Breton, Kirkwood F. Adams, Jana Glotzer, Gregg Fonarow, Michele Hamilton, Julie Sorg, Mark Drazner, Shannon Hoffman, Leslie W. Miller, Judith A. Graziano, Mary Ellen Berman, Robert Frantz, Karen Hartman, Carl V. Leier, William T. Abraham, Laura Yamokoski,

Thomas G. DiSalvo, Janice Camuso, Mihai Gheorghiade, Karen Fachet, Alain Heroux, Jin Kim Soo, J. Wayne Warnica, Jane Grant, Mian Hasan, Lydia Withrow, James Young, Barbara Gus, Javed Butler, Laurie Hawkins, Barry K. Rayburn, Jessica Robinson, Ileana Piña, Lori Shelby, Joseph Rogers, Heidi Craddock, Melvin Tonkon, Shane Miller, Teresa DeMarco, Debra Lau, Maryl Johnson, and Cassondra Vander Ark. Evaluation study of congestive heart failure and pulmonary artery catheterization effectiveness. *Journal of the American Medical Association*, 294(13):1625–1633, October 2005.

[44] Christian Richard, Josiane Warszawski, Nadia Anguel, Nicolas Deye, Alain Combes, Didier Barnoud, Thierry Boulain, Yannick Lefort, Muriel Fartoukh, Frederic Baud, Alexandre Boyer, Laurent Brochard, and Jean Louis Teboul. Early Use of the Pulmonary Artery Catheter and Outcomes in Patients with Shock and Acute Respiratory Distress Syndrome: A Randomized Controlled Trial. *Journal of the American Medical Association*, 290(20):2713–2720, November 2003.

[45] Wheeler AP, Bernard GR, Thompson BT, Schoenfeld D, Wiedemann HP, DeBoisblanc B, Connors AF, Hite RD, and Harabin AL. Pulmonary-Artery versus Central Venous Catheter to Guide Treatment of Acute Lung Injury. *New England Journal of Medicine*, 354(21):2213–2224, May 2006.

[46] Sheila Harvey, David A. Harrison, Mervyn Singer, Joanne Ashcroft, Carys M. Jones, Diana Elbourne, William Brampton, Dewi Williams, Duncan Young, and Kathryn Rowan. Assessment of the clinical effectiveness of pulmonary artery catheters in management of patients in intensive care (PAC-Man): A randomised controlled trial. *Lancet*, 366(9484):472–477, August 2005.

[47] Sheila Harvey, Duncan Young, William Brampton, Andrew Cooper, Gordon S Doig, William Sibbald, and Kathy Rowan. Pulmonary artery catheters for adult patients in intensive care. *Cochrane Database of Systematic Reviews*, 19(3), July 2006.

[48] August Krogh. *The respiratory exchange of animals and man.* London : Longmans, Green and Co., 1916.

[49] C Douglas. A method for determining the total respiratory exchange in man. *J Physiol.*, 42:17–23, 1911.

[50] A. Heather Haugen, Lingtak Neander Chan, and Fanny Li. Indirect calorimetry: A practical guide for clinicians. *Nutrition in Clinical Practice*, 22(4):377–388, August 2007.

[51] Idelle M Weisman, Darcy Marciniuk, Fernando J Martinez, Exercise Testing Measurements Frank Sciurba, Darryl Sue, Jonathan Myers Bruce Johnson, Brian Whipp, Jorge Zeballos, Ken Beck, Donald Mahler, John Cotes, Kathy Sietsema, Unexplained Dyspnea, Kieran Killian, and Richard Casaburi. ATS/ACCP Statement on cardiopulmonary exercise testing. *American journal of respiratory and critical care medicine*, 167(2):211–277, December 2003.

[52] Murat Pekdemir, Orhan Cinar, Serkan Yilmaz, Elif Yaka, and Melih Yuksel. Disparity between mainstream and sidestream end-tidal carbon dioxide values and arterial carbon dioxide levels. *Respiratory Care*, 58(7):1152–1156, July 2013.

[53] C. E. W. Hahn. Tutorial Review Electrochemical analysis of clinical blood-gases, gases and vapours. *The Analyst*, 123(6):57–86, 1998.

[54] Rakesh Garg and Ramesh Chand Gupta. Analysis of oxygen, anaesthesia agent and flows in anaesthesia machine. *Indian Journal of Anaesthesia*, 57(5):481–488, September 2013.

[55] A Burris. *The Magnetic Suscetptibility of oxygen and nitric oxide at low field strengths*. PhD thesis, Michigan State College of Agriculture and Applied Science, 1943.

[56] N. J.H. Davies and D. M. Denison. The measurement of metabolic gas exchange and minute volume by mass spectrometry alone. *Respiration Physiology*, 36(2):261–267, 1979.

[57] I E Sodal. The medical mass spectrometer. *Biomed Instrum Technol.*, 23(6):469–76, 1989.

[58] Long Guo, Yong Cui, Prashant Bobhate, Shine Kumar, Shreepal Jain, Mohamed Elgendi, Scott Pharis, Lindsay Ryerson, and Ian Adatia. Measurement of oxygen consumption in critically ill children: Breath-by-breath method vs mass spectrometry. *American Journal of Critical Care*, 25(3):243–248, May 2016.

[59] J A Langton, Frca A Hutton, and Mbbs Mrcp Frca. Respiratory gas analysis. *Continuing Education in Anaesthesia, Critical Care and Pain*, 9:19–23, 2009.

[60] Paul D. Robinson, Philipp Latzin, Sylvia Verbanck, Graham L. Hall, Alexander Horsley, Monika Gappa, Cindy Thamrin, Hubertus G.M. Arets, Paul Aurora, Susanne I. Fuchs, Gregory G. King, Sooky Lum, Kenneth Macleod, Manuel Paiva, Jane J. Pillow, Sarah Ranganathan, Felix Ratjen, Florian Singer, Samatha Sonnappa, Janet Stocks, Padmaja Subbarao, Bruce R. Thompson, and Per M. Gustafsson. Consensus statement for inert gas washout measurement using multiple- and singlebreath tests. *European Respiratory Journal*, 41(3):507–522, March 2013.

[61] Peter A. Robbins, James Mountain, David O'Neill, Luca Ciaffoni, John Couper, Jon Whiteley, Gus Hancock, and Grant Ritchie. Measuring lung inhomogeneity in early chronic lung disease. *European Respiratory Journal*, 48(suppl 60):PA2265, September 2016.

[62] M. R. Miller, J. Hankinson, Vito Brusasco, F. Burgos, R. Casaburi, A. Coates, R. Crapo, P. Enright, C. P.M. van der Grinten, P. Gustafsson, R. Jensen, D. C. Johnson, N. MacIntrye, R. McKay, D. Navajas, O. F. Pedersen, R. Pellegrino, G. Viegi, and J. Wagner. Standardisation of spirometry. *European Respiratory Journal*, 26(2):319–338, August 2005.

[63] V. C. Moore. Spirometry: Step by step. *Breathe*, 8(3):233–240, March 2012.

[64] Richard E. Kanner, Attilio D. Renzetti, Melville R. Klauber, Charles B. Smith, and Carole A. Golden. Variables associated with changes in spirometry in patients with obstructive lung diseases. *The American Journal of Medicine*, 67(1):44–50, 1979.

[65] Reed M. Gardner and John L. Hankinson. Standardization of Spirometry—1987 Update. *American Review of Respiratory Disease*, 136(5):1285–1298, November 1987.

[66] O. Crapo, John L. Hankinson, Charles Irvin, Neil R. MacIntyre, Karen Z. Voter, Robert A. Wise, B. Graham, C. O'Donnell, P. Paoletti, J. Roca, and G. Veigi. Standardization of spirometry: 1994 Update. *American Journal of Respiratory and Critical Care Medicine*, 152(3):1107–1136, December 1995.

[67] Ph. H Quanjer. Standardized lung function testing : report working party Standardization of lung function tests. 1983. Publisher: Luxembourg : European community for coal and steel, 1983.

[68] Brian L. Graham, Irene Steenbruggen, Igor Z. Barjaktarevic, Brendan G. Cooper, Graham L. Hall, Teal S. Hallstrand, David A. Kaminsky, Kevin McCarthy, Meredith C. McCormack, Martin R. Miller, Cristine E. Oropez, Margaret Rosenfeld, Sanja Stanojevic, Maureen P. Swanney, and Bruce R. Thompson. Standardization of spirometry 2019 update an official American Thoracic Society and European Respiratory Society technical statement. *American Journal of Respiratory and Critical Care Medicine*, 200(8):E70–E88, October 2019.

[69] Timothy Barreiro and Irene Perillo. An Approach to Interpreting Spirometry - American Family Physician. *American Family Physician*, 69(5):1107–1114, March 2004.

[70] Global strategy for the diagnosis, management and prevention of chronic obstructive pulmonary disease. Technical report, Global Inititiative for Chronic Obstructive Pulmonary Disease, 2020. `https://goldcopd.org/wp-content/uploads/2019/12/GOLD-2020-FINAL-ver1.2-03Dec19_WMV.pdf`, date accessed 2021-10-01.

[71] Eric J. Heckman and George T. O'Connor. Pulmonary Function Tests for Diagnosing Lung Disease. *JAMA*, 313(22):2278–2279, June 2015.

[72] R. A. Pauwels, A. S. Buist, P. M.A. Calverley, C. R. Jenkins, and S. S. Hurd. Global strategy for the diagnosis, management, and prevention of chronic obstructive pulmonary disease: NHLBI/WHO Global Initiative for Chronic Obstructive Lung Disease (GOLD) workshop summary. *American Journal of Respiratory and Critical Care Medicine*, 163(5):1256–1276, April 2001.

[73] Ellie Oostveen, D. MacLeod, H. Lorino, R. Farré, Z. Hantos, K. Desager, and F. Marchal. The forced oscillation technique in clinical practice: Methodology, recommendations and future developments. *European Respiratory Journal*, 22(6):1026–1041, December 2003.

[74] Eleanor Main. Airway clearance research in CF: the 'perfect storm' of strong preference and effortful participation in long-term, non-blinded studies. *Thorax*, 68(8):701–702, August 2013.

[75] Eleni Skylogianni, Konstantinos Douros, Michael B. Anthracopoulos, and Sotirios Fouzas. The Forced Oscillation Technique in Paediatric Respiratory Practice. *Paediatric Respiratory Reviews*, 18:46–51, March 2016.

[76] S. Brennan, G. L. Hall, F. Horak, A. Moeller, P. M.C. Pitrez, A. Franzmann, S. Turner, N. De Klerk, P. Franklin, K. R. Winfield, E. Balding, S. M. Stick, and P. D. Sly. Correlation of forced oscillation technique in preschool children with cystic fibrosis with pulmonary inflammation. *Thorax*, 60(2):159–163, February 2005.

[77] F. Child, S. Clayton, S. Davies, A.A. Fryer, P.W. Jones, and W. Lenney. How should airways resistance be measured in young children: mask or mouthpiece? *European Respiratory Journal*, 17(6), 2001.

[78] Janet Stocks and Sooky Lum. Pulmonary Function Tests in Infants and Preschool Children. In *Kendig and Chernick's Disorders of the Respiratory Tract in Children*, pages 169–210. Elsevier Inc., January 2012.

[79] A L Coates, R Peslin, D Rodenstein, and J Stocks. Measurement of lung volumes by plethysmography. *Eur Respir J*, 10:1415–1427, 1997.

[80] C. P. Criée, S. Sorichter, H. J. Smith, P. Kardos, R. Merget, D. Heise, D. Berdel, D. Köhler, H. Magnussen, W. Marek, H. Mitfessel, K. Rasche, M. Rolke, H. Worth, and R. A. Jörres. Body plethysmography - Its principles and clinical use. *Respiratory Medicine*, 105(7):959–971, July 2011.

[81] Insa Korten, Angela Zacharasiewicz, Nina Bittkowski, Alexander Hofmann, and Christiane Lex. Asthma control in children: Body plethysmography in addition to spirometry. *Pediatric Pulmonology*, 54(8):ppul.24320, June 2019.

[82] B. Dünges, J. Karmrodt, J. E. Baumgardner, and K. Markstaller. Ventilations-perfusions-verteilungen in der lunge: Eine neue technik zur schnellen bestimmung. *Anaesthesist*, 56(6):612–616, June 2007.

[83] Susan R. Hopkins and Peter D. Wagner. *The Multiple Inert Gas Elimination Technique (MIGET)*. Springer US, 2017.

[84] Peter D. Wagner. The multiple inert gas elimination technique (MIGET). *Intensive Care Medicine*, 34(6):994–1001, June 2008.

[85] Stephen E. Rees, S. Kjærgaard, S. Andreassen, and G. Hedenstierna. Reproduction of inert gas and oxygenation data: A comparison of the MIGET and a simple model of pulmonary gas exchange. *Intensive Care Medicine*, 36(12):2117–2124, December 2010.

[86] Roberto Rodríguez-Roisin, Mitra Drakulovic, Diego A. Rodríguez, Josep Roca, Joan Albert Barberà, and Peter D. Wagner. Ventilation-perfusion imbalance and chronic obstructive pulmonary disease staging severity. *Journal of Applied Physiology*, 106(6):1902–1908, June 2009.

[87] Justus E. Roos, Holman P. McAdams, S. Sivaram Kaushik, and Bastiaan Driehuys. Hyperpolarized Gas MR Imaging: Technique and Applications. *Magnetic Resonance Imaging Clinics of North America*, 23(2):217–229, May 2015.

[88] R. R. Kennedy, J. W. Stokes, and P. Downing. Anaesthesia and the 'inert' gases with special reference to xenon. *Anaesthesia and Intensive Care*, 20(1):66–70, 1992.

[89] David Kramer. For some, helium-3 supply picture is brightening. *Physics Today*, 64(5):20–22, May 2011.

[90] I. C. Ruset, S. Ketel, and F. W. Hersman. Optical pumping system design for large production of hyperpolarized Xe129. *Physical Review Letters*, 96(5), 2006.

[91] Bastiaan Driehuys, Santiago Martinez-Jimenez, Zackary I. Cleveland, Gregory M. Metz, Denise M. Beaver, John C. Nouls, S. Sivaram Kaushik, Rafael Firszt, Christine Willis, Kevin T. Kelly, Jan Wolber, Monica Kraft, and H. Page McAdams. Chronic obstructive pulmonary disease: Safety and tolerability of hyperpolarized 129Xe MR imaging in healthy volunteers and patients. *Radiology*, 262(1):279–289, January 2012.

[92] R. E. Latchaw, H. Yonas, S. L. Pentheny, and D. Gur. Adverse reactions to xenon-enhanced CT cerebral blood flow determination. *Radiology*, 163(1):251–254, 1987.

[93] J. S. Robertson, W. E. Siri, and H. B. Jones. Lung ventilation patterns determined by analysis of nitrogen elimination rates; use of mass spectrometer as a continuous gas analyzer. *The Journal of clinical investigation*, 29(5):577–590, 1950.

[94] A. Van Muylem, P. De Vuyst, J. C. Yernault, and M. Paiva. Inert gas single-breath washout and structural alteration of respiratory bronchioles. *American Review of Respiratory Disease*, 146(5):1167–1172, December 1992.

[95] Birgitta Houltz, Marita Gilljam, Monica Rosberg, Fanny Fors, Dorota Persson, Anders Lindblad, and Per Gustafsson. Sensitivity of N2 single breath washout (SBW) compared multiple breath washout (MBW) in adults with cystic fibrosis (CF). *European Respiratory Journal*, 42(Suppl 57), 2013.

[96] Katie J Bayfield, Alex Horsley, Eric Alton, Samantha Irving, Andrew Bush, and Jane C Davies. Simultaneous sulfur hexafluoride and nitrogen multiple-breath washout (MBW) to examine inherent differences in MBW outcomes. *ERJ Open Research*, 5(4):00234–2018, 2019.

[97] Padmaja Subbarao, Carlos Milla, Paul Aurora, Jane C. Davies, Stephanie D. Davis, Graham L. Hall, Sonya Heltshe, Philipp Latzin, Anders Lindblad, Jessica E. Pittman, Paul D. Robinson, Margaret Rosenfeld, Florian Singer, Tim D. Starner, Felix Ratjen, and Wayne Morgan. Multiple-breath washout as a lung function test in cystic fibrosis: A cystic fibrosis foundation workshop report. *Annals of the American Thoracic Society*, 12(6):932–939, June 2015.

[98] L. Kent, P. Reix, J. A. Innes, S. Zielen, M. Le Bourgeois, C. Braggion, S. Lever, H. G.M. Arets, K. Brownlee, J. M. Bradley, K. Bayfield, K. O'Neill, D. Savi, D. Bilton, A. Lindblad, J. C. Davies, I. Sermet, and K. De Boeck. Lung clearance index: Evidence for use in clinical trials in cystic fibrosis. *Journal of Cystic Fibrosis*, 13(2):123–138, March 2014.

[99] Julia E. Kao, Jacquelyn M. Zirbes, Carol K. Conrad, and Carlos E. Milla. Lung clearance index is sensitive to small airway disease in pediatric lung transplant recipients. *Journal of Heart and Lung Transplantation*, 36(9):980–984, September 2017.

[100] Madeleine Driskel, Alex Horsley, Laurice Fretwell, Nigel Clayton, and Mohamed Al-Aloul. Lung clearance index in detection of post-transplant bronchiolitis obliterans syndrome. *ERJ Open Research*, 5(4):00164–2019, October 2019.

[101] François Vermeulen, Marijke Proesmans, Mieke Boon, Trudy Havermans, and Kris De Boeck. Lung clearance index predicts pulmonary exacerbations in young patients with cystic fibrosis. *Thorax*, 69(1):39–45, January 2014.

[102] Paul Aurora, Wanda Kozlowska, and Janet Stocks. Gas mixing efficiency from birth to adulthood measured by multiple-breath washout. *Respiratory Physiology and Neurobiology*, 148(1-2 SPEC. ISS.):125–139, August 2005.

[103] Sylvia Verbanck, Bruce R. Thompson, Daniel Schuermans, Harpal Kalsi, Martyn Biddiscombe, Chris Stuart-Andrews, Shane Hanon, Alain Van Muylem, Manuel Paiva, Walter Vincken, and Omar Usmani. Ventilation heterogeneity in the acinar and conductive zones of the normal ageing lung. *Thorax*, 67(9):789–795, September 2012.

[104] M. Paiva. Two New Pulmonary Functional Indexes Suggested by a Simple Mathematical Model. *Respiration*, 32(5):389–403, 1975.

[105] A. B.H. Crawford, M. Makowska, S. Kelly, and L. A. Engel. Effect of breath holding on ventilation maldistribution during tidal breathing in normal subjects. *Journal of Applied Physiology*, 61(6):2108–2115, 1986.

[106] S. Verbanck, D. Schuermans, A. Van Muylem, M. Paiva, M. Noppen, and W. Vincken. Ventilation distribution during histamine provocation. *Journal of Applied Physiology*, 83(6):1907–1916, 1997.

[107] Sylvia Verbanck, Daniel Schuermans, and Walter Vincken. Inflammation and airway function in the lung periphery of patients with stable asthma. *Journal of Allergy and Clinical Immunology*, 125(3):611–616, March 2010.

[108] Sue R. Downie, Cheryl M. Salome, Sylvia Verbanck, Bruce Thompson, Norbert Berend, and Gregory G. King. Ventilation heterogeneity is a major determinant of airway hyperresponsiveness in asthma, independent of airway inflammation. *Thorax*, 62(8):684–689, August 2007.

[109] Bruce R. Thompson, Jo A. Douglass, Matthew J. Ellis, Vanessa J. Kelly, Robyn E. O'Hehir, Gregory G. King, and Sylvia Verbanck. Peripheral lung function in patients with stable and unstable asthma. *Journal of Allergy and Clinical Immunology*, 131(5):1322–1328, May 2013.

[110] David A Kaminsky. Multiple breath nitrogen washout profiles in asthmatic patients: What do they mean clinically? *J Allergy Clin Immunol*, 2013.

[111] Sue R. Downie, Cheryl M. Salome, Sylvia Verbanck, Bruce R. Thompson, Norbert Berend, and Gregory G. King. Effect of methacholine on peripheral lung

mechanics and ventilation heterogeneity in asthma. *Journal of Applied Physiology*, 114(6):770–777, March 2013.

[112] Sylvia Verbanck, Daniël Schuermans, Manuel Paiva, and Walter Vincken. Nonreversible conductive airway ventilation heterogeneity in mild asthma. *Journal of Applied Physiology*, 94(4):1380–1386, April 2003.

[113] Sylvia Verbanck, Daniël Schuermans, Manuel Paiva, and Walter Vincken. The functional benefit of anti-inflammatory aerosols in the lung periphery. *Journal of Allergy and Clinical Immunology*, 118(2):340–346, August 2006.

[114] Katie Bayfield, Clare Saunders, Eric Alton, and Jane Davies. Comparison of CF and non CF FRC and LCI values measured with Exhalyzer D and InnocorTM devices. *European Respiratory Journal*, 46(suppl 59):PA2288, September 2015.

[115] James E. Mountain, Peter Santer, David P. O'Neill, Nicholas M. J. Smith, Luca Ciaffoni, John H. Couper, Grant A. D. Ritchie, Gus Hancock, Jonathan P. Whiteley, and Peter A. Robbins. Non-invasive assessment of lung inhomogeneity using highly precise, highly time-resolved, measurements of gas exchange. *Submitted to J. Appl. Physiol.*, 2017.

[116] Henry Wollaston. A method of examining refractive and dispersive powers by prismatic reflexion. *Philosophical Transactions of the Royal Society*, 102:378, 1802.

[117] Andrew B. Christensen, Jeng-Hwa Yee, Rebecca L. Bishop, Scott A. Budzien, James H. Hecht, Gulamabas Sivjee, and Andrew W. Stephan. Observations of molecular oxygen Atmospheric band emission in the thermosphere using the near infrared spectrometer on the ISS/RAIDS experiment. *Journal of Geophysical Research: Space Physics*, 117(A4):n/a–n/a, April 2012.

[118] Cheng Zhang, Rami ElAfandy, and Jung Han. Distributed Bragg Reflectors for GaN-Based Vertical-Cavity Surface-Emitting Lasers. *Applied Sciences*, 9(8):1593, April 2019.

[119] M Nowakowski, J Wojtas, Z Bielecki, and J Mikołajczyk. Cavity Enhanced Absorption Spectroscopy Sensor. *ACTA PHYSICA POLONICA A*, 116:363–367, 2009.

[120] B. Ouyang and R. L. Jones. Understanding the sensitivity of cavity-enhanced absorption spectroscopy: pathlength enhancement versus noise suppression. *Applied Physics B*, 109(4):581–591, December 2012.

[121] Robert R. Gamache and Anne L. Laraia. N2-, O2-, and air-broadened half-widths, their temperature dependence, and line shifts for the rotation band of H216O. *Journal of Molecular Spectroscopy*, 257(2):116–127, October 2009.

[122] L. S. Rothman, I. E. Gordon, Y. Babikov, A. Barbe, D. Chris Benner, P. F. Bernath, M. Birk, L. Bizzocchi, V. Boudon, L. R. Brown, A. Campargue, K. Chance, E. A. Cohen, L. H. Coudert, V. M. Devi, B. J. Drouin, A. Fayt, J. M. Flaud, R. R. Gamache, J. J. Harrison, J. M. Hartmann, C. Hill, J. T. Hodges, D. Jacquemart, A. Jolly, J. Lamouroux, R. J. Le Roy, G. Li, D. A. Long, O. M. Lyulin, C. J. Mackie, S. T. Massie, S. Mikhailenko, H. S.P. Müller, O. V. Naumenko, A. V. Nikitin, J. Orphal, V. Perevalov, A. Perrin, E. R. Polovtseva, C. Richard, M. A.H. Smith, E. Starikova, K. Sung, S. Tashkun, J. Tennyson, G. C. Toon, Vl G. Tyuterev, and G. Wagner. The HITRAN2012 molecular spectroscopic database. *Journal of Quantitative Spectroscopy and Radiative Transfer*, 130:4–50, November 2013. ISBN: 0022-4073.

[123] Luca Ciaffoni, John Couper, Gus Hancock, Robert Peverall, Peter A. Robbins, and Grant A. D. Ritchie. RF noise induced laser perturbation for improving the performance of non-resonant cavity enhanced absorption spectroscopy. *Optics Express*, 22(14):17030, July 2014.

[124] Paul J. LaNasa and E. Loy Upp. 2 - Basic Flow Measurement Laws. In Paul J. LaNasa and E. Loy Upp, editors, *Fluid Flow Measurement (Third Edition)*, pages 19–29. Butterworth-Heinemann, Oxford, January 2014.

[125] Erwin. Fried and I. E. Idel'chik. *Flow resistance : a design guide for engineers*. Hemisphere, New York ;, 1989.

[126] Toolbox Engineering. Gases - Densities. `https://www.engineeringtoolbox.com/gas-density-d_158.html`, date accessed 2020-06-15.

[127] William Sutherland. The viscosity of gases and molecular force. *The London, Edinburgh, and Dublin Philosophical Magazine and Journal of Science*, 36(223):507–531, 1893.

[128] Viola Teske, Eckhard Vogel, and Eckard Bich. Viscosity measurements on water vapor and their evaluation. *Journal of Chemical and Engineering Data*, 50(6):2082–2087, November 2005.

[129] William Sutherland. XXXVII. The viscosity of mixed gases. *The London, Edinburgh, and Dublin Philosophical Magazine and Journal of Science*, 40(246):421–431, 1895.

[130] R S Brokaw. Viscosity of gas mixtures. *NASA Technical Note*, TN D-4496, 1968.

[131] Mervyn Singer, Clifford S. Deutschman, Christopher Warren Seymour, Manu Shankar-Hari, Djillali Annane, Michael Bauer, Rinaldo Bellomo, Gordon R. Bernard, Jean-Daniel Chiche, Craig M. Coopersmith, Richard S. Hotchkiss, Mitchell M. Levy, John C. Marshall, Greg S. Martin, Steven M. Opal, Gordon D. Rubenfeld, Tom van der Poll, Jean-Louis Vincent, and Derek C. Angus. The Third International Consensus Definitions for Sepsis and Septic Shock (Sepsis-3). *JAMA*, 315(8):801–810, February 2016.

[132] Vinay K. Sharma and RPhillip Dellinger. The International Sepsis Forum's frontiers in sepsis: high cardiac output should not be maintained in severe sepsis. *Critical Care*, 7(4):272, July 2003.

[133] Roman Pareznik, Rajko Knezevic, Gorazd Voga, and Matej Podbregar. Changes in muscle tissue oxygenation during stagnant ischemia in septic patients. *Intensive Care Med*, 32(1):87–92, January 2006.

[134] M. H. Schoenberg, M. Weiss, and P. Radermacher. Outcome of patients with sepsis and septic shock after ICU treatment. *Langenbecks Arch Surg*, 383(1):44–48, March 1998.

[135] Michael Bauer, Herwig Gerlach, Tobias Vogelmann, Franziska Preissing, Julia Stiefel, and Daniel Adam. Mortality in sepsis and septic shock in Europe, North America and Australia between 2009 and 2019— results from a systematic review and meta-analysis. *Critical Care*, 24(1):239, May 2020.

[136] Sean Dineen and Paul Schumacher. Cardiovascular support and management in the intensive care unit. In *Parkland Trauma Handbook*, pages 425–433. Elsevier Inc., January 2009.

[137] Ichiro Hirayama, Toshifumi Asada, Miyuki Yamamoto, Naoki Hayase, Takahiro Hiruma, and Kent Doi. Changes in carbon dioxide production and oxygen uptake evaluated using indirect calorimetry in mechanically ventilated patients with sepsis. *Critical Care*, 25(1):416, December 2021.

[138] Ccm express®: Indirect calorimeter. `https://mgcdiagnostics.com/images/uploads/documents/CCM_Express_sell_sheet_060065-001.pdf`, date accessed 2023-09-05.

[139] R. M. Leach and D. F. Treacher. The pulmonary physician in critical care · 2: Oxygen delivery and consumption in the critically ill. *Thorax*, 57(2):170–177, February 2002.

[140] S. A. McLellan and T. S. Walsh. Oxygen delivery and haemoglobin. *Continuing Education in Anaesthesia Critical Care \& Pain*, 4(4):123–126, August 2004.

[141] Vincent Caille and Pierre Squara. Oxygen uptake-to-delivery relationship: A way to assess adequate flow. *Critical Care*, 10(SUPPL. 3):S4, November 2006.

[142] Leonardo Rocha, Camila Pessoa, Thiago Correa, Adriano Pereira, Murillo Assuncao, and Eliézer Silva. [Current concepts on hemodynamic support and therapy in septic shock]. *Revista brasileira de anestesiologia*, August 2015.

[143] P. T. Schumacker and S. M. Cain. The concept of a critical oxygen delivery. *Intensive Care Medicine*, 13(4):223–229, June 1987.

[144] W. C. Shoemaker, P. L. Appel, H. B. Kram, K. Waxman, and T. S. Lee. Prospective trial of supranormal values of survivors as therapeutic goals in high-risk surgical patients. *Chest*, 94(6):1176–1186, 1988.

[145] W. C. Shoemaker, P. L. Appel, and H. B. Kram. Hemodynamic and oxygen transport responses in survivors and nonsurvivors of high-risk surgery. *Critical Care Medicine*, 21(7):977–990, 1993.

[146] Hoong Sern Lim. Cardiogenic Shock: Failure of Oxygen Delivery and Oxygen Utilization. *Clinical Cardiology*, 39(8):477–483, 2016.

[147] Feihu Zhou, Zhi Mao, Xiantao Zeng, Hongjun Kang, Hui Liu, Liang Pan, and Peter C Hou. Vasopressors in septic shock: a systematic review and network meta-analysis. *Ther Clin Risk Manag*, 11:1047–1059, July 2015.

[148] Nicole P. Juffermans, Cécile Aubron, Jacques Duranteau, Alexander P. J. Vlaar, Daryl J. Kor, Jennifer A. Muszynski, Philip C. Spinella, and Jean-Louis Vincent. Transfusion in the mechanically ventilated patient. *Intensive Care Med*, 46(12):2450–2457, 2020.

[149] Roeland F. Stolk, Tom van der Poll, Derek C. Angus, Johannes G. van der Hoeven, Peter Pickkers, and Matthijs Kox. Potentially Inadvertent Immunomodulation: Norepinephrine Use in Sepsis. *Am J Respir Crit Care Med*, 194(5):550–558, September 2016.

[150] Hitoshi Yamamura, Yu Kawazoe, Kyohei Miyamoto, Tomonori Yamamoto, Yoshinori Ohta, and Takeshi Morimoto. Effect of norepinephrine dosage on mortality in patients with septic shock. *J Intensive Care*, 6:12, February 2018.

[151] Constantine A. Manthous, Paul T. Schumacker, Anne Pohlman, Gregory A. Schmidt, Jesse B. Hall, Richard W. Samsel, and Lawrence D.H. Wood. Absence of supply dependence of oxygen consumption in patients with septic shock. *Journal of Critical Care*, 8(4):203–211, 1993.

[152] Richard H. Kallet and Michael A. Matthay. Hyperoxic acute lung injury. *Respiratory Care*, 58(1):123–140, January 2013.

[153] Emanuel Rivers, Bryant Nguyen, Suzanne Havstad, Julie Ressler, Alexandria Muzzin, Bernhard Knoblich, Edward Peterson, and Michael Tomlanovich. Early Goal-Directed Therapy in the Treatment of Severe Sepsis and Septic Shock. *New England Journal of Medicine*, 345(19):1368–1377, November 2001.

[154] H. Bryant Nguyen, Anja Kathrin Jaehne, Namita Jayaprakash, Matthew W. Semler, Sara Hegab, Angel Coz Yataco, Geneva Tatem, Dhafer Salem, Steven Moore, Kamran Boka, Jasreen Kaur Gill, Jayna Gardner-Gray, Jacqueline Pflaum, Juan Pablo Domecq, Gina Hurst, Justin B. Belsky, Raymond Fowkes, Ronald B. Elkin, Steven Q. Simpson, Jay L. Falk, Daniel J. Singer, and Emanuel P. Rivers. Early goal-directed therapy in severe sepsis and septic shock: insights and comparisons to ProCESS, ProMISe, and ARISE. *Critical Care*, 20(1):160, July 2016.

[155] Anna Patkova, Vera Joskova, Eduard Havel, Simona Najpaverova, Daniela Uramova, Miroslav Kovarik, Zdenek Zadak, and Miloslav Hronek. Prognostic value of respiratory quotients in severe polytrauma patients with nutritional support. *Nutrition*, 49:90–95, May 2018.

[156] Stephen A. McClave, Cynthia C. Lowen, Melissa J. Kleber, J. Wesley McConnell, Laura Y. Jung, and Linda J. Goldsmith. Clinical use of the respiratory quotient obtained from indirect calorimetry. *JPEN J Parenter Enteral Nutr*, 27(1):21–26, 2003.

[157] McClave Sa, Taylor Be, Martindale Rg, Warren Mm, Johnson Dr, Braunschweig C, McCarthy Ms, Davanos E, Rice Tw, Cresci Ga, Gervasio Jm, Sacks Gs, Roberts Pr, Compher C, and undefined. Guidelines for the Provision and Assessment of Nutrition Support Therapy in the Adult Critically Ill Patient: Society of Critical Care Medicine (SCCM) and American Society for Parenteral and Enteral Nutrition (A.S.P.E.N.). *JPEN J Parenter Enteral Nutr*, 40(2):159–211, February 2016.

[158] J. B. de V. Weir. New methods for calculating metabolic rate with special reference to protein metabolism. *The Journal of Physiology*, 109(1-2):1–9, 1949.

[159] Hanneke Pierre Franciscus Xaverius Moonen, Karin Josephina Hubertina Beckers, and Arthur Raymond Hubert van Zanten. Energy expenditure and indirect calorimetry in critical illness and convalescence: current evidence and practical considerations. *Journal of Intensive Care*, 9(1):8, January 2021.

[160] Sandra N. Stapel, Harm-Jan S. de Grooth, Hoda Alimohamad, Paul W. G. Elbers, Armand R. J. Girbes, Peter J. M. Weijs, and Heleen M. Oudemans-van Straaten. Ventilator-derived carbon dioxide production to assess energy expenditure in critically ill patients: proof of concept. *Critical Care*, 19(1):370, October 2015.

[161] Mark Lillelund Rousing, Mie Hviid Hahn-Pedersen, Steen Andreassen, Ulrike Pielmeier, and Jean-Charles Preiser. Energy expenditure in critically ill patients estimated by population-based equations, indirect calorimetry and CO2-based indirect calorimetry. *Annals of Intensive Care*, 6(1):16, February 2016.

[162] MD Mifflin, ST St Jeor, LA Hill, BJ Scott, SA Daugherty, and YO Koh. A new predictive equation for resting energy expenditure in healthy individuals. *The American Journal of Clinical Nutrition*, 51(2):241–247, February 1990.

[163] Frank B. Cerra, Marta Rios Benitez, George L. Blackburn, Richard S. Irwin, Khursheed Jeejeebhoy, David P. Katz, Susan K. Pingleton, James Pomposelli,

John L. Rombeau, Eva Shronts, Robert R. Wolfe, and Gary Paul Zaloga. Applied Nutrition in ICU Patients: A Consensus Statement of the American College of Chest Physicians. *CHEST*, 111(3):769–778, March 1997.

[164] D Frankenfield, Js Smith, and Rn Cooney. Validation of 2 approaches to predicting resting metabolic rate in critically ill patients. *Journal of Parenteral and Enteral Nutrition*, 28(4):259–264, 2004.

[165] Hérnan Aguirre-Bermeo and Jordi Mancebo. Pressure support ventilation. In Andrew Webb, Derek Angus, Simon Finfer, Luciano Gattinoni, and Mervyn Singer, editors, *Oxford Textbook of Critical Care*, page 0. Oxford University Press, April 2016.

[166] Andres L. Mora Carpio and Jorge I. Mora. Ventilator Management. In *StatPearls*. StatPearls Publishing, 2023.

[167] Masanori Uehara, Lindsay D. Plank, and Graham L. Hill. Components of energy expenditure in patients with severe sepsis and major trauma: A basis for clinical care. *Critical Care Medicine*, 27(7):1295, July 1999.

[168] Philip F. Stahel, Michael A. Flierl, and Ernest E. Moore. "Metabolic staging" after major trauma - a guide for clinical decision making? *Scandinavian Journal of Trauma, Resuscitation and Emergency Medicine*, 18(1):34, June 2010.

[169] Georgia Vasileiou, Sinong Qian, Rahul Iyengar, Michelle B. Mulder, Lindsey M Gass, Jonathan Parks, Gerd D. Pust, Rishi Rattan, Edward Lineen, Patricia Byers, and D. Dante Yeh. Use of Predictive Equations for Energy Prescription Results in Inaccurate Estimation in Trauma Patients. *Nutrition in Clinical Practice*, 35(5):927–932, 2020.

[170] John Whittle, Jeroen Molinger, David MacLeod, Krista Haines, Paul E. Wischmeyer, John Whittle, Jeroen Molinger, David MacLeod, Krista Haines, Paul E. Wischmeyer, Anthony Sung, Marat Fudim, Lindsie Boerger, Kathryn Lessig, Jessica Lumbard, Leslie C. Murray, Sue Steves, Jhana Parikh, Jacob Ribet, Melanie Hollidge, and for the LEEP-COVID Study Group. Persistent hypermetabolism and longitudinal energy expenditure in critically ill patients with COVID-19. *Critical Care*, 24(1):581, September 2020.

[171] Ido G. Bikker, Jasper van Bommel, Dinis Reis Miranda, Jan Bakker, and Diederik Gommers. End-expiratory lung volume during mechanical ventilation: a comparison with reference values and the effect of positive end-expiratory pressure in intensive care unit patients with different lung conditions. *Critical Care*, 12(6):R145, November 2008.

[172] P. H. Quanjer, G. J. Tammeling, J. E. Cotes, O. F. Pedersen, R. Peslin, and J. C. Yernault. Lung volumes and forced ventilatory flows. In *European Respiratory Journal, Supplement*, volume 6, pages 5–40. European Respiratory Society, March 1993. Issue: 16 ISSN: 09041950.

[173] A. B. Lumb and J. F. Nunn. Respiratory function and ribcage contribution to ventilation in body positions commonly used during anesthesia. *Anesth Analg*, 73(4):422–426, October 1991.

[174] Luciano Gattinoni and Antonio Pesenti. The concept of "baby lung". *Intensive Care Medicine*, 31(6):776–784, June 2005.

[175] Hiran Patel, Connor C. Kerndt, and Abhishek Bhardwaj. Physiology, Respiratory Quotient. In *StatPearls*. 2023.

[176] Rungsinee A. Liusuwan Manotok, Tina L. Palmieri, and David G. Greenhalgh. The respiratory quotient has little value in evaluating the state of feeding in burn patients. *J Burn Care Res*, 29(4):655–659, 2008.

[177] Indubala Maurya, Mridula Pawar, Rakesh Garg, Mohandeep Kaur, and Rajesh Sood. Comparison of respiratory quotient and resting energy expenditure in two regimens of enteral feeding – continuous vs. intermittent in head-injured critically ill patients. *Saudi J Anaesth*, 5(2):195–201, 2011.

[178] Curtis N. Sessler, Mark S. Gosnell, Mary Jo Grap, Gretchen M. Brophy, Pam V. O'Neal, Kimberly A. Keane, Eljim P. Tesoro, and R. K. Elswick. The Richmond Agitation–Sedation Scale. *Am J Respir Crit Care Med*, 166(10):1338–1344, November 2002.

[179] Metaraminol 10mg/mL Solution for Injection or Infusion - Summary of Product Characteristics (SmPC) - (emc). `https://www.medicines.org.uk/emc/product/7111/smpc#gref`, date accessed 2023-09-06.

[180] E. M. M. Besterman. Treatment of Cardiac Shock by Metaraminol. *Br Med J*, 1(5129):1081–1083, April 1959.

[181] Khashayar Farzam, Ariel Kidron, and Anand D. Lakhkar. Adrenergic Drugs. In *StatPearls*. StatPearls Publishing, 2023.

[182] Matthew D. Smith and Christopher V. Maani. Norepinephrine. In *StatPearls*. StatPearls Publishing, 2023.

[183] Christopher B. Overgaard and Vladimír Džavík. Inotropes and Vasopressors. *Circulation*, 118(10):1047–1056, September 2008.

[184] Soubhi Alhayek and Charles V. Preuss. Beta 1 Receptors. In *StatPearls*. StatPearls Publishing, 2023.

[185] James S. Dean II and Anil Kumar Reddy Reddivari. Alpha-1 Receptor Agonists. In *StatPearls*. StatPearls Publishing, 2023.

[186] James R. Nestler. Relationships between Respiratory Quotient and Metabolic Rate during Entry to and Arousal from Daily Torpor in Deer Mice (Peromyscus maniculatus). *Physiological Zoology*, 63(3):504–515, 1990.

[187] National Clinical Guideline Centre (UK). Repositioning. In *The Prevention and Management of Pressure Ulcers in Primary and Secondary Care*. National Institute for Health and Care Excellence (NICE), April 2014.

[188] N. D. Ciesla. Chest physical therapy for patients in the intensive care unit. *Phys Ther*, 76(6):609–625, June 1996.

[189] Virteeka Sinha, George Semien, and Brian M. Fitzgerald. Surgical Airway Suctioning. In *StatPearls*. StatPearls Publishing, 2023.

[190] Jonathan Myers, Leonard Kaminsky, Ricardo Lima, Jeffrey Chistle, Euan Ashley, and Ross Arena. A Reference Equation for Normal Standards for VO2 Max: Analysis from the Fitness Registry and the Importance of Exercise National Database (FRIEND Registry). *Progress in cardiovascular diseases*, 60, April 2017.

[191] Nicholas M.J. Smith, John Couper, Graham Richmond, Dominic Sandhu, Gus Hancock, Peter A. Robbins, and Grant A.D. Ritchie. Development of in-airway laser absorption spectroscopy for respiratory based measurements of cardiac output. *Scientific Reports*, 11(1):1–13, December 2021.

[192] Anders Larsson and Claude Guerin. Monitoring of lung function in acute respiratory distress syndrome. *Ann Transl Med*, 5(14):284, July 2017.

[193] Snapper Magor-Elliott. *A new technique for diagnosing pulmonary embolism based on respiratory exchange*. DPhil thesis, University of Oxford, 2022.

[194] Anna Pathak. *The effect of posture on pulmonary inhomogeneity assessed using the technique of in-airway molecular flow sensing*. Research project dissertation (FHS), University of Oxford, 2019.

[195] Nayia Petousi, Nick P. Talbot, Ian Pavord, and Peter A. Robbins. Measuring lung function in airways diseases: current and emerging techniques. *Thorax*, 74(8):797–805, August 2019.

[196] Susanne I. Fuchs, Helmut Ellemunter, Johannes Eder, Uwe Mellies, Jörg Grosse-Onnebrink, Burkhard Tümmler, Doris Staab, Andrea Jobst, Matthias Griese, Jan Ripper, Ernst Rietschel, Susanne Zeidler, Frank Ahrens, and Monika Gappa. Feasibility and Variability of Measuring the Lung Clearance Index in a Multi-Center Setting. *Pediatric Pulmonology*, 47(7):649–657, July 2012.

[197] P. M. Gustafsson, P. Aurora, and A. Lindblad. Evaluation of ventilation maldistribution as an early indicator of lung disease in children with cystic fibrosis. *European Respiratory Journal*, 22(6):972–979, December 2003.

[198] Elpis Hatziagorou, Vasiliki Avramidou, Fotis Kirvasillis, and John Tsanakas. Ventilation inhomogeneity in children with severe asthma and normal spirometry indicates residual airways disease. *European Respiratory Journal*, 42(Suppl 57), September 2013.

[199] Zihang Lu, Rachel E Foong, Krzysztof Kowalik, Theo J Moraes, Ayanna Boyce, Aimee Dubeau, Susan Balkovec, Per Magnus Gustafsson, Allan B Becker, Piush J Mandhane, Stuart E Turvey, Wendy Lou, Felix Ratjen, Malcolm Sears, and Padmaja Subbarao. Ventilation inhomogeneity in infants with recurrent wheezing. *Thorax*, 73(10):936–941, October 2018.

[200] Nicholas M.J. Smith, John Couper, Christopher J. Fullerton, Graham Richmond, Nick P. Talbot, Gus Hancock, Ian Pavord, Grant A.D. Ritchie, Peter A. Robbins, and Nayia Petousi. Novel measure of lung function for assessing disease activity in asthma. *BMJ Open Respiratory Research*, 7(1):531, March 2020.

[201] P. D. Wagner, D. R. Dantzker, R. Dueck, J. L. de Polo, K. Wasserman, and J. B. West. Distribution of ventilation-perfusion ratios in patients with interstitial lung disease. *Chest*, 69(2 Suppl):256–257, February 1976.

[202] James Mountain. *The Lognormal Lung: Quantifying Inhomogeneity of Ventilation*. PhD thesis, University of Oxford.

[203] T. A. Wilson and K. C. Beck. Contributions of ventilation and perfusion inhomogeneities to the VA/Q distribution. *Journal of applied physiology (Bethesda, Md. : 1985)*, 72(6):2298–2304, 1992.

[204] Kenneth C. Beck, Bruce D. Johnson, Thomas P. Olson, and Theodore A. Wilson. Ventilation-perfusion distribution in normal subjects. *Journal of Applied Physiology*, 113(6):872, September 2012.

[205] A. St J. Lee, R. W. Patterson, and R. D. Kaufman. Relationships among ventilation-perfusion distribution, multiple inert gas methodology and metabolic blood-gas tensions. *British journal of anaesthesia*, 59(12):1579–1598, 1987.

[206] Sven M 'Berggren. *The Oxygen deficit of arterial blood caused by non-ventilating parts of the lung*, volume 11. Stockholm : Kungl. Boktryckeriet, 1942.

[207] H. Thomas Robertson. Dead space: the physiology of wasted ventilation. *European Respiratory Journal*, 45(6):1704–1716, June 2015.

[208] Snapper Richard Myran Magor-Elliott, Christopher J. Fullerton, Graham Richmond, Grant A.D. Ritchie, and Peter A. Robbins. A dynamic model of the body gas stores for carbon dioxide, oxygen and inert gases that incorporates circulatory transport delays to and from the lung. *Journal of Applied Physiology*, January 2021.

[209] P. D. Wagner, D. R. Dantzker, R. Dueck, J. L. Clausen, and J. B. West. Ventilation-perfusion inequality in chronic obstructive pulmonary disease. *The Journal of clinical investigation*, 59(2):203–216, 1977.

[210] J. A. Barbera, J. Ramirez, J. Roca, P. D. Wagner, J. Sanchez-Lloret, and R. Rodriguez-Roisin. Lung structure and gas exchange in mild chronic obstructive pulmonary disease. *The American review of respiratory disease*, 141(4 Pt 1):895–901, 1990.

[211] Roberto Rodríguez-Roisin, Mitra Drakulovic, Diego A. Rodríguez, Josep Roca, Joan Albert Barberà, and Peter D. Wagner. Ventilation-perfusion imbalance and chronic obstructive pulmonary disease staging severity. *Journal of applied physiology (Bethesda, Md. : 1985)*, 106(6):1902–1908, June 2009.

[212] Okada Y Kawai A Mori M Yokoyama T Yamasawa F, Kawashiro T. Uneven ventilation-perfusion ratio distribution during acute exacerbation of chronic pulmonary diseases. *Kokyu To Junkan*, pages 40(4):369–73, 1992.

[213] Hallemans R Mols P Lejeine P Melot C, Naeije R. Beneficial effects of almitrine bismesylate on pulmonary gas exchange in COPD. *Eur J Respir Dis Suppl .*, pages 126:249–54, 1983.

[214] C. Melot, R. Naeije, T. Rothschild, P. Mertens, P. Mols, and R. Hallemans. Improvement in ventilation-perfusion matching by almitrine in COPD. *Chest*, 83(3):528–533, 1983.

[215] Lisa D.M. Verberne, Chantal J. Leemrijse, Ilse C.S. Swinkels, Christel E. Van Dijk, Dinny H. De Bakker, and Mark M.J. Nielen. Overweight in patients with chronic obstructive pulmonary disease needs more attention: a cross-sectional study in general practice. *NPJ Primary Care Respiratory Medicine*, 27(1):63, December 2017.

[216] P. D. Wagner, H. A. Saltzman, and J. B. West. Measurement of continuous distributions of ventilation-perfusion ratios: theory. *https://doi.org/10.1152/jappl.1974.36.5.588*, 36(5):588–599, 1974.

[217] Rui Carlos Sá, A. Cortney Henderson, Tatum Simonson, Tatsuya J. Arai, Harrieth Wagner, Rebecca J. Theilmann, Peter D. Wagner, G. Kim Prisk, and Susan R. Hopkins. Measurement of the distribution of ventilation-perfusion ratios in the human lung with proton MRI: comparison with the multiple inert-gas elimination technique. *Journal of Applied Physiology*, 123(1):136–146, July 2017.

[218] Nicholas M. J. Smith, Snapper R. M. Magor-Elliott, Christopher J. Fullerton, John H. Couper, Graham Richmond, Gus Hancock, Grant A. D. Ritchie, Peter A. Robbins, Nick P. Talbot, and Nayia Petousi. The Lognormal Lung: A new approach to quantifying lung inhomogeneity in COPD. *Front Physiol*, 13:1032126, October 2022.

[219] NMJ Smith, S Magor-Elliot, J Redmond, GAD Ritchie, PA Robbins, N Petousi, and NP Talbot. S114 Non-invasive assessment of lung inhomogeneity for early identification of COPD. In *Thorax*, volume 74, pages A71–A72. BMJ, December 2019. Issue: Suppl 2 ISSN: 0040-6376.

[220] D. E. O'Donnell and P. Laveneziana. Physiology and consequences of lung hyperinflation in COPD. *European Respiratory Review*, 15(100):61–67, December 2006.

[221] Anne E. Dixon and Ubong Peters. The effect of obesity on lung function. *Expert review of respiratory medicine*, 12(9):755, September 2018.

[222] Richard L. Jones and Mary Magdalene U. Nzekwu. The Effects of Body Mass Index on Lung Volumes. *Chest*, 130(3):827–833, September 2006.

[223] D. G. Altman and J. M. Bland. Measurement in Medicine: The Analysis of Method Comparison Studies. *The Statistician*, 32(3):307, September 1983.

[224] Davide Giavarina. Understanding Bland Altman analysis. *Biochemia Medica*, 25(2):141, 2015.

[225] Sagar Patel, Alvin Jose, and Shamim S. Mohiuddin. Physiology, Oxygen Transport And Carbon Dioxide Dissociation Curve. *StatPearls*, March 2022.

[226] D. Vanuxem, C. Guillot, and C. Grimaud. Tabagisme et monoxyde de carbone. *Respiration*, 40(3):136–141, 1980.

[227] Rafael Laniado-Laborin. Smoking and chronic obstructive pulmonary disease (COPD). Parallel epidemics of the 21st century. *International Journal of Environmental Research and Public Health*, 6(1):209–224, January 2009.

[228] Daiana Stolz, Takudzwa Mkorombindo, Desiree M. Schumann, Alvar Agusti, Samuel Y. Ash, Mona Bafadhel, Chunxue Bai, James D. Chalmers, Gerard J. Criner, Shyamali C. Dharmage, Frits M.E. Franssen, Urs Frey, Mei Lan Han, Nadia N. Hansel, Nathaniel M. Hawkins, Ravi Kalhan, Melanie Konigshoff, Fanny W. Ko, Trisha M. Parekh, Pippa Powell, Maureen Rutten-van Mölken, Jodie Simpson, Don D. Sin, Yuanlin Song, Bela Suki, Thierry Troosters, George R. Washko, Tobias Welte, and Mark T. Dransfield. Towards the elimination of chronic obstructive pulmonary disease: a Lancet Commission. *The Lancet*, 400(10356):921–972, September 2022.

[229] Julia A. Walters, E. Haydn Walters, Mark Nelson, Andrew Robinson, Jenn Scott, Paul Turner, and Richard Wood-Baker. Factors associated with misdiagnosis of COPD in primary care. *Primary Care Respiratory Journal*, 20(4):396–402, 2011.

[230] David M. Mannino and A. Sonia Buist. Global burden of COPD: risk factors, prevalence, and future trends. *Lancet*, 370(9589):765–773, September 2007.

[231] Andrew Higham, Anne Marie Quinn, José Eduardo D. Cançado, and Dave Singh. The pathology of small airways disease in COPD: Historical aspects and future directions. *Respiratory Research*, 20(1):1–11, March 2019.

[232] Roberto W. Dal Negro, Matteo Paoletti, and Massimo Pistolesi. Standard spirometry to assess emphysema in patients with chronic obstructive pulmonary disease: the Emphysema Severity Index (ESI). *Multidisciplinary Respiratory Medicine*, 16(1):805, January 2021.

[233] Prescott G. Woodruff, R. Graham Barr, Eugene Bleecker, Stephanie A. Christenson, David Couper, Jeffrey L. Curtis, Natalia A. Gouskova, Nadia N. Hansel, Eric A. Hoffman, Richard E. Kanner, Eric Kleerup, Stephen C. Lazarus, Fernando J. Martinez, Robert Paine, Stephen Rennard, Donald P. Tashkin, and MeiLan K. Han. Clinical Significance of Symptoms in Smokers with Preserved Pulmonary Function. *The New England journal of medicine*, 374(19):1811–1821, May 2016.

[234] Alvar Agusti, Peter M.A. Calverley, Bartolome Celli, Harvey O. Coxson, Lisa D. Edwards, David A. Lomas, William MacNee, Bruce E. Miller, Steve Rennard, Edwin K. Silverman, Ruth Tal-Singer, Emiel Wouters, Julie C. Yates, and Jørgen Vestbo. Characterisation of COPD heterogeneity in the ECLIPSE cohort. *Respiratory research*, 11(1), September 2010.

[235] David P. Johns, Julia A E Walters, and E. Haydn Walters. Diagnosis and early detection of COPD using spirometry. *Journal of Thoracic Disease*, 6(11):1557–1569, 2014.

[236] A Guide to Performing Quality Assured Diagnostic Spirometry 2 © PCC 2013 PCC |. 2013. `https://www.brit-thoracic.org.uk/media/70454/spirometry_e-guide_2013.pdf`, date accessed 2022-10-20.

[237] Sylvia Verbanck, Daniël Schuermans, Marc Meysman, Manuel Paiva, and Walter Vincken. Noninvasive assessment of airway alterations in smokers: The small airways revisited. *American Journal of Respiratory and Critical Care Medicine*, 170(4):414–419, August 2004.

[238] Dennis E. Niewoehner, Jerome Kleinerman, and Donald B. Rice. Pathologic Changes in the Peripheral Airways of Young Cigarette Smokers. *New England Journal of Medicine*, 291(15):755–758, October 1974.

[239] Kristen Deane, James J. Stevermer, and John Hickner. Help smokers quit: Tell them their "lung age". *The Journal of Family Practice*, 57(9):584, September 2008.

[240] Thomas Bithell. *Molecular Flow Sensing: A Tool For Cardiopulmonography.* MChem Part II thesis, University of Oxford, 2023.

[241] Natalie Terzikhan, Katia M.C. Verhamme, Albert Hofman, Bruno H. Stricker, Guy G. Brusselle, and Lies Lahousse. Prevalence and incidence of COPD in smokers and non-smokers: the Rotterdam Study. *European Journal of Epidemiology*, 31(8):785, August 2016.

[242] Alejandra Ramírez-Venegas, Raul H. Sansores, Roger H. Quintana-Carrillo, Monica Velázquez-Uncal, Rafael J. Hernandez-Zenteno, Candelaria Sánchez-Romero, Alejandra Velazquez-Montero, and Fernando Flores-Trujillo. FEV1 decline in patients with chronic obstructive pulmonary disease associated with biomass exposure. *American Journal of Respiratory and Critical Care Medicine*, 190(9):996–1002, November 2014.

[243] P. A. Dawkins, C. L. Dawkins, A. M. Wood, P. G. Nightingale, J. A. Stockley, and R. A. Stockley. Rate of progression of lung function impairment in alpha-1-antitrypsin deficiency. *European Respiratory Journal*, 33(6):1338–1344, June 2009.

[244] Graciela E. Silva, Duane L. Sherrill, Stefano Guerra, and Robert A. Barbee. Asthma as a risk factor for COPD in a longitudinal study. *Chest*, 126(1):59–65, 2004.

[245] Andrew Tai, Haily Tran, Mary Roberts, Nadeene Clarke, John Wilson, and Colin F. Robertson. The association between childhood asthma and adult chronic obstructive pulmonary disease. *Thorax*, 69(9):805–810, 2014.

[246] Bhagyashree Madan, Akshay Panchal, and Dilip Chavan. Lung Cancer Detection Using Deep Learning. *SSRN Electronic Journal*, April 2019.

[247] NICE. Cystic fibrosis: diagnosis and management, NICE. *Cystic fibrosis: diagnosis and management*, 2017. Publisher: NICE.

[248] Jane C Davies, Steve Cunningham, Eric W F W Alton, and J A Innes. Lung clearance index in CF: a sensitive marker of lung disease severity. *Thorax*, 63(2):96–7, February 2008.

[249] Susan Charman, Elliot McGlenaghan, Rebecca Cosgriff, Andrew Lee, and Siobhan Carr. UK Cystic Fibrosis Registry Annual Data Report 2018. Technical report, UK Cystic Fibrosis Registry, 2019.

[250] Janice Kelly. Environmental scan of cystic fibrosis research worldwide. *Journal of Cystic Fibrosis*, 16(3):367–370, May 2017.

[251] Penny Agent and Helen Parrott. Inhaled therapy in cystic fibrosis: Agents, devices and regimens. *Breathe*, 11(2):111–118, June 2015.

[252] Isabelle Sermet-Gaudelus. Ivacaftor treatment in patients with cystic fibrosis and the G551D-CFTR mutation. *European Respiratory Review*, 22(127):66–71, March 2013.

[253] Sara Cuevas-Ocaña, Onofrio Laselva, Julie Avolio, and Raffaella Nenna. Landmark papers in respiratory medicine: The era of cftr modulators: Improvements made and remaining challenges. *Breathe*, 16(2):1–5, June 2020.

[254] Claire E. Wainwright, J. Stuart Elborn, Bonnie W. Ramsey, Gautham Marigowda, Xiaohong Huang, Marco Cipolli, Carla Colombo, Jane C. Davies, Kris De Boeck, Patrick A. Flume, Michael W. Konstan, Susanna A. McColley, Karen McCoy, Edward F. McKone, Anne Munck, Felix Ratjen, Steven M. Rowe, David Waltz, and Michael P. Boyle. Lumacaftor–Ivacaftor in Patients with Cystic Fibrosis Homozygous for Phe508del CFTR. *New England Journal of Medicine*, 373(3):220–231, July 2015.

[255] David Weill, Christian Benden, Paul A. Corris, John H. Dark, R. Duane Davis, Shaf Keshavjee, David J. Lederer, Michael J. Mulligan, G. Alexander Patterson, Lianne G. Singer, Greg I. Snell, Geert M. Verleden, Martin R. Zamora, and Allan R. Glanville. A consensus document for the selection of lung transplant

candidates: 2014 - An update from the Pulmonary Transplantation Council of the International Society for Heart and Lung Transplantation. *Journal of Heart and Lung Transplantation*, 34(1):1–15, January 2015.

[256] Rhonda Szczesniak, Sonya L. Heltshe, Sanja Stanojevic, and Nicole Mayer-Hamblett. Use of FEV1 in cystic fibrosis epidemiologic studies and clinical trials: A statistical perspective for the clinical researcher. *Journal of Cystic Fibrosis*, 16(3):318–326, May 2017.

[257] Anna Rybacka and Katarzyna Karmelita-Katulska. The role of computed tomography in monitoring patients with cystic fibrosis. *Polish Journal of Radiology*, 81:141–145, April 2016.

[258] Helena Ferris, Maria Twomey, Fiachra Moloney, Siobhan B O'Neill, Kevin Murphy, Owen J O'Connor, and Michael Maher. Computed tomography dose optimisation in cystic fibrosis: A review. *World Journal of Radiology*, 8(4):331, 2016.

[259] P. A. De Jong, A. Lindblad, L. Rubin, W. C.J. Hop, J. C. De Jongste, M. Brink, and H. A.W.M. Tiddens. Progression of lung disease on computed tomography and pulmonary function tests in children and adults with cystic fibrosis. *Thorax*, 61(1):80–85, January 2006.

[260] S. Rao and J. Grigg. New insights into pulmonary inflammation in cystic fibrosis. *Archives of Disease in Childhood*, 91(9):786–788, September 2006.

[261] Anita Balázs and Marcus A. Mall. Mucus obstruction and inflammation in early cystic fibrosis lung disease: Emerging role of the IL-1 signaling pathway. *Pediatric Pulmonology*, 54(S3):S5–S12, November 2019.

[262] H. B. Mann and D. R. Whitney. On a Test of Whether one of Two Random Variables is Stochastically Larger than the Other. *The Annals of Mathematical Statistics*, 18(1):50–60, March 1947.

[263] Helen Jones, Peter Millward Knight, and Babatunde Buraimo. Adult participation in sport: analysis of the Taking Part Survey. 2011.

[264] S. Mazic, B. Lazovic, M. Djelic, J. Suzic-Lazic, S. Djordjevic-Saranovic, T. Durmic, I. Soldatovic, D. Zikic, Z. Gluvic, and V. Zugic. Respiratory parameters in elite athletes – does sport have an influence? *Pulmonology*, 21(4):192–197, July 2015.

[265] Güner Çiçek, Abdullah Güllü B-C, Esin Güllü, and Faruk Yamaner. The Effect of Aerobic and Core Exercises on Forced Vital Capacity. *Physical Culture and Sport: Studies and Research*, 2018.

[266] Virginia A. Stallings, Lori J. Stark, Karen A. Robinson, Andrew P. Feranchak, and Hebe Quinton. Evidence-Based Practice Recommendations for Nutrition-Related Management of Children and Adults with Cystic Fibrosis and Pancreatic Insufficiency: Results of a Systematic Review. *Journal of the American Dietetic Association*, 108(5):832–839, May 2008.

[267] Eitan Kerem, Laura Viviani, Anna Zolin, Stephanie MacNeill, Elpis Hatziagorou, Helmut Ellemunter, Pavel Drevinek, Vincent Gulmans, Uros Krivec, and Hanne Olesen. Factors associated with FEV1 decline in cystic fibrosis: Analysis of the ECFS patient registry. *European Respiratory Journal*, 43(1):125–133, January 2014.

[268] Laurie J. Smith, Kenneth A. Macleod, Guilhem J. Collier, Felix C. Horn, Helen Sheridan, Ina Aldag, Chris J. Taylor, Steve Cunningham, Jim M. Wild, and Alex Horsley. Supine posture changes lung volumes and increases ventilation heterogeneity in cystic fibrosis. *PLoS ONE*, 12(11), November 2017.

[269] Jean Donadieu, Candice Roudier, Magali Saguintaah, Carlo Maccia, and Raphaël Chiron. Estimation of the radiation dose from thoracic CT scans in a cystic fibrosis population. *Chest*, 132(4):1233–1238, 2007.

[270] Gaël Dournes, Laura L. Walkup, Ilyes Benlala, Matthew M. Willmering, Julie Macey, Stephanie Bui, François Laurent, and Jason C. Woods. The Clinical Use of Lung MRI in Cystic Fibrosis: What, Now, How? *Chest*, 159(6):2205–2217, June 2021.

[271] Meenakshi Bhalla, Nelson Turcios, Victor Aponte, Margaret Jenkins, Barry S. Leitman, Dorothy I. McCauley, and David P. Naidich. Cystic fibrosis: scoring system with thin-section CT. *https://doi.org/10.1148/radiology.179.3.2027992*, 179(3):783–788, June 1991.

[272] Francesca Santamaria, Giacomo Grillo, Guido Guidi, Antonio Rotondo, Valeria Raia, Giorgio De Ritis, Paola Sarnelli, Marinella Caterino, and Luigi Greco. Cystic fibrosis: when should high-resolution computed tomography of the chest Be obtained? *Pediatrics*, 101(5):908–913, May 1998.

[273] Thomas H. Helbich, Gertraud Heinz-Peer, Irmgard Eichler, Patrick Wunderbaldinger, Manfred Götz, Claudia Wojnarowski, Robert C. Brasch, and Christian J. Herold. Cystic fibrosis: CT assessment of lung involvement in children and adults. *Radiology*, 213(2):537–544, November 1999.

[274] Alan S. Brody, Paul L. Molina, Jeffrey S. Klein, Brian S. Rothman, Maya Ramagopal, and Donald R. Swartz. High-resolution computed tomography of the chest in children with cystic fibrosis: Support for use as an outcome surrogate. *Pediatric Radiology*, 29(10):731–735, October 1999.

[275] Pim A. De Jong, Mark D. Ottink, Simon G.F. Robben, Maarten H. Lequin, Wim C.J. Hop, Johan J.E. Hendriks, Peter D. Paré, and Harm A.W.M. Tiddens. Pulmonary Disease Assessment in Cystic Fibrosis: Comparison of CT Scoring Systems and Value of Bronchial and Arterial Dimension Measurements. *Radiology*, 231(2):434–439, May 2004.

[276] Alan S. Brody, Jeffrey S. Klein, Paul L. Molina, Joanne Quan, Judy A. Bean, and Robert W. Wilmott. High-resolution computed tomography in young patients with cystic fibrosis: Distribution of abnormalities and correlation with pulmonary function tests. *The Journal of Pediatrics*, 145(1):32–38, July 2004.

[277] Alan S. Brody, Heidi Sucharew, Jonathan D. Campbell, Steven P. Millard, Paul L. Molina, Jeffrey S. Klein, and Joanne Quan. Computed tomography correlates with pulmonary exacerbations in children with cystic fibrosis. *American journal of respiratory and critical care medicine*, 172(9):1128–1132, November 2005.

[278] Alistair D. Calder, Andrew Bush, Alan S. Brody, and Catherine M. Owens. Scoring of chest CT in children with cystic fibrosis: state of the art. *Pediatric radiology*, 44(12):1496–1506, November 2014.

[279] Mannudeep K. Kalra, Michael M. Maher, Stefania Rizzo, David Kanarek, and Jo Anne O. Shephard. Radiation exposure from Chest CT: Issues and Strategies. *Journal of Korean Medical Science*, 19(2):159, 2004.

[280] Allen F. Shaughnessy. Incidental Findings Are Common with Chest CT and MRI of the Spine and Brain. *American Family Physician*, 98(11):682–682, December 2018.

[281] Alda Marques, Joana Cruz, Cristina Jácome, Ana Oliveira, Alda Marques, Joana Cruz, Cristina Jácome, and Ana Oliveira. Outcome Measures for Respiratory Physiotherapy in Cystic Fibrosis — Challenges and Advances. *Cystic Fibrosis in the Light of New Research*, August 2015.

[282] Judy M. Bradley, Fidelma M. Moran, and J. Stuart Elborn. Evidence for physical therapies (airway clearance and physical training) in cystic fibrosis: an overview of five Cochrane systematic reviews. *Respiratory medicine*, 100(2):191–201, 2006.

[283] Maggie Patricia McIlwaine, Nancy Alarie, George F. Davidson, Larry C. Lands, Felix Ratjen, Ruth Milner, Blythe Owen, and Jennifer L. Agnew. Long-term multicentre randomised controlled study of high frequency chest wall oscillation versus positive expiratory pressure mask in cystic fibrosis. *Thorax*, 68(8):746–751, 2013.

[284] Maggie McIlwaine, Lawrence T Wong, Mark Chilvers, and George F. Davidson. Long-term comparative trial of two different physiotherapy techniques; postural drainage with percussion and autogenic drainage, in the treatment of cystic fibrosis. *Pediatric Pulmonology*, 45(11):1064–1069, November 2010.

[285] A R Horsley, P M Gustafsson, K A Macleod, C Saunders, A P Greening, D J Porteous, J C Davies, S Cunningham, E W F W Alton, and J A Innes. Lung clearance index is a sensitive, repeatable and practical measure of airways disease in adults with cystic fibrosis. *Thorax*, 63(2):135–140, September 2007.

[286] Helmut Ellemunter, Susanne I. Fuchs, Karin M. Unsinn, Martin C. Freund, Maria Waltner-Romen, Gratiana Steinkamp, and Monika Gappa. Sensitivity of lung clearance index and chest computed tomography in early cf lung disease. *Respiratory Medicine*, 104(12):1834–1842, December 2010.

[287] Andrew Fretzayas, Konstantinos Douros, Maria Moustaki, and Ioanna Loukou. Applications of lung clearance index in monitoring children with cystic fibrosis. *World Journal of Clinical Pediatrics*, 8(2):15, April 2019.

[288] BreAnna Kinghorn, Sharon McNamara, Alan Genatossio, Erin Sullivan, Molly Siegel, Irma Bauer, Charles Clem, Robin C. Johnson, Miriam Davis, Anne Griffiths, William Wheeler, Katherine Johnson, Stephanie D. Davis, Margaret W. Leigh, Margaret Rosenfeld, and Jessica Pittman. Comparison of Multiple

Breath Washout and Spirometry in Children with Primary Ciliary Dyskinesia and Cystic Fibrosis and Healthy Controls. *Ann Am Thorac Soc*, 17(9):1085–1093, September 2020.

[289] Margaret Rosenfeld, Ronald L. Gibson, Sharon McNamara, Julia Emerson, Jane L. Burns, Robert Castile, Peter Hiatt, Karen McCoy, Christopher B. Wilson, Andrew Inglis, Arnold Smith, Thomas R. Martin, and Bonnie W. Ramsey. Early pulmonary infection, inflammation, and clinical outcomes in infants with cystic fibrosis*. *Pediatric Pulmonology*, 32(5):356–366, November 2001.

[290] Gillian M. Nixon, D. S. Armstrong, R. Carzino, J. B. Carlin, A. Olinsky, C. F. Robertson, and K. Grimwood. Early airway infection, inflammation, and lung function in cystic fibrosis. *Archives of Disease in Childhood*, 87(4):306–311, October 2002.

[291] A. R. Horsley, P. M. Gustafsson, K. A. Macleod, C. Saunders, A. P. Greening, D. J. Porteous, J. C. Davies, S. Cunningham, E. W.F.W. Alton, and J. A. Innes. Lung clearance index is a sensitive, repeatable and practical measure of airways disease in adults with cystic fibrosis. *Thorax*, 63(2):135–140, February 2008.

[292] Ah Fong Hoo, Lena P. Thia, The Thanh Diem Nguyen, Andrew Bush, Jane Chudleigh, Sooky Lum, Deeba Ahmed, Ian Balfour Lynn, Siobhan B. Carr, Richard J. Chavasse, Kate L. Costeloe, John Price, Anu Shankar, Colin Wallis, Hilary A. Wyatt, Angela Wade, and Janet Stocks. Lung function is abnormal in 3-month-old infants with cystic fibrosis diagnosed by newborn screening. *Thorax*, 67(10):874–881, 2012.

[293] P. M. Gustafsson, P. A. De Jong, H. A.W.M. Tiddens, and A. Lindblad. Multiple-breath inert gas washout and spirometry versus structural lung disease in cystic fibrosis. *Thorax*, 63(2):129–134, February 2008.

[294] Yvonne Belessis, Barbara Dixon, Glenn Hawkins, John Pereira, Jenny Peat, Rebecca MacDonald, Penny Field, Andrew Numa, John Morton, Kei Lui, and Adam Jaffe. Early Cystic Fibrosis Lung Disease Detected by Bronchoalveolar Lavage and Lung Clearance Index. *https://doi.org/10.1164/rccm.201109-1631OC*, 185(8):862–873, December 2012.

[295] Paul D. Robinson, Michael D. Goldman, and Per M. Gustafsson. Inert Gas Washout: Theoretical Background and Clinical Utility in Respiratory Disease. *Respiration*, 78(3):339–355, 2009.

[296] Refika Hamutcu, Jon M. Rowland, Monica V. Horn, Cornelia Kaminsky, Eithne F. MacLaughlin, Vaughn A. Starnes, and Marlyn S. Woo. Clinical findings and lung pathology in children with cystic fibrosis. *American Journal of Respiratory and Critical Care Medicine*, 165(8):1172–1175, April 2002.

[297] Refika Hamutcu, Jon M. Rowland, Monica V. Horn, Cornelia Kaminsky, Eithne F. MacLaughlin, Vaughn A. Starnes, and Marlyn S. Woo. Clinical Findings and Lung Pathology in Children with Cystic Fibrosis. *https://doi.org/10.1164/ajrccm.165.8.2104090*, 165(8):1172–1175, December 2012.

[298] Elpis Hatziagorou, Asterios Kampouras, Vasiliki Avramidou, Ilektra Toulia, Elisavet Anna Chrysochoou, Maria Galogavrou, Fotios Kirvassilis, and John Tsanakas. Toward the Establishment of New Clinical Endpoints for Cystic Fibrosis: The Role of Lung Clearance Index and Cardiopulmonary Exercise Testing. *Frontiers in Pediatrics*, 9:116, February 2021.

[299] E. Hatziagorou, V. Avramidou, F. Kirvassilis, and J. Tsanakas. Use of lung clearance index to assess the response to intravenous treatment in cystic fibrosis. *Hippokratia*, 19(1):47, June 2015.

[300] Jane Davies, Helen Sheridan, Nicholas Bell, Steve Cunningham, Stephanie D. Davis, J. Stuart Elborn, Carlos E. Milla, Timothy D. Starner, Daniel J. Weiner, Po Shun Lee, and Felix Ratjen. Assessment of clinical response to ivacaftor with lung clearance index in cystic fibrosis patients with a G551D-CFTR mutation and preserved spirometry: a randomised controlled trial. *The Lancet. Respiratory medicine*, 1(8):630–638, 2013.

[301] Jane C. Davies, Isabelle Sermet-Gaudelus, Lutz Naehrlich, R. Scott Harris, Daniel Campbell, Neil Ahluwalia, Christopher Short, Eric Haseltine, Paul Panorchan, Clare Saunders, Caroline A. Owen, and Claire E. Wainwright. A phase 3, double-blind, parallel-group study to evaluate the efficacy and safety of tezacaftor in combination with ivacaftor in participants 6 through 11 years of

age with cystic fibrosis homozygous for F508del or heterozygous for the F508del-CFTR mutati. *Journal of cystic fibrosis : official journal of the European Cystic Fibrosis Society*, 20(1):68–77, January 2021.

[302] Michelle Shaw, Martinus C. Oppelaar, Renee Jensen, Sanja Stanojevic, Stephanie D. Davis, George Retsch-Bogart, and Felix A. Ratjen. The utility of moment ratios and abbreviated endpoints of the multiple breath washout test in preschool children with cystic fibrosis. *Pediatric Pulmonology*, 55(3):649–653, March 2020.

[303] Lokesh Guglani, Ajay Kasi, Miah Starks, Knud E. Pedersen, Jørgen G. Nielsen, and Daniel J. Weiner. Difference between SF6 and N2 multiple breath washout kinetics is due to N2 back diffusion and error in N2 offset. *Journal of Applied Physiology*, 125(4):1257–1265, October 2018.

[304] Alexander Horsley and Chantal Darquenne. Better late than never: correcting the error in the Exhalyzer nitrogen washout system. *Journal of Applied Physiology*, 131(4):1286, October 2021.

[305] Sylvia Verbanck, Daniël Schuermans, and Walter Vincken. Small airways ventilation heterogeneity and hyperinflation in COPD: Response to tiotropium bromide. *International Journal of Chronic Obstructive Pulmonary Disease*, 2(4):625, 2007.

[306] Sanja Stanojevic, Renee Jensen, Dasiga Sundaralingam, Juliana Giraldo Salazar, Sophie Yammine, Florian Singer, Philipp Latzin, Reshma Amin, Padmaja Subbarao, Per Gustafsson, and Felix Ratjen. Alternative outcomes for the multiple breath washout in children with CF. *Journal of Cystic Fibrosis*, 14(4):490–496, July 2015.

[307] B. L. Welch. The Generalization of 'Student's' Problem When Several Different Population Variances are Involved. *Biometrika*, 34(1-2):28–35, January 1947.

[308] David Taylor-Robinson, Margaret Whitehead, Finn Diderichsen, Hanne Vebert Olesen, Tania Pressler, Rosalind L. Smyth, and Peter Diggle. Understanding the natural progression in %FEV1 decline in patients with cystic fibrosis: A longitudinal study. *Thorax*, 67(10):860–866, 2012.

[309] William L. Eschenbacher. Defining Airflow Obstruction. *Chronic Obstructive Pulmonary Diseases: Journal of the COPD Foundation*, 3(2):515–518, 2016.

[310] Michel A. Hofman, Alfons C. Laan, and Harry B.M. Uylings. Bivariate linear models in neurobiology: problems of concept and methodology. *Journal of neuroscience methods*, 18(1-2):103–114, 1986.

[311] A. Trujillo-Ortiz and R Hernandez-Walls. gmregress: Geometric Mean Regression (Reduced Major Axis Regression). A MATLAB file. [WWW document]., 2010.

[312] Pierre Jolicoeur. Interval Estimation of the Slope of the Major Axis of a Bivariate Normal Distribution in the Case of a Small Sample. *Biometrics*, 24(3):679, September 1968.

[313] B. H. McArdle. The structural relationship: regression in biology. *Canadian Journal of Zoology*, 66(11):2329–2339, November 1988.

[314] Peter J. Rousseeuw, Ida Ruts, and John W. Tukey. The bagplot: A bivariate boxplot. *American Statistician*, 53(4):382–387, 1999.

[315] A. C. Groom, R. Morin, and L. E. Farhi. Determination of dissolved N2 in blood and investigation of N2 washout from the body. *https://doi.org/10.1152/jappl.1967.23.5.706*, 23(5):706–712, 1967.

[316] A. Barry Baker and Andrew D. Farmery. Inert Gas Transport in Blood and Tissues. *Comprehensive Physiology*, 1(2):569–592, April 2011.

[317] Blake M. Handley, Edward Jeagal, Robin E. Schoeffel, Tanya Badal, David G. Chapman, Catherine E. Farrow, Gregory G. King, Paul D. Robinson, Stephen Milne, and Cindy Thamrin. Controlled versus free breathing for multiple breath nitrogen washout in healthy adults. *ERJ Open Research*, 7(1), January 2021.

[318] Sylvia Verbanck, Daniel Schuermans, Manuel Paiva, Paul D. Robinson, and Eef Vanderhelst. Mitigating increased variability of multiple breath washout indices due to tidal breathing. *European Respiratory Journal*, 57(2), February 2021.

[319] G. Kim Prisk, Sandra Rutting, Jack Bozier, Cindy Thamrin, Paul D. Robinson, and Bruce R. Thompson. Assessing the calculation of conductive and acinar ventilatory heterogeneity indices Scond and Sacin from multiple-breath washout data. *Journal of Applied Physiology*, 134(4):879–886, April 2023.

[320] Florian Wyler, Marc-Alexander Oestreich, Bettina S. Frauchiger, Kathryn A. Ramsey, and Philipp Latzin. Correction of sensor crosstalk error in Exhalyzer D multiple-breath washout device significantly impacts outcomes in children with cystic fibrosis. *Journal of Applied Physiology*, 131(3):1148–1156, September 2021.

[321] Sherif Gonem, Alys Scadding, Marcia Soares, Amisha Singapuri, Per Gustafsson, Chandra Ohri, Simon Range, Christopher E. Brightling, Ian Pavord, Alex Horsley, and Salman Siddiqui. Lung clearance index in adults with non-cystic fibrosis bronchiectasis. *Respiratory Research*, 15(1):59, May 2014.

[322] Per M. Gustafsson. Peripheral airway involvement in CF and asthma compared by inert gas washout. *Pediatric pulmonology*, 42(2):168–176, February 2007.

[323] G Davies, P Aurora, A Mcdonald, A Prasad, D Bilton, J Stocks, and S Stanojevic. S67 Lung Clearance Index (lci) Is A Sensitive Predictor Of High Resolution Computed Tomography (hrct) Scores In Children With Non-cf Bronchiectasis. *Thorax*, 69(Suppl 2):A37–A38, December 2014.

[324] Johanna Manuela Kurz, Jeannette Frey, Reto Auer, Nicolas Rodondi, Sylvia Nyilas, Nikolay Pavlov, Manuela Funke-Chambour, and Florian Singer. Influence of ventilation inhomogeneity on diffusing capacity of carbon monoxide in smokers without COPD. *ERJ Open Research*, 7(1), 2021.

[325] Don B. Sanders, George M. Solomon, Valeria V. Beckett, Natalie E. West, Cori L. Daines, Sonya L. Heltshe, Donald R. VanDevanter, Jonathan E. Spahr, Ronald L. Gibson, Jerry A. Nick, Bruce C. Marshall, Patrick A. Flume, and Christopher H. Goss. Standardized Treatment of Pulmonary Exacerbations (STOP) study: Observations at the initiation of intravenous antibiotics for cystic fibrosis pulmonary exacerbations. *Journal of Cystic Fibrosis*, 16(5):592–599, September 2017.

[326] NICE Guideline, No. 78. In *NICE Guideline, No. 78.* National Guideline Alliance (UK), 2017. `https://www.ncbi.nlm.nih.gov/books/NBK535670/`, date accessed 2023-08-07.

[327] Susan Charman, Elliot McGlenaghan, Rebecca Cosgriff, Andrew Lee, and Siobhan Carr. UK Cystic Fibrosis Registry Annual Data Report 2019. Technical report, UK Cystic Fibrosis Registry, 2020.

[328] Alan R. Smyth, Scott C. Bell, Snezana Bojcin, Mandy Bryon, Alistair Duff, Patrick Flume, Nataliya Kashirskaya, Anne Munck, Felix Ratjen, Sarah Jane Schwarzenberg, Isabelle Sermet-Gaudelus, Kevin W. Southern, Giovanni Taccetti, Gerald Ullrich, and Sue Wolfe. European cystic fibrosis society standards of care: Best practice guidelines. *Journal of Cystic Fibrosis*, 13(S1):S23–S42, May 2014.

[329] Uk cystic fibrosis registry annual data report 2012: Summary. `https://www.cysticfibrosis.org.uk/sites/default/files/2020-12/2012%20Registry%20Annual%20Data%20Report%20SUMMARY.pdf`, date accessed 2023-08-10.

[330] Paul Aurora, Andrew Bush, Per Gustafsson, Cara Oliver, Colin Wallis, John Price, John Stroobant, Siobhan Carr, and Janet Stocks. Multiple-breath washout as a marker of lung disease in preschool children with cystic fibrosis. *American Journal of Respiratory and Critical Care Medicine*, 171(3):249–256, February 2005.

[331] Kathryn A. Ramsey, Rachel E. Foong, Jasmine Grdosic, Alana Harper, Billy Skoric, Charles Clem, Miriam Davis, Lidija Turkovic, Stephen M. Stick, Stephanie D. Davis, Sarath C. Ranganathan, and Graham L. Hall. Multiple-breath washout outcomes are sensitive to inflammation and infection in children with cystic fibrosis. *Annals of the American Thoracic Society*, 14(9):1436–1442, September 2017.

[332] R. Amin, P. Subbarao, W. Lou, A. Jabar, S. Balkovec, R. Jensen, S. Kerrigan, P. Gustafsson, and F. Ratjen. The effect of dornase alfa on ventilation inhomogeneity in patients with cystic fibrosis. *European Respiratory Journal*, 37(4):806–812, April 2011.

[333] Reshma Amin, Padmaja Subbarao, Alisha Jabar, Susan Balkovec, Renee Jensen, Shawn Kerrigan, Per Gustafsson, and Felix Ratjen. Hypertonic saline improves the LCI in paediatric patients with CF with normal lung function. *Thorax*, 65(5):379–383, May 2010.

[334] Lucy Perrem, Jonathan H. Rayment, and Felix Ratjen. The lung clearance index as a monitoring tool in cystic fibrosis: ready for the clinic? *Current opinion in pulmonary medicine*, 24(6):579–585, November 2018.

[335] Mirjam Stahl, Cornelia Joachim, Mark O. Wielpütz, and Marcus A. Mall. Comparison of lung clearance index determined by washout of N2 and SF6 in infants and preschool children with cystic fibrosis. *J Cyst Fibros*, 18(3):399–406, May 2019.

[336] Tamás Kovács, Wuhu Feng, Anna Totterdill, John M C Plane, Sandip Dhomse, Juan Carlos Gómez-Martín, Gabriele P Stiller, Florian J Haenel, Christopher Smith, Piers M Forster, Rolando R García, Daniel R Marsh, and Martyn P Chipperfield. Determination of the atmospheric lifetime and global warming potential of sulfur hexafluoride using a three-dimensional model. *Atmos. Chem. Phys*, 17:883–898, 2017.

[337] Amy G. L. Nuttall, Werner Velásquez, Caroline S. Beardsmore, and Erol A. Gaillard. Lung clearance index: assessment and utility in children with asthma. *European Respiratory Review*, 28(154), December 2019.

[338] WHO child growth charts. `https://www.who.int/tools/child-growth-standards/standards/weight-for-age`, date accessed 2023-08-09.

[339] A. V. Nikitin, O. M. Lyulin, S. N. Mikhailenko, V. I. Perevalov, N. N. Filippov, I. M. Grigoriev, I. Morino, Y. Yoshida, and T. Matsunaga. GOSAT-2014 methane spectral line list. *Journal of Quantitative Spectroscopy and Radiative Transfer*, 154:63–71, March 2015.

[340] Orazio Svelto. *Principles of lasers*. Springer, 2010.

[341] P. D. Wagner, P. F. Naumann, and R. B. Laravuso. Simultaneous measurement of eight foreign gases in blood by gas chromatography. *https://doi.org/10.1152/jappl.1974.36.5.600*, 36(5):600–605, 1974.

[342] L. E. Farhi, A. W. Edwards, and T. Homma. Determination of dissolved N2 in blood by gas chromatography and (a-A)N2 difference. *https://doi.org/10.1152/jappl.1963.18.1.97*, 18:97–106, January 1963.

[343] Paul Aurora, Andrew Bush, Per Gustafsson, Cara Oliver, Colin Wallis, John Price, John Stroobant, Siobhan Carr, and Janet Stocks. Multiple-Breath Washout as a Marker of Lung Disease in Preschool Children with Cystic Fibrosis. *Am J Respir Crit Care Med*, 171(3):249–256, February 2005.

[344] Elisabeth Kieninger, Sophie Yammine, Insa Korten, Pinelopi Anagnostopoulou, Florian Singer, Urs Frey, Anne Mornand, Maura Zanolari, Isabelle Rochat, Daniel Trachsel, Dominik Mueller-Suter, Alexander Moeller, Carmen Casaulta, Philipp Latzin, SCILD study group, and BILD study group. Elevated lung clearance index in infants with cystic fibrosis shortly after birth. *Eur Respir J*, 50(5):1700580, November 2017.

[345] Annelies Zwitserloot, Susanne I. Fuchs, Christina Müller, Kornelia Bisdorf, and Monika Gappa. Clinical application of inert gas Multiple Breath Washout in children and adolescents with asthma. *Respir Med*, 108(9):1254–1259, 2014.

[346] W. James Gauderman, Hita Vora, Rob McConnell, Kiros Berhane, Frank Gilliland, Duncan Thomas, Fred Lurmann, Edward Avol, Nino Kunzli, Michael Jerrett, and John Peters. Effect of exposure to traffic on lung development from 10 to 18 years of age: a cohort study. *The Lancet*, 369(9561):571–577, 2007.

[347] S. Sonnappa, C. M. Bastardo, P. Aurora, D. Whyatt, F. J. Kelly, S. D. Beevers, and J. Grigg. Residential proximity to main roads and lung function in healthy young children. *European Respiratory Journal*, 37(6):1525–1526, June 2011.

[348] Gary Nieman, Michaela Kollisch-Singule, Harry Ramcharran, Joshua Satalin, Sarah Blair, Louis A. Gatto, Penny Andrews, Auyon Ghosh, David W. Kaczka, Donald Gaver, Jason Bates, and Nader M. Habashi. Unshrinking the baby lung to calm the VILI vortex. *Critical Care*, 26(1):242, August 2022.

[349] Snapper R. M. Magor-Elliott, Asma Alamoudi, Rebecca R. Chamley, Haopeng Xu, Tishan Wellalagodage, Rory P. McDonald, David O'Brien, Jonathan Collins, Ben Coombs, James Winchester, Ed Sellon, Cheng Xie, Dominic Sandhu, Christopher J. Fullerton, John H. Couper, Nicholas M. J. Smith, Graham Richmond, Mark P. Cassar, Betty Raman, Nick P. Talbot, Alexander N. Bennett, Edward D. Nicol, Grant A. D. Ritchie, Nayia Petousi, David A. Holdsworth, and Peter A. Robbins. Altered lung physiology in two cohorts after COVID-19 infection as assessed by computed cardiopulmonography. *Journal of Applied Physiology (Bethesda, Md.: 1985)*, 133(5):1175–1191, November 2022.

[350] Steve Goodacre, Catherine Nelson-Piercy, Beverley Hunt, and Wee-Shian Chan. When should we use diagnostic imaging to investigate for pulmonary embolism in pregnant and postpartum women? *Emergency medicine journal: EMJ*, 32(1):78–82, January 2015.